The PERK(s) of having your own niche: how Acute Myeloid Leukaemia transforms the Bone Marrow Microenvironment

Doriana Di Bella

Declaration

I, Doriana Di Bella, confirm that the research included within this thesis is my own work or that where it has been carried out in collaboration with or supported by others, that this is duly acknowledged below and my contribution indicated.

I attest that I have exercised reasonable care to ensure that the work is original, and does not to the best of my knowledge break any UK law, infringe any third party copyright or other Intellectual Property Right, or contain any confidential material.

I accept that the College has the right to use plagiarism detection software to check the electronic version of the thesis.

I confirm that this thesis has not been previously submitted for the award of a degree by this or any other university. The copyright of this thesis rests with the author and no quotation from it or information derived from it may be published without the prior written consent of the author.

Signature:

Date: December 2022

Statement of contribution

Eleni Maniati (BCI, London) performed RNA-sequencing analysis.

Pedro Maria Casado-Izquierdo (BCI, London) performed the Proteomic and Phosphoproteomic analysis, while Ruth Osuntola (BCI, London) and Vinothini Rajeeve (BCI, London) prepared and acquired the samples.

Diana Passaro and Jorgina Reginold (Cochin Institute, Paris) performed the bioengineered humanised bone marrow experiment.

Diana Passaro (Crick institute, London) performed the patient-derived-xenograft experiment.

Eleanor Jane Tyler (BCI, London) performed the matrisome analysis.

Acknowledgements

Firstly, I would like to thank my supervisor for the opportunity to be the first PhD student in his lab. Thanks also to my second supervisor Jessica Okosun for been always very encouraging and enlightening. A special thanks to Ana Rio-Machin and Jude Fitzgibbon who first welcomed me and never stopped sustaining me throughout these years.

Next, I would like to thank the members of the lab, Céline and Wei Wei: chance made us colleagues, but all the time spent together made us friends. I feel so lucky to have had you as partners in science, who allowed me to grow so much both as a scientist and as a person. Thank you Céline for being of great inspiration and support, for never losing patience with my never-ending questions and doubts, and for sharing tips and teaching me techniques. You bestowed so many good suggestions upon me and I will always cherish our friendship. Also, thank you for introducing me to S. Rita, undoubtedly an essential support in cloning! Thank you Wei for being such a caring, kind and helpful person. Your presence has made such a positive impact and I feel fortunate that I could share my PhD path with you and build our lovely memories.

It has been a pleasure working in the haemato-oncology department, and I thank the present and past members for creating such a pleasant working atmosphere. I would like to express my deepest gratitude to all the collaborators that were keen on my project and have contributed with their unique expertise to this work.

I am extremely grateful to all the people that made these years amazing. Filomena and Pablo, thanks for the countless weekends spent together, the discussions, the games, the walks and the nights out. Thank you Vilma for being such an inspirational woman and scientist. Thank you Mariette for your trust, support and words of encouragement. Thank you Joana for being always so nice and caring. Thank you all for the memorable moments we shared and for being part of my London family.

A super special thank you goes to Vir, my long-distance yet closest friend. I am grateful that I could share the up-and-downs of the PhD process with you. Thank you

for our phone calls and the endless entertaining discussions, both scientific and otherwise, that gave me comfort but also fostered me to better myself.

Thank you to my family: Mum, Dad, my brothers Danilo and Damiano and my sister Domitilla, who despite being miles away have always been there for me.

Finally, words cannot express my gratitude to Francesco, my pillar. Thank you for your constant love and encouragement that kept my spirit and motivation high during this process. Lastly, to London, for welcoming us and being our home for five incredible years.

Contents

List of Figures

List of Tables

Abbreviations

ACN	Acetonitrile
AML	Acute Myeloid Leukaemia
APC	Allophycocyanin
APC-Cy7	APC-Cyanine® 7
ASK1	Apoptosis Signal-Regulating Kinase 1
ATF4	Activation Transcription Factor 4
ATF6	Activation Transcription Factor 6
ATF6f	Activation Transcription Factor 6 Fragment
ATF6α	Activation Transcription Factor 6α
ATP	Adenosine Triphosphate
ATP5H	Mitochondrial ATP Synthase
BCA	Bicinchoninic Acid
BCL-2	B-Cell Lymphoma 2
BIM	Bcl-2 Interacting Mediator Of Cell Death
BIX	Bip Inducer X
BM	Bone Marrow
BMP2	Bone Morphogenic Protein 2
BMP4	Bone Morphogenic Protein 4
BMPs	Bone Morphogenic Proteins
BV421	Brilliant Violet 421
C/EBPα	CCAAT/Enhancer Binding Protein A
C/EBPβ	CCAAT/Enhancer Binding Protein B
C/EBPδ	CCAAT/Enhancer Binding Protein Δ
Ca2+	Calcium
CB	Cord Blood
CD	Cluster Of Differentiation
CFD	Complement Factor D (Adipsin)
CFU-F	Colony-Forming Unit-Fibroblastic
CFU-S	Colony-Forming Unit-Spleen
CHOP	C/EBP Homologous Protein
CMP	Common Myeloid Progenitor
CNX	Calnexin

COL1A1	Collagen Type I Alpha 1 Chain
COL3A1	Collagen Type III Alpha 1 Chain
COL5A1	Collagen Type V Alpha 1 Chain
CREB	Camp-Response Element-Binding
CRT	Calreticulin
CSNK1E	Casein Kinase 1 Epsilon
CXCL12	C-X-C Motif Chemokine Ligand 12
CXCL2	C-X-C Motif Chemokine Ligand 2
DAPI	4',6-Diamidino-2-Phenylindole
db/db	Diabetes/Diabetes
DCN	Decorin
DMEM	Dulbecco's Modified Eagle Medium
DNA	Deoxyribonucleic Acid
DNase	Deoxyribonuclease
DNMT3A	DNA (Cytosine-5)-Methyltransferase 3A
EC	Endothelial Cell
ECM	Extracellular Matrix
EDEM	ER Degradation Enhancing Alpha-Mannosidase Like Protein 1
EDTA	Ethylenediaminetetraacetic Acid
EGFP	Enhanced Green Florescence Protein
EIF2AK3	Eukaryotic Translation Initiation Factor 2 Alpha Kinase 3
ER	Endoplasmic Reticulum
ERAD	Endoplasmic-Reticulum-Associated Protein Degradation
ERCC6L2	ERCC Excision Repair 6 Like 2
ERdj4	ER-Resident Protein
FA	Fatty Acid
FABP	Fatty-Acid-Binding Proteins
FABP4	Fatty-Acid-Binding Protein 4
FACS	Fluorescence-Activated Cell Sorting
FBS	Foetal Bovine Serum
FDR	False Discovery Rate
FGF2	Fibroblast Growth Factor 2
FLT3	Fms Related Receptor Tyrosine Kinase 3
FLT3-L	Foetal Liver Tyrosine Kinase-3 Ligand
FPKM	Fragments Per Kilobase Million

FWHM	Full Width At Half Maximum
GADD34	Growth Arrest And DNA Damage-Inducible Protein 34
GATA2	GATA Binding Protein 2
GATA3	GATA Binding Protein 3
GCN2	General Control Nonderepressible 2
GFP	Green Fluorescence Protein
GLUT4	Glucose Transporter Type 4
GMP	Granulocyte-Monocyte Progenitor
GRP78	Glucose Regulated Protein 78
GRP94	Glucose Regulated Protein 94
GSEA	Gene Set Enrichment Analysis
HA	Human Influenza Hemagglutinin
HBSS	Hanks' Balanced Salt Solution
HCT	Haematopoitic Cell Transplantation
HD	Healthy Donor
HD-MSC	Healthy Donor-Mesenchymal Stromal Cell
HEK293T	Human Embryonic Kidney 293 Cells
HEPES	4-(2-Hydroxyethyl)-1-Piperazineethanesulfonic Acid
HERPUD1	Homocysteine-Responsive Endoplasmic Reticulum-Resident Ubiquitin-Like Domain Member 1 Protein
HL60	Human Leukemia 60 Cells
HLA-DR	Human Leukocyte Antigen – DR Isotype
HRI	Heme-Regulated Eif2α Kinase
HSC	Haematopoitic Stem Cell
HSPC	Haematopoitic Stem And Progenitor Cell
IGF1	Insulin-Like Growth Factor 1
IGF2	Insulin-Like Growth Factor 2
IGFBP2	Insulin Like Growth Factor Binding Protein 2
IL-11	Interleukin 11
IL-6	Interleukin 6
IMDM	Iscove's Modified Dulbecco's Media
IRE1	Inositol-Requiring Enzyme 1
IRE1-LZ	Inositol-Requiring Enzyme 1-Leucine Zipper
IRE1α	Inositol-Requiring Enzyme 1 A
JNK	C-Jun N-Terminal Kinases

KLF	Kruppel-Like Factor
LDS	Lithium Dodecyl Sulfate
LEPR	Leptin Receptor
MAPK	Mitogen-Activated Protein Kinase
MEFs	Mouse Embryonic Fibroblasts
MEMα	Minimum Essential Medium A
MEP	Megakaryocyte–Erythroid Progenitor Cell
MLL-AF9	Mixed-Lineage Leukemia-AF9
MLP	Multilineage Progenitor
MNC	Mononuclear Cell
MOPS	3-(N-Morpholino)Propanesulfonic Acid
MPP	Multi-Potent Progenitor
MS	Mass Spectrometry
MS-5	Murine Stromal Cell Line 5
MSC	Mesenchymal Stromal Cells
NG2	Neural/Glial Antigen 2
NK	Neutral Killer Cell
NO	Nitrogen Oxide
NOTCH1	Neurogenic Locus Notch Homolog Protein 1
NPM1	Nucleophosmin
OSX	Osterix
PAK2	P21 (RAC1) Activated Kinase 2
PBS	Phosphate-Buffered Saline
PCA	Principal Component Analysis
PCR	Polymerase Chain Reaction
PDI	Protein Disulphide Isomerase
PDIA5	Protein Disulphide Isomerases A5
PDX	Patient-Derived Xenograft
PE	Phycoerythrin
PE-Cy7	PE-Cyanine® 7
PERK	Protein Kinase R (PKR)-Like Endoplasmic Reticulum Kinase
PERK-LZ	Protein Kinase R (PKR)-Like Endoplasmic Reticulum Kinase-Leucine Zipper
PP2a	Protein Phosphatase 2
PPARγ	Peroxisome Proliferator-Activated Receptor Gamma

PVDF	Polyvinylidene Difluoride
qPCR	Quantitative Polymerase Chain Reaction
RIN	RNA Integrity Number
RLT	RNA Lysis Buffer
RNA	Ribonucleic Acid
RNase	Ribonuclease
RNA-Seq	RNA Sequencing
ROS	Reactive Oxygen Species
RPKM	Reads Per Kilobase Of Transcript Per Million Reads Mapped
RPMI	Roswell Park Memorial Institute Medium
RSEM	RNA-Seq By Expectation-Maximization
RT-qPCR	Reverse Transcription Quantitative Real-Time PCR
RUNX2	Runt-Related Transcription Factor 2
SCF	Stem Cell Factor
SDS	Sodium Dodecyl Sulfate
SERCA2	Sarco/Endoplasmic Reticulum Ca2+-ATPase
TBS-T	Tris-Buffered Saline - Tween
TFA	Trifluoroacetic Acid
TNF	Tumour Necrotic Factor
TPM	Transcript Per Million
TPO	Thrombopoietin
UPR	Unfolded Protein Response
WRS	Wolcott-Rallison Syndrome
XBP1	X-Box Binding Protein 1
XBP1s	X-Box Binding Protein 1 Spliced
XBP1t	X-Box Binding Protein 1 total
XIC	Extracted Ion Chromatograms

Abstract

Mesenchymal stromal cells (MSC), that generate multiple bone marrow (BM) cell types, such as adipocytes and osteoblasts, contribute to the BM microenvironment cellular diversity, critical to supporting functional haematopoiesis. Mouse model research has shown that acute myeloid leukaemia (AML) alters the BM niche, inducing MSC quiescence, impeding adipogenic differentiation, and compromising haematopoiesis. In this context, it is still unclear whether AML cells directly inhibit haematopoiesis or if this is mediated via alterations of the BM niche. We hypothesized that AML propagation induces stresses, such as oxidative stress, starvation or hypoxia, that lead to endoplasmic reticulum (ER) stress in the BM niche, ultimately leading to the BM failure observed in patients. Here, with combined ex vivo and in vivo studies, we show that AML induces in MSCs an ER stress response known as unfolded protein response (UPR). UPR signals through three branches, PERK, IRE1 and ATF6 to regulate protein synthesis rates, lipid metabolism and apoptosis. Our data reveal the activation of UPR in MSC undergoing adipogenic differentiation. Using a lentiviral conditional overexpression approach, we show that PERK activation reduces MSC proliferative capacities, triggers a cytostatic effect, and shows no apoptosis. Remarkably, MSC adipogenic differentiation is impaired upon conditional PERK activation, while not upon IRE1 overexpression. These data are in line with the adipogenic differentiation blockage observed in AML patients' BM. Furthermore, by using an ectopic humanised BM niche in mice, we show that PERK activation in MSC results in hematopoietic lineage skewing with increased myeloid cells. These findings demonstrate the role of UPR activation as a mechanism responsible for BM alteration. Our study provides new therapeutic opportunities to restore BM functions by targeting UPR.

"For the things we have to learn before we can do them,

we learn by doing them."

Aristotle, The Nicomachean Ethics

Chapter 1

Introduction

1.1. The bone marrow microenvironment in normal haematopoiesis

1.1.1. Haematopoiesis

Haematopoiesis is the hierarchical multi-step process that describes the production of the diverse blood cell repertoire in the bone marrow (BM) throughout postnatal life. All the blood cells originate from a rare population of hematopoietic stem cells (HSCs) which are defined by their ability to self-renew while capable of differentiating into the multiple types of blood cells through a series of intermediary progenitors that undergo gradual fate restrictions (Doulatov et al., 2012).

The first to postulate that haematopoiesis was organised as a hierarchy deriving from a common precursor cell was the scientist Alexander A. Maximow in 1909 (reviewed in Doulatov et al., 2012) after the discovery of the diverse cellular morphologies present in the BM. A more significant indication of the existence of blood-forming cells in the BM came later in the 1950s when two independent research groups rescued the lethal consequences of irradiation through transplantation of the bone marrow or spleen from non-irradiated donors (Jacobson et al., 1951; Lorenz et al., 1951). Further *in vivo* stem cell function assays demonstrated that blood lineages were derived from clonogenic multipotent BM cells, capable of forming macroscopic multi-lineage haematopoietic colonies in the spleen (colony-forming unit or CFU-S) following transplantation of lethally irradiated recipient mice (Till & McCulloch, 1961). These experiments led to the first definitive proof of *in vivo* multipotent progenitor cell function based on tracking cytogenetic abnormalities within individual CFU-S colonies (Becker et al., 1963; Laurenti & Göttgens, 2018).

These early findings, along with the prospective isolation of hematopoietic cells using specific cell surface markers and further *in vitro* or *in vivo* functional assays, contributed to the development of the classical model of haematopoiesis (Doulatov et al., 2012; Laurenti & Göttgens, 2018) (Figure 1.1). This model pictures haematopoiesis as a tree-like differentiation hierarchy, where HSCs with their self-renew capacity reside at the top while terminally differentiated cells constitute the bottom. As they differentiate, HSCs gradually lose their self-renewal properties and differentiation potential, progressing from multi- to oligo- and finally unipotent progenitors (Laurenti & Göttgens, 2018). In the first branch of the tree-like hierarchy, HSCs differentiate into multipotent progenitors (MPPs) characterised by multi-lineage potential but reduced self-renewal capacities. In turn, MPPs give rise to more committed progenitors, namely the common myeloid progenitors (CMPs) and the multilymphoid progenitors (MLPs). CMPs can differentiate into the granulocyte/macrophage progenitors (GMPs) and the megakaryocyte/erythroid progenitors (MEPs), which then respectively give rise to myeloid and erythroid lineages. MLPs are also able to generate GMPs, while capable of differentiation into B, T, and Natural killer (NK) cell precursors, giving rise to the lymphoid lineage (Doulatov et al., 2012; Laurenti & Göttgens, 2018).

While the classical haematopoietic hierarchy roadmap illustrates haematopoiesis as a stepwise process constituted of discrete intermediated steps, recent single-cell murine studies have challenged this model, providing new insights into haematopoiesis and revealing more complexity in the differentiation process. Newly revised models propose that the classically defined progenitors do not represent discrete cell types but rather heterogeneous populations, composed mostly of unilineage committed cells (Laurenti & Göttgens, 2018; Notta et al., 2016), and that the HSCs differentiation, with the acquisition of lineage-specific fates, is a continuous process (Laurenti & Göttgens, 2018; Velten et al., 2017).

1.1.1.1. Immunophenotypic characterisation

The success of cell surface markers for immunophenotypic characterisation and prospective isolation of HSCs and blood cells have significantly fuelled and accelerated the study of haematopoiesis and its hierarchy. The first marker

discovered to enrich human HSCs and progenitor cells was CD34 (Civin et al., 1984), which was found to be expressed in 1-2% of human BM cells (Civin et al., 1984). CD34 has been then successfully proven in numerous clinical transplantation studies over the past decade to mark HSCs (Doulatov et al., 2012) and CD34+ hematopoietic cells obtained from the BM or blood are in clinical use in transplantation and gene therapy studies, including ongoing attempts to expand them *ex vivo* (Krause et al., 1996). While being useful to enrich human HSCs, CD34 marks also more differentiated progenitors, so the CD34+ population is usually referred to as haematopoietic stem and progenitor cells (HSPCs) (Figure 1.1). The purification and identification of human HSCs require the simultaneous detection of several independent cell surface markers. Baum et al. identified CD90 (Thy1) as a stem cell marker (Baum et al., 1992), which in combination with CD34 but no known lineage (Lin) markers, it demarcated a small population of Lin-CD34+CD90+ cells that contained most multilineage capacity (Murray et al., 1995). Further studies introduced CD45RA (Majeti et al., 2007) and CD38 (Bhatia et al., 1997) as markers of more differentiated progenitors that negatively enrich for HSCs. More recently, CD49f was found to be expressed in 50% of Lin-CD34+CD38-CD90-CD45RA- HSCs (Notta et al., 2011), indicating that could be used as a positive selection to further fractionate HSCs, while MPPs can be identified by the loss of CD49f expression as Lin-CD34+CD38-CD45RA-CD90-CD49f- (Doulatov et al., 2012). More committed progenitors such as MLP, CMP, GMP and MEP can also be studied with a combination of markers that include CD38, CD45RA, CD10, CD135 and CD7 (Figure 1.1) (Doulatov et al., 2012; Van Galen et al., 2014;

Wasnik et al., 2012). The different markers used for the identification and isolation of HSC and progenitor cells are summarised in the review by Rix et al., 2022.

CD45 pan-hematopoietic and lineage (Lin+) specific markers identify and characterise the differentiated progeny of CMP (erythrocytes, granulocytes, megakaryocytes, and macrophages) and MLP (B cell, T cell, NK cell). For instance, B-cells are CD45+CD20+; T-lymphocytes CD45+CD3+ or CD45+CD19+ and NK cells are CD45+CD56+. Cells of myeloid lineages such as erythrocytes are CD235a+; megakaryocytes are CD41+; monocytes are CD45+CD14+ and granulocytes are CD45+CD15+ (Wasnik et al., 2012).

1.1.1.2. Regulation of Haematopoiesis
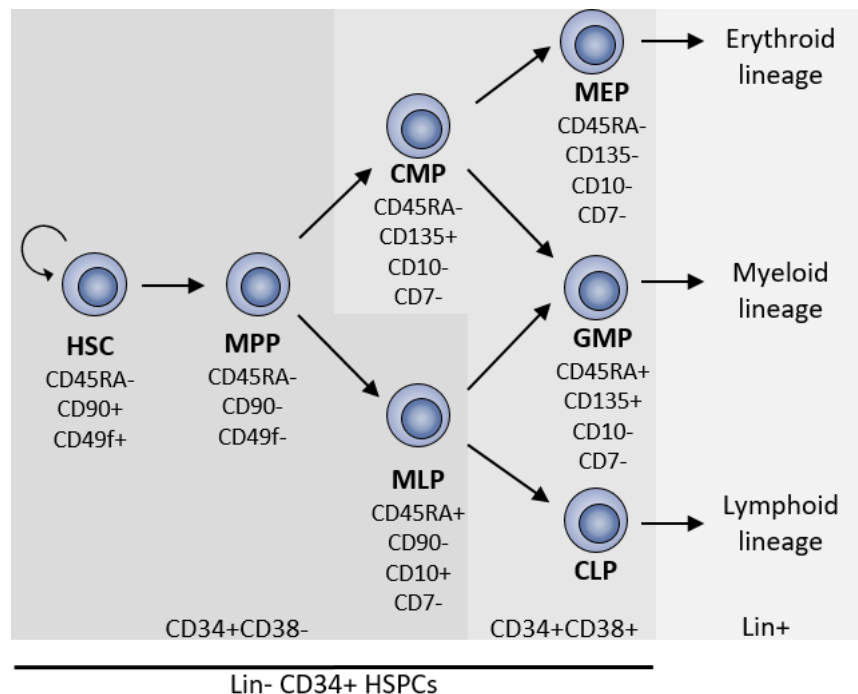
Figure 1.1: Human haematopoiesis hierarchy and immunophenotypic characterisation of haematopoietic cells. HSCs are commonly identified as lineage marker negative (Lin−) CD34+CD38−CD45RA−CD90+CD49f+, and MPPs can be identified by the loss of CD49f expression. While only one population of immature lymphoid progenitors (MLPs) has been described, well-defined populations of myelo-erythroid progenitors have been identified: CMPs, GMPs, and MEPs. [MPP, multipotent progenitor; MLP, multipotent lymphoid progenitor; CMP, common myeloid progenitor; MEP, megakaryocyte/erythroid progenitor; GMP, granulocyte/macrophage progenitor; CLP, common lymphoid progenitor; HSPCs, hematopoietic stem and progenitor cells; Lin, lineage].

Haematopoiesis is a very complex and dynamic process that requires tight regulation to balance between HSC fates, including differentiation, self-renewal, proliferation and migration (Laurenti & Göttgens, 2018). Decisions in cell fates are orchestrated

by both cell-autonomous (or intrinsic factors) as well as non-cell-autonomous (or extrinsic signals) derived from specific tissue microenvironments within the BM, also called niches (Morrison & Scadden, 2014).

Crucial to the intracellular decision-making processes are transcription factors and their interactions within gene regulatory networks. Thanks to their capacity to bind specific DNA sequences within regulatory regions, and simultaneously activate and repress hundreds of genes, transcription factors are essential for guiding gene expression and thus control phenotypes. Over 50 different transcription factors have been shown to be master regulators of long-term HSC self-renewal, survival, quiescence and lineage commitment fates (Göttgens, 2015; Laurenti & Dick, 2012; Orkin & Zon, 2008). Genes encoding hematopoietic regulators need to be expressed in a strictly controlled and timely manner. If this hierarchy is altered by ectopic gene expression at an inappropriate developmental stage, differentiation might be deregulated and cells can be reprogrammed into alternate lineages or subverted into leukaemia (Chapter 1.2.1). Indeed, genes important for HSCs functionality such as Runt-related transcription factor 1 (RUNX1) and GATA Binding Protein 2 (GATA2), are mutated in haematological malignancies, indicating the importance of regulatory networks in both normal and malignant haematopoiesis. Changes in the expression of genes that govern HSCs maintenance and differentiation are accompanied and often preceded by epigenetic modifications. These changes are orchestrated by epigenetic regulators that, through control of the DNA chromatin structure and organisation, modify the chromatin accessibility, marking regulatory regions as active, silent, or poised (Corces et al., 2016; Doulatov et al., 2012; Hoogenkamp et al., 2009). Other cellular intrinsic signals that are involved in HSCs fates decision include molecular regulators of the cell cycle division that regulate the balance between proliferation and quiescence (Laurenti et al., 2015; Pietras et al., 2011), and anti-apoptotic signals (Domen et al., 2000). In addition, HSCs receive extrinsic signals from surrounding cells in the BM through direct cell-cell interactions and various factors secreted by the stromal cells that regulate HSCs functionality (discussed in Chapter 1.1.2).

Importantly, disruptions of this fine balance of factors and defects in the complex regulatory network, such as the acquisition of genetic mutations, changes in important signalling pathways and alterations in extracellular signals, can result in pathological disorders including BM failure or haematological malignancies (Doulatov et al., 2012). Therefore, understanding the mechanisms that regulate normal HSCs is crucial for understanding the process of leukemogenesis.

1.1.2. The bone marrow niche

As mentioned before (Chapter 1.1.1), haematopoiesis is a very complex and dynamic process that requires tight regulation to balance HSC differentiation and self-renewal (Laurenti & Göttgens, 2018). Decisions in cell fates are regulated by both cell-autonomous and non-cell-autonomous signals derived from specific tissue microenvironments within the BM, also called niches (Morrison & Scadden, 2014). The concept of the HSC niche was first proposed by Schofield (Schofield, 1978) in his pioneering review article on spleen colony-forming units (CFU-S): observing that haematopoietic cells derived from the spleen had a decreased proliferative potential compared to those from the BM, he hypothesised that the BM harboured specialised microenvironments that support HSCs and maintains their functions. Since then, taking advantage of new technologies, such as flow cytometry, intravital imaging and genetic mouse models, several studies have led to a better understanding of the HSC niche. Besides HSCs and their progeny, the BM microenvironment (Figure 1.2a) is composed of heterogeneous cell populations of stromal cells with complex phenotypes and poorly defined trajectories of maturation which include mesenchymal stroma cells (MSCs), adipocytes, osteoblasts, endothelial cells (EC) and sympathetic nervous system (SNS) (Morrison & Scadden, 2014). In addition, extracellular matrix proteins, cytokines and growth factors, as well as elements such as oxygen and mineral concentrations, have been indicated to play an important role within the BM niche.

Currently, mouse niches have been defined by their anatomical location within the BM and can be divided into the endosteal (or osteoblastic) niche, lining the bone

surface, and the vascular niches, which reside in the central marrow cavity and contain the majority of vessels, sinusoids and arterioles (Figure 1.2a). The nature and function of these niches remain to be elucidated, and controversies exist about their influence on haematopoietic stem and progenitor cells (HSPCs) maturation and functions. In both mice and humans, HSPCs reside in perivascular niches, in both endosteal and vascular, where MSCs and ECs are critical to regulating HSCs' fate (Méndez-Ferrer et al., 2020).

1.1.2.1. Mesenchymal stromal cells

MSCs are a heterogeneous population of multipotent cells capable of differentiating into osteoblasts (bone-forming cells), adipocytes (fat-forming cells) or chondrocytes (cartilage-forming cells). Moreover, *in vitro* studies suggest that MSCs can differentiate into others cell types including myoblast, hepatocytes, β-cells and neurons (Andrzejewska et al., 2019).
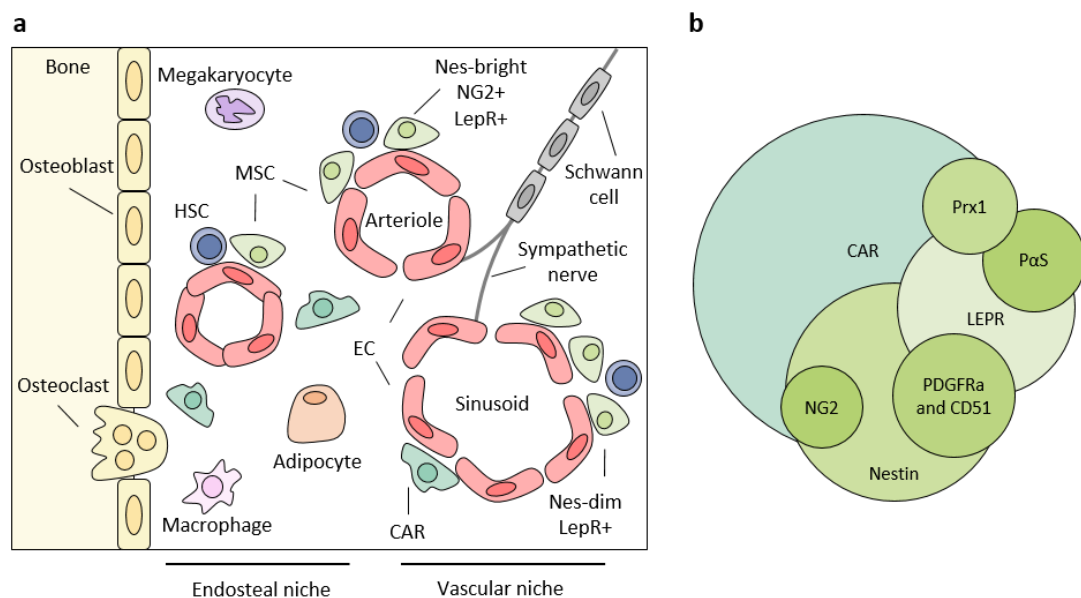
Figure 1.2: Anatomy of the bone marrow niche. (a) *The BM is a heterogeneous environment composed of different types of cells, regulating the tissue homeostasis and the normal (haematopoietic stem cells) HSC fate in health and disease. Mesenchymal stem cells (MSCs) give rise to osteoblasts and adipocytes, whereas osteoclasts share a common ancestor with monocytic/macrophages cells. Nestin-dim (Nes-dim) and leptin receptor (LepR+) MSCs are associated with sinusoids, Nes-bright and neural–glial antigen 2 (NG2)+ MSCs are associated with arterioles. CXC-chemokine ligand 12 (CXCL12)-abundant reticular (CAR) MSCs surround sinusoidal endothelial cells (EC) or are located near the endosteum. Sympathetic nerve fibres regulate the migration of HSCs through the sinusoids.* ***(b)*** *Correlation between distinct murine MSC populations in the bone marrow as defined by expression markers.*

The first evidence describing MSCs dates back to studies of Friedenstein et al. who reported the isolation of BM-derived stromal cells with fibroblast-like shape and colony-forming unit fibroblast (CFU-F) potential (Friedenstein et al., 1970), capable of supporting haematopoiesis *in vitro* and regenerating bone tissue when re-transplanted *in vivo* (Friedenstein et al., 1974).

In mice, several subtypes of MSCs have been identified based on the expression of specific marker genes. These include Nestin (Ding & Morrison, 2013; Kunisaki et al., 2013; Méndez-Ferrer et al., 2010), Leptin Receptor (LEPR) (Baryawno et al., 2019; Ding et al., 2012; Ding & Morrison, 2013; Kunisaki et al., 2013; Tikhonova et al., 2019; Zhou et al., 2014), Neuron-glial 2 (NG2) (Kunisaki et al., 2013), paired-related-homeobox-1 (PRX1) (Greenbaum et al., 2013), platelet-derived growth factor receptor alpha (PDGFRA or CD140) in combination with Sca-1 (population named PαS) (Morikawa et al., 2009) or with CD51 (Pinho et al., 2013). Another MSC population is composed of CXC12-abundant reticular (CAR) cells, which express high levels of the C-X-C motif chemokine 12 (CXCL12) (Sugiyama et al., 2006). MSCs subtypes labelled by the different markers largely overlap between them (Figure 1.2b) and how they relate to one another is still not fully understood. These MSC populations in part differ with regard to their abundance and locations within the BM cavity, the level of CFU-F activity, clonogenic potential and quiescence. MSC subtypes also differ by the levels of expression of important HSC regulatory factors such as CXCL12, stem cell factor (SCF), thrombopoietin (TPO), interleukin-3, 6, 11 (IL-3, IL-6, IL-11) and foetal liver tyrosine kinase-3 ligand (FLT3-L). Although these cytokines are also produced by other cell types within the BM niche, it is believed that MSC signalling is crucial for the regulation of HSCs. Indeed, the deletion of CXCL12 or SCF in MSCs subtypes reduces HSPCs frequency (Méndez-Ferrer et al., 2010; Zhou et al., 2014), depletes quiescent HSPCs (Ding et al., 2012; Kunisaki et al., 2013; Omatsu et al., 2010) and results in a loss in the long-term repopulation ability of HSPCs (Greenbaum et al., 2013). In contrast, deletion of these factors from other constituents of the HSC niche such as osteoblasts and endothelial cells has a much smaller effect on HSCs (Ding & Morrison, 2013; Greenbaum et al., 2013; Zhou et al.,

2014), arguing for MSCs as key components of the BM niche and as major players in the regulation of normal HSPCs.

Compared to the mouse system, much less is known regarding human MSCs. Minimal criteria to define human MSCs have been defined by the Mesenchymal and Tissue Stem Cell Committee of the International Society for Cellular Therapy (Table 1.1). It indicates that: (1) MSC must be plastic-adherent when maintained in standard culture conditions; (2) MSC must express CD105, CD73 and CD90, and lack expression of CD45, CD34, CD14 or CD11b, CD79a or CD19 and HLA-DR surface molecules; (3) MSC must differentiate to osteoblasts, adipocytes and chondroblasts *in vitro* (Dominici et al., 2006). Other markers have been used to identify and characterise different subtypes of human MSCs, such as CD271 (LNGFR) which is known to label perisinusoidal BM stromal cells (Cattoretti et al., 1993) in the BM central cavity (Cox et al., 2012) and enrich for CFU-F activity. CD271+ MSCs can be subdivided by CD146 expression, which identifies perivascular MSCs (Sacchetti et al., 2007) or with CD140a, used as a negative selection marker (Li et al., 2014). Other used markers include STRO-1 (Bensidhoum et al., 2004; Gronthos et al., 2003), CD51 and Nestin (Pinho et al., 2013) and LEPR (Li et al., 2014) which are expressed also in mice MSCs, indicating HSC niche, at least in part, may be conserved between the murine and human species.

Table 1.1: Summary of criteria to identify MSC

1) Adherence to plastic in standard culture conditions		
2) Phenotype	Positive (>95%+)	Negative (<2%+)
	CD105	CD45
	CD73	CD34
	CD90	CD14 or CD11b
		CD79a or CD19 HLA-DR
3) *In-vitro* differentiation: osteoblasts, adipocytes, chondroblasts (demonstrated by staining of *in-vitro* cell culture)		

Cultured human MSCs have been shown to produce several cytokines and express cell adhesion molecules important for the regulation of haematopoiesis (Corselli et al., 2013; H. Li et al., 2014; Muguruma et al., 2006; Pinho et al., 2013; Sacchetti et al., 2007). For these reasons, MSCs have been extensively used to maintain and expand

human HSPCs in co-culture (Corselli et al., 2013; Pinho et al., 2013) and mediate the *ex vivo* expansion of transplantable CD34+ HSPCs (Bensidhoum et al., 2004; H. Li et al., 2014). Importantly, human MSCs are capable of inducing ectopic hematopoietic marrow when transplanted in mice (Pinho et al., 2013; Sacchetti et al., 2007), and reconstituting the functional human hematopoietic microenvironment (H. Li et al., 2014; Muguruma et al., 2006). Furthermore, MSCs have been shown to support HSC engraftment in mice (Bensidhoum et al., 2004) and patients (Le Blanc & Ringdén, 2007) when co-transplanted.

1.1.2.2. Osteoblastic niche

The osteoblastic cells represent another BM niche population that derives from mesenchymal stromal cells (MSCs) and can be divided into osteoprogenitors and mature osteoblasts. The differentiation of osteoblasts from MSCs requires the activity of specific transcription factors, which are expressed and active at distinct time points during the differentiation process, thereby defining various developmental stages of the osteoblast lineage. These stages are frequently considered to consist of mesenchymal progenitors, pre-osteoblasts and osteoblasts, despite their identities remain not well understood due to the lack of specific molecular markers (Long, 2012). Osteoblasts, which morphologically present as cuboidal non-dividing cells in direct contact with the bone surface, are often characterised by the expression of osteocalcin, the most abundant non-collagenous protein in bone secreted exclusively by osteoblasts into bone matrix and blood. Pre-osteoblasts instead are dividing cells that encompass all cells transitioning from progenitors to mature osteoblasts and therefore are, by definition, heterogeneous (Long, 2012). They are usually considered to express the transcription factor Runt-related transcription factor 2 (RUNX2) or, at a more advanced stage of differentiation, both RUNX2 and osterix (OSX; also known as SP7) (Figure 1.3).

RUNX2 was the first osteogenic transcription factor to be identified (Ducy et al., 1997) and is still the earliest cell-specific transcriptional determinant known in this cell lineage. Once RUNX2 is activated, the cells are defined as pre-osteoblasts (Long, 2012; Rutkovskiy et al., 2016). RUNX2 belongs to the evolutionarily conserved family of Runt-containing transcription factors, characterised by a DNA-binding domain

called the Runt domain, which allows interactions with DNA and other nuclear proteins. Several molecular biology experiments combined with mouse and human genetic studies converge to establish RUNX2 as a master regulator of osteoblast differentiation. Mice with a homozygous mutation in *Runx2* die of respiratory failure just after birth, because their ribcage cannot produce air traction. Examination of their skeletal systems showed a complete lack of ossification and the absence of osteoblasts (Komori et al., 1997; Otto et al., 1997). Indeed in *Runx2-/-* mice, osteoblasts differentiation is arrested at the early stage, as osteocalcin and osteopontin are completely absent and alkaline phosphatase is barely detectable (Komori et al., 1997). Heterozygous *Runx2* knockout mice present as well impaired osteogenesis and show specific skeletal abnormalities that are characteristic of a human congenital skeletal disorder, called cleidocranial dysplasia (CCD) (Lee et al., 1997; Mundlos et al., 1997; Otto et al., 1997). Conversely, *Runx2*-forced expression outside the skeleton manifests the onset of ectopic calcification (Komori et al., 1997) and allows MSCs to express many osteoblast-specific genes, whose expression is directly controlled by RUNX2 (Ducy et al., 1997), thereby establishing RUNX2 as an osteoblast differentiation factor. Indeed, RUNX2 regulates the expression of multiple genes expressed in osteoblasts (Ducy et al., 1997), such as osteopontin, bone sialoprotein (Bsp), osteocalcin, osteoprotegerin, collagen type 1 alpha 1 (Col1a1) (Ducy et al., 1997; Y. Li et al., 2012). Furthermore, Runx2 positively regulates the activity of its promoter (Ducy et al., 1999).

The second osteoblast-specific transcription factor is Osterix (Osx) (Figure 1.3), a zinc-finger-containing protein that was initially identified by subtractive screening of bone morphogenetic protein 2 (BMP2) induced genes. OSX is required for osteoblast differentiation and bone formation as in *Osx-/-* mice, no bone formation occurs (Nakashima et al., 2002). *Osx* knockout mice have normal levels of *Runx2*, while *Osx* is not expressed in *Runx2* null mice, and arrest in osteoblast differentiation in *Osx-/-* occurs at a later step than in *Runx2-/-* mice, indicating that OSX may act downstream of RUNX2 during osteoblast differentiation (Nakashima et al., 2002). Consistently with the sequential activation of these transcription factors, sequencing and targeted mutation analysis showed that RUNX2 specifically binds to DNA elements in the *OSX*

promoter, upregulating its transcription. Furthermore, this up-regulation is abrogated when the RUNX2 responsive element on the *OSX* promoter are mutated (Nishio et al., 2006). Besides mediating the commitment of MSCs to osteoblastic lineage along with RUNX2, OSX promotes later stages of differentiation with the expression of osteoblastic genes as in *Osx* null mice both early osteoblastic markers,
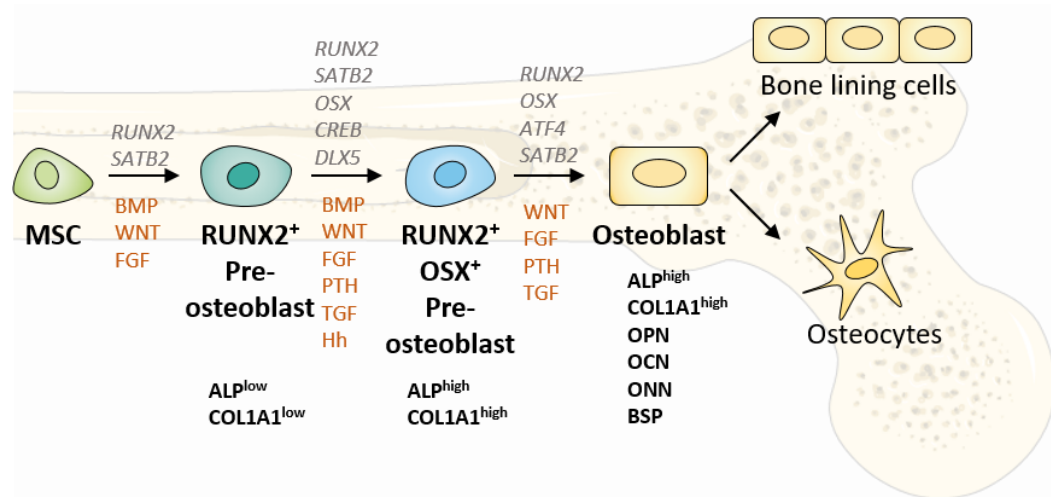
Figure 1.3: Stages of osteoblast cell differentiation. *Mesenchymal stromal cells (MSC) that give rise to osteoblasts are marked by the expression of RUNX2, followed by osterix (OSX), ultimately leading to the development of mature osteoblasts. Several transcription factors (in italics and grey) and signalling molecules (in orange) guide the differentiation process into pre-osteoblasts and osteoblasts, which are marked by the expression of marker genes (in bold). A subset of osteoblasts can become osteocytes upon being entombed in the bone matrix. [BMP, bone morphogenetic protein. FGF, fibroblast growth factor. RUNX2, runt-related transcription factor 2. PTH, parathyroid hormone. TGF, transforming growth factor. Hh, hedgehog. SATB2, special AT-rich sequence-binding protein 2. OSX, osterix. ATF4, activating transcription factor 4. CREB, cAMP-responsive element-binding. ALP, alkaline phosphatase. OPN, osteopontin. OCN, osteocalcin. ONN, osteonectin. BSP, bone sialoprotein. COL1A1, collagen type 1 alpha 1 chain]. Adapted from Long, 2012 and Amarasekara et al., 2021.*

such as Col1a1, Bsp and osteonectin and later markers such as osteocalcin are absent (Nakashima et al., 2002). This also indicates that several osteoblast marker genes need both Osx and Runx2 for their expression (Nakashima et al., 2002).

Activating transcription factor 4 (ATF4) is also downstream of RUNX2 and is crucial in the late stages of osteoblast differentiation, by directly regulating osteocalcin expression in complex with RUNX2 at the promoter of osteocalcin. Indeed, *Atf4* knockout mice have reduced osteocalcin and Bsp expression, while overexpression

of Atf4 gives a dose-dependent increase of osteocalcin (Xiao et al., 2005). ATF4 functions in osteogenesis are described in more detail in Chapter 1.3.4.2.

The transcription factors described above are regulated by a range of developmental signals, which have important roles at various stages of osteoblast lineage cell development (Long, 2012). The bone morphogenetic proteins (BMPs) BMP2 and BMP4, which are members of the transforming growth factor-β (TGFβ) superfamily, have essential roles in promoting osteoblast differentiation, as loss of both BMP2 and BMP4 results in a severe impairment of osteogenesis (Bandyopadhyay et al., 2006). Indeed, BMP2 regulates gene expression of osteoblast markers such as osteocalcin, Bone sialoprotein (Bsp) and osteopontin (D. Chen et al., 1997; Jang et al., 2012). For these reasons, BMP2 has been commonly used to induce bone formation and osteogenesis both *in vivo* and *in vitro* (Bandyopadhyay et al., 2006; Cai et al., 2021; Jang et al., 2012; Saito et al., 2011). Besides BMPs, some other growth factors influence osteoblast differentiation, and these include fibroblast growth factors (FGFs). For instance, mice lacking FGF2 show a reduction in total bone mass at the adult stage, which was probably due to reduced pre-osteoblast proliferation and decreased osteoblast function (Montero et al., 2000). Another family of growth factors implicated in osteoblast differentiation is the Wnt proteins, which control the differentiation of osteoblast progenitor cells into mature osteoblasts. Indeed, disruption of β-catenin, the intracellular downstream effector of the canonical Wnt signalling pathway, in MSCs, prevents differentiation into osteoblasts and instead favours their differentiation into chondrocytes (Day et al., 2005). Conversely, mouse genetic studies suggest that Notch signalling suppresses osteoblast differentiation, probably by diminishing RUNX2 activity, as Notch inhibition increases bone formation by stimulating osteogenesis from BM MSCs. Consistent with the negative role of Notch signalling in osteoblast differentiation, NOTCH1 haploinsufficiency in humans causes ectopic ossification in the aortic valves (Hilton et al., 2008). Also Leptin, a small polypeptide hormone secreted primarily by the adipocytes, negatively regulates bone formation via the sympathetic nervous system (Ducy et al., 2000; Takeda et al., 2002).

Osteoblastic cells were the first cell population in the BM to be linked to HSC regulation with a seminal study showing that an increase in the number of collagen α1 (I)-expressing osteoblasts, conditionally manipulated by altering the parathyroid hormone, a potent regulator of bone turnover, correlates with an increase in the number of HSPCs (Calvi et al., 2003). A similar phenotype was observed in wild-type mice injected with recombinant parathyroid hormone (Calvi et al., 2003). Similarly, the conditional inactivation of bone morphogenetic protein receptor type IA using Cre recombinase expressed from the Mx1 promoter (Mx1–Cre) increases the number of N-cadherin-positive osteoblasts, which also leads to HSC expansion (J. Zhang et al., 2003). However, the direct role of osteoblasts in influencing HSC frequency was challenged by later findings. Osteoblast ablation (Visnjic et al., 2004; J. Zhu et al., 2007) or increased osteoblast numbers with strontium treatment (Lymperi et al., 2008) did not - or only mildly - affected HSC frequency, although causing acute alterations in haematopoiesis, including a reduced number of lymphoid, erythroid and myeloid progenitors. Genetic ablation of osterix-expressing osteoprogenitors (Raaijmakers et al., 2010) affects HSPC proliferation and differentiation, whereas the same modification in mature osteocalcin-expressing osteoblasts does not. Deletion of CXCL12 from osteoblasts does not affect HSPC, while deletion from osterix-expressing osteoprogenitors results in constitutive HSPC mobilization and a loss of B-lymphoid progenitors, while HSC function is normal (Greenbaum et al., 2013). Furthermore, *in vivo* imaging studies have shown that HSCs are not significantly associated with osteoblasts (Morrison & Scadden, 2014). Overall, these data indicate that osteoblast lineage cells are a component of the HSC niche, although may not be directly required for HSC maintenance, but rather involved in the regulation of more committed hematopoietic progenitors.

1.1.2.3. Adipocytes

The adipogenic commitment, during which a multipotent MSC precursor becomes restricted to the adipocyte lineage and incapable of forming other mesenchymal cell types, involves the sequential activation of a series of transcription factors (Figure 1.4 and Figure 1.5). Peroxisome proliferator-activated receptor γ (PPARγ), a member of the nuclear receptor superfamily, is considered the master regulator of

adipogenesis, and both necessary and sufficient for adipogenesis. Indeed, PPARγ-deficient cells fail to differentiate into adipocytes *in vivo* and *in vitro* (Rosen et al., 1999; Wang et al., 2013; W. H. Yu et al., 2012), and mice present with a dramatic loss of adipose tissue causing insulin resistance, diabetes and a series of abnormalities in adipose-containing organs including bone, skin, and mammary glands. Furthermore, dominant-negative mutations in human PPARγ are associated with severe insulin resistance and diabetes mellitus (Barroso et al., 1999), overall indicating that PPARγ is indispensable for adipogenic differentiation and adipose tissue function. Conversely, ectopic expression of PPARγ causes fibroblasts to differentiate into adipocytes (Tontonoz et al., 1994) and the addition of PPARγ to cultured myoblasts causes them to accumulate lipid and express adipocytes-specific markers in a phenomenon called transdifferentiation (E. Hu et al., 1995), indicating that PPARγ is also sufficient to induce adipogenesis.

PPARγ is also required for the maintenance of the differentiated state. Inducible knockout of PPARγ in differentiated adipocytes causes them to die within a few days (Imai et al., 2004), while overexpression of a dominant-negative PPARγ in mature 3T3-L1 adipocytes results in a de-differentiation with loss of lipid accumulation and decreased expression of adipocyte markers (Tamori et al., 2002), such as GLUT4, insulin receptor and CCAAT-enhancer-binding protein α (C/EBPα).

CCAAT-enhancer-binding proteins (C/EBPs) are also important regulators of adipogenesis (Figure 1.4) and four members of the C/EBP family, C/EBPα, β, δ, (see below) and CAAT/enhancer binding protein-homologous protein (CHOP) (see Chapter 1.3.4.3), are expressed at specific times during the differentiation (Cao et al., 1991; Ron & Habener, 1992). The temporal pattern of expression of C/EBPs reflects a regulatory cascade that controls the process of cell differentiation. C/EBPβ and δ are transiently induced at an early phase of adipogenesis, with their expression declining very sharply at later phases to be replaced by C/EBPα, which instead regulates terminal differentiation (Cao et al., 1991). Mouse embryonic fibroblasts (MEFs) from *c/ebpβ-/-* mice fail to differentiate into adipocytes and do not express PPARγ (Q. Q. Tang et al., 2003); defective adipogenesis is also observed upon C/EBPδ knockdown (Hishida et al., 2009) or in double-knockout mice (Tanaka et al., 1997),

indicating that C/EBPβ and C/EBPδ are required for adipogenesis. C/EBPα as well is essential for adipogenic differentiation as mice deficient in C/EBPα have defective development of adipose tissue, and *C/EBPα-/-* fibroblasts accumulate fewer lipids and do not induce endogenous PPARγ (Wu et al., 1999).

Despite the importance of C/EBPs in adipogenesis, these transcription factors cannot function efficiently in absence of PPARγ. Ectopic expression of C/EBPα is sufficient to induce adipogenesis in a variety of fibroblastic cells (Freytag et al., 1994), but not in absence of PPARγ (Rosen et al., 2002), whereas PPARγ alone can promote adipogenesis in C/EBPα-deficient cells (Z Wu et al., 1999). Similarly, C/EBPβ cannot induce expression of C/EBPα in the absence of PPARγ (Zuo et al., 2006).
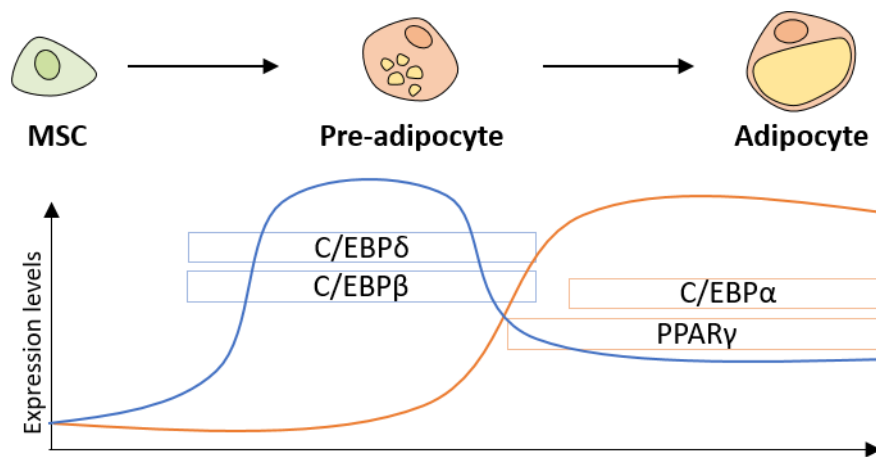
Figure 1.4: Stages of adipogenic cell differentiation and expression kinetic of master regulators of adipogenesis. *Mesenchymal stromal cells (MSC) give rise to pre-adipocytes, which are marked by expression of CCAAT-enhancer-binding protein β (C/EBPβ) and C/EBPδ. C/EBPβ and C/EBPδ decrease in expression to be substituted by C/EBPα and peroxisome proliferator-activated receptor γ (PPARγ) which induce terminal differentiation with formation of fully mature adipocytes.*

C/EBPs participate in adipogenesis by regulating and maintaining PPARγ expression. C/EBPβ and C/EBPδ have been shown to play a crucial role in initiating the differentiation of pre-adipocytes by activating the expression of PPARγ and C/EBPα (Z Wu et al., 1996; Yeh et al., 1995). Furthermore, while PPARγ activates the promoter of the gene encoding C/EBPα, C/EBPα induces PPARγ expression creating a positive-feedback loop that is essential to activate the mature adipocyte programme. Genome-wide binding analyses showed that PPARγ and C/EBPα cooperate on multiple binding sites in promoter regions, synergistically regulating a

wide range of genes expressed in developing and mature adipocytes. These include genes involved in insulin sensitivity, lipogenesis and lipolysis, such as glucose transporter GLUT4, fatty-acid-binding protein (FABP4, also known as adipocyte protein 2, aP2), lipoprotein lipase (LPL), sn-1-acylglycerol-3-phosphate acyltransferase 2 (AGPAT2), perilipin and the secreted factors adiponectin and leptin (Lefterova et al., 2008; Madsen et al., 2014; Nielsen et al., 2008).

A cascade of different Krüppel-like factors (KLFs), a large family of C2H2 zinc-finger proteins, has been shown to affect adipocyte biology (Figure 1.5). KLF15, for instance, is highly upregulated by C/EBPs during adipogenesis and its expression promotes lipid accumulation and adipocyte differentiation, while its deletion abrogates it (Mori et al., 2005). Furthermore, KLF15 induces GLUT4 (Gray et al., 2002) and, acting in synergy with C/EBPα, increases the activity of the PPARγ gene promoter (Mori et al., 2005). Similarly, KLF5 is induced early during adipocyte differentiation by C/EBPβ and C/EBPδ and, in turn, KLF5 binds to and activates the PPARγ promoter, functioning in concert with the C/EBPs (Oishi et al., 2005). KLF6 promotes pre-adipocyte differentiation through inhibition of delta-like-1/pre-adipocyte factor-1 (DLK1/PREF1), an inhibitor of adipogenesis frequently considered a marker of pre-adipocytes, while cells with reduced amounts of KLF6 show decreased adipogenesis (D. Li et al., 2005).

Other KLFs act instead as negative regulators of adipogenesis. KLF2, for example, that is expressed in pre-adipocytes but not in mature adipocytes, potently inhibits PPARγ expression when overexpressed by directly inhibiting its promoter, with no effect on the upstream regulators C/EBPβ and C/EBPδ (Sen Banerjee et al., 2003). KLF7 overexpression in human adipocytes inhibits the expression of adipocyte-specific genes such as adiponectin and leptin.

Besides KLF2 and KLF7, other transcription factors are anti-adipogenic, including CHOP, which seems to repress adipogenesis through protein–protein interactions rather than directly binding the DNA (see Chapter 1.3.4.3), DLK1/PREF1 and members of the GATA family of transcription factors (Figure 1.5). GATA-binding factor 2 (GATA2) and GATA3 are specifically expressed in adipocyte precursors and their downregulation sets the stage for terminal differentiation. Indeed, GATA3-deficient

embryonic stem cells exhibit an enhanced capacity to differentiate into adipocytes, while constitutive GATA2 and GATA3 expression suppress adipogenesis, trapping cells at the pre-adipocyte stage (Tong et al., 2000). This is achieved through the direct binding to the PPARγ promoter and suppression of its activity (Tong et al., 2000) but
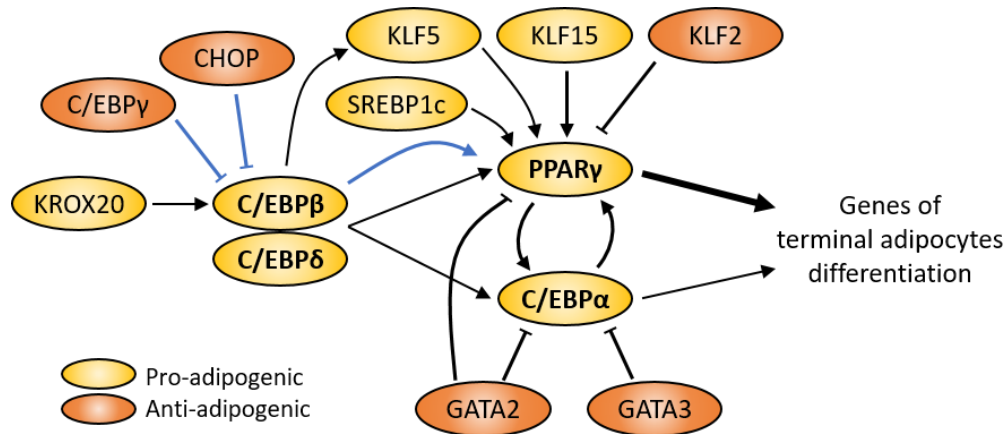
Figure 1.5: Transcriptional cascade regulating adipogenesis. *Peroxisome proliferator-activated receptor γ (PPARγ) lies at the core of the transcriptional cascade that regulates adipogenesis. The expression of PPARγ is regulated by several pro-adipogenic (yellow) and anti-adipogenic (orange) factors. CCAAT-enhancer-binding proteins are also central factors in adipogenesis: C/EBPβ and C/EBPδ are expressed at early stages of differentiation and induce C/EBPα and PPARγ expression. Some transcription factor families have several members that participate in adipogenesis, such as the Krüppel-like factors (KLFs). Other factors include sterol regulatory element-binding protein 1c (SREBP1c) and early growth response gene 2 (EGR2, also known as KROX20). Black lines indicate effects on gene expression, whereas blue lines represent effects on protein activity. Adapted from Rosen & MacDougald, 2016.*

also by forming protein complexes with C/EBPα and C/EBPβ, interfering with their functions (Tong et al., 2005).

The adipocyte is the most abundant stromal cell type found in the adult marrow but its role in the BM niche still needs to be fully explored (Morrison & Scadden, 2014). It is thought that adipocytes may negatively regulate haematopoiesis since human primary stromal cultures enriched in adipocytes do not support HSCs (Corre et al., 2004; Touw & Lowenberg, 1983) and adiponectin (adipoq), an adipocyte-secreted protein, impairs the proliferation of haematopoietic progenitors in vitro (Yokota et al., 2000). Adipocyte-rich murine bones have reduced HSCs frequency when compared with adipocyte-poor bones (Naveiras et al., 2009), and pharmacological inhibition of adipocytes increases osteogenesis and accelerates BM recovery after transplantation or chemotherapy (Naveiras et al., 2009; R. J. Zhu et al., 2013). By contrast, adiponectin from cultured murine BM stroma cells was shown to enhance

HSC proliferation and *in vivo* reconstitution (DiMascio et al., 2007) while adipocyte progenitors derived from adipoq-labelled cells transiently supported the regeneration of HSCs by producing SCF (Zhou et al., 2017). Furthermore, human adipocytes supported complete myeloid and lymphoid differentiation from human CD34+ cells (Corre et al., 2004). Further studies are needed to clarify these findings and the mechanisms of adipocyte cell regulation of the HSC niche. However, since MSCs contribute to osteogenesis and adipocyte formation, the balance between these two processes likely regulates niche activity (Méndez-Ferrer et al., 2010; Omatsu et al., 2010).

1.2. The bone marrow microenvironment in acute myeloid leukaemia

1.2.1. Acute myeloid leukaemia, an overview

Acute myeloid leukaemia (AML) is the most common form of acute leukaemia in adults, with approximately 3000 new cases each year in the United Kingdom (UK) and a median age of disease presentation of about 70 years old (Cancer Research UK). It is a malignant disorder of the BM, characterised by clonal expansion, uncontrolled growth and abnormal differentiation of hematopoietic stem/progenitor cells (HSPCs), leading to the accumulation of immature blast cells, called myeloblast, in the BM and peripheral blood (De Kouchkovsky & Abdul-Hay, 2016). These myeloblasts can also infiltrate other tissues in the body including the liver, spleen, skin, lymph nodes and central nervous system (Lowenberg et al., 1999). The expansion of malignant cells occurs at the expense of terminally differentiated BM healthy cells, such as red blood cells, platelets and white blood cells whose production is impaired due to ineffective normal haematopoiesis (Boyd et al., 2017; Miraki-Moud et al., 2013). Indeed, AML patients typically present with the symptoms of bone marrow failure: fatigue and shortness of breath due to anaemia; recurrent infections due to neutropenia; and excessive bleeding and a tendency to bruise due to thrombocytopenia.

AML represents an archetypal stem cell disorder and, similarly to the normal haematopoiesis, is organised as a hierarchy (Figure 1.6) that arises from transformed HSPCs (Bonnet & Dick, 1997; Corces-Zimmerman et al., 2014; Shlush et al., 2014) due the accumulation of multiple stepwise genetic and epigenetic lesions. These series of mutations give rise to pre-leukaemic stem cells (pre-LSCs) and fully transformed leukaemic stem cells (LSCs) which have a selective advantage over normal HSPCs, allowing clonal expansion and subsequent acquisition of further mutations, leading to overt cancer and disease propagation and relapse. (Bonnet & Dick, 1997; Corces-Zimmerman et al., 2014; Shlush et al., 2014).
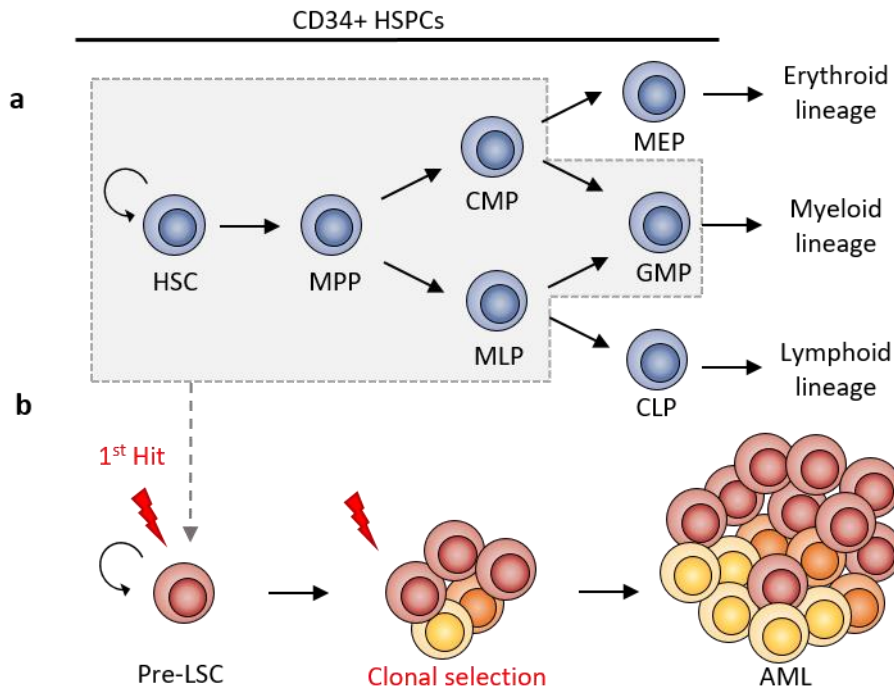
Figure 1.6: Hierarchy of normal and leukemic haematopoiesis. (a) *Haematopoiesis is a hierarchical process originating from self-renewing hematopoietic stem cells (HSCs) that provide a life-long supply of different types of mature blood cells, through a series of intermediary progenitor cells.* ***(b)*** *Similarly, AML is organised as a hierarchy and arise from transformed hematopoietic stem/progenitor cells (HSPCs) due to the accumulation of genetic and epigenetic lesions, giving rise to pre-leukaemic stem cells (pre-LSC) and fully transformed leukemic stem cells (LSC), responsible for disease propagation and relapse. [MPP, multipotent progenitor; MLP, multilymphoid progenitor; CMP, common myeloid progenitor; CLP, common lymphoid progenitor; MEP, megakaryocyte/erythroid progenitor; GMP, granulocyte/macrophage progenitor].*

AML is diagnosed based on the accumulation of myoblasts in the BM and peripheral blood, displaying over 20% of blast cells (De Kouchkovsky & Abdul-Hay, 2016). In addition, immunophenotyping, cytogenetic and molecular genetic analyses of the myeloblasts are used in parallel to define AML subtypes and optimal treatment options. Chromosomal abnormalities can be found in about 50% of AML cases and represent the best-established prognostic markers, segregating patients according to favourable, intermediate and poor risk groups. The chromosomal translocations t(8;21), t(15;17), or inversion inv(16)/t(16;16) have a favourable prognosis, with a 3-year overall survival rate of about 66% and 33% in patients younger than 60 and older than 60 years of age, respectively. The poor risk group represents ~17% of AML patients and includes those with monosomies or deletions of chromosomes 5 and 7, chromosome 3q or 11q abnormalities or with complex karyotypes (≥4 unrelated

abnormalities). The intermediate risk category represents ~50% of AML cases, including all normal karyotype AML and those not otherwise classified as favourable or poor risk (Grimwade et al., 2016; Seraihi et al., 2019). Although cytogenetics provides powerful independent prognostic information and continues to be useful for patient stratification, there are some important limitations. Indeed, a considerable level of heterogeneity exists within cytogenetic risk groups, with variations in the outcomes of patients with the same primary chromosomal abnormality. Moreover, AML with normal karyotype, which account for 40% of adult AML, are highly heterogeneous in terms of clinical outcome, prompting the research for additional prognostic markers to further stratify the disease and offer a more accurate prognosis. Research efforts have thereby focused on deciphering the molecular basis of AML, leading to the discovery of recurrently mutated genes. Several comprehensive genetic studies have revealed that mutations in the receptor tyrosine kinase FMS-like tyrosine kinase 3 (FLT3), Nucleophosmin 1 (NPM1) and DNA Methyltransferase 3 Alpha (DNMT3A) genes are frequently identified in AML patients (Kiyoi et al., 2020).

FLT3 is a cytokine receptor that plays a key role in cell survival and normal development of haematopoiesis and is mutated in a third of AML cases (Kiyoi et al., 2020). Mutations in the FLT3 genes can be divided into in-frame duplications within the juxtamembrane region (FLT3-ITD) and point mutations in the tyrosine kinase domain (FLT3-TKD), which occur respectively in 25% and 7% of AML. Even though both classes of mutation lead to constitutive activation of the receptor that promotes blast proliferation causing severe leukocytosis, their prognostic implications are different, with FLT3-TKD characterised by a better survival than FLT3-ITD (Grimwade et al., 2016).

Another frequently mutated gene is NPM1, and with a frequency of approximately 30%, AML with mutated NPM1 represents the largest class of AML (Bullinger et al., 2017). NPM1 encodes a multifunctional nucleocytoplasmic shuttling protein, and mutations in its gene sequence result in the aberrant cytoplasmic localisation of NPM1 and NPM1-interacting proteins (Johansson & Harrison, 2010), leading, in mouse models, to enhanced self-renewal of hematopoietic progenitors, associated

with expanded myelopoiesis and AML development (Vassiliou et al., 2011). NPM1 and FLT3-ITD mutations cooperate to induce AML with an adverse prognosis (Mupo et al., 2013), while NPM1 mutations in the absence of FLT3-ITD have a relatively favourable prognosis.

The epigenetic modifier DNMT3A, a methyl-transferase that catalyses *de novo* DNA methylation via the conversion of cytosine to 5-methylcytosine, is mutated in 20-25% of AML cases. DNMT3A mutations do not change 5-methylcytosine content in AML genomes, and mouse knockout studies have revealed a crucial role for DNMT3A in limiting the self-renewal of HSPCs and in regulating myeloid differentiation. DNMT3A mutations are associated with poor overall survival, independent of age, presence of other mutations and regardless of the type of mutation or genetic location (Khwaja et al., 2016; Ley et al., 2010).

Table 1.2: Summary of functional groups of mutated genes in AML with relative frequencies

Functional groups*	Examples of mutated genes	Frequency (%)
Signalling pathways	FLT3, KIT, KRAS, NRAS and serine/threonine kinases	59
DNA methylation	DNMT3A, TET2, IDH1 and IDH2	44
Chromatin modifiers	MLL (also known as KMT2A) fusions, ASXL1 and EZH2	30
Nucleophosmin	NPM1	27
Myeloid transcription factors	RUNX1 and CEBPA	22
Transcription factors	PML–RARA, MYH11–CBFB and RUNX1–RUNX1T1	18
Tumour suppressors	TP53, WT1 and PHF6	16
Spliceosome complex	SRSF2 and U2AF1	14
Cohesin complex	STAG2, RAD21, SMC1 and SMC3	13

*ASXL1, additional sex combs-like 1 transcriptional regulator; CBFB, core-binding factor subunit-β; CEBPA, CCAAT/enhancer-binding protein-α; DNMT3A, DNA methyltransferase 3A; EZH2, enhancer of zeste 2 polycomb repressive complex 2 subunit; FLT3, FMS-related tyrosine kinase 3; IDH, isocitrate dehydrogenase; MLL, myeloid/lymphoid mixed-lineage leukaemia; MYH11, myosin heavy chain 11 smooth muscle; NPM1, nucleophosmin; PHF6, PHD finger protein 6; PML, promyelocytic leukaemia; RARA, retinoic acid receptor-α; RUNX1, Runt-related transcription factor 1; RUNX1T1, RUNX1 translocated to 1; SMC, structural maintenance of chromosomes protein; SRSF2, serine/arginine-rich splicing factor 2; STAG2, stromal antigen 2; TET2, tet methylcytosine dioxygenase 2; U2AF1, U2 small nuclear RNA auxiliary factor 1; WT1, Wilms tumour 1. *Changes within a category are largely mutually exclusive. Data from Cancer Genome Atlas Research Network (2013) N. Engl. J. Med. 368, 2059–2074*

With the advances in Next Generation Sequencing (NGS) technologies, there have been further improvements in understanding the genetic basis of AML (Duncavage et al., 2021; Ley et al., 2013; Papaemmanuil et al., 2016) revealing a plethora of new recurrently mutated genes, with the potential to inform classification and selection

of therapies. The so far identified mutations can be categorised into nine functional groups (Table 1.2) that affect distinct cellular activities: (1) activated cell signalling pathways, that regulate cell proliferation and survival; (2) epigenetic modifiers, that regulate the expression of various genes, (3) chromatin modifiers; (4) the gene encoding nucleophosmin (NPM1); (5) genes encoding transcription factors; (6) genes encoding myeloid transcription factors, that are involved in the regulation of cell differentiation and self-renewal; (7) tumour suppressors; (8) mutation in the spliceosome machinery, involved in pre-messenger RNA processing before protein translation; and (9) mutations in cohesin complex members, involved in sister chromatid exchange during anaphase, regulation of DNA repair, and transcriptional control (Khwaja et al., 2016). There are now more than 100 genes known to be recurrently mutated in AML, although many occur at low frequencies (<5%) (Ley et al., 2013; Papaemmanuil et al., 2016; Seraihi et al., 2019).

The improved understanding of AML genetic basis in the past decade, which has revealed a marked level of clonal heterogeneity and genomic complexity, has not been however accompanied by substantial improvements in the clinical outcomes for patients with AML, which remain poor, with high mortality rates and a five-year relative survival of 20% (Cancer Research UK). Survival has improved considerably in the last forty years for AML patients under 65 years old; however, a similar advance has not been made in the older age group, for which the five-year survival is about 5% (Cancer Research UK). This is in part due to the fact the standard therapeutic approach for AML has not been significantly altered in over 40 years (Döhner et al., 2017; Grimwade et al., 2016; Seraihi et al., 2019), and treatments for the older age group remain limited (Döhner et al., 2022). AML standard of care typically involves induction chemotherapy, followed by further cycles of consolidation chemotherapy. The induction phase is referred to as the "7 + 3" regimen, which includes the continuous infusion of cytarabine for seven days along with anthracycline (typically daunorubicin or idarubicin) on days 1 to 3. After achieving complete remission (blast count of less than 5%) with induction therapy, consolidation therapy is initiated and standard post-remission strategies include intensive chemotherapy and high-dose therapy as well as hematopoietic cell transplantation (HCT) (Döhner et al., 2017,

2022). The dose intensity of cytotoxic chemotherapy that can be delivered varies with performance status (the general well-being of the patient), which is strongly linked to age, and similar considerations also apply to HCT (Khwaja et al., 2016). As such, therapeutic options remain limited in elderly patients, for whom intensive therapy is not possible and, where most patients are ineligible for HCT due to lower fitness (Khwaja et al., 2016).
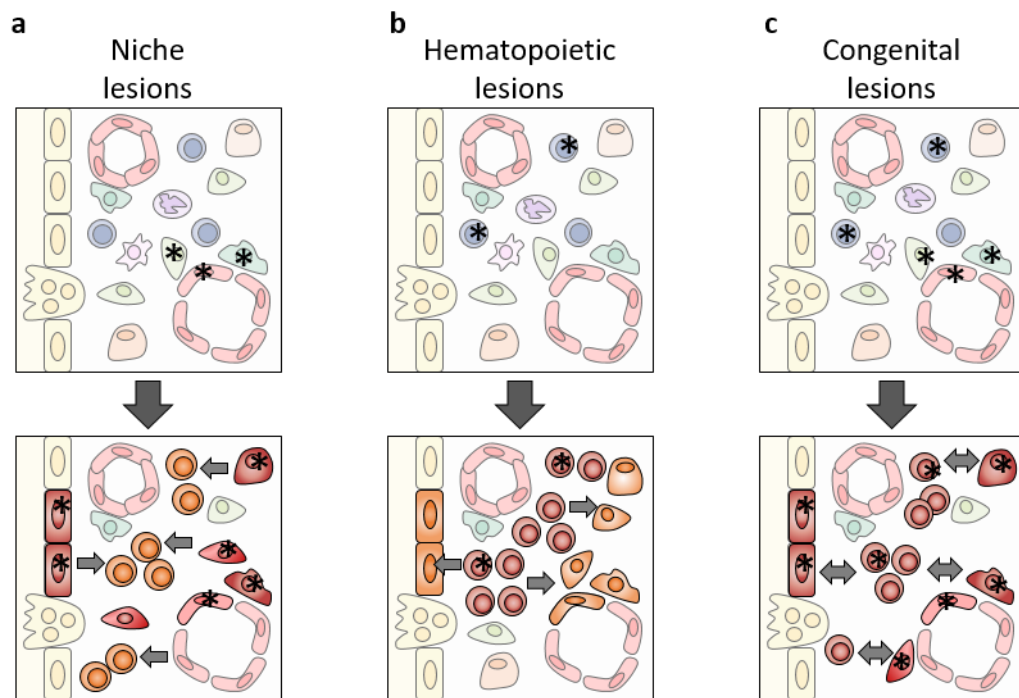
Figure 1.7: Models of disease initiation and BM contribution to leukaemogenesis. (a) Genetic lesions and alterations (asterisks) in stromal cells can lead to myeloid malignancies with predisposition to secondary mutations in hematopoietic cells. (b) The majority of myeloid malignancies are caused by genetic lesions (asterisks) occurring in hematopoietic cells, which lead to generation of LSCs and remodelling of the BM niche. These two modes of disease initiation are not mutually exclusive. (c) Finally, congenital lesions present in both hematopoietic and stromal cells are observed in myeloid malignancies and likely synergize as well as predispose to changes in the BM microenvironment and to acquisition of additional transforming mutations in hematopoietic cells. Arrows indicate the directionality of these events. Adapted from Schepers et al., 2015.

1.2.2. Malignant bone marrow

Genetic and epigenetic lesions in HSPCs are well established as the main drivers of leukaemogenesis and they were initially thought to be the sole cause of the disease. However, in recent years, the BM microenvironment has increasingly been recognised as playing an important role in the pathogenesis and chemoresistance of

AML. Two non-mutually exclusive models of BM niche contribution to leukaemogenesis have been proposed: (1) a microenvironment-induced oncogenesis model, where the acquisition of genetic alterations in BM microenvironment predisposes to AML; (2) a leukaemia-induced reconfiguration of the BM microenvironment, caused by the transformed leukaemic blast and that supports and promotes disease expansion (Figure 1.7).

1.2.2.1.Niche-induced disease

The concept of niche-induced disease initiation in haematological malignancies (Figure 1.7a) has been mainly demonstrated using animal models. The first demonstration that lesions in BM niche cells could initiate AML appeared in 2010 when Raaijmakers et al. showed that the conditional deletion of the microRNA processing the endonuclease Dicer1 in mesenchymal osteoprogenitors, but not in mature osteoblast, results in impaired osteoblast differentiation and leads to myeloid dysplastic syndrome (MDS) and sporadic transformation to AML (Raaijmakers et al., 2010). Another study in 2014 by Kode et al., reported that the overexpression of β-catenin in mouse osteoblasts alters the differentiation potential of myeloid and lymphoid progenitors leading to the development of AML (Kode et al., 2014). In particular, activated β-catenin triggers the expression of the Notch Ligand Jagged 1 in osteoblasts, with the subsequent activation of Notch signalling in HSPCs, inducing the malignant changes. Importantly, Kode et al. also showed that BM biopsies from AML patients had increased β-catenin signalling in osteoblasts and elevated activation of Notch signalling in hematopoietic cells, suggesting that stromal genetic changes shown to drive leukaemogenesis in mice are also found in human tissues and could similarly contribute to disease development. Other evidence supporting the niche-induced disease model in human AML is based on the occurrence of rare cases of donor-derived leukaemia, where pre-existing niche alterations in the patients receiving the BM transplant are thought to initiate leukaemogenesis (Wiseman, 2011). However, the underlying mechanism driving donor-derived cell transformation remains highly speculative, due to the limited data available. Finally, another correlative although controversial evidence of niche-

induced leukaemogenesis relies on studies performed on *ex vivo* expanded MSCs from AML patients that exhibited a wide range of genetic abnormalities, including chromosomal aberrations (Blau et al., 2011), transcriptional and epigenetic changes (Geyh et al., 2016), that were different from the mutations found on the leukaemic blasts (Blau et al., 2011). AML patients-derived MSCs showed functional alterations in their growth capacities, and differentiation potential (Geyh et al., 2016) and had reduced HSPC-supportive capacities (Chandran et al., 2015; Geyh et al., 2016). It is important to note these MSCs aberrations could not be pre-existing, but rather acquired following chemotherapy, during the course of the diseases (AML-induced BM alterations) or even during the *ex vivo* culture. On the other hand, these results could support the idea that genetic changes could independently occur in BM niche cells during the disease (Schepers et al., 2013). An interesting example of pre-existing genetic changes within the BM niche consists in familial AML cases, in which the predisposition to leukaemia derives from inherited mutations. In these cases, which remain largely unexplored, both hematopoietic and stromal compartments harbour the germline mutations and could induce leukaemia independently or collaboratively (Figure 1.7c). Our lab showed that germline ERCC excision repair 6 like 2 (ERCC6L2) loss-of-function mutations, known to give rise to bone marrow failure and AML, cause defects in haematopoiesis and BM microenvironments reshaping by altering MSCs homeostasis, with both patient-derived and ERCC6L2-silenced MSCs exhibiting enhanced osteogenesis and suppressed adipogenesis (Armes et al., 2022). How genetic changes within the niche induce leukaemia remains to be explored, but new surrogate models are being developed to address stroma cell contribution to leukaemogenesis.

1.2.2.2. AML-induced BM alterations

More experimental evidence in both humans and mice supports the opposite concept; AML, resulting from transformed HSPCs, reconfigures the BM microenvironment to support and promote disease expansion (Figure 1.7b). For example, alterations in BM innervation and stroma have been described at late stages of disease in mice injected with MLL-AF9 leukemic cells (Hanoun et al., 2014). AML development led to disruptions of sympathetic nervous system nerves causing

sympathetic neuropathy and disruption of quiescence of Nestin-GFP+ niche cells, leading to expansion of MSCs primed for osteoblastic differentiation at the expense of HSC-maintaining NG2+ peri-arteriolar niche cells. The potential relevance of these alterations in human AML remained unexplored. Another MLL-AF9-driven mouse model of AML demonstrated BM reshaping at different stages of the disease. Using intravital microscopy, Duarte et al. found that AML progression leads to differential remodelling of vasculature in central and endosteal BM regions with a progressive loss of vessels in the endosteum over time, at intermediate (40%–50% BM infiltration) and advanced (>80% BM infiltration) disease stages. Interestingly, BM trephine biopsies from AML patients with >80% infiltration showed a similar decrease in the endosteal vessels. In the areas with high levels of leukaemic infiltration, the vasculature remodelling was accompanied by a significant decrease in osteoblasts and HSCs. Remodelling of the vasculature was also described by Passaro et al.; using patient-derived xenograft (PDX) and intravital microscopy, the authors showed that AML engraftment leads to vascular leakiness and hypoxia, identifying the endothelial-derived nitric oxide (NO) as a major mediator of this phenotype. Importantly, a significant increase in the NO level was also observed in AML patient-derived BM biopsies, and NO levels remained elevated in the majority of post-treatment BM samples (Passaro, Di Tullio, et al., 2017). Osteogenesis (Baryawno et al., 2019; Duarte et al., 2018; Krevvata et al., 2014; Kumar et al., 2018) and adipogenesis (Baryawno et al., 2019; Boyd et al., 2017; Passaro et al., 2021) were also found to be impaired in AML in patients and mouse models, with a profound remodelling of BM stromal cell proportions. The changes in the stroma were also accompanied by the deregulation of the expression of key HSC niche factors across different mesenchymal populations, especially *Cxcl12* and *Kitl*, which may contribute to altered support of normal blood cell growth (Baryawno et al., 2019). Integrated omics analysis and single-cell RNA sequencing in PDX models also reveals a number of deregulated pathways involving multiple components of the BM niche upon human AML engraftment, with a profound change in the cell identities and homeostatic balance within the niche (Baryawno et al., 2019; Passaro et al., 2021). The AML-induced changes of these cells also greatly affected the secretome of stromal cells, with upregulation of proteins involved in AML-associated signalling and

downregulation of mediators of normal HSC maintenance and expansion, or pathways related to the immune function and chemotaxis (Baryawno et al., 2019; Passaro et al., 2021). AML-engraftment was also associated with increased production of proteins involved in the interaction with the extracellular matrix (ECM) in BM niche cells (Passaro et al., 2021), all of which can affect normal haematopoiesis. Indeed, the loss of adipocytes in PDX mouse models, for instance, leads to a compromised myelo-erythroid maturation (Boyd et al., 2017). Similarly, osteoblast ablation compromises myeloid and lymphocytic development with the accumulation of immature progenitors (Krevvata et al., 2014), while increasing the leukemic burden (Krevvata et al., 2014; Kumar et al., 2018).

Other clinical evidence consists of studies in human BM MSC, derived from AML patients, that exhibit some molecular alterations, including chromosomal aberrations (Blau et al., 2011) and transcriptional and epigenetic changes (Geyh et al., 2016). While it cannot always be excluded that these alterations are pre-existing and thereby fall in a niche-induced model of leukaemogenesis (Chapter 1.2.2.1), it supports the hypothesis that alterations within the BM niche, whether pre-existing or acquired upon AML expansion, are deleterious for BM function and haematopoiesis while overall beneficial to AML. Besides displaying molecular and functional alterations like reduced clonogenic potential, decreased proliferation, and impaired *in vitro* adipogenic and osteogenic differentiation, AML patient-derived MSCs have also reduced HSPC-supportive capacities due to alterations in HSC-regulating factors, while showing increased support of leukaemia growth (Battula et al., 2017; Chandran et al., 2015; Geyh et al., 2016; Pievani et al., 2021; Waclawiczek et al., 2020). It is worth mentioning that studies have reported conflicting results, as some found that AML patients-derived MSCs have a normal ability to form adipocytes and only osteogenesis is impaired (Geyh et al., 2016), while others found the opposite results (Azadniv et al., 2020; Battula et al., 2017). However, these differences may be due to different experimental settings or different AML mutational backgrounds.

The BM microenvironment provides signals to regulate normal haematopoiesis and thus perturbations of BM inevitably affect HSCs and normal blood development.

Combined clinical and experimental model results (Baryawno et al., 2019; Boyd et al., 2017; Miraki-Moud et al., 2013) have demonstrated that AML impairs healthy haematopoiesis, by impeding HSCs differentiation, consequently inducing cytopenia and BM failure, one of the major causes of morbidity and mortality of AML. In these contexts, it is still debated whether AML cells directly inhibit normal hematopoietic cells or if this is mediated via the BM microenvironment. However, several groups showed evidence that chemical and/or genetic rescue of endosteal vessels (Duarte et al., 2018), vascular leakiness (Passaro, Di Tullio, et al., 2017), adipogenesis (Boyd et al., 2017) or osteogenesis (Krevvata et al., 2014) in mouse models were able to offset the niche-damaging effects of AML. Indeed rescue and maintenance of the various components of BM restore normal marrow function, preventing the loss of healthy HSCs and rescuing healthy haematopoietic maturation, while reducing tumour burden with improve response to the chemotherapeutic agent cytarabine, and hence prolonging survival.

The efficacy of treatment is limited in AML and the identification of additional therapeutic targets is needed. This new evidence opens the possibilities for the development of therapies targeting the BM microenvironment in conjunction with existing therapies, intending to reboot the BM niche and HSC functions, while eliminating leukemic cells.

1.3. Endoplasmic reticulum stress and unfolded protein response

1.3.1. The endoplasmic reticulum and its functions

The endoplasmic reticulum (ER), observed for the first time by Porter and colleagues in 1945 using electron microscopy (Almanza et al., 2019; Porter et al., 1945), is a large cellular organelle localised in the cytoplasm of eukaryotic cells. It consists of a dynamic network of membrane-enclosed flattened sacs and tubular structures that extends evenly throughout the cytoplasm. The tubules and sacs are all interconnected so that the ER membrane forms a continuous lipid bilayer enclosing a single internal space called ER lumen, which often occupies more than 10% of the total cell volume (Alberts et al., 2002; Schwarz & Blower, 2016). The ER membrane, which itself accounts for 50% of all cell membranes, separates the ER lumen from the cytosol, mediating the selective transfer of molecules between the two compartments (Alberts et al., 2002). Besides being the largest organelle of the eukaryotic cell, the ER also exerts numerous important functions (Figure 1.8) distributed in and associated with specialised structural regions within the ER:

- The rough endoplasmic reticulum, or rough ER, so called because of membrane-bound ribosomes coating its cytosolic surface, is the site of protein synthesis;
- The smooth endoplasmic reticulum, or smooth ER, lacks bound ribosomes and is an important site of lipid metabolism and hormone biosynthesis. In specialised cells, it is also the site where various membrane-associated detoxifying enzymes oxide and modify toxic hydrophobic molecules, rendering them more hydrophilic and less toxic. Furthermore, the lumen of the smooth ER also serves as an important storage site for intracellular calcium (Ca2+);
- The transitional endoplasmic reticulum, or transitional ER, constitutes regions of smooth ER that contain exit sites from where transport vesicles, carrying

newly synthesized proteins and lipids, bud off for transport to the Golgi apparatus.

1.3.1.1. Protein synthesis and folding

As mentioned, one of the major functions of the ER is to serve as a site for protein synthesis for most of the secreted and transmembrane proteins, as well as some cytosolic ones, so that the ER governs the synthesis, folding, and processing of over a third of all cellular proteins (Almanza et al., 2019; Féral et al., 2021). Their translation initiates in the cytosol and, upon recognition of the amino-terminal signal sequence within the nascent polypeptide by signal recognition particles (SRP), these ER-targeted proteins are recruited to docking sites of the rough ER membrane, while still attached to the ribosome (Alberts et al., 2002; Schwarz & Blower, 2016). Translation continues on the ER and the emerging polypeptide can co-translationally enter the ER through a translocon, a dynamic complex of proteins that form an aqueous pore in ER membrane (Alberts et al., 2002; Schwarz & Blower, 2016). At this stage, typically before translation of the polypeptide is completed, proteases remove the ER signal peptide, allowing the newly synthesized polypeptide to enter the ER lumen. Once in the ER lumen, the protein folds into its unique three-dimensional structure, while concomitantly undergoing various post-translational modifications, such as N-glycosylation, formation of disulphide bonds, isomerization of proline, lipid conjugation or oligomerisation (Hetz & Papa, 2018). These processes are catalysed by an ER-resident protein folding and modification machinery comprising a network of chaperones, glycosylating enzymes, and oxidoreductases. If the protein is destined for secretion or the plasma membrane, it will be released by the chaperones, packed into transport vesicles from adjacent regions of smooth transitional ER, and finally delivered through the Golgi onto its final destination (Hetz & Papa, 2018).

1.3.1.2. Lipid biogenesis

While the ER is a major site of protein synthesis and quality control, it is also a major site of lipid biogenesis, as it contains numerous enzymes involved in lipid metabolism (Han & Kaufman, 2016). Lipid synthesis occurs in regions of the ER that are in close juxtaposition to the Golgi apparatus, from where lipids are then distributed to other cellular locations, through organelle contacts or secretory vesicles. The ER

participates in the synthesis of all major classes of cellular lipids, constituting therefore a major influence on cellular lipid biomass and composition, by balancing the production of different lipid categories in response to homeostatic external and internal stimuli (Alberts et al., 2002; Jacquemyn et al., 2017). The ER indeed produces the membrane building-block lipids, the phospholipids, of which the major one made is phosphatidylcholine, formed in three steps from choline, two fatty acids (FA), and glycerol phosphate by ER-resident enzymes. During the phospholipid synthesis, acyl transferases add two FA to glycerol phosphate to produce phosphatidic acid that remains in the ER lipid bilayer membrane and contributes to its enlargement. The ER also houses the enzymes that synthesise cholesterol, and sterol regulatory element-binding protein family of cholesterol sensors (SREBPs) that ensure homeostasis of cholesterol, which functions as a precursor of various steroid hormones and in maintaining cell membrane fluidity. Finally, the ER is also involved in the production of triacylglycerides, important for energy storage.

1.3.1.3. Calcium homeostasis

Calcium (Ca^{2+}) is a ubiquitous and versatile signalling molecule that plays a fundamental role in many intracellular and extracellular processes, including physiological activities within the ER, maintenance of the oxidation-reduction potential, gene expression, protein synthesis and trafficking, cell proliferation, differentiation, metabolism, contraction and apoptosis (Park et al., 2021). The ER is the main intracellular Ca^{2+} reservoir and has an essential role in controlling Ca^{2+} homeostasis, throughout the regulation and maintenance of Ca^{2+} levels in the ER lumen and the cytosol. The typical Ca^{2+} concentration in the ER lumen is 100–800 μM, while cytosolic and extracellular Ca^{2+} concentrations are respectively 100 nM and 2mM (Schwarz & Blower, 2016). To modulate these concentrations and maintain Ca^{2+} homeostasis, the ER uses integrated and coordinated processes of Ca^{2+} uptake, release, and binding, which consist of:

- the sarcoendoplasmic reticular Ca^{2+} ATPase (SERCA), which pumps Ca^{2+} inside the ER in an ATP-dependent fashion;

- the ER membrane channels, that regulate the release of Ca2+ from the ER lumen into the cytosol and include the ryanodine receptor (RyR) and inositol 1,4,5- trisphosphate receptor channel (IP3R);
- and intraluminal chaperones, which sequester free Ca2+ buffering its effects (Almanza et al., 2019; Schwarz & Blower, 2016). These chaperones include the 78-kDa glucose-regulated protein (GRP78), which accounts for approximately 25% of the calcium buffering capacity within the ER (Park et al., 2021), Calreticulin (CRT) and Calnexin (CNX).

The Ca2+ stored in the ER lumen is essential for the regulation of protein post-translational modification, folding, and transport. The Ca2+ released from the ER to the cytosol provides instead sustained and precise Ca2+-mediated cellular responses, including apoptosis, cell proliferation and differentiation (Park et al., 2021). Thus, the maintenance of ER Ca2+ homeostasis is crucial for cell function and survival.
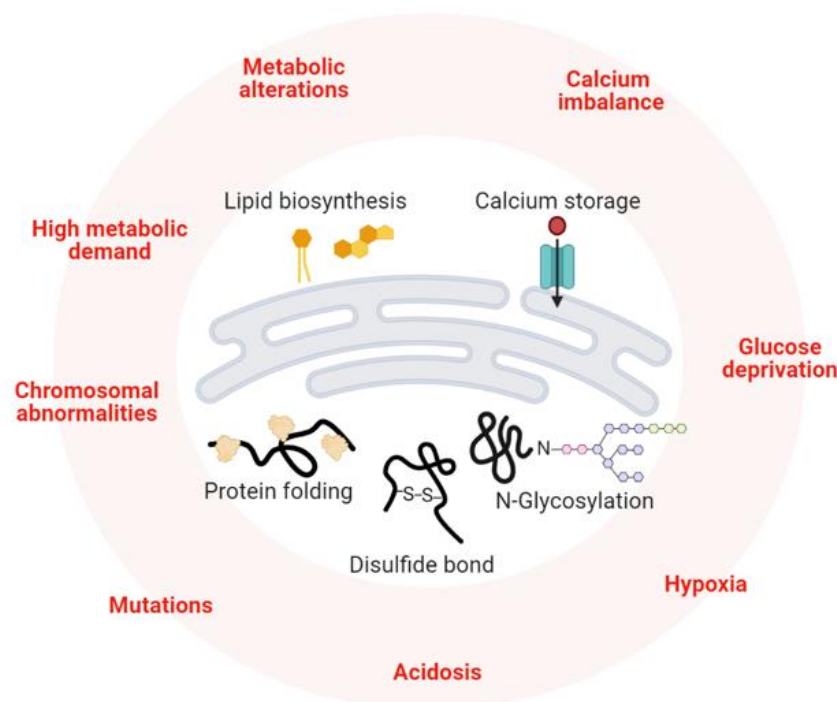
Figure 1.8: ER functions and general mechanisms of ER stress induction. *The ER is involved in many different cellular functions. It acts in protein synthesis and folding, disulphide bonds formation and contributes to the storage and regulation of calcium, lipids biosynthesis and storage and, and to glucose metabolism. Conditions (in red) that lead to perturbation of the ER homeostasis and deregulate its functions trigger an ER stress. This image was created using BioRender.*

1.3.2. Endoplasmic reticulum stress

Given these diverse important functions, disturbances of the homeostasis of protein synthesis and folding, lipid metabolism or calcium levels directly affect the environment of the ER compartment, with a profound impact on cell fate decisions. Conditions that disrupt ER homeostasis induce a cellular state commonly referred to as "ER stress", which describes an imbalance between the demand on the ER function(s) and the ER capacity of the cell (Figure 1.8) (Ron, 2002, Schroder and Kaufman, 2005b).

1.3.2.1. Perturbations in protein folding

The homeostasis of the ER protein folding is the balance between the influx of newly synthesised unfolded polypeptides entering the ER and the sum of the effluxes of correctly folded proteins to the Golgi and unfolded proteins targeted for proteasome degradation (Schröder, 2008). If the influx of nascent, unfolded polypeptides exceeds the folding and/or processing capacity of the ER, the normal physiological state of the ER is perturbed (Schröder, 2008). To ensure that the protein-folding capacity is in balance with protein-folding demand, cells constantly monitor the number of misfolded proteins in the ER lumen and adjust the efficiency of protein synthesis, folding and trafficking throughout a series of feedback mechanisms (Hetz, 2012; Ron & Walter, 2007). One of the first evidence for the existence of such feedback mechanisms came from pioneering studies in mammalian cells, in which the pharmacological inhibition of protein folding led to the transcriptional upregulation of several key ER chaperones, known as glucose-response proteins: the 78-kDa glucose-regulated protein (GRP78) and the 94-kDa glucose-regulated protein (GRP94) (Hetz, 2012; Kozutsumi et al., 1988). GRP78, also known as binding immunoglobulin protein (BiP), and GRP94 are ER-resident molecular chaperones that promote correct protein folding by preferentially binding the hydrophobic residues on the unfolded, misfolded or partially folded proteins. In this way, GRP78 shields unfolded proteins from aggregation with each other, thereby impeding the formation of toxic agglomerates (Féral et al., 2021; Schröder, 2008).

Both intrinsic and extrinsic factors can alter ER protein folding homeostasis causing ER stress. Intrinsic factors include high demand for protein secretion or oncogene

activation. Secretory cells, such as hepatocytes and pancreatic β cells, are characterised by physiologically high protein synthesis rates, being able to synthesize approximately 13 and 2.6 million secretory proteins per minute, respectively (J. Wu & Kaufman, 2006). To manage this physiological high demand of protein synthesis, fold, process, and secretion, the professional secretory cells harbour an extensive, highly evolved ER structure and a sophisticated surveillance system. This highly developed ER allows pancreatic β cells, for instance, to manage insulin production and release in response to increases in blood glucose and to sense and respond to ER stress before it becomes detrimental. If pancreatic β cells become unable to fold the increased levels of insulin needed to maintain blood glucose, ER stress occurs.

Besides being indispensable to ensuring proper cell functions, ER stress is also actively involved to establish cell fates, participating in the differentiation process of B-lymphocytes into plasma cells. Plasma cells are capable of secreting immunoglobulins (Ig) and their maturation is accompanied by a five-fold expansion of the ER compartment and an increase in GRP78 expression, presumably to accommodate the high level of Ig secretion (J. Wu & Kaufman, 2006).

Genomic instability and somatic mutations that alter correct protein folding are also intrinsic mechanisms of ER stress induction. Many cancers have high mutation rates, which result in an intrinsically higher level of ER stress. For example, melanoma has the highest mutation burden of any cancer and the sheer number of mutated proteins is a source of intrinsically higher ER stress levels (Almanza et al., 2019). Solid tumours often exhibit elevated levels of ER chaperones including GRP78, and this is associated with increased proliferation rate and invasion and correlates with poor prognosis (Urra et al., 2016). Furthermore, highly proliferative cancer cells require higher levels of protein synthesis, thereby presenting with higher levels of ER stress (Almanza et al., 2019).

This ER stress observed in tumours is exacerbated by the fact that increased proliferation eventually depletes the microenvironment of nutrients and oxygen, causing local micro-environmental stress and resulting in hypoxia, starvation and acidosis, all of which cause ER stress and perturb protein (Almanza et al., 2019). Indeed, hypoxia, starvation and acidosis are among the so-called extrinsic factors

that cause ER stress by perturbing protein synthesis homeostasis. Nutrient deprivation, and particularly glucose starvation, can promote ER stress by impairing glycosylation, an important ER biosynthetic function that involves the covalent addition of sugars to nascent polypeptides co-translationally entering the ER. The most common glycosylation type is the N-glycosylation, during which an oligosaccharide is transferred to the side-chain NH_2 group of an asparagine amino acid of the nascent protein, by an ER-bound oligosaccharyl-transferase (Alberts et al., 2002). The added carbohydrate residue makes the protein more hydrophilic, reducing the risk of aggregation and thereby increasing its stability. A glucose deficiency can therefore be the cause of an accumulation of malformed proteins (Urra et al., 2016).

The ER also provides an oxidizing environment that is highly optimized for the formation of disulphide bonds in folding proteins, a process known as oxidative protein folding (Almanza et al., 2019). The formation and isomerisation of disulphide bonds (S-S) is achieved through the oxidation of free sulfhydryl groups (SH) on cysteines and is catalysed by oxidoreductases called protein disulphide isomerases (PDIs) (Alberts et al., 2002) which, in turn, are maintained in an oxidized state by the ER oxidoreductin 1 (Ero1p) (Tu & Weissman, 2004). An extremely reducing ER environment is unfavourable to disulphide bond formation, whereas an overly oxidizing ER may result in the trapping of proteins in a misfolded state. Indeed, the formation of disulphide bridges itself generates reactive oxygen species (ROS) and if ROS production exceeds the antioxidant capacity of the cell, altering the redox balance within the ER, oxidative stress occurs leading to excessive oxidation of proteins and ER stress (Almanza et al., 2019; Tu & Weissman, 2004). While oxidative folding is believed to contribute to as much as 25% of the overall ROS generated (Almanza et al., 2019; Schröder, 2008), several external agents can induce intracellular ROS, including inflammation and chemotherapy (Urra et al., 2016). On the other hand, intracellular oxygen depletion due to hypoxic conditions can also disrupt the formation and isomerisation of disulphide bonds, hence leading to the accumulation of misfolded proteins and ER stress (Chipurupalli et al., 2019).

Finally, pH and body temperature are also important factors for the correct folding of proteins and deviations from normal ranges can disrupt cellular homeostasis, causing protein denaturation and/or aggregation (Almanza et al., 2019; Urra et al., 2016). An increase in the expression of several heat shock proteins and ER stress markers is observed, for instance, at mildly elevated temperatures (up to 40 °C), while fragmentation of both ER and Golgi can occur upon acute temperature increase, or heat shock (Almanza et al., 2019).

1.3.2.2. Perturbations in lipid metabolism

Eukaryotic cells have developed control mechanisms to regulate lipid metabolism, as excessive accumulation of lipids and their intermediate products can have detrimental effects on cell function, a phenomenon known as lipotoxicity, which can cause metabolic abnormalities and cell death. This has been observed in numerous peripheral tissues, including pancreatic β cells, hepatocytes, skeletal myocytes, and cardiomyocytes (Han & Kaufman, 2016).

In the liver, for instance, a surplus of nutrients and energy stimulates synthetic pathways such as lipogenesis for energy storage, which may lead to overloading in the ER. The increase of specific phospholipids synthesis apt for packaging and storing the new products of lipogenesis further contributes to creating an imbalance in ER lipid composition and phospholipids ratios, which exacerbates ER functions. Furthermore, alterations in the ER fatty acids and lipid composition result in the inhibition of Sarco/endoplasmic reticulum calcium ATPase (SERCA) activity, alimenting ER stress (Fu et al., 2011).

Chronically elevated levels of free fatty acids are also detrimental to pancreatic β cell function. The treatment with saturated and/or unsaturated free fatty acids itself causes ER stress (Cunha et al., 2008), with a differential stress response depending on the type of fatty acid. For instance, saturated fatty acids, such as palmitate, activate ER stress with subsequent induction of apoptosis, owing to a sustained depletion of ER Ca2+ stores, whereas the unsaturated free fatty acid, like oleate, leads to milder ER stress (Cunha et al., 2008).

In the heart, hypoxia and ischemia are associated with intracellular accumulation of lipids, accompanied by ER stress that likely contributes to cardiomyocyte dysfunction upon stress-mediated lipid accumulation and apoptosis (Drevinge et al., 2013; Han & Kaufman, 2016; Perman et al., 2011).

Interestingly, in each organ/cell type, inhibition of ER stress can prevent free fatty acids-mediated lipotoxicity, further indicating the importance of maintaining ER homeostasis (Han & Kaufman, 2016).

1.3.2.3. Perturbations in calcium homeostasis

ER Ca2+ homeostasis critically controls cell survival and death, as Ca2+ participates in a variety of cellular functions. As mentioned in section 1.3.1, a coordinated network of ER-resident proteins allows for precise Ca2+ release in the cytosol and ATP-dependent uptake to maintain cytosolic and ER luminal levels, ensuring correct ER Ca2+ homeostasis (Schwarz & Blower, 2016). An imbalance between ER Ca2+ release and uptake mechanisms can occur in pathologic conditions, such as diabetes mellitus, neurologic disorders, cancer, and kidney disease, causing ER stress. For instance, renal ischemia causes the accumulation of massive unfolded and misfolded proteins in the ER of renal tubular cells due to cellular ATP depletion and changes in Ca2+ homeostasis (Park et al., 2021). In diabetic nephropathy, the most common cause of end-stage renal disease worldwide, SERCA2 activity and expression are diminished in the islet, heart, and liver of animal models, as well as in the kidney cortex of db/db mice, a mouse model of type 2 diabetes. SERCA2 impaired expression and activity causes ER Ca2+ depletion, triggering ER stress (Park et al., 2021).

The correct ER luminal Ca2+ concentration is also a fundamental requirement for the protein folding and post-translational modification activities of this organelle, since chaperones, PDIs, N-glycosylating enzymes and other proteins require the correct oxidoreductase potential to function properly. Disruptions in the function of these chaperones and/or Ca2+ release/uptake can therefore result in the accumulation of unfolded proteins, which in turn causes ER stress. For instance, the CNX and CRT cycle is essential to fold glycosylated proteins produced in the secretory pathway, representing a major protein quality control mechanism. Alterations of these protein folding and quality control systems result in alterations in the Ca2+ dynamics,

accumulation of immature or misfolded proteins, and ER stress (Bousette et al., 2014).

1.3.2.4. Exposure to ER stressors

Chemical agents can be used to induce ER stress *in vitro* or *in vivo* by perturbing the different aspects of the ER homeostasis explained so far. These ER stressors include:

- Thapsigargin, a non-competitive inhibitor of the Sarco/endoplasmic reticulum Ca2+ ATPase (SERCA). Treatment with thapsigargin induces ER stress by reducing ER Ca2+ concentration, thereby perturbing calcium homeostasis and impairing protein-folding capacity.
- Tunicamycin blocks the N-linked glycosylation of proteins, disrupting their maturation and folding which results in an accumulation of misfolded proteins, broadly activating ER stress.
- Dithiothreitol (DTT) is a reducing agent that disrupts (DTT) inhibits protein disulphide bond formation and interferes with oxidative protein folding in the ER.
- Brefeldin A (BFA) impairs ER- to-Golgi trafficking, thus causing a rapid and reversible inhibition of protein secretion.

Several other small molecules have been reported to modulate ER stress, including some current cancer treatments. For instance, vemurafenib, a BRAF inhibitor that is used to treat advanced malignant melanoma, has been shown to induce ER stress and ER-stress-mediated apoptosis (Beck et al., 2013). Similarly, romidepsin, a histone deacetylase used for the treatment of peripheral and cutaneous T-cell lymphoma, may induce apoptosis in malignant T-cells through ER stress (Valdez et al., 2015). ER-stress-induced cell apoptosis plays a key role in the therapeutic effects of ibrutinib (Tang et al., 2014), an irreversible Bruton's tyrosine kinase (BTK) inhibitor used for the treatment of Chronic Lymphocytic Leukaemia (CLL).

1.3.3. Unfolded protein response

The cellular response mounted in these conditions of ER stress involves the activation of a series of adaptive mechanisms that aim at overcoming the stress and restoring the ER functions. The type of response is dependent on the perturbing stimulus as

well as the intensity and duration of the stress. This series of complementary adaptive mechanisms to cope with ER stress are together known as the unfolded protein response (UPR). The UPR transduces information about the status within the ER lumen to the nucleus and cytosol to buffer fluctuations in unfolded protein load and lipids and calcium demand. When cells undergo irreversible ER stress, this pathway eliminates damaged cells by apoptosis, indicating the existence of mechanisms that integrate information about the duration and intensity of stress stimuli.
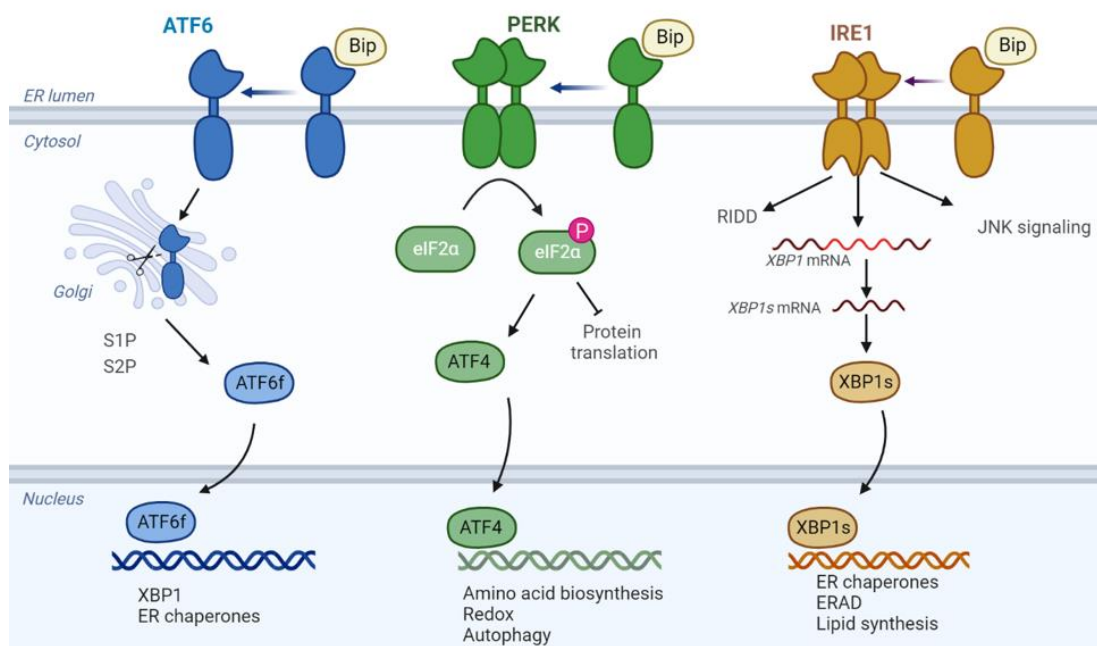
Figure 1.9: The unfolded protein response. *In homeostatic conditions, the lumenal domain of PERK, IRE1 and ATF6, binds a chaperone protein called BiP/GRP78. Following the accumulation of unfolded proteins, BiP is released from the luminal domain, triggering activation of IRE1, PERK and ATF6 and their downstream effectors: XBP1s, ATF4 and ATF6f that act as transcription factors. The immediate response of UPR aims to re-establish proteostasis through global attenuation of the translation, increase of protein folding capacity and mRNA degradation. If ER homeostasis is not restored, apoptotic programs are triggered.*

The UPR (Figure 1.9) is a cellular stress response controlled by three sensors, residing in the ER membrane: inositol-requiring enzyme 1 (IRE1), protein kinase RNA (PKR)-like endoplasmic reticulum kinase (PERK) and activating transcription factor 6 (ATF6). In homeostatic conditions, the lumen domain of PERK, IRE1 and ATF6, binds a chaperone protein called binding immunoglobulin protein (BiP) or glucose-regulated protein 78-kDa (GRP78). Following the accumulation of unfolded proteins, BiP is

released by the luminal domain due to its high affinity for misfolded proteins, leading to dimerization and trans-auto-phosphorylation of the cytosolic domains of IRE1 and PERK and triggering their activation. Other chaperone proteins, residing in the ER, may be involved in the regulation of the activation/inactivation of UPR sensors. For example, protein disulphide-isomerase A5 (PDIA5) has been described to interact with ATF6 by modifying its conformation and facilitating its export from ER (Higa et al., 2014). Protein disulphide-isomerase A6 (PDIA6) binds active IRE1 and PERK promoting their inactivation (Eletto et al., 2014). Another chaperone, heat shock protein 47 (HSP47) can directly bind the luminal domain of IRE1, dislodging BiP and promoting its activation (Sepulveda et al., 2018). Also, mitochondrial ATPase ATP5H or the phosphatase PP2a can regulate IRE1 activity (Sepulveda et al., 2018).

Once activated, the IRE1 RNase domain catalyses the non-conventional splicing of X-box binding protein-1 (XBP1) mRNA resulting in spliced XBP1 protein (XBP1s) that translocates to the nucleus and regulates the transcription of UPR target genes, including genes involved in ER-associated degradation (ERAD) and protein folding. These include the ER-resident chaperone p58[IPK], BiP co-factor ER-Resident Protein (ERdj4), PDIA5 protein disulphide isomerase family A member 5 (PDIA5) (Xiong et al., 2021). In addition, IRE1 RNase activity degrades mRNAs and microRNAs through regulated IRE1-dependent decay (RIDD). IRE1 has also been proposed to play a role in ER stress-mediated apoptosis by interacting with TNF receptor-associated factor-2 (TRAF2) and apoptosis signal-regulating kinase 1 (ASK1) leading to the activation of ASK1 and (c-Jun amino-terminal kinase) JNK, and subsequent cell death (J. Wu & Kaufman, 2006).

Once activated, PERK phosphorylates the eIF2α inhibiting its activity and leading to global translation attenuation. In contrast, the phosphorylation of eIF2α allows the selective translation of activation transcription factor 4 (ATF4), which controls the expression of UPR target genes. A direct target of ATF4 is, for instance, the transcription factor C/EBP-homologous protein (CHOP) that, by promoting the transcription of BIM (Bcl-2 Interacting Mediator of cell death) and the downregulation of the anti-apoptotic BCL-2 (B-cell lymphoma 2) expression, contributes to the induction of apoptosis. CHOP also induces the expression of

growth arrest and DNA damage-inducible gene 34 (GADD34) which, involved in the dephosphorylation of P-eIF2a, serves in a negative feedback loop that antagonises apoptosis, p-eIF2a-dependent translation inhibition and restores protein synthesis.

ATF6, upon ER stress and accumulation of unfolded proteins, translocates to the Golgi where it is processed by Site-1 protease (S1P) and Site-2 protease (S2P), which release the cytosolic fragment ATF6f that acts as a transcription factor. Among ATF6 targets are prominent ER-resident proteins involved in protein folding, such as BiP/GRP78, protein disulphide isomerase (PDI), and glucose-regulated protein 94 (GRP94) (Walter & Ron, 2011). Furthermore, ATF6 activates specific transcriptional programmes apt to increase the protein turnover through ERAD by inducing proteins like ER degradation enhancing alpha-mannosidase like protein 1 (EDEM) and homocysteine-responsive endoplasmic reticulum-resident ubiquitin-like domain member 1 protein (HERPUD1) (Jaud et al., 2020; Yamamoto et al., 2007).

The immediate response of UPR aims at aligning cellular physiology to the demands imposed by the ER stress and re-establishing proteostasis and redox balance. In this initial pro-survival phase, the three UPR branches induce a transcriptional rewiring through the activation of transcription factors such as ATF4, XBP1s and ATF6f. Together, ATF4, XBP1s and ATF6f govern the expression of a large range of partially overlapping target genes that modulate adaptation to stress through global attenuation of the translation, an increase of protein folding capacity and mRNA degradation (Hetz, 2012). UPR-target genes involved in this protective response include those encoding ER chaperones such as BiP/GRP78, GRP94, calreticulin (CRT), and calnexin (CNX) and proteins that catalyse protein-folding such as the protein disulphide isomerases (PDIs), ER Protein 57 ERp57/PDIA3 and endoplasmic oxidoreductin-1-like protein (ERO1L) (Wu & Kaufman, 2006). In addition, UPR-activated genes stimulate ER biogenesis to compensate for the increased demand for the protein-folding machinery and accelerate ERAD to remove terminally misfolded proteins (Féral et al., 2021).

If ER homeostasis is not restored and the ER stress persists, the UPR response enters the pro-apoptotic phase, named also terminal UPR, during which apoptotic programs are triggered (J. Jaud et al., 2020), although at what point and by which mechanism

the cell commits to death in response to excessive ER stress is still not fully elucidated (Wu & Kaufman, 2006). Cellular death under ER stress involves the mitochondrial apoptosis pathway and the regulation of pro-apoptotic and anti-apoptotic proteins of the B cell lymphoma 2 (BCL-2) protein family. Chronic ER stress leads to the transcriptional upregulation of pro-apoptotic BCL-2 homology 3 (BH3)-only proteins such as BCL-2-interacting mediator of cell death (BIM) and BH3 interacting-domain death agonist (BID), that antagonizes the anti-apoptotic proteins, BCL-2 and BCL-X. This triggers the oligomerisation of (Bcl-2-associated X protein) BAX and BH antagonist or killer (BAK) proteins to permeabilise the outer mitochondrial membrane, leading to the release of mitochondrial proteins in the cytoplasm and the activation of the intrinsic apoptotic pathway (Hetz, 2012). Ample evidence supports that the two UPR kinases, PERK and IRE1α, engage a distinct set of pro-apoptotic outputs that contribute to cell degeneration and death if ER stress cannot be resolved. A key UPR pro-apoptotic player is CHOP, which is transcriptionally upregulated by the PERK–ATF4 axis. CHOP promotes both the transcription of BIM and the downregulation of BCL-2 expression, contributing to the induction of apoptosis. Under certain conditions, IRE1α activation is also linked to apoptosis through activation of ASK1 and JNK, as well as the degradation of ER-localised mRNAs RIDD (Hetz & Papa, 2018), depleting ER protein-folding components to further worsen ER stress at later time points.

1.3.4. UPR and cell fates control

Although the UPR is classically linked to protein folding under both physiological and pathological conditions, it has become clear that it has further important functions. Indeed, various components of the UPR regulate several processes, ranging from lipid and cholesterol metabolism and energy homeostasis to inflammation and cell differentiation.

1.3.4.1. UPR and plasma cells differentiation

As mentioned in section 1.3.2, accumulating evidence supports the fundamental role of the UPR in sustaining the activity and differentiation of secretory cells such as plasma cells. The B-cell lymphopoiesis can be considered to be constituted of two phases: an early phase, which is antigen-independent and occurs in the bone

marrow, during which pro-B cells give rise to pre-B cells, and a later antigen-driven phase, that leads to the formation of mature B cells and then antibody-secreting plasma cells (J. Wu & Kaufman, 2006). Compared to pre-B cells whose ER is a relatively small structure, the differentiation into plasma cells is accompanied by a five-fold increase in the ER (J. Wu & Kaufman, 2006), together with increased expression and activation of some UPR marker genes such as GRP78, GRP94 and XBP1 (Gass et al., 2002; Reimold et al., 2001). Particularly, XBP1 is required for the differentiation of B cells into plasma cells as *xbp1-/-* B cells fail to respond to antigen presentation, secrete immunoglobulins (Ig) and differentiate into plasma cells *in vivo* (Reimold et al., 2001). On the other hand, the introduction of XBP1 in B cells is sufficient to stimulate plasma cell terminal differentiation (Reimold et al., 2001) and its overexpression enhances Ig production in B cells (Lee et al., 2003). XBP1 is thought to elicit its effects on B cells and plasma cells, at least in part, by controlling the production of interleukin 6 (IL-6), a cytokine known to be essential for plasma cell survival, and by increasing the protein-folding machinery in the cell, through induction of ER chaperones and foldases (Iwakoshi et al., 2003).

As plasma cells are 'antibody factories' capable of secreting thousands of antibody molecules per second (Gass et al., 2004), it was initially thought that B cells activated UPR to cope with the increased demand for protein synthesis for the antibodies production. However, the upregulation of UPR components occurs before the upregulation of Ig, with their maximal expression level being reached when differentiation is completed (Gass et al., 2002). Furthermore, XBP1 is induced during differentiation even when Ig production is abrogated (C. C. A. Hu et al., 2009), indicating that UPR is activated regardless of Ig accumulation, and IRE1α is required for Ig gene rearrangement (K. Zhang et al., 2005). However, XBP1s post-transcriptional processing and translation are dependent on the synthesis of Ig during B cell differentiation (Iwakoshi et al., 2003), and both the IRE1α kinase and RNase catalytic activities are required to splice the mRNA encoding X-box–binding protein 1 (XBP1) for terminal differentiation of mature B cells into antibody-secreting plasma cells (K. Zhang et al., 2005). This indicates that UPR is finely tuned across the differentiation and Ig production. Furthermore, while ER stress may be sustained in

B cells partly to cope with the protein overload and to guide differentiation, upstream mechanisms activating UPR, before protein accumulation, may be involved. Further research found, indeed, that signals such as interleukin 4 (IL4), a multifunctional cytokine produced by T cells, mast cells and basophils that acts in early B cell activation by inducting their proliferation and stimulating Ig class switching, could control the transcription of XBP1 (Iwakoshi et al., 2003). Overall, this indicated that signals both upstream and downstream of XBP1 link plasma cell differentiation to UPR.

ATF6 was also found to be upregulated during terminal differentiation (Gass et al., 2002), and inhibition of its pathway by expression of a dominant-negative form of ATF6 reduced Ig production in differentiating B cells (Gunn et al., 2004). ATF6 however does not seem to be essential for differentiation as its depletion does not affect the maturation of plasma cells. Conversely, eIF2α phosphorylation is not required for B lymphocyte maturation and/or plasma cell differentiation (K. Zhang et al., 2005) and it has been suggested that differentiation-induced signals that silence the PERK branch (Ma et al., 2010).

1.3.4.2. UPR and osteogenesis

Osteoblasts, the bone-making cells that derive from mesenchymal progenitor cells (Chapter 1.1.2), produce a large number of extracellular proteins, including osteocalcin, alkaline phosphatase and type I collagen (Long, 2012). Being professional secretory cells that produce these large amounts of extracellular matrix proteins to form the bone, osteoblasts must expand their secretory machinery to handle the increase in the production of secreted proteins, by expanding the capacity of the ER (Hino et al., 2010). As a proof-of-concept, ER molecular chaperones, such as GRP78/BiP and PDI are down-regulated in osteoblasts from osteoporosis patients (Hino et al., 2010). Treatment of murine model for osteoporosis with BIX (BiP inducer X) a selective inducer of BiP, effectively prevents bone loss and improves decline in bone formation through the activation of folding and secretion of bone matrix proteins (Hino et al., 2010).

The cell commitment into the osteoblast lineage requires the activity of specific transcription factors, such as RUNX2, a member of the Runt-containing family,

followed by osterix (OSX or SP7), a zinc-finger-containing transcription factor (Chapter 1.1.2.2) and ATF4, a basic leucine zipper (bZIP) transcription, member of the CREB family and downstream effector of the PERK branch of the UPR. Indeed, treatment of wild-type primary osteoblasts with BMP2, commonly used and required for osteoblast differentiation, induces ER stress and expression of several UPR marker genes, including ATF4 (Saito et al., 2011; Tohmonda et al., 2011). ATF4 is required for osteoblast differentiation as ATF4 deficiency results in delayed bone formation during embryonic development and severe reduction in bone volume throughout postnatal life in mice (Yang et al., 2004). *Atf4*-deficient mice have normal levels of Runx2 and Osterix, both required factors for early osteoblast differentiation. However, the expression of markers for terminally differentiated osteoblasts such as bone sialoprotein and osteocalcin are markedly reduced in *Atf4*-deficient osteoblasts (Yang et al., 2004), suggesting that ATF4 is not required for the early stage of osteoblast differentiation, but rather regulates osteoblast terminal differentiation and function (Yang & Karsenty, 2004). Further analysis showed that ATF4 directly regulates osteocalcin expression (Yang et al., 2004) by binding specific sites in the osteocalcin promoter and cooperatively interacting with RUNX2 forming a functional complex (L. Xiao et al., 2010). Incisively, ATF4 can induce the expression of osteoblast-specific genes like osteocalcin in non-osteoblastic cell types (Yang & Karsenty, 2004).

Besides directly regulating the expression of the osteoblast-specific genes (L. Xiao et al., 2010), ATF4 affects osteoblast function to a larger extent by regulating amino acid imports to ensure proper protein synthesis (Long, 2012; Yang & Karsenty, 2004) such as the production of type I collagen. Indeed, ATF4 deficiency results in a decrease in type I collagen synthesis without affecting its mRNA expression. The decrease in collagen can be rescued upon the addition of essential amino acids (Yang et al., 2004), also establishing that part of the skeletal phenotype observed in absence of *Atf4* can be attributed to a posttranscriptional defect (Yang et al., 2004). The pathway controlling amino acid import is initiated by phosphorylation of the eukaryotic initiation factor 2 α (eIF2α), followed by P-eIF2α-dependent expression of ATF4; eIF2α can be phosphorylated by four kinases (Figure 1.10), including PERK (Chapter

1.3.3). Interestingly, mice deficient in PERK have the same abnormal developmental defects observed in *Atf4*-deficient mice (Delépine et al., 2000; Wei et al., 2008; Zhang et al., 2002), while mouse knockout mutations of the other three eIF2α kinases (PKR, HRI, and GCN2) (Figure 1.10) are not associated with overt developmental skeletal defects (Zhang et al., 2002). Furthermore, in humans, mutations in the *EIF2AK3* gene that results in loss of function of PERK cause Wolcott–Rallison syndrome (WRS), an autosomal recessive disorder characterised by the early onset of type I diabetes, growth retardation and multiple skeletal dysphasia, including bone fractures and later osteoporosis (Delépine et al., 2000; Wei et al., 2008). Interestingly, other clinical manifestations have been described in association with WRS, including renal failure,
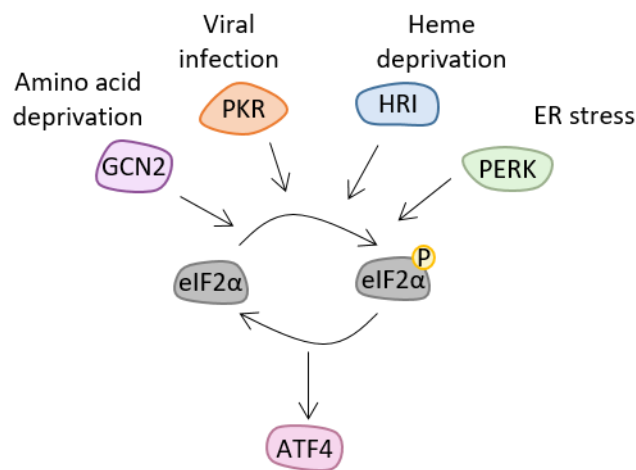
Figure 1.10: The integrated stress response. *ER stress, viral infection, amino acid deprivation and heme deprivation activate PERK, PKR, GCN2 and HRI kinases, respectively, that converge on phosphorylation of eIF2α. This leads to global attenuation of protein translation while concomitantly initiates the preferential translation of ATF4. [PERK: PKR-like ER kinase; PKR: double-stranded RNA-dependent protein kinase; HRI: heme-regulated eIF2α kinase; GCN2: general control non-derepressible 2; ATF4: activating transcription factor 4; eIF2α: eukaryotic initiation factor 2α].*

primary hypothyroidism, developmental delay and symptoms of bone marrow failure such as neutropenia and anaemia (Lundgren et al., 2019; Špehar Uroić et al., 2014). *Perk-/-* mice exhibit severe osteopenia, with reduced osteoblast and osteocyte numbers and impaired osteoblast activity. In particular, the expression of mature osteoblast markers osteocalcin, alkaline phosphatase, bone sialoprotein and type I collagen are dramatically reduced *in vivo* and *in vitro* (Wei et al., 2008). Osteopontin,

an early osteoblast marker is instead normally expressed in the absence of PERK, thus implying a role for PERK in late differentiation and maturation of osteoblasts, rather than in determining their fates (Wei et al., 2008). The levels of ATF4 are also severely diminished in *Perk-/-* osteoblasts, indicating that PERK signalling is required for ATF4 activation during osteoblast differentiation (Saito et al., 2011). Indeed, the abnormalities observed in absence of PERK (Wei et al., 2008), such as decrease in alkaline phosphatase activities and delayed mineralized nodule formation, are almost completely restored by the introduction of ATF4 into *Perk-/-* osteoblasts (Saito et al., 2011). Overall these data show that ER stress occurs during osteoblast differentiation and activates the PERK-eIF2α-ATF4 signalling pathway followed by the promotion of gene expression essential for osteogenesis (Saito et al., 2011).

The IRE1-XBP1 axis plays an important role in osteoblast differentiation, too. Indeed, treatment of wild-type mouse embryonic fibroblasts (MEFs) with BMP2 is enough to induce the expression of *Xbp1* and its spliced form *Xbp1s,* along with other UPR maker genes such as *Grp78* and *Atf4* (Tohmonda et al., 2011). On the other hand, *Ire1α-/-* mouse embryonic fibroblasts (MEFs) treated with the osteogenesis-inducer BMP2 fail to differentiate, despite growing and expanding normally (Tohmonda et al., 2011), and harbour reduced expression levels of osteoblast markers such as bone sialoprotein, osteopontin and osteonectin. A similar phenotype is observed upon *Xbp1* silencing in MEFs, overall indicating that the IRE1α–XBP1 pathway is essential for BMP2-induced osteoblast differentiation and maturation. Additional analyses revealed that XBP1s functions as a transcription factor for Osterix, one of the master regulators of osteoblast differentiation (Tohmonda et al., 2011).

In summary, these data indicate that UPR may have two functions during osteoblast differentiation: (1) to expand the capacity of the ER to cope with the increase in the production of extracellular matrix proteins, and (2) to stimulate osteoblast-specific gene expression, promoting their differentiation and maturation.

1.3.4.3. UPR and adipogenesis
Adipogenesis describes the commitment of multipotent mesenchymal stem cells (MSCs) into pre-adipocytes, and subsequent terminal differentiation into mature adipocytes (Chapter 1.1.2.3). It occurs through a temporally regulated cascade of

transcription factors, with the two master regulators, PPARγ and C/EBPα, controlling the entire terminal differentiation process, while early transcription factors such as C/EBPβ and C/EBPδ regulate the expression of C/EBPα. At later stages of differentiation, adipocytes gain insulin sensitivity, with an increase in the number of insulin receptors and glucose transporters. Furthermore, lipid droplets form in mature adipocytes, while de novo lipogenesis continues and expression of proteins, such as adipocyte-specific FABP (aP2), the fatty acid transporter FAT/CD36, and the lipid droplet protein perilipin, increases dramatically. Mature adipocytes then synthesise and secrete adipokines such as adiponectin, adipsin (also known as CFD) and leptin. It is therefore intuitive that secretory cell types such as adipocytes rely on the ER for efficient and proper protein folding and maturation, and lipogenesis (Agostinis & Afshin, 2012). Indeed, markers of ER stress and UPR, such as GRP78/BiP, P-eIF2α, CHOP, ATF4, XBP1s and ATF6α are upregulated during adipogenesis of 3T3-L1 pre-adipocytes and mouse embryonic fibroblasts (MEFs) (Basseri et al., 2009; H. Chen et al., 2016; Han et al., 2013; Sha et al., 2009; K. Yu et al., 2014).

Further research revealed that a physiological level of the UPR may be required for adipogenesis to occur, as suppression of UPR with the chemical chaperone 4-phenylbutyrate (4-PBA) results in attenuation of adipogenesis and reduction of lipid accumulation and adiponectin secretion (Basseri et al., 2009). Similarly, mice fed a high-fat diet supplemented with 4-PBA showed a significant reduction in weight gain and fat mass, with decreased GRP78 expression in adipose tissue and lowered plasma triglyceride, glucose, leptin, and adiponectin levels (Basseri et al., 2009). All three branches of UPR have been suggested to be essential for adipogenesis.

PERK-deficiency in mouse embryonic fibroblasts (MEFs) and 3T3-L1 pre-adipocytes reduces the adipogenic capacity and expression of lipogenic genes and attenuates lipid accumulation (Bobrovnikova-Marjon et al., 2008). Similarly, depletion of ATF4 by siRNAs dramatically inhibits the differentiation of 3T3-L1 adipocytes (H. Chen et al., 2016; K. Yu et al., 2014) and primary human MSCs (Cohen et al., 2015), reduces fatty acids synthesis (H. Chen et al., 2016) and lipid accumulation, and expression of marker genes (H. Chen et al., 2016; K. Yu et al., 2014). Furthermore, ATF4-deficient mice are lean (H. Chen et al., 2016), overall indicating that the PERK-ATF4 axis is

required for successful adipogenesis. Conversely, expression of ATF4 in 3T3-L1 pre-adipocytes promotes adipogenic differentiation and induces an increase in the content of fatty acids and triglycerides and the expression of several key adipogenic transcription factors, such as PPARγ, C/EBPα, adiponectin and FABP4 (H. Chen et al., 2016; K. Yu et al., 2014). Chromatin immunoprecipitation (ChIP) experiments indicate that ATF4 directly binds to the promoter of both C/EBPβ and PPARγ and stimulates their transcription (K. Yu et al., 2014). Furthermore, it has been proposed that ATF4 dimerises with C/EBPβ to drive a unique set of genes that prime MSCs into a pre-adipocyte state (Cohen et al., 2015). PERK and ATF4 play also an essential role in regulating fatty acids biosynthesis by controlling the expression of important transcription factors of lipogenesis, including the sterol regulatory element binding protein (SREBP) family (Bobrovnikova-Marjon et al., 2008; H. Chen et al., 2016).

Another study demonstrated that the IRE1α-XBP1 pathway is indispensable for adipogenesis, as *Xbp1s-/-* mice are smaller with a negligible white adipose mass, compared to wild-type mice. Furthermore, XBP1-deficient in MEFs and 3T3-L1 cells, through XBP1 or IRE1α knockdown, fail to differentiate, and only transduction of the XBP1s rescues the cells (Sha et al., 2009). Sha et al. found also that XBP1 is a direct target of C/EBPβ during adipogenesis, and that in turn XBP1s binds the promoter of and upregulates C/EBPα, indicating that XBP1 is integral in the loop of transcriptional activation of adipocyte differentiation (Sha et al., 2009).

It is not clear whether ATF6 is significantly upregulated during adipogenesis, as some reported upregulation of ATF6α during adipogenesis of 3T3-L1 cell lines, while others did not observe any upregulation in C3H10T1/2 (Han et al., 2013; C. E. Lowe et al., 2012). However, reduction of ATF6α expression in adipogenic cell line C3H10T1/2 impairs the ability of the cells to differentiate into mature adipocytes, with reduced lipid accumulation and expression of key adipogenic genes such as PPARγ, the lipogenic transcription factor SREBP1c, the insulin-sensitive glucose transporter, GLUT4 and fatty acid-binding protein, aP2 (C. E. Lowe et al., 2012), indicating that ATF6α may have in fact a role in adipogenesis. However, the mechanism responsible for ATF6α-mediated blockage of adipogenesis remains unexplored.

While induction of the UPR pathway and its targets such as XBP1 and ATF4 appears to represent a physiological requirement for adipogenesis, acute persistent ER stress is instead detrimental and a potent repressor of adipogenesis (Agostinis & Afshin, 2012) (Figure 1.11). ER stress-inducing agents, such as tunicamycin or thapsigargin, or ER stress-inducing conditions, such as hypoxia, inhibit adipogenesis, decrease lipid accumulation and reduce expression of adipogenic marker genes, including C/EBPα, PPARγ, adiponectin, adipsin and GLUT4 (Batchvarova et al., 1995; Han et al., 2013; Miller et al., 2007; Ryu et al., 2020). A proposed mechanism is that such acute and unresolved ER stress leads to the induction of CHOP, which stoichiometrically dimerises with C/EBP transcription factors and, functioning as a dominant negative inhibitor, represses their activity, sequestering them and preventing their binding to adipogenic target genes (Batchvarova et al., 1995; Kaspar et al., 2021; Miller et al.,
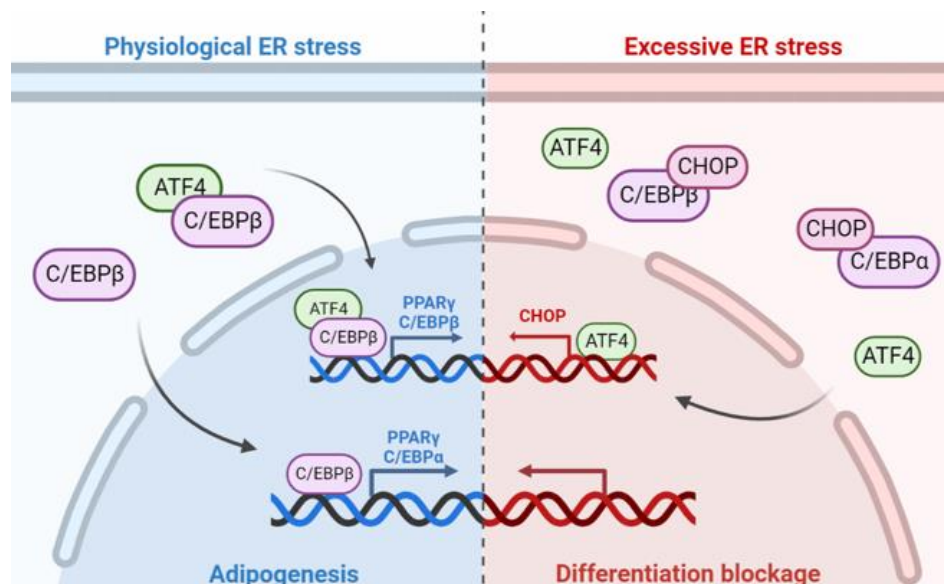
Figure 1.11: PERK-ATF4 signalling in adipogenesis. *Induction of UPR represents a physiological requirement for adipogenesis; however, acute and persistent ER stress is a potent repressor of adipogenesis. A mechanism proposed for this activation involves induction of CHOP, which dimerises with C/EBP factors preventing them to induce adipogenesis. [ATF4: activating transcription factor 4; CHOP: C/EBP homologous protein: C/EBP: CCAAT/enhancer binding proteins; PPARγ: Peroxisome proliferation activated receptor gamma]. This image was created using BioRender.*

2007; Ron & Habener, 1992). In murine models, ectopic expression of an active form of PERK, which activates CHOP, or ectopic expression of CHOP reduces adipogenesis, with reduced lipid accumulation and reduced expression of mature adipocyte marker genes adiponectin, *Ppary* and *C/ebpα* (Han et al., 2013). Deletion of the DNA-binding

basic region or leucine zipper dimerization domain of CHOP abolishes its anti-adipogenic effects (Batchvarova et al., 1995), suggesting that CHOP activity is transcriptional dependent. However, consistent with a model whereby CHOP-induced attenuation of differentiation is mediated by interference with C/EBP activity, ectopic expression of C/EBPα rescues the adipogenic phenotype of CHOP-expressing cells (Batchvarova et al., 1995). Finally, *Chop-/-* MEFs treated with ER stress inducers can differentiate (Han et al., 2013), overall indicating that CHOP is essential for ER stress-mediated suppression of adipogenesis.

It cannot be ruled out that CHOP may be directly involved in regulating C/EPBs and PPARγ gene expression, since ectopic expression of CHOP results in attenuation of expression of C/EBPα, PPARγ and, to a lesser degree, C/EBPβ (Batchvarova et al., 1995; Han et al., 2013). CHOP could inhibit adipogenesis by activating anti-adipogenic target genes, with attenuated expression of C/EBPs being a marker of failed differentiation rather than, at least in part, its cause. However, C/EPBs are involved in an auto-regulatory feedback loop cascade that drives their expression and expression of PPARγ. Thereby, speculatively speaking, the decrease in C/EPBs expression observed upon CHOP over-activation may be due to an indirect effect of CHOP heterodimerising with C/EBPs, which, trapped, cannot induce their expression anymore. Regardless, CHOP interferes with the normal differentiation-associated induction of C/EBPα and C/EBPβ and impedes adipogenesis. Downregulation of adipsin upon ER stress is not mediated by C/EBPα as its silencing does not alter adipsin levels in mature 3T3-L1 adipocytes (Ryu et al., 2020), but it is rather a direct cause of ER stress-induced PPARγ downregulation, indicating that other non-mutually exclusive mechanisms may be involved in ER-stress induced inhibition of adipogenesis.

Acute stress through IRE1-XBP1 signalling, instead, does not seem to alter adipogenesis, as ectopic expression of an active form of IRE1 does not affect the capacity of 3T3-L1 cells to differentiate into adipocytes and form lipid deposits (Han et al., 2013). However, Han et al. also showed that inhibition of IRE1α does not block differentiation, which is in contraposition to what was previously reported by (Sha et

al., 2009), thus more efforts are necessary to tackle the importance of IRE1-XBP1 signalling in adipogenesis.

1.3.5. UPR in cancers

In recent years, the UPR has emerged as an adaptive mechanism that sustains and promotes tumorigenesis in solid cancers, with mounting evidence that the UPR may modulate all the cardinal hallmarks of cancer, such as angiogenesis, metastasis, genome stability, inflammation, and drug resistance (Obacz et al., 2019; Urra et al., 2016). Indeed, cancer cells, owing to their high proliferative capacities, require elevated levels of protein and lipid synthesis, which can perturb ER homeostasis. Furthermore, cancer cells are also constantly exposed to environmental pressure such as hypoxia, glucose shortage, oxidative stress, or low pH, all known to cause ER stress. To cope with these challenges, cancer cells can activate UPR. The overexpression of UPR sensors has been reported in several human cancers including that of breast, brain, liver, kidney, pancreas, lung, prostate and gastrointestinal tract. An elevated level of GRP78 is often found in tumour tissues and is associated with metastasis, poor prognosis, and resistance to treatment (Obacz et al., 2019). Similarly, in AML patients, increased expression of XBP1, GRP78/BiP, and Calreticulin has been detected (M. Jaud et al., 2020) and functional studies suggest a UPR role in HSCs/LSCs maintenance and survival (Rouault-Pierre et al., 2013; van Galen et al., 2018; Van Galen et al., 2014).

Similar to hematopoietic and leukaemic cells, also BM niche cells are exposed to microenvironmental stress, resulting from nutrient and oxygen depletion and acidosis, in part caused by high proliferative AML cells, all of which can lead to ER stress (Almanza et al., 2019). Indeed, activation of ER stress has been reported in the BM microenvironment of AML mouse models, with consequent deregulation of the differentiation capabilities of stromal cells (Doron et al., 2018). Interestingly, the authors suggest that ER stress was transmitted by AML cells to the microenvironment (Doron et al., 2018), causing a reconfiguration of the BM niche. How these changes affect haematopoiesis and leukaemogenesis remains to be assessed, particularly in a human context.

1.4. Aims of the thesis

New models of acute myeloid leukaemia (AML) disease progression include a reconfiguration of the bone marrow (BM) microenvironment induced by AML blasts to support and promote disease expansion. Perturbations of the BM microenvironment inevitably affect haematopoietic stem cells. AML impairs healthy haematopoiesis, by impeding haematopoietic stem cell differentiation, consequently inducing cytopenia and bone marrow failure. In these contexts, it is still unclear whether AML cells directly inhibit haematopoiesis or if this is mediated via alterations of the BM niche.

This project aims to study the functional dynamics that occur among acute myeloid leukaemia cells, the bone marrow niche and haematopoiesis in a human context. To tackle these questions, this PhD work focuses on mesenchymal stromal cells (MSCs), representing an essential component of the BM niche, being capable of generating other BM cells, such as adipocytes and osteoblasts, and supporting haematopoiesis. The experiments in this work have been designed for the following aims:

1) To identify molecular and functional changes in MSCs induced by AML (Chapter 3).

2) To investigate the effect of UPR activation on MSCs homeostasis (Chapter 4).

3) To evaluate how changes within the MSC niche affect healthy haematopoiesis (Chapter 4).

Chapter 2

Methods

2.1. Cell lines

OCI-AML3, THP1, HL60 AML cell lines, MS-5 cells and HEK239T cells were originally obtained from the Francis Crick Institute Cell services. Each cell line was validated by short tandem repeat (STR) profiling using the PowerPlex 16HS system. were cultured at 37 °C in a 5% CO_2 humidified incubator and maintained in RPMI 1640 with 10% (v/v) heat-inactivated foetal bovine serum (FBS) and 1% (v/v) Penicillin/Streptomycin. MS-5 cells were cultured at 37 °C in a 5% CO_2 humidified incubator and maintained in Iscove's Modified Dulbecco's Media (IMDM) containing 10% (v/v) heat-inactivated FBS and 1% (v/v) Penicillin/Streptomycin. HEK293T cells were cultured at 37 °C in a 5% CO_2 humidified incubator and maintained in DMEM containing 10% (v/v) heat-inactivated FBS and 1% (v/v) Penicillin/Streptomycin.

2.2. Primary AML and umbilical cord blood samples

AML samples were obtained after informed consent from the Barts Cancer Institute Tissue Bank (Table 2.1 and Supplementary Table 6.12). The cells were collected and frozen at diagnosis or relapse. AML mononuclear cells (MNCs) were isolated by centrifugation using Ficoll-Paque (GE Healthcare Life Sciences, Buckinghamshire, UK). CD45$^+$ cells were magnetically sorted from AML MNCs by using EasySep™ Human CD45 Depletion Kit II (Stem Cell Technologies, cat.: 17898) according to the manufacturer's instructions. Umbilical cord blood (UCB) samples were purchased from Anthony Nolan through normal full-term deliveries after signed informed consent. MNCs were purified by Ficoll-Paque density centrifugation (GE Healthcare Life Sciences, Buckinghamshire, UK) and red blood cell lysis (BioLegend). CD34$^+$ cells

were magnetically sorted from CB MNCs by using EasySep™ Human CD34 Positive Selection Kit II (Stem Cell Technologies, cat.: 17856) according to the manufacturer's instructions.

Table 2.1: MSC isolated from BM patients samples

Patient ID	Sample Type	Diagnosis	Patient Status	Gender	Age at sample collection	Age at diagnosis
HD1	BM	HD	-	M	20	-
HD2	BM	HD	-	M	20	-
HD3	BM	HD	-	F	23	-
AML01	BM	AML	Diagnosis/Pre-treatment	M	-	74
AML02	BM	MDS/AML	Diagnosis/Pre-treatment	M	-	24
AML03	BM	2nd AML	Post-treatment response	M	-	72
AML04	BM	2nd AML	Post-treatment response	N/A	-	N/A

2.3. Isolation of mesenchymal stromal cells from bone marrow aspirates

BM samples (Table 2.1) were obtained after signed informed consent. Mononuclear cells (MNCs) were purified by Ficoll-Paque density centrifugation (GE Healthcare Life Sciences, Buckinghamshire, UK) and red blood cell lysis (BioLegend). CD34$^-$ or CD45$^-$ MNCs (see Chapter 2.2: Primary AML and umbilical cord blood samples) were seeded in MSC medium (Gibco™ MEMα, nucleosides, GlutaMAX™ Supplement, containing 10% (v/v) Gibco MSC-qualified, USDA-approved regions Gibco™, 1% (v/v) Penicillin/Streptomycin) to isolate MSCs by plastic adherence and incubated at 37 °C and 5 % CO_2. The medium was replaced 24 hours after plating and later every 3-4 days until confluence was reached. At 80%-90% confluence, the cells were incubated with trypsin/EDTA solution (0.025% trypsin, 0.01% EDTA) and subsequently passaged by splitting them into three to four flasks. Cells were frozen at passage 2 and used up to passage 7.

2.4. Co-cultures

MSCs or MS-5 were seeded at 10,000 cells/cm^2 and allowed to adhere. 1 x 10^5, or otherwise indicated, AML primary cells or AML cell lines or healthy donor CB CD34$^+$ cells or mononuclear cells (MNC) were added using Myelocult H5100 (StemCell Technologies, Vancouver, BC, Canada) in the presence of cytokines: 20 ng/ml stem cell factor (SCF), 20 ng/ml Interleukin 3 (IL-3) and 20 ng/ml thrombopoietin (TPO) (all from PeproTech, London, UK). The medium was replaced every 3-4 days by means of half-depopulation. At the specified time-point, cells were harvested and immunomagnetic human CD45 Depletion (Stem Cell Technologies) was performed following the manufacturer's instruction. To check the purity of the sorted CD45-population, representing MSCs or MS-5, cells were incubated with human CD90 (Thy-1)-APC (clone 5E10; eBioscience, cat: 17-0909-42) or APC-Cy7 anti-mouse Ly-6A/E (Sca-1) (Biolegend, cat: 108125 and CD45-Pe-Cy7 (Clone HI30; BD Biosciences, 557748) for 20 min at +4°C in the dark and washed with FACS buffer (2% (v/v) FBS, 1% (v/v) Penicillin/Streptomycin). Before analysis on a BD LSR flow cytometer, 1:2000 4',6-diamidino-2-phenylindole (DAPI; 1mg/ml stock concentration) was added to the cells. Cells with purity >98% are selected for further analysis.

2.5. In vitro differentiation assays

MSCs were grown to confluence before the initiation of multilineage differentiation assays. The adipogenic maturation potential of MSCs was tested using a commercially available adipogenesis kit (PT-3004, Lonza), according to the manufacturer's instructions. The medium was refreshed every 2-3 days for 18-21 days. Differentiating and mature adipocytes were harvested for qPCR array on adipogenesis marker genes (Table 2.2). After differentiation, mature adipocytes were fixed with 4% paraformaldehyde for 20 min, washed three times with PBS, once with 60% isopropanol and stained with Oil Red O (Sigma Ref. O-0625) in 60% isopropanol. Osteoblast maturation potential was tested using a commercially available osteogenesis kit (PT-3002, Lonza), following the manufacturer's instructions. The medium was refreshed every 2-3 days for a total duration of 18-21 days. Differentiating and mature osteoblasts were harvested for qPCR array on

osteogenesis marker genes (Table 2.2). Terminally differentiated osteoblasts were fixed with ice-cold 70% ethanol for 1 hour and mineralization was assessed by Alizarin Red staining (Sigma). Cells were imaged using a phase-contrast microscope (EVOS™) and cellular staining was quantified using ImageJ. Briefly, the RGB picture is converted into greyscale and the green channel is subtracted from the red channel, to remove any white and yellow objects while keeping the red and pink objects. The threshold tool is then used to select and measure the areas of positive staining.

Table 2.2: qPCR primer for human cDNA

	Forward	Reverse
UPR target genes		
ATF4	GCTAAGGCGGGCTCCTCCGA	ACCCAACAGGGCATCCAAGTCG
ATF6	ATGAAGTTGTGTCAGAGAACC	CTCTTTAGCAGAAAATCCTAG
CHOP	GGAGCATCAGTCCCCCACTT	TGTGGGATTGAGGGTCACATC
CNX	GGTGCTTGGAACTGCTATTG	CCCTGTTGGAACTGGAGCTT
CRT	TGGGATGAAGAGATGGACGGAGA	GCATAGATACTGGGATCGGGAGAA
ERDJ4	CCGATTTTGGCACACCTAAG	GAGGAGCAGCAGTAGTCGGA
ERO1LB	TATTGCTGAACCCAGAGCGT	TCCAGACACAAACCTTCTAGCC
ERp57	AAGAAATATGAAGGTGGCCGTG	GTCCTCCCCAATGGTTTTCC
GADD34	CCTCTACTTCTGCCTTGTCTCCAG	TTTTCCTCCTTCTCCTCGGACG
GRP78	GGAAATTGCGCTGTGCTCC	GCCGACGCAGGAGTAGGTG
GRP94	ATCTCCGTGTGCTTTGGTGG	TTCGTCGAAGCATGTCTCTG
HERPUD1	TCCTCCTCCTGACGTTGTAAA	TGCTCGCCATCTAGTACATCC
IRE 1	AGTCAGTTCTGCGTCCGCT	TGGTACTTCCAAAAATCCCGAGG
MIR22HG	CCTCGTGCAGCAACCCC	GTGAGGGCGTGAGAGGAAC
ORP150	GGCAGACAAAGTTAGGAGGCA	TCCTCCGAGATTCCTTATTCAAGAC
PDIA5	ACTGCTCAGAACCCGGAATA	GATGGTCCCTTGTCCTTTCA
PERK	ATGCTTTCACGGTCTTGGTC	TCATCCAGCCTTAGCAAACC
THBS1	TCATTAGAGTGGTGATGTATGAAGG	ACCAGCATTGGTTTATGATCAGTC
XBP1 spliced	TTGCTGAAGAGGAGGCGGAA	CTGCACCTGCTGCGGACTCAG
XBP1 Total	TTCCGGAGCTGGGTATCTCA	GAAAGGGAACCCCCGTATCC
Osteogenesis marker genes		
RUNX2	CAACAGAGTCATTTAAGGCTGCAA	ACATGGTGTCACTGTGCTGA
BMP2	CTGCGGTCTCCTAAAGGTCG	CAACTCGAACTCGCTCAGGA
Adipogenesis marker genes		
PPARg	TGTGAAGGATGCAAGGGTTTCT	ATCCGCCCAAACCTGATGG
CFD	GATGTGCGCGGAGAGCAAT	CTGTCGATCCAGGCCGCATA
ADIPOQ	CGTGATGGCAGAGATGGCAC	GGTACTCCGGTTTCACCGAT
CEBPA	TATAGGCTGGGCTTCCCCTT	AGCTTTCTGGTGTGACTCGG
CEBPB	TTTGTCCAAACCAACCGCAC	GCATCAACTTCGAAACCGGC
FABP4	AACTGGTGGTGGAATGCGT	GGTCAACGTCCCTTGGCTTA
DLK1	GAGATGACCGCGACCGAAG	AGCATTCAGCCCCATAGGTG
GATA3	CTCTTCGCTACCCAGGTGAC	ACGACTCTGCAATTCTGCGA
Housekeeping genes		
actB	GCCGCCAGCTCACCAT	TCGTCGCCCACATAGGAATC
B2m	AGCAGCATCATGGAGGTTTGA	TCAAACATGGAGACAGCACTCA

2.6. Flow cytometry analysis

Flow cytometry analysis was performed using an LSR Fortessa Analyzer (Becton Dickinson, CA, USA). Dead cells and debris were excluded from the analysis using 4,6, diamidino-2-phenylindole (DAPI). MSCs were immunophenotyped using monoclonal antibodies specific for human antigens: APC CD90 (Biolegend 328118), PerCP/Cyanine5.5 CD105 (Biolegend 323215), PE CD73 (Biolegend 344003), PE-Cy7 CD45 (BD Bioscience 557748). All data were analysed using FlowJo software (Becton Dickinson, CA, USA).

2.7. Cell death assay

Apoptosis analysis was performed by staining cells with an Annexin V antibody (Alexa Fluor® 647 Annexin V, Biolegend, 640912 or PE/Cyanine7 Annexin V, Biolegend 640950) and DAPI in Annexin V Binding Buffer (BD Bioscience, 556454). Before staining cells, a fresh 1X Annexin V Binding Buffer working solution was made by diluting the 10X concentrate 1:10 with distilled water. Cells were then analysed on a Fortessa Analyzer (Becton Dickinson, CA, USA). Data were analysed using FlowJo software (Becton Dickinson, CA, USA) (Figure 2.1).
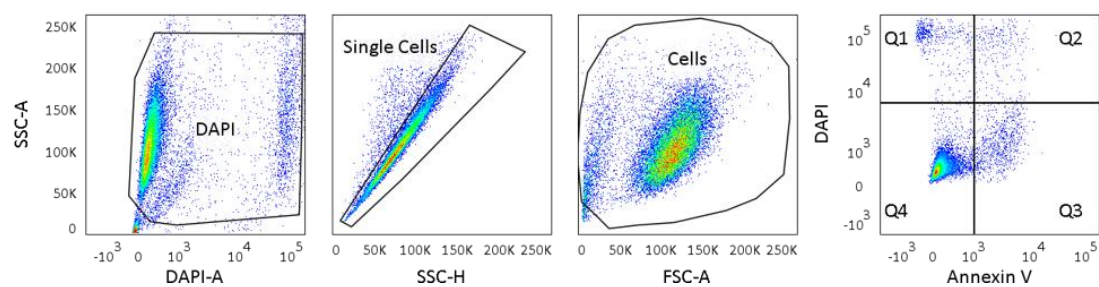
Figure 2.1: Gating strategy for apoptosis analysis.

2.8. Cell cycle assay

Fixation and permeabilisation of cells were performed using the BD Cytofix/Cytoperm™ kit (554714) following the manufacturer's instructions. Cells were then stained with a 1:100 DAPI solution and analysed on a Fortessa Analyzer

(Becton Dickinson, CA, USA). Data were analysed using FlowJo software (Becton Dickinson, CA, USA) (Figure 2.2).
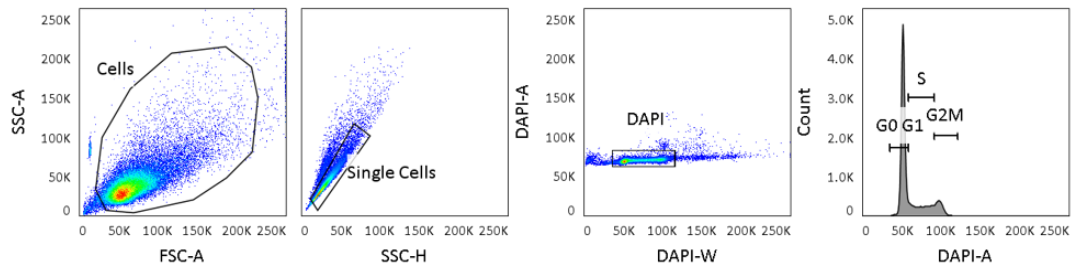
Figure 2.2: Gating strategy for cell cycle analysis.

2.9. Cell proliferation assay by flow cytometry

CountBright™ Absolute Counting Beads (ThermoFisher Scientific C36950, Lot 1932240, 0.52×10^5 beads/50 µl) were used for the quantification of cell populations. Cells from co-cultures were first incubated with human CD90 (Thy-1)-APC (clone 5E10; eBioscience, 17-0909-42) and human CD45-Pe-Cy7 (Clone HI30; BD Biosciences, 557748). After washing, cells were resuspended in 300 µl of FACS buffer with DAPI and a specific volume of the microsphere suspension (10 µl) was added. Samples were analysed on a BD LSR Fortessa Analyzer (Becton Dickinson, CA, USA). Data were analysed using FlowJo software (Becton Dickinson, CA, USA). The absolute numbers of cells in the sample were calculated by comparing the ratio of bead events to cell events by using the formula.

$$Cell\ concentration = number\ of\ cell\ events\ \times \frac{beads\ concentration}{number\ of\ beads\ event}$$

2.10. Cell proliferation assay

At specific time points, cells are carefully resuspended in a fresh medium or wash buffer. Under sterile conditions, an aliquot of cell suspension is removed and an equal volume of Trypan Blue (dilution factor 2) is added, mixing by gentle pipetting. The chamber of the haemocytometer is filled with the cell suspension (approximately 10 µl) and viewed under an inverted phase contrast microscope using x20 magnification. The number of viable (seen as bright cells) and non-viable cells

79

(stained blue) are counted, noting the number of squares counted to obtain a count of >100 cells. The concentration of viable and non-viable cells was measured by using the formula:

$$Cell\ contration = \frac{Number\ of\ counted\ cells}{Number\ of\ squares} \times dilution\ factor\ \times 10,000$$

2.11. Plasmid constructions and bacterial transformation

pTRIP-TRE-PLZ, pTRIP-TRE-ILZ and pTRIP-TRE-ATF6p50 (ΔATF6) gain-of-function constructs plasmids and rtTA (pLenti-rtta3, Addgene 26429) (Figure 2.3 and 2.4) were kindly gifted by Dr Christian Touriol (Cancer Research Center of Toulouse, Inserm, Université Toulouse III). IRES-EGFP cassette from pIRES2-EGFP (Addgene) was cloned as a eukaryotic selectable marker in the original vectors by using In-Fusion® HD Cloning (Takara 102518) following the manufacturer's instructions. PERK-LZ and IRE1-LZ vectors were linearized using the restriction enzyme KpnI and the IRES-EGFP sequence was amplified with CloneAmp HiFi PCR Premix Kit (639298, Clonetech) by using the iresEGFP-pTRIP primers (Table 2.3), and inserted in the linearized vector by homologous recombination to generate pTRIP-TRE-PLZ-iresEGFP (PERK-LZ), pTRIP-TRE-ILZiresEGFP (IRE1-LZ) (Figure 2.4).

Table 2.3: Primers for plasmid construction

	Forward
iresEGFP-pTRIP	CCAGTCACACCTCAGCCGCCCCTCTCCCTCCCC
pTRIP-ATF6p50	TTTGGCTGATACGCGACGCGTTCACTCGAGTTTACTCC
PGK	GGTCCTTAAGATTAATGATATCGAATTCCCACGGGGT
PGK-xbp1	GCGGCGACGCGTATGATATCGAATTCCCACGGG
pLenti	TTTGGCTGATACGCGTATAACCGTATTACCGCCATGC
	Reverse
iresEGFP-pTRIP	TCATTGGTCTTAAAGCTTGTACAGCTCGTCCATGCCG
pTRIP-ATF6p50	TTTTCTAGGTCTCGAGAGCGGCCGCCCTATCTTCG
PGK	TAATTCTATAGCTAGCATCCCCCTGGGGAGAGAGGT
PGK-xbp1	GCGGCGATCGATGCTGATTATGATCTAGAGTCGC
pLenti	GATCCGGGCCCATCGATCCTCTACAAATGTGGTATGGC

ΔATF6 was linearized by using the restriction enzymes MluI-HF and XhoI and the IRES-EGFP sequence was amplified with CloneAmp HiFi PCR Premix Kit (639298, Clonetech) by using the pTRIP-ATF6p50 primers (Table 2.3) and cloned in the linearized ΔATF6 vector by homologous recombination. Plasmid size was checked by restriction enzyme digestion and gel electrophoresis with 0.5% (w/v) agarose gel in Tris Borate EDTA (TBE) buffer and sequences were confirmed by DNA sequencing (Eurofins). Plasmids were amplified by transformation of NEB 5-alpha competent E. Coli (High Efficiency, NEB C2987H) and overnight growth in lysogeny broth (LB) supplemented with ampicillin or kanamycin at 37 °C under agitation. Plasmids were purified using Invitrogen™ PureLink™ HiPure Plasmid Maxiprep Kit (K210007, Thermofisher).
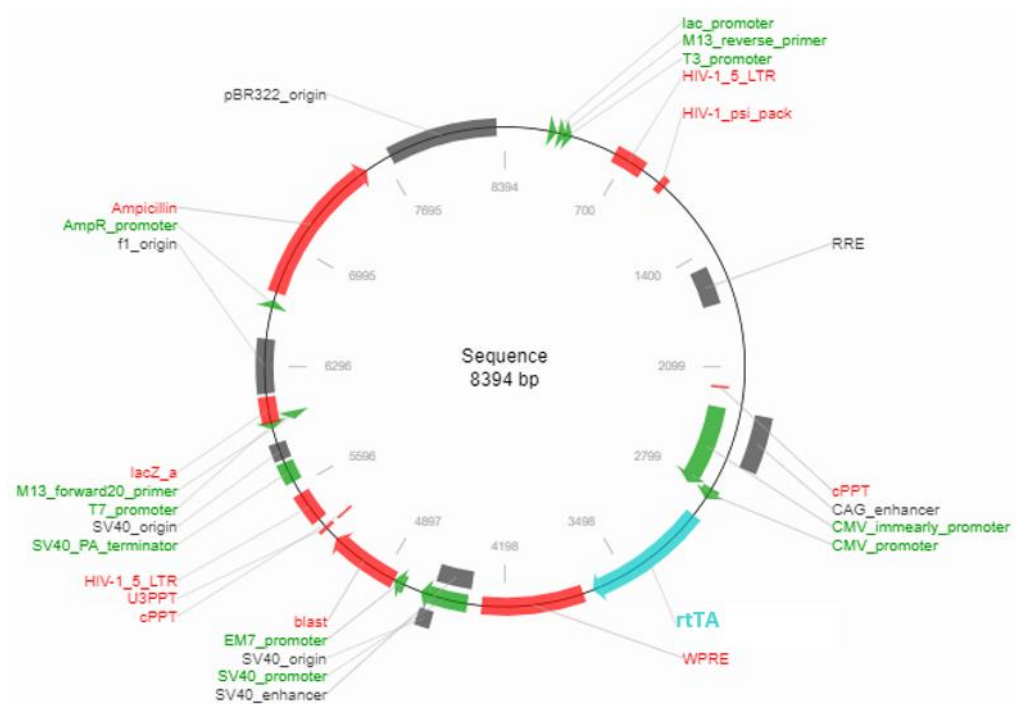
Figure 2.3: Graphic map of the reverse tetracycline transactivator (rtTA) expression vector. *[HA: Human influenza hemagglutinin; IRES: internal ribosomal entry site; EGFP: enhanced green fluorescent protein; cPPT: central polypurine tract; U3PPT: U3 polypurine tract; HIV-1_3_LTR: human immunodeficiency virus 1_ 3'-long terminal repeats; AmpR: ampicillin resistance; SV40: simian virus 40; NLS: nuclear localisation signal; HIV-1_5_LTR: human immunodeficiency virus 1_ 5'-long terminal repeats; HIV-1_psi_pack: human immunodeficiency virus 1_packing signal; RRE: HIV-1 Rev response element; CMV: cytomegalovirus; CAG: CMV immediate enhancer/β-actin; WPRE: woodchuck hepatitis virus; bp: base pair].*
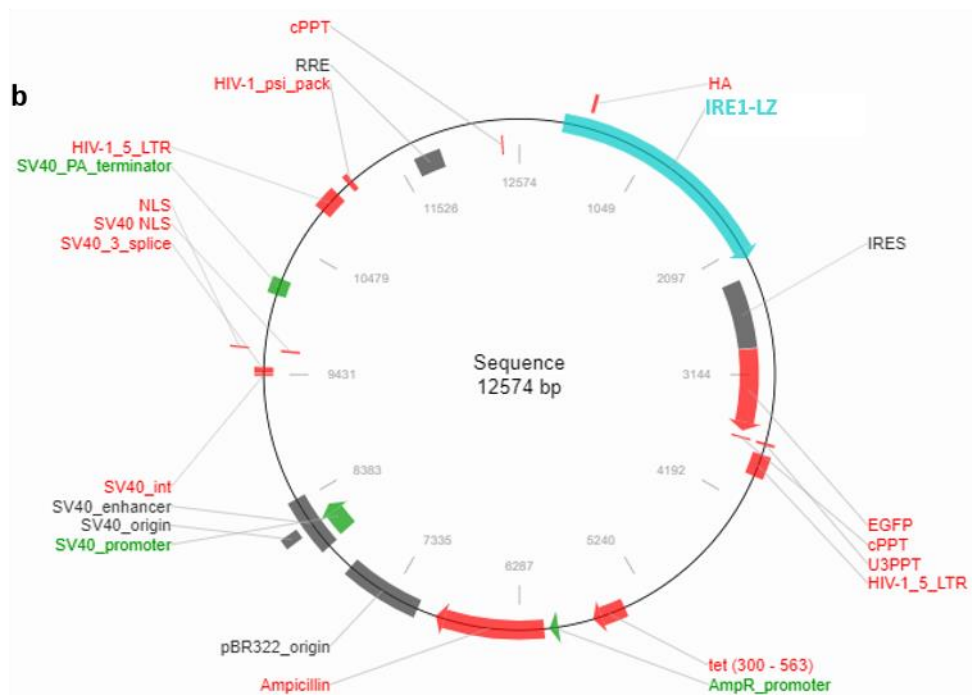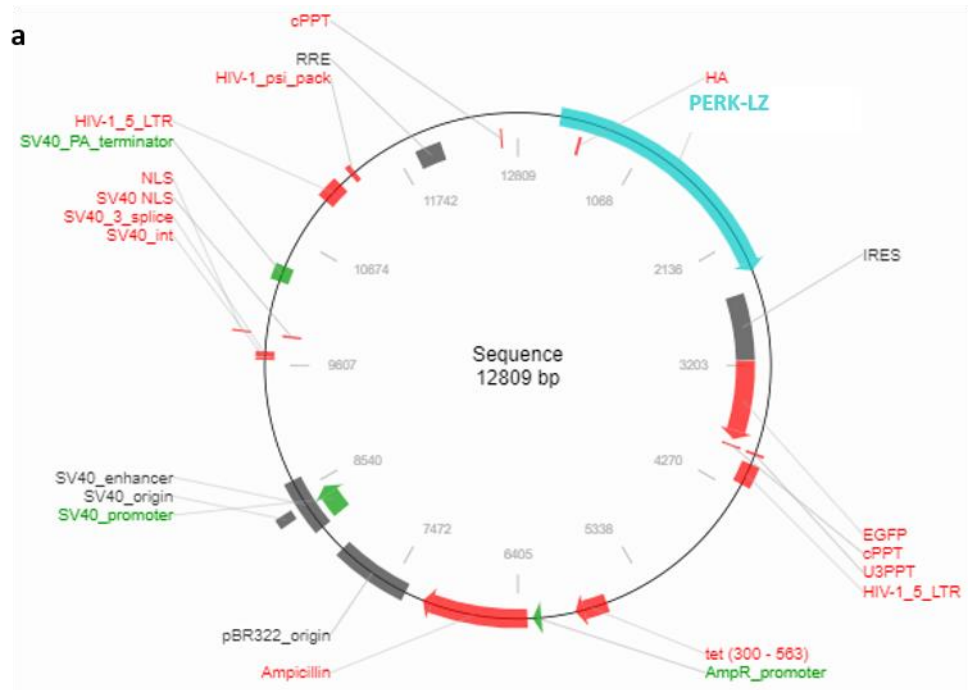
Figure 2.4: Graphic maps of gain-of-function expression vectors. (a) pTRIP-TRE-PLZ-iresEGFP (PERK-LZ) (b) pTRIP-TRE-ILZ-iresEGFP (IRE1-LZ). *[HA: Human influenza hemagglutinin; IRES: internal ribosomal entry site; EGFP: enhanced green fluorescent protein; cPPT: central polypurine tract; U3PPT: U3 polypurine tract; HIV-1_3_LTR: human immunodeficiency virus 1_ 3'-long terminal repeats; AmpR: ampicillin resistance; SV40: simian virus 40; NLS: nuclear localisation signal; HIV-1_5_LTR: human immunodeficiency virus 1_ 5'-long terminal repeats; HIV-1_psi_pack: human immunodeficiency virus 1_packing signal; RRE: HIV-1 Rev response element; tet: Tetracycline Inducible Expression; bp: base pair].*

2.12.   Transfection and viral production

Viruses were produced by transfecting HEK293T cells with each plasmid along with packaging components pCMVdR8.74 and pMD.G2 using the $CaCl_2$ method. Medium containing the virus was collected at 24 and 48 hours, centrifuged at 500xg for 8min and filtered through a 0.22μm filter to eliminate cell debris. The viruses were then concentrated using an ultracentrifuge at 22000 rpm for 2 hours at +4 °C and resuspended in 200 μl of MSC medium (Gibco™ MEMα, nucleosides, GlutaMAX™ Supplement with 1% (v/v) Penicillin/Streptomycin). Aliquots of concentrated viral particles were kept at -80 °C for long-term storage.

2.13.   Transduction

To generate MSCs stably expressing the gain-of-function plasmids, $3.5x10^6$ cells were harvested and resuspended in 12 ml of the virus-containing medium at a multiplicity of infection (MOI) of 10. MSCs were co-transduced with rtTA and PERK-LZ or IRE1-LZ gain-of-function plasmids at 1:1 ratios (rtTA:PERK-LZ or rtTA:IRE1-LZ). MSCs transduced with rtTA alone are used as controls for experiments. Resuspended cells are then seeded in 150mm flasks at high confluence. After ~12 hours, the cells were washed, resuspended in fresh medium and expanded.

2.14.   Fluorescence-activated cell sorting (FACS)

Cell sorting was performed using a FACS Aria Fusion Flow Cytometer Analyzer (Becton Dickinson, CA, USA). Transduced MSCs were treated with doxycycline hydrochloride (1 μg/mL; Sigma, D3447) the day before. The next day, MSCs were harvested and stained with DAPI. Dead cells and debris were excluded from the analysis using 4,6, diamidino-2-phenylindole (DAPI). MSCs were sorted based on GFP^+ expression and then seeded directly for downstream assays and/or expanded for a few days.

2.15.   Quantitative PCR

Total RNA from cells was extracted using the RNeasy Micro Kit (QIAGEN). RNA was quantified and quality was assessed using Nanodrop. cDNA was synthesised with the High-Capacity cDNA Reverse Transcription Kit (Applied Biosystems) and the following qPCR analysis was performed on the CFX384 Touch™ Real-Time PCR Detection System (Bio-Rad) by using PowerUp™ SYBR™ Green Master Mix (Applied Biosystems™). All signals were quantified using the ΔΔCt method. See Table 2.2 for primer sequences.

2.16.   Western Blot Analysis

MSC cells were seeded at 90% confluence in 60mm dish or 6-well plates. After specified treatment at the specified contractions and time points, cells were harvested and washed twice with PBS. Cell extracts were obtained by using a Lysis Buffer (50 mM Tris-HCl, pH 7.4; 100 mM NaCl; 1% Igepal CA-630 (Sigma I8896); 0.1% SDS; 0.5% sodium deoxycholate) supplemented with Halt™ Protease and Phosphatase Inhibitor Cocktail, EDTA-free (100X; Sigma 78441). Protein extracts were quantified using the Pierce BCA Protein assay kit (Thermo Scientific™, 23225) and denatured by the addition of NuPAGE LDS Sample Buffer (4X; ThermoFisher NP007) and NuPAGE Sample Reducing Agent (10X; Thermofisher NP0009) and heating at 95°C for 5 minutes. Samples were loaded into a pre-cast gel (Gel NuPAGE™ 4-12% Bis-Tris Protein Gels, 1.0 mm, 10-well, Thermofisher NP0321BOX or NuPAGE™ 4 to 12%, Bis-Tris, 1.0 mm, Mini Protein Gel, 15-well NP0323BOX) and run using NuPAGE™ MOPS SDS Running Buffer (20X) 500 mL (NP0001) at 120-140V. The transfer was performed overnight using a PVDF membrane and NuPAGE™ Transfer Buffer (20X, Thermofisher NP00061) with 10% methanol. Membranes were blocked with 3% (w/v) bovine serum albumin (BSA; Merk A2153) in TBS-T (TRIS-buffered saline with 0.01% Tween P1379 Sigma) for 1 hour under gentle agitation (30 rpm), followed incubation with primary and secondary antibody. HA-tagged proteins were detected using HA-Tag mouse mAb (dilution 1:5000; clone 6E2; Cell Signalling Technology 2367). Other antibodies used were: IRE1 total (dilution 1:1000, Cell Signalling Technology 3294), PERK total (dilution 1:1000, Cell Signalling Technology

5683S), P-eIF2α (Ser51) (dilution 1:1000, Cell Signalling Technology 9721), eIF2a total (dilution 1:1000, Cell Signalling Technology 9722 or 2103), ATF4 (dilution 1:1000, Cell Signalling Technology 11815), XBP1s (dilution 1:1000, Cell Signalling Technology 83418), GADD34 (dilution 1:500, Santa Cruz sc-373815), CHOP mouse mAb (dilution 1:1000, clone L63F7, Cell Signalling Technology 2895), GATA3 (dilution 1:1000, clone D13C9, Cell Signalling Technology 5852). Protein signals were normalised using anti-tubulin mouse mAb (dilution 1:10,000, Abcam ab7291) or anti-actin mAb (dilution 1:10,000; Sigma-Aldrich A2066). Anti-rabbit IgG, HRP-linked Antibody (dilution 1:5000, Cell Signalling Technology, 7074) or anti-mouse IgG, HRP-linked (dilution 1:5000, Cell Signalling Technology, 7076) were used as secondary antibodies. Signals were detected using the Clarity chemiluminescence kit (Bio-Rad) and imaged with the Amersham Imager 600.

2.17. Patient-derived xenograft experiment

Dr Diana Passaro performed these animal experiments in the laboratory of Professor Dominque Bonnet at the Francis Crick Institute, under the project license (PPL 70/8904) approved by the Home Office of the UK and following The Francis Crick institute animal ethics committee guidelines. Detailed methods are available at Passaro et al., 2021. Okt3-treated AML patient-derived samples ($2\text{-}8\text{x}10^6$) and healthy HSPC ($1\text{x}10^6$) were transplanted into 8 to 12-week-old unconditioned Nestin-GFP NOD-SCID IL2Rgnull (NSG) mice by intravenous injection. Each experimental cohort contained an equal number of male and female mice. BM engraftment was assessed by the BM aspirate. Mice were sacrificed when human engraftment was > 50% (or 1%–10% for early time point experiments), with an age of 13 to 20 weeks. At the end of each experiment, animals were sacrificed by cervical dislocation and the six rear bones, tibia, femur and pelvis, were collected in cold PBS. To retrieve BM niche cells, bones were dissected in small pieces of 2-3 mm diameter and incubated for 20 min at 37 °C in a Hanks' Balanced Salt Solution (HBSS) digestion solution containing 2% FBS, DNase I (10 mg/ml), Collagenase (1 mg/ml), Dispase II (5 mg/ml) and Heparin (20 U/ml), all from Sigma-Aldrich. Bone pieces were next crushed with mortar and pestle in the same digestion solution and incubated at 37 °C for 20 min.

The cell suspension was then homogenized with a micropipette and filtered with a 100 μm cell strainer. Cell sorting was performed using a FACS Aria SORP (BD Biosciences, Oxford, UK). To sort BM niche cells, human and murine hematopoietic cells were excluded using an EasySep Human CD45 Positive Selection kit and a murine CD45 positive selection kit (Stem Cell Technologies, Vancouver, Canada) according to the manufacturer's instructions, with a purity of 85 to 99%. The remaining cells were sorted in RNeasy RLT buffer (RNeasy Mini kit, QIAGEN) based on the expression fluorescent reporters (GFP for Nestin). RNA was extracted using the RNeasy Mini kit (QIAGEN) following manufacturer instructions. The quality and concentration of total RNA were determined on Agilent 2100 Bioanalyzer using the Eukaryote Total RNA Pico Assay. Most of the total RNA has an average (RNA integrity number) RIN number of 5-8, with a concentration of at least 4 pg/ml. Some of the samples were concentrated on a speed vac without heat to obtain a final volume of 5 ml. 3.5 ng of Total RNA in 5 mL volume was used to generate cDNA synthesis with Nugen Ovation RNA-Seq System V2 kit (part No. 7102). The resulting SPIA-cDNA were normalized to 100 ng in 15 mL based on Qubit DNA HS assay. Fragmentation was done using 8 microTUBE-15 AFA Beads Strip V2 (PN 520159) on Covaris E-series at setting 20%DF, 18W, 200 burst, 20C tempt, 120s treatment time and no Intensifier. Only 10-30 ng in 10 mL of fragmented cDNA was used starting from the End Repair step of the Ovation Ultralow Library Systems V2 (part No. 0344NB) protocol, with 10 cycles PCR. The RNA-Seq libraries were quality checked on Qubit DNA HS assay, Bioanalyser and Illumina Ecoreal qPCR followed by Illumina PE51 sequencing on Hiseq 2500 V3 reagents.

2.18. Bioengineered humanised bone marrow niche in mice

Diana Passaro and Jorgina Reginold performed these animal experiments in the laboratory of Diana Passaro at the Cochin Institute, Paris. A detailed protocol to generate bioengineered scaffolds can be found in Passaro et al., 2017. MSC stably expressing rtTA and PERK-LZ or rtTA alone were obtained as previously described in Methods 2.13 and 2.14. Successfully generated PERK-MSCs or rtTA-MSCs were

injected into sterile pieces of gel foam (Pfizer, 0315-08) by using a 1mL 26G syringe (BD Medical, 305501). Pieces of gel foam were prepared in advance by cutting the gel foam into 24 pieces in sterile conditions, washed with Ethanol 70% for 5 min and twice with PBS. Per each condition, 12 scaffolds with 45,000 MSCs per scaffold were prepared and incubated at 37°C, 5% CO2 for 30 min in low attachment 24 well plate (Corning, CLS3473). 1mL of MSC medium (Gibco™ MEMα, nucleosides, GlutaMAX™ Supplement, containing 10% (v/v) Gibco MSC-qualified, USDA-approved regions Gibco™, 1% (v/v) Penicillin/Streptomycin) was then added and scaffolds were incubated at 37°C, 5% CO2 for 3 days. After 3 days, 41,600 hematopoietic CD34$^+$ cells were injected into each of the 24 scaffolds by using 26G 1mL syringes. Scaffolds were incubated at 37°C, 5% CO2 for 30 min. After 30 min, cells were fed with 1mL of CD34$^+$ cells medium, consisting of Stem Span (Stemcell, 9650) supplemented with recombinant human SCF (150ng/mL; Peprotech, 300-07), recombinant human Flt3 Ligand (150ng/mL; Peprotech, 300-19), recombinant human TPO (20ng/mL; Peprotech, 300-18), 1% HEPES buffer saline (Sigma, 51558) and 1% P/S, and incubated at 37°C, 5% CO2 overnight. On the day of implantation, scaffolds were treated with 5 µl of rhBMP-2 (Noricum) at 5 mg/ml in acetic acid 50 mM, with 20 µL of thrombin (Sigma T8885) at 10U/500 µl in CaCl2 2% and 20 µl fibrinogen (Sigma F3879) at 40 mg/mL in water for 10 - 15 min at 37 °C. The treated scaffolds were then implanted subcutaneously into 8 mice. After six weeks, to allow organoids formation, mice were treated with doxycycline hydrochloride (1 µg/mL; Sigma, D3447) in acid-free water with 5% sucrose (Euromedex, 200-301) to induce the expression of the recombinant protein PERK-LZ. Doxycycline-untreated control mice were watered with 5% sucrose acid-free water. Water was replaced with a freshly prepared solution every week until sacrifice. After 12 weeks, animals were sacrificed by cervical dislocation. The 19 organoids and all the bones of the six rear legs (tibia, femur and pelvis) and spleen from the 8 mice were collected in PBS with 2% FBS. Each organoid was cut into pieces and incubated at 37°C for 25 min in a digestion solution containing 2% FBS, Dispase II (5mg/ml; Sigma, D4693), 2000U/ml heparin, bovine pancreas Deoxyribonuclease I (1 mg/ml; Sigma, D4627), Collagenase (100mg/ml; Sigma, C0130). The digested organoid was then filtered with a 100 µm strainer (Fisher, 22363549), and pieces were crushed and washed with PBS 2% FBS. Cells were

then incubated with red blood cell lysis buffer for 10 min, washed with PBS 2% FBS and stained for flow cytometry analysis or frozen down. Flow analysis of the organoids-derived cells was performed with a 'haematopoietic panel' and a 'niche panel'. The haematopoietic panel included anti-mouse CD45 BV421 (Biolegend, 103134), anti-mouse Ter119 BV421 (Biolegend, 116234), anti-human CD45 APC-Cy7 (ThermoFisher, 47-0459-42), anti-human CD33 PE (Biolegend, 303404), anti-human CD19 APC (BD, 555415), anti-human CD3-Qdot605 (ThermoFisher, Q10054), anti-human CD34 PerCP-Cy5.5 (BD, 347222), anti-human CD38 PeCy7 (ThermoFisher, 25-0388-42). The niche panel included anti-mouse CD45 BV421 (Biolegend,103134), anti-mouse Ter119 BV421 (Biolegend,116234), anti-human CD45 PerCP-Cy5.5 (Biolegend,304028), anti-human CD90 APC (ThermoFisher,17-090942), anti-human CD73 APC (ThermoFisher, 17-0739-42), anti-mouse CD51 PE (ThermoFisher, 12-0512-42), anti-mouse CD31 PeCy7 (Biolegend,102418), anti-mouse Sca1 APC-Cy7 (Biolegend,108126), anti-human CD271 Biotin (Milteny, 130-113-419), Streptavidin Qdot605 (ThermoFisher, Q10101MP). To retrieve BM hematopoietic cells, bones were crushed with a mortar, passed through a 100 µm strainer, incubated in red blood cell lysis buffer for 10 min and washed with PBS 2% FBS. To retrieve spleen hematopoietic cells, the spleen was passed on a 100 µm strainer, crushed, treated with red blood cell lysis buffer for 10 min and washed with PBS 2% FBS. Hematopoietic cells isolated from the BM or the spleen were frozen down or stained for flow cytometry with anti-mouse CD45 BV421 (Biolegend, 103134), anti-mouse Ter119 BV421 (Biolegend, 116234), anti-human CD45 APC-Cy7 (ThermoFisher, 47-0459-42), anti-human CD33 PE (Biolegend,303404), anti-human CD19 APC (BD, 555415), anti-human CD38 PeCy7 (ThermoFisher, 25-0388-42), anti-human CD34 PerCP-Cy5.5 (BD, 347222). Cells were then stained with DAPI and analysed on an LSR II cytometer. Data were analysed using FlowJo software and the graphs were made on GraphPad Prism Software.

2.19. RNA sequencing

RNA sequencing was performed on: MSCs isolated from the BM of AML patients (AML-MSC) and of healthy donors (HD-MSC), on MSCs transduced with the gain-of-

function vectors (PERK-MSC, IRE1-MSC or rtTA-MSC) and on PERK-MSC and rtTA-MSC cultured in adipogenic differentiation conditions for 14 days. MSC stably expressing rtTA and PERK-LZ or rtTA alone were obtained as previously described in Methods 2.13 and 2.14 and for two days with doxycycline hydrochloride (1 µg/mL; Sigma, D3447). RNA integrity was assessed by 4200 TapeStation (Agilent Technologies). Novogene (China) performed library preparation with NEB Next® Ultra™ RNA Library Prep Kit with unstranded protocol and mRNA sequencing at 43 million reads per sample using an Illumina PE150 platform. FASTQC was performed using trim galore and FASTQ files were aligned to the human reference genome (GRCh38.p10) using STAR alignment with a 2-pass procedure. Counting of reads was performed with (RNA-Seq by Expectation-Maximization) RSEM using the Ensemble annotation GRCh38.101. Only genes that achieved at least one read count per million reads (TPM, transcript per million) in at least 25% of samples were kept. TPM and FPKM log2 expression matrices were generated as part of the RSEM count pipeline. Conditional quantile normalisation (cqn) (PMID: 22285995) was performed by counting for gene length and GC content, and a log2 transformed RPKM (Log2RPKM) expression matrix was generated. Differential gene expression analyses were carried out using the lm model of the 'limma' R package and voom normalization with a 0+Group design (PMID:25605792). Gene-set enrichment analysis (GSEA) was performed using R package fgsea GSEA pre-ranked and ranked t-statistic of all genes for the four contrasts. Heatmaps illustrating the expression pattern of the genes were generated using the R package ComplexHeatmap. Row clustering was performed on euclidean distance and the "complete" clustering method. Volcano plots were generated using the R package EnhancedVolcano.

2.20. Proteomic and Phosphoproteomic analysis

Dr Pedro Casado performed Proteomic and Phosphoproteomic analysis in the lab of Dr Pedro R Cutillas on MSCs isolated from the BM of AML patients (AML-MSC) and of healthy donors (HD-MSC), and on MSCs transduced with the gain-of-function vectors (PERK-MSC, IRE1-MSC or rtTA-MSC). MSC stably expressing rtTA and PERK-LZ or rtTA

alone were obtained as previously described in Methods 2.13 and 2.14 and treated for two days with doxycycline hydrochloride (1 μg/mL; Sigma, D3447) before collection. Cell medium was aspirated from the cell containing flasks or dishes and washed twice with 5mL of ice-cold PBS containing protease and phosphatase inhibitors (20 μL NaF and 100 μL Na3VO4 to 10 mL of PBS), keeping dishes on ice. 500 μl of cell lysis buffer (8M urea in 20mM HEPES, pH 8.0, 100 mM sodium orthovanadate Na_3VO_4, 500 mM sodium fluoride NaF, 1M β-glycerol phosphate, 250mM disodium pyrophosphate $Na_2H_2P_2O_7$) were added directly to cell layer, maintaining flasks or dishes on ice. Cells were harvested using a scraper and transferred to sonication tubes. Samples were sonicated using a Bioruptor® Pico sonication device for 20 Cycles, 30 seconds on and 30 seconds off, at high intensity. After sonication, the cell suspension was centrifuged at 13,000 rpm for 10 minutes at 5^oC to remove debris and the supernatant was recovered into a 1.5 mL Eppendorf Protein Lo-bind tube. Protein extracts were quantified using the Pierce BCA Protein assay kit (Thermo Scientific™, 23225) and analysed on LC-MS/MS platform, a Dionex UltiMate 3000 RSLC coupled to Q Exactive™ Plus Orbitrap Mass Spectrometer (Thermo Fisher Scientific) through an EASY-Spray source. For the acquisition of phosphoproteomics data, peptide pellets were reconstituted in 10 μL of reconstitution buffer (20 fmol/μL enolase in 3% acetonitrile (ACN), 0.1% trifluoroacetic acid (TFA)) and 5 μL were loaded onto an LC-MS/MS system. For proteomics data acquisition, peptide pellets were reconstituted in 8 μL of 0.1% TFA, 2 μL of this solution were further diluted in 18 μL of reconstitution buffer and 2 μL were injected into the LC-MS/MS system. Mobile phases for the chromatographic separation of the peptides were Solvent A (0.1% FA) and Solvent B (99.9% ACN; 0.1% FA). Peptides were loaded in a μ-precolumn and separated in an analytical column using a gradient running from 3% to 28% B over 60 min for phosphoproteomics or 90 min for proteomics. The Ultra high-performance liquid chromatography (UPLC) system delivered a flow of 2 μL/min (loading) and 250 nL/min (gradient elution). The Q Exactive Plus acquired full scan survey spectra (m/z 375–1500) with a 70,000 Full width at half maximum (FWHM) resolution followed by data-dependent acquisition (DDA) in which the 15 most intense ions were selected for higher energy collisional dissociation (HCD) and MS/MS scanning (200–2000 m/z) with a resolution of 17,500

FWHM. A dynamic exclusion list of the 30s with an m/z window of ±10 ppm was enabled. A maximum duty cycle of 2.1s was operated by the instrument. Peptide identification from MS data was automated using a Mascot Daemon (v2.8.0.1) workflow in which Mascot Distiller generated peak list files (MGF) from RAW data and the Mascot search engine matched the MS/MS data stored in the mascot generic format (MGF) files to peptides using the SwissProt Database restricted to the Homo sapiens taxon (SwissProt_2021_02.fasta; 20396 sequences). Searches had an FDR of ~1% and allowed two trypsin missed cleavages, a mass tolerance of ±10 ppm for the MS scans and ±25 mmu for the MS/MS scans, carbamidomethyl cysteine as a fixed modification and oxidation of methionine, pyroglutamic acid (pyroGlu) on N-terminal glutamine as variable modifications. Phosphorylation on serine, threonine, and tyrosine as variable modifications was also considered for searches performed on phosphoproteomics data. Pescal was used for label-free quantification of the identified peptides. The software constructed Extracted ion chromatograms (XICs) for all the peptides identified in at least one of the LC-MS/MS runs across all samples. XIC mass and retention time windows were ±7 ppm and ±2 min, respectively. Quantification of peptides was achieved by measuring the area under the peak of the XICs. Individual peptide intensity values in each sample were normalized to the sum of the intensity values of all the peptides quantified in that sample. Data points not quantified for a particular peptide were given a peptide intensity value equal to the minimum intensity value quantified in the sample divided by 10. For phosphoproteomics experiments, a phosphorylation index (ppIndex) was obtained by summing the signals of all peptide ions containing the same modification site. For the proteomics experiment, protein intensity values were calculated by adding the intensities of all the peptides derived from a protein. Protein score values were expressed as the maximum Mascot protein score value obtained across samples. Statistical analysis was carried out in Excel or R (v4.0.0) using base functions or the ggpubr package (https://CRAN.R-project.org/package=ggpubr). Term enrichment analysis of subsets of proteins differentially expressed or phosphorylated was performed using the cluster Profiler package (https://bioconductor.org/packages/release/bioc/html/clusterProfiler.html). Data

were visualized using the ggplot2 package (https://cran.r-project.org/web/packages/ggplot2/index.html).

2.21. Matrisome analysis

Matrisome analysis was performed by Eleanor Jane Tyler in the lab of Dr Oliver Pierce on differentially expressed genes and proteins generated by RNA-sequencing and proteomic analysis (Methods 2.19 and 2.20) of MSCs transduced with the gain-of-function vectors, PERK-MSC and rtTA-MSC. Lollipop and volcano plots for the matrisome signature of altered genes from were generated transcriptome and proteome data, with inclusion parameters of adjusted p-value <0.05 and logFC < 1.

2.22. Statistical analysis

Statistical analysis was performed on GraphPad Prism Software, using an unpaired two-tailed t-test or repeated measures one-way ANOVA followed by Dunnett's test for multiple comparisons. Error bars indicate the standard deviation (s.d.) or standard error of the mean (s.e.m.) of data from replicate experiments. Observed differences were considered statistically significant if the calculated p-value was below 0.05. *$p < 0.05$; **$p < 0.001$; ***$p < 0.0001$; ****$p < 0.00001$.

Chapter 3

Results

Acute Myeloid Leukaemia-induced alterations on Mesenchymal Stromal Cells

Acute myeloid leukaemia (AML) is a heterogeneous disorder characterized by the clonal proliferation of blasts in the bone marrow (BM), where haematopoietic stem cells reside. The BM is a complex multicellular tissue located in the central cavities of the bone and comprises blood vessels, nerve fibres and a heterogeneous population of stromal cells which includes mesenchymal stromal cells (MSCs), osteoblasts and adipocytes (Baryawno et al., 2019; Méndez-Ferrer et al., 2010; Shafat et al., 2017; Wolock et al., 2019). Emerging evidence suggests that leukemic cells compete with normal hematopoietic stem and progenitors cells for niche occupation resulting in the remodelling of the BM niche into a leukaemia-permissive microenvironment (Medyouf, 2017) while suppressing normal haematopoiesis (Boyd et al., 2017; Miraki-Moud et al., 2013). *In vivo* studies using murine models have shown that these changes include alterations in BM innervation and stroma, with the disruption of quiescence of Nestin-GFP^{+} niche cells and expansion of mesenchymal stromal cells (MSCs) primed for osteoblastic differentiation at the expense of HSC-maintaining NG2^{+} periarteriolar niche cells (Hanoun et al., 2014). Furthermore, AML progression leads to differential remodelling of the vasculature (Duarte et al., 2018; Kumar et al., 2018; Passaro, Di Tullio, et al., 2017) in central and endosteal BM regions with a progressive loss of vessels in the endosteum and significant decrease of osteoblasts (Duarte et al., 2018). Osteogenesis (Baryawno et al., 2019; Duarte et al., 2018; Kumar et al., 2018) and adipogenesis (Baryawno et al., 2019; Boyd et al., 2017) were also found to be impaired in mouse models. Similarly, alterations in BM stromal cells have been described in AML patients, including impaired *in vitro* adipogenic and
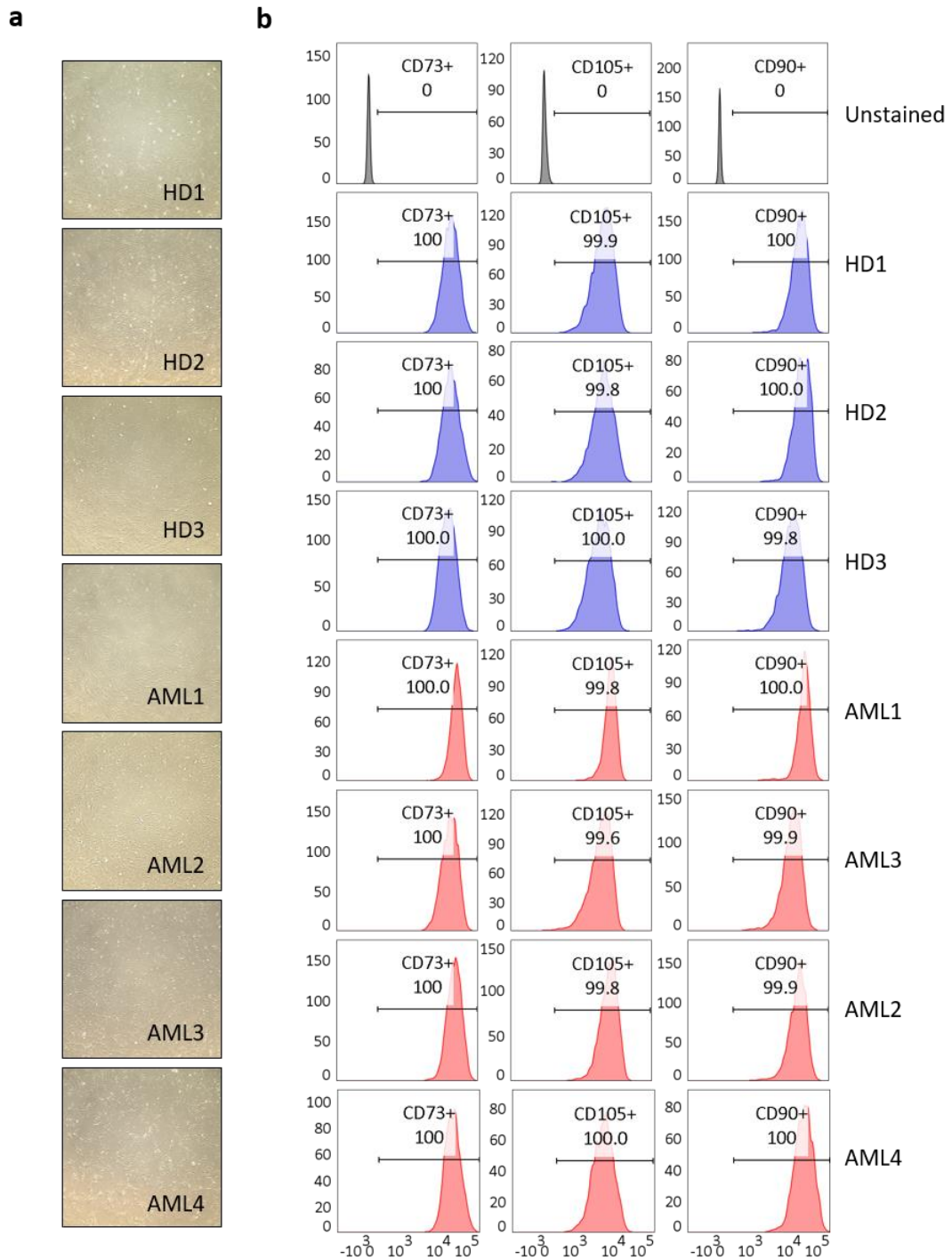
Figure 3.1: Characterisation of BM-derived MSCs. (a) *Representative pictures of fibroblasts-like shaped BM-derived MSCs from acute myeloid leukaemia patients (AML) or from healthy donor (HD), taken with a bright-field microscope. (b) Histogram plots showing known MSC markers CD73, CD90 and CD105 (Dominici at al., 2006). Unstained cells were used as control to set the threshold for the analysis with flow cytometry.*

osteogenic differentiation (Azadniv et al., 2020; Battula et al., 2017; Bonilla et al., 2019; Boyd et al., 2017; Kumar et al., 2018). Furthermore, MSC derived from AML patients exhibit molecular and functional alterations, such as translocations, gene

expression modifications, reduced clonogenic potential, decreased proliferation, higher senescence, increased support of leukaemia growth, and imbalanced regulation of endogenous haematopoiesis (Azadniv et al., 2020; Battula et al., 2017; Blau et al., 2011; Bonilla et al., 2019; Chandran et al., 2015; Diaz de la Guardia et al., 2017; Geyh et al., 2016; Huang et al., 2015; Konopleva et al., 2002; Kornblau et al., 2018; Pievani et al., 2021). However, molecular mechanisms used by the malignant cells to alter and reshape the BM niche remain elusive and many unknowns remain, particularly in a human context. To shed light on the molecular basis of such changes, we focus on MSCs, which represent one of the main cellular components of the BM microenvironment and are essential for BM function. Within the BM niche, MSCs elicit a dual function being essential for the regulation of haematopoiesis, while also being able to give rise to other cellular entities, such as adipocytes and osteoblasts, that contribute to the integrity and function of the BM niche.

3.1. Characterisation of BM-derived MSCs

Human BM-derived MSCs from healthy donors (HD) and patients with acute myeloid leukaemia (AML) were isolated by plastic adherence and expanded in standard MSC culture conditions. Stable MSC cultures were generated from three healthy donor samples, while adherent cells were obtained from primary cultures of four AML patients (Table 2.1). Isolated MSCs from healthy donors and AML samples showed plastic adherence and the characteristic fibroblastic-shaped spindled morphology (Figure 3.1a) (Dominici et al., 2006). MSCs obtained were further characterised for surface antigen expression, in accordance with the criteria established by the International Society for Cellular Therapy (Dominici et al., 2006). All MSCs isolated from the BM of healthy donors and AML patients expressed mesenchymal stromal markers CD73, CD105 and CD90 as shown by histogram plots in Figure 3.1b. Unstained cells were used as a control to set the threshold for the analysis with flow cytometry. MSCs from healthy donor primary cultures were further evaluated for
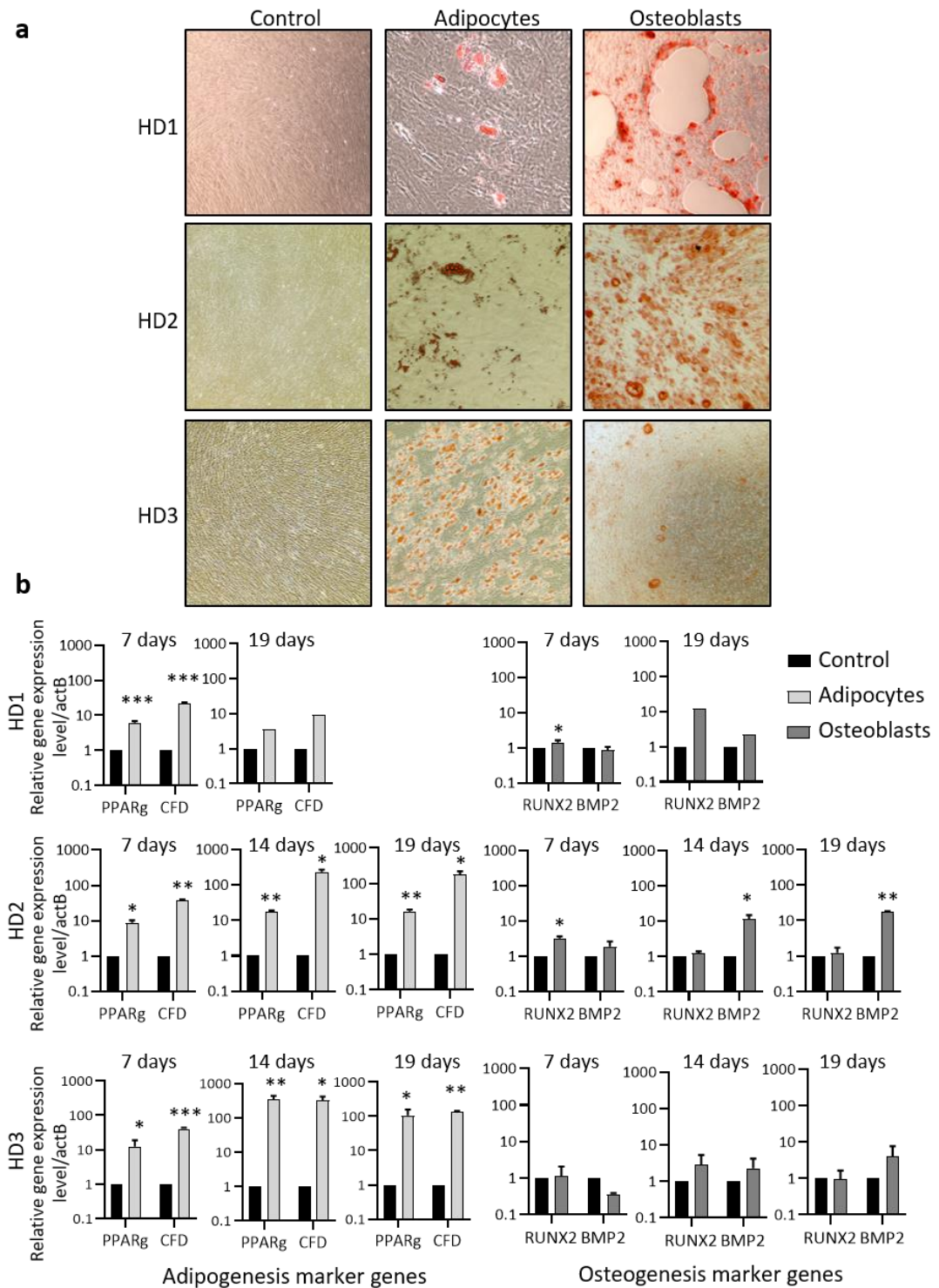
Figure 3.2: Differentiation of BM-derived MSCs. (a) *Picture taken with a bright-field microscope of undifferentiated control MSCs, adipocytes and osteoblasts from three different heathy donor BM samples after 3 weeks culture using normal MSC, adipogenic or osteogenic medium, respectively. Adipocytes were stained with Oil Red O and osteoblast with Alizarin red. Undifferentiated MSC did not present any staining.* ***(b)*** *Expression at different time points of adipogenesis markers genes (PPARγ and CFD) and osteogenesis marker genes (RUNX2 and BMP2) of adipogenic-induced and osteogenic-induced MSCs respectively as compared to undifferentiated MSCs. Results represent average of 3 technical replicates, with the exception of day 19 from sample HD1. Y-axis is displayed in logarithmic scale. Asterisks, where indicated, are *p<0.05; **p<0.01; ***p<0.001; unpaired two-tailed t-test. All error bars indicate S.E.M.*

their osteogenic and adipogenic differentiation potential by culturing them for three weeks using standard *in vitro* tissue culture differentiating conditions (Dominici et al., 2006). Differentiation status was monitored through the assessment of differentiation markers genes' expression (Table 2.2) at different time points (days 7, 14, and 19), while successful differentiation was confirmed through chemical staining at day 21. Markers genes of adipogenesis and osteogenesis were selected based on commonly used genes in the literature and validated on induced MSCs and/or on cell lines reportedly to express the target genes according to the human atlas website (https://www.proteinatlas.org/). All the tested MSC cultures were capable to form osteoblasts, as proven by the increased overtime expression of osteogenic-lineage-associated genes such as *RUNX2* and *BMP2* (Figure 3.2b & Table 2.2) (Hamamura & Yokota, 2007; Pinho et al., 2013). Osteogenic-induced cells showed changes in cell morphology, from spindle-shaped to cuboidal-shaped, with the formation of gaps in the cell layer (Figure 3.2a). The osteoblasts formed aggregates of calcium deposits, confirmed by alizarin staining (Figure 3.2a). Adipogenic-induced MSCs expressed adipogenic-lineage-associated genes such as *PPARγ* and *CFD* (Figure 3.2b & Table 2.2) (Boyd et al., 2017; Pinho et al., 2013). The adipocyte's ability to form lipids was demonstrated by staining the vacuoles using Oil Red O (Figure 3.2a). It is important to note that differences were evident both qualitatively and quantitatively between MSCs from different healthy donors, highlighting heterogeneity between primary human samples. Overall, the adherence to the plastic surface, surface marker expression and differentiation capability (Dominici et al., 2006), demonstrate that bona fide MSC cultures could be successfully derived.

3.2. AML growth alters MSC transcriptional program

To assess the dynamic molecular changes of the MSC niche under AML development and better understand the mechanisms of leukaemogenesis within the BM niche, the
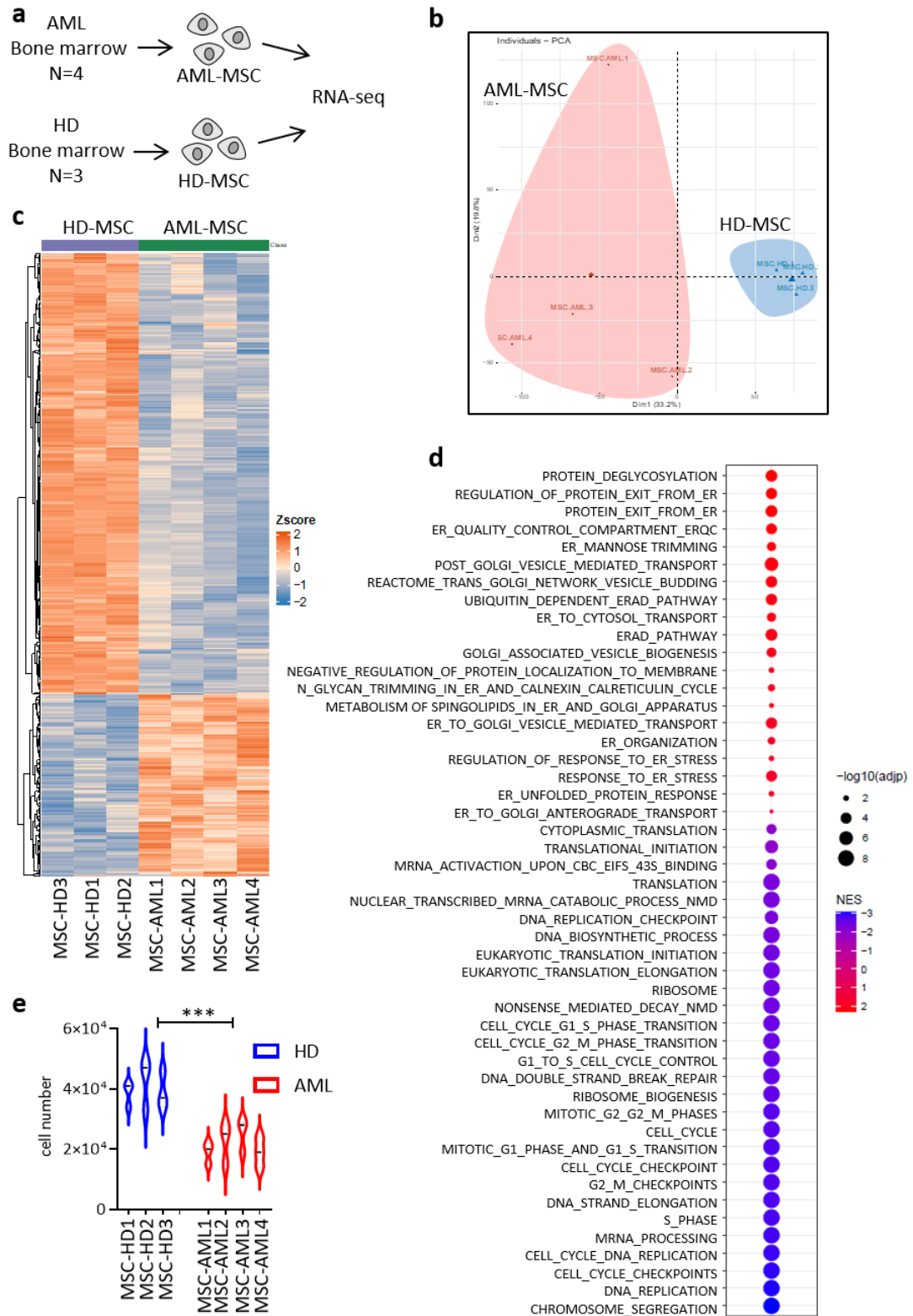
Figure 3.3: AML alters the MSC transcriptional programme. (a) *Human BM-derived MSCs from three healthy donors (HD) and four acute myeloid leukaemia (AML) patients were isolated by standard MSC isolation protocol and analysed with RNA-seq at passage p3. **(b)** Principle component analysis (PCA) plot of HD-MSCs and AML-MSCs. **(c)** Heatmap showing hierarchical clustering of differentially expressed genes in AML-MSCs compared to healthy donor MSCs. **(d)** Dot plots of GSEA showing positive or negative normalized enrichment scores (NES) in AML-MSCs compared to healthy donor MSCs. **(e)** Violin plot showing cell proliferation analysis of HD-MSCs and AML-MSCs upon one week of culture in standard MSC culture conditions. Asterisks, where indicated, are *p<0.05; **p<0.01; ***p<0.001; unpaired two-tailed t-test. All error bars indicate S.E.M.*

transcriptome of three healthy MSCs and four MSCs from the BM of AML patients at the passage p3 expansion stage was analysed via RNA sequencing (Figure 3.3a). Unbiased principal component analysis (PCA) (Figure 3.3b) and heatmap of differentially expressed genes (Figure 3.3c) differentiated AML-MSCs from their healthy counterparts, indicating disease-specific transcriptional modulation. While the PCA revealed a tight clustering among HD-MSCs, AML-MSCs were more transcriptionally distinct, suggestive of disease heterogeneity. Nonetheless, analyses of biological processes and cellular functions allowed us to determine specific functional features of AML-MSCs, with the most up-regulated pathways being involved in endoplasmic reticulum (ER) biology and ER stress-related processes, including significant upregulation of the ER stress pathway called unfolded protein response (UPR), while protein translation and mRNA processes were downregulated (Figure 3.3d). Further gene set enrichment analysis (GSEA) of the global RNA-seq datasets identified genes involved in multiple aspects of the cell cycle pathway and DNA replication (Figure 3.3d) as preferentially downregulated in AML-MSCs. This was reflective of a slower *in vitro* kinetic and reduced proliferative capacities of AML-MSCs compared to their healthy counterparts, as shown by the cell proliferation analysis (Figure 3.3e).

3.3. AML growth alters MSC proteome and phosphoproteome

The transcriptomic data unravelled molecular insights into MSCs response to the presence of AML within the BM. To have a complete picture of the molecular changes occurring in MSCs retrieved from AML patients, proteomic and phosphoproteomic analyses on the four AML-MSCs and the three HD-MSCs were also performed (Figure 3.4a). AML-MSCs presented with more downregulated protein as compared to their healthy counterparts (Figure 3.4b), which is in agreement with the downregulated protein translation pathways observed in the transcriptomic data (Figure 3.3d).
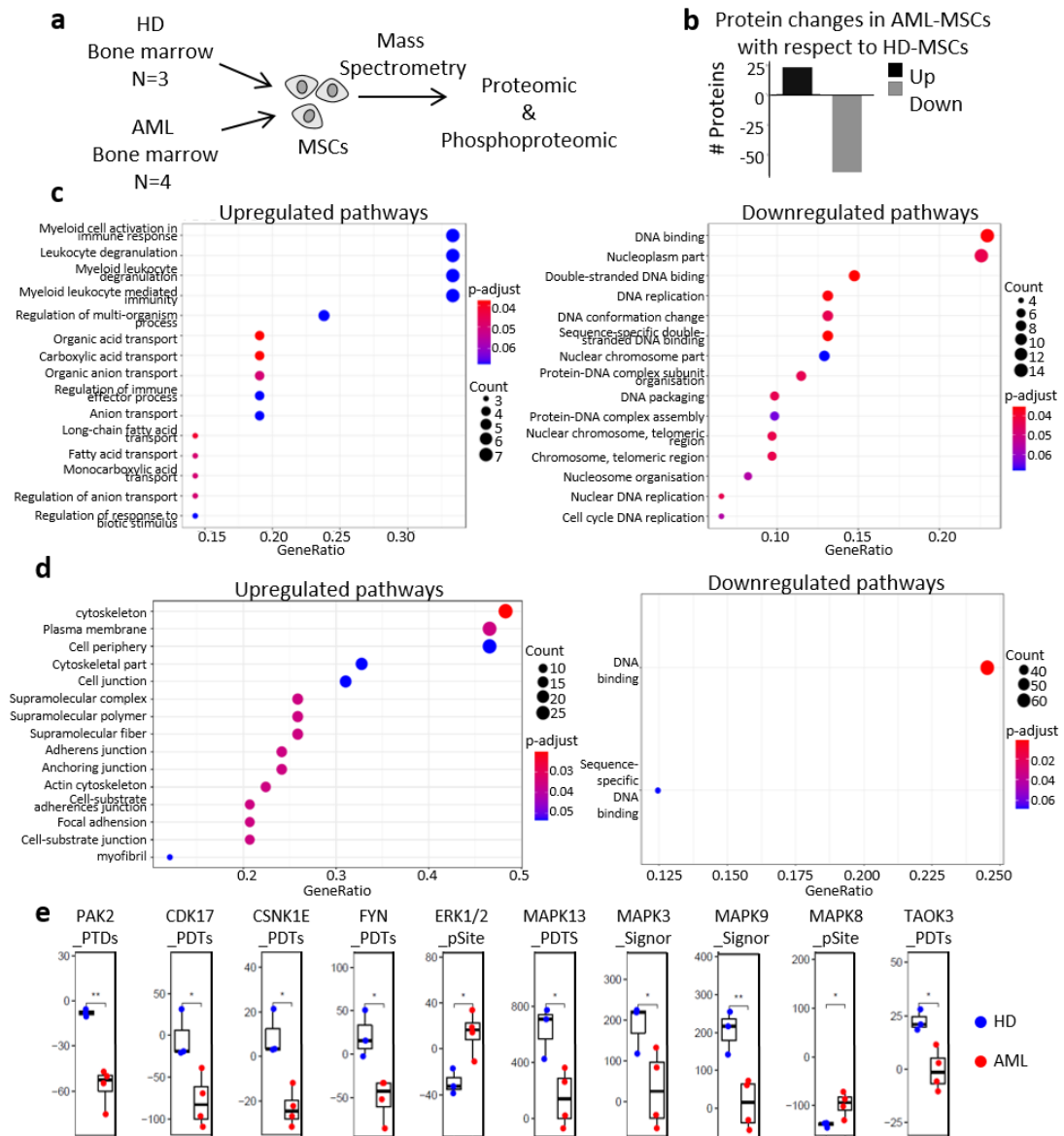
Figure 3.4: AML alters MSC proteome and phosphoproteome. (a) *Human BM-derived MSCs from three healthy donors (HD) and four acute myeloid leukaemia (AML) patients were isolated by standard MSC isolation protocol and analysed with proteomic and phosphoproteomic at passage p3.* **(b)** *Total protein changes in AML-MSCs as compared to HD-MSCs.* **(c)** *Gene ontology analysis based on differentially expressed proteins in AML-MSCs compared to HD-MSCs, showing upregulated and downregulated pathways. The X-axis is the ratio of the number of DE proteins in the corresponding pathway to the number of total proteins identified in the pathway. The greater the value, the higher the enrichment degree of the DE proteins in the pathway. The colour of the points represent the p-value of the hypergeometric test. The redder the colour, the smaller the value, indicating that the reliability of the test is greater and more statistically significant. The size of the dot represents the number of DE proteins in the corresponding pathway.* **(d)** *Gene ontology analysis based on global phosphoproteomic data showing upregulated and downregulated pathways in AML-MSCs compared to HD-MSCs.* **(e)** *Kinase activity kinase based on kinase-substrate enrichment analysis (KSEA) on global phosphoproteomic data.*

Furthermore, gene ontology analysis of global proteome identified pathways involved in the cell cycle and DNA replication as preferentially downregulated in AML-MSCs (Figure 3.4c), recapitulating again the transcriptomic data (Figure 3.3). Similarly, global phosphoproteomic analysis by mass spectrometry showed a downregulation of DNA repair and DNA binding in AML-MSCs (Figure 3.4d) and a decrease in the kinase activity of pro-survival kinases involved in cell growth, DNA replication and cell differentiation such as MAPK3, MAPK13, PAK2 and CSNK1E (Figure 3.4e). Overall, these data advocate for the remodelling of MSC proteome and phosphoproteome upon AML growth, with a downregulation of cell survival pathways.

Chapter 4

Results

Investigating the role of ER stress and UPR activation in the AML BM microenvironment

Chapter 3 provided experimental evidence that AML alters human mesenchymal stromal cells (MSC) transcriptome and proteome, complementing recent findings in mouse models that shows AML-induced molecular alterations in different compartments of the murine BM niche (Baryawno et al., 2019; Passaro et al., 2021; Tikhonova et al., 2019). However, the molecular mechanisms remain elusive, particularly in a human context. We hypothesized that AML propagation induces stresses, such as oxidative stress, starvation or hypoxia, that lead to endoplasmic reticulum (ER) stress in the BM niche, ultimately leading to the BM failure observed in patients. In Figure 3.3, the gene ontology analysis performed on MSC isolated from the BM of AML patients showed a positive enrichment of endoplasmic reticulum (ER) biology-related pathways and ER stress, with an upregulation of the unfolded protein response (UPR), as compared to MSC isolated from the BM of healthy donors. As mentioned in the introduction (Chapter 1.3.3), the UPR is a conserved stress cellular response originating in the ER and is regulated by three transmembrane sensors residing in the ER: protein kinase RNA (PKR)-like endoplasmic reticulum kinase (PERK), inositol-requiring enzyme 1 (IRE1), and activating transcription factor 6 (ATF6) (Figure 1.9) (Hetz, 2012). In homeostatic conditions, the lumenal domain of PERK, IRE1 and ATF6 binds a chaperone protein called binding immunoglobulin protein (BiP) or glucose-regulated protein 78-kDa (GRP78), which keeps the three proteins in an inactive state. Following the ER stress induction, BiP is released leading to dimerization and trans-auto-phosphorylation of the cytosolic domains of IRE1 and PERK and triggering their activation. Once activated, the IRE1 RNase domain

catalyses the splicing of X-box binding protein-1 (XBP1) mRNA resulting in spliced XBP1 protein (XBP1s) that translocates to the nucleus and regulates the transcription of UPR target genes. PERK phosphorylates the eIF2α inhibiting its activity and leading to global attenuation of protein translation while allowing the selective translation of some proteins, including the activation transcription factor 4 (ATF4). BiP decoupling from the sensors also leads to ATF6 translocation to the Golgi where it is proteolytically cleaved to release the cytosolic fragment, ATF6f, which translocates to the nucleus and activates the transcription of target genes. Collectively, UPR activation governs several biological pathways including lipid metabolism, cell cycle and apoptosis, while inducing attenuation of protein translation.
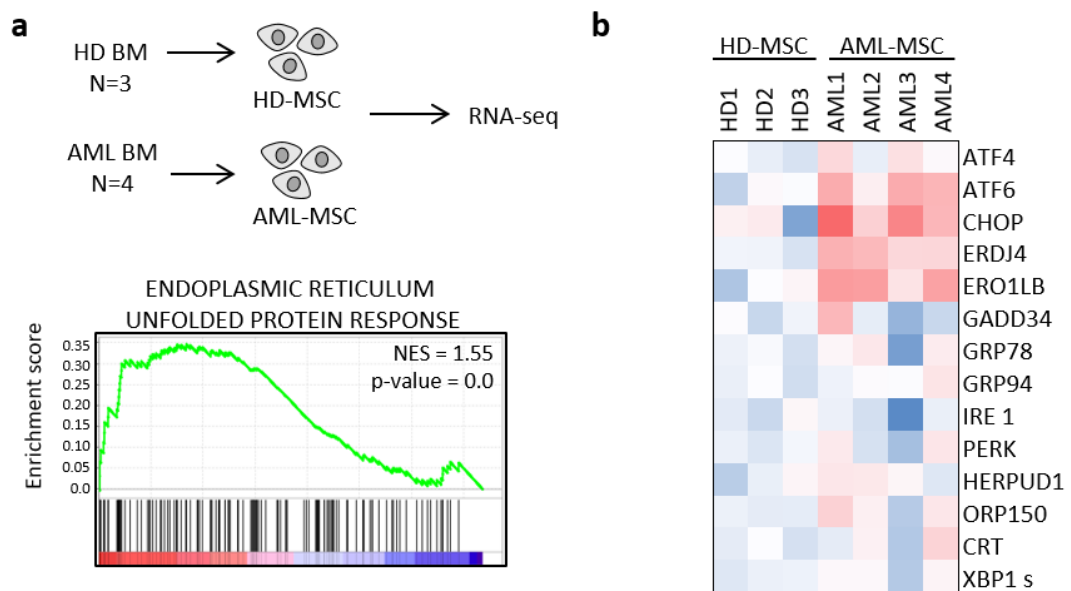
Figure 4.1: AML induces an ER stress signature in MSCs. (a) *Human MSCs were isolated from the BM of four AML patients (AML BM; AML-MSC) and three healthy donors (HD BM; HD-MSC) by standard MSC isolation protocol and analysed with RNA-sequencing. The GSEA revealed an upregulation of unfolded protein response (UPR) [gene set M22993] in AML-MSCs as compared to HD-MSCs.* ***(b)*** *Heat map shows differentially regulated UPR-related genes measured by qPCR in AML-MSCs and HD-MSCs at passage 2, showing upregulation of the genes in AML-MSCs.*

4.1 ER stress and UPR activation in the AML BM microenvironment

4.1.1. AML growth induces ER stress and UPR activation in MSCs

After showing an upregulation of the UPR pathway in MSC isolated from the BM of AML patients (Figure 3.3d and 4.1a), I thought to validate RNA-seq data and study AML-induced UPR activation in MSCs. For this purpose, I assembled an RT-qPCR survey panel of established UPR-target genes (Table 2.2) (Rouault-Pierre et al., 2013;
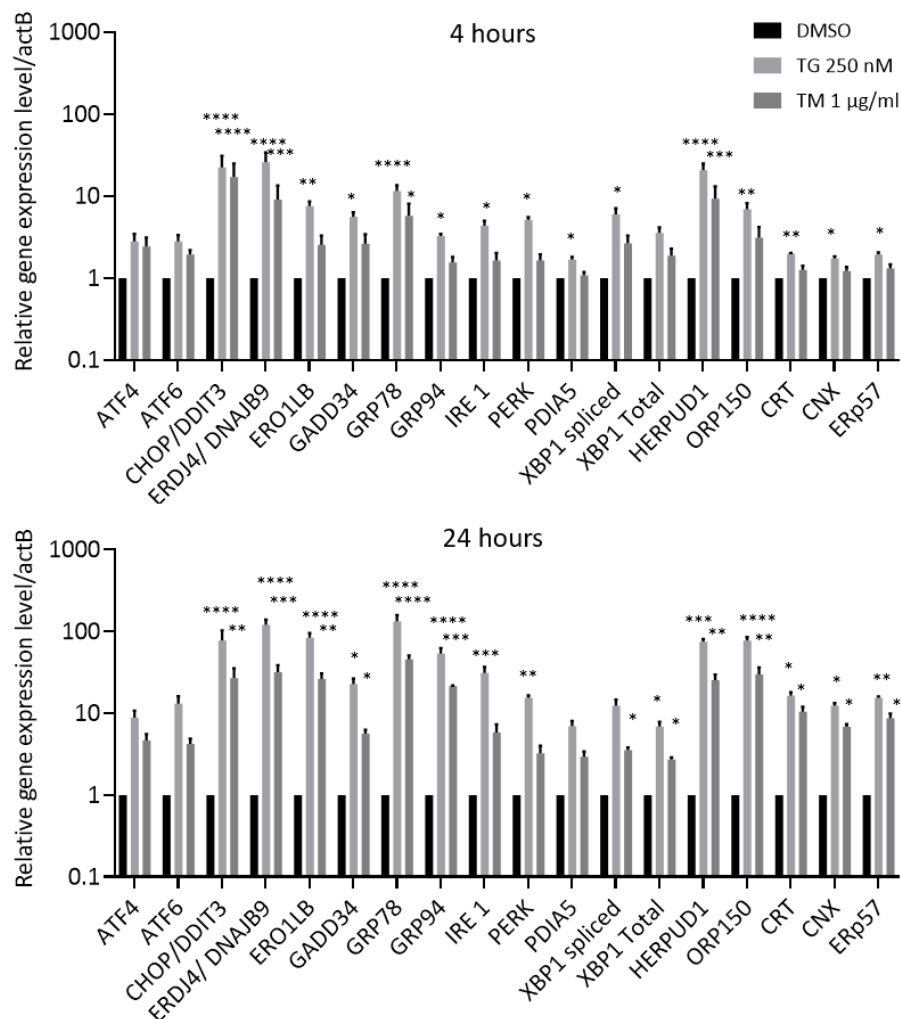
Figure 4.2: UPR-related genes qPCR panel validation. *mRNA levels for UPR-related genes measured by qPCR in MSC treated for 4 hours and 24 hours with 250 nM Thapsigargin (TG) or 1µg/ml Tunicamycin (TM). mRNA levels are expressed as fold-change relative to vehicle (DMSO 0.1%)-treated cells. Results are shown as mean S.D. of three bone marrow MSC samples (HD1, HD2, HD3). Y-axis is displayed in logarithmic scale. All error bars indicate S.D.*

van Galen et al., 2018; Van Galen et al., 2014). The panel was first validated by using

two chemical ER stress inducers, thapsigargin and tunicamycin (Figure 4.2). Thapsigargin (TG) disrupts calcium (Ca2$^+$) homeostasis in the ER by inhibiting the Sarco/endoplasmic reticulum Ca2$^+$ ATPase (SERCA) pump, rapidly activating all three branches of the UPR, while tunicamycin (TM) blocks the synthesis of N-linked glycoproteins, causing accumulation of unfolded proteins in the ER. Healthy donor MSCs (HD-MSC) were treated with the two ER stress inducers for 4 or 24 hours, to measure early and late UPR (Chapter 1.3.3). MSCs showed a distinct UPR response to the two stressors, being more sensitive to thapsigargin (TG) than tunicamycin (TM) (Figure 4.2). I then used this RT-qPCR panel on MSCs isolated from the BM of AML patients (AML BM) and healthy donors (HD BM) by standard MSC isolation protocol. The heatmap in figure 4.1b shows a widespread overexpression of the well-known UPR target genes in AML-MSCs across all samples, as compared to HD-MSCs, indicating that AML induces an ER stress signature in MSCs, thereby validating RNA-seq findings. Similar to RNA-seq analysis (Figure 3.3), the qPCR analysis revealed some differences across AML-MSCs samples, indicative of patient heterogeneity.

To model the BM niche *in vitro* during AML expansion and recapitulate these findings, I developed a 2D co-culture system where MSCs from healthy donors (HD-MSC) are exposed to AML patients' or healthy donors' primary cells for three weeks (Figure 4.3a) (see also Supplementary Chapter 6.1). After three weeks and prior to further analysis, haematopoietic CD45$^+$ cells were depleted by immunomagnetic selection from the co-cultures to purify MSCs. Purity of CD45$^-$ MSCs fractions were assessed by flow cytometry and samples with 98-100% purity levels were selected for further analysis (Figure 4.3b). UPR activation was observed in healthy donor-derived MSCs upon co-culture with AML cells, as compared to cultures with healthy donor controls (Figure 4.3c), indicated by increased expression of CHOP and decreased expression of GADD34, downstream effectors of the PERK pathway, and by increased expression of XBP1s and ERdj4, downstream effectors of the IRE1 pathway. This indicated that AML specifically induces ER stress in MSCs. Of note, CD45$^+$ cells from healthy donors were more proliferative than CD45$^+$ AML cells, in the co-culture setting (Figure 4.3d),
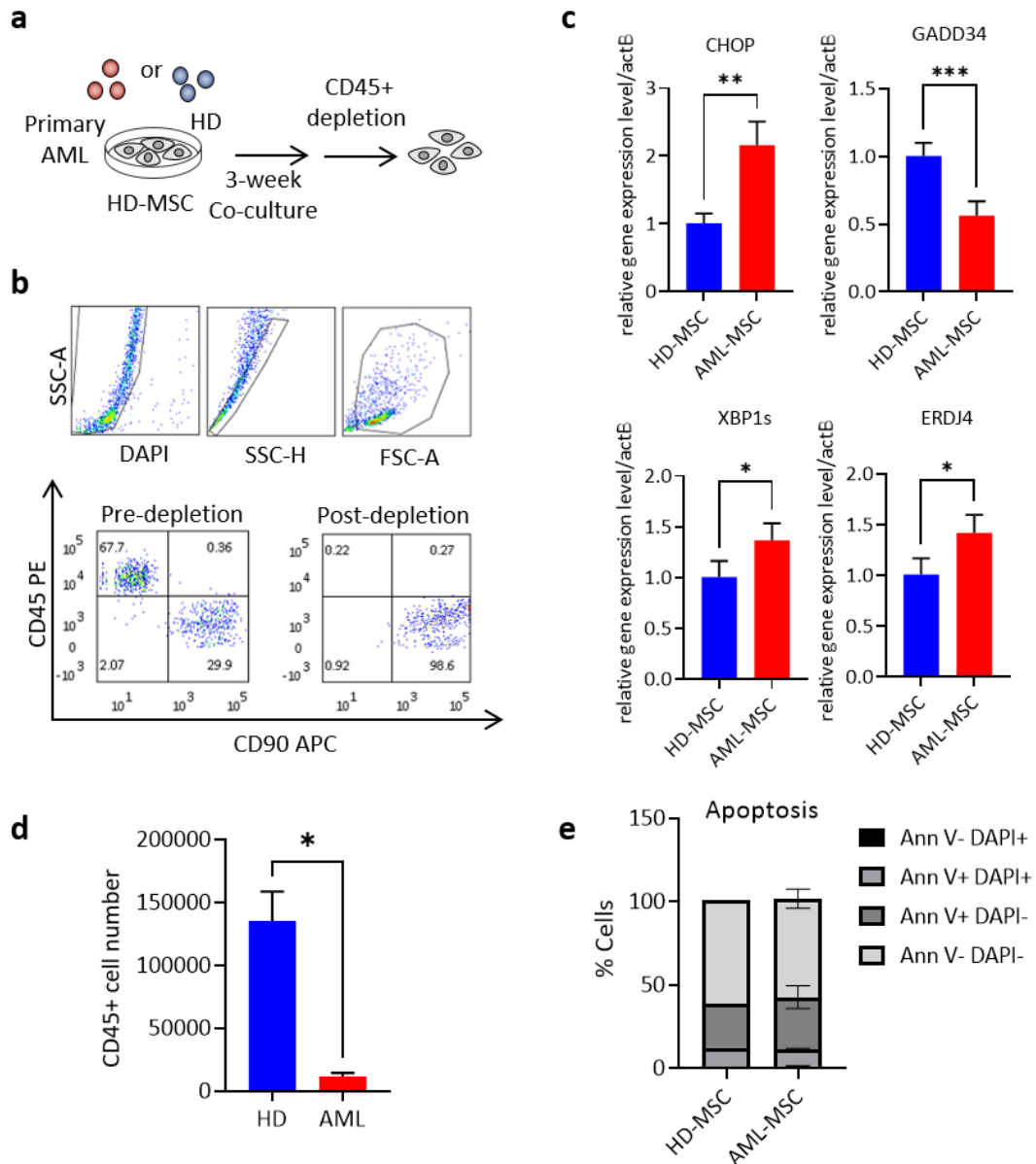
Figure 4.3: AML growth induces ER stress and UPR activation in in vitro. (a) *Schematic representation of the experimental outline of MSC co-cultures: healthy-donor MSCs (HD-MSCs) are co-cultured with 100,000 AML primary cells or 100,000 healthy donor (HD) CD34+ cord blood cells for three weeks. At the time point, hematopoietic CD45+ cell are depleted from the co-culture with immunomagnetic isolation to purify MSCs.* **(b)** *Gating strategy used to evaluate purity level of CD90+ MSC fractions after haematopoietic CD45+ cells depletion. Samples with CD90+ MSCs purity percentages >98% are selected for further analysis.* **(c)** *Bar plot showing mRNA levels of UPR-related genes measured by qPCR in HD-MSCs co-cultured with AML patients' cells (AML-MSC) or HD cord blood cells (HD-MSC) for three weeks. MSCs co-cultured with AML cells (AML-MSCs) showed a significant upregulation of several UPR target genes as compared to MSCs co-cultured with HD cells (HD-MSCs).* **(d)** *Cell numbers of HD or AML primary cells after three-week co-cultures with MSCs and CD45+ depletion. Haematopoietic CD45+ cells are counted by using counting beads during flow cytometry analysis of the CD45+ cells.* **(e)** *Apoptosis analysis of MSCs co-cultured respectively with HD (HD-MSCs) or AML primary samples (AML-MSCs) for three weeks, by measuring Annexin V+ levels. Y-axis is displayed in linear scale. Asterisks, where indicated, are *p<0.05; **p<0.01; ***p<0.001; **** p ≤ 0.0001; unpaired two-tailed t-test. All error bars indicate S.E.M.*

suggesting that ER stress activation in MSC cultured with AML cells cannot be accounted by density or nutrition deprivation. As UPR is a regulator of apoptosis, we wondered if ER stress induction of AML in MSC would lead to increase apoptosis in MSCs. As per Annexin V levels analysis, co-cultures with AMLs or with healthy donors did not induce apoptosis in MSC (Figure 4.3e).

To assess if AML growth could induce UPR activation in the BM microenvironment *in vivo*, we collaborated with Dr Diana Passaro (Institute Cochin, Paris) and curated data now published in (Passaro et al., 2021). In brief, patient-derived xenograft (PDX) models were generated by transplanting AML patients' cells or healthy donors' CD34^{+} blood cells in NOD/SCID/IL2rγ-/- (NSG) mice. After 8 to 12 weeks, MSCs were isolated by flow cytometry (FACS) and profiled by RNA-seq (Figure 4.4). Gene set enrichment analysis (GSEA) showed a positive enrichment for unfolded protein response (UPR), in particular the PERK/ATF4 branch, supporting an ER stress signature in MSCs *in vivo*.
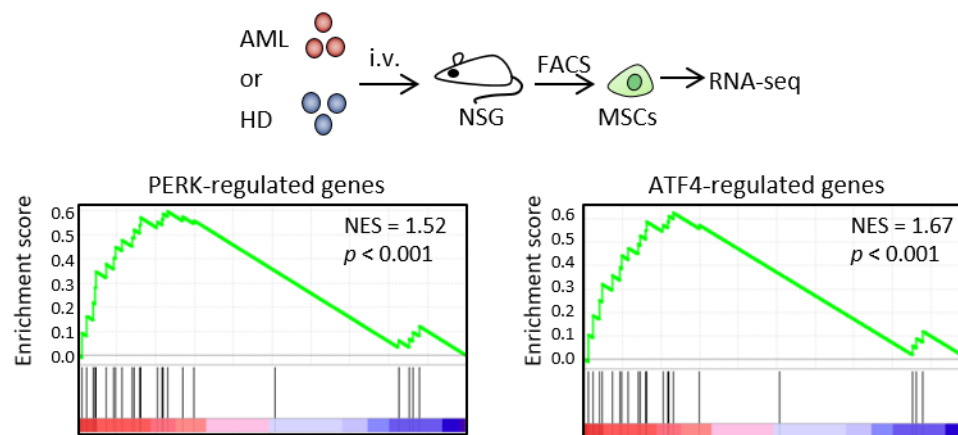
Figure 4.4: AML growth leads to ER stress and UPR activation in vivo. *AML patients' cells or healthy-donors' cord blood (CB) cells were transplanted into NOD/SCID/IL2rγ-/- (NSG) mice. After 8 to 12 weeks, mice were sacrificed and MSC populations were isolated by FACS and profiled by RNA-seq. GSEA a positive enrichment for the UPR branches PERK/ATF4 [PERK: gene set M792; ATF4: gene set: M796]. [NES: normalised enrichment score; p: nominal p-value].*

Overall, these results indicate that AML growth induces a specific ER stress signature in MSCs *in vivo* and that this signature is maintained *ex vivo*. Thus, ER stress activation can be recapitulated both *in vitro* and *in vivo*.

4.1.2.Differentiating MSCs activate UPR signalling

As mentioned in the introduction (Chapter 1.3.4), UPR signalling governs the activity of transcriptions factors involved in the differentiation of murine stromal cells into adipocytes and osteoblasts (H. Chen et al., 2016; Hamamura & Yokota, 2007; Han et al., 2013; Yang & Karsenty, 2004; K. Yu et al., 2014). To test if UPR signalling is involved in the adipogenesis and osteogenesis of human MSCs as well, I applied our established UPR target genes panel (Table 2.2 and Figure 4.2) to healthy donor MSCs grown in adipogenic and osteogenic differentiating conditions (Figure 3.2 and Figure 4.5a). This analysis revealed a widespread activation of UPR target genes in differentiating adipocytes at day 14, which slightly decreased when adipocytes reached maturation at day 19 (Figure 4.5b). Upregulation of UPR-targeted genes also occurred upon osteoblastic differentiation with a further increase at maturation at day 19 (Figure 4.5c). Interestingly, 24-hour treatment of healthy donor MSCs with ER stress inducers in standard MSC culturing conditions led to increased expression of various adipogenic marker genes, (*PPARγ*, *CFD*, *CEBPβ*, *CEBPα*, Figure 4.5d). Overall, these results suggest that UPR signalling governs the activity of these genes.
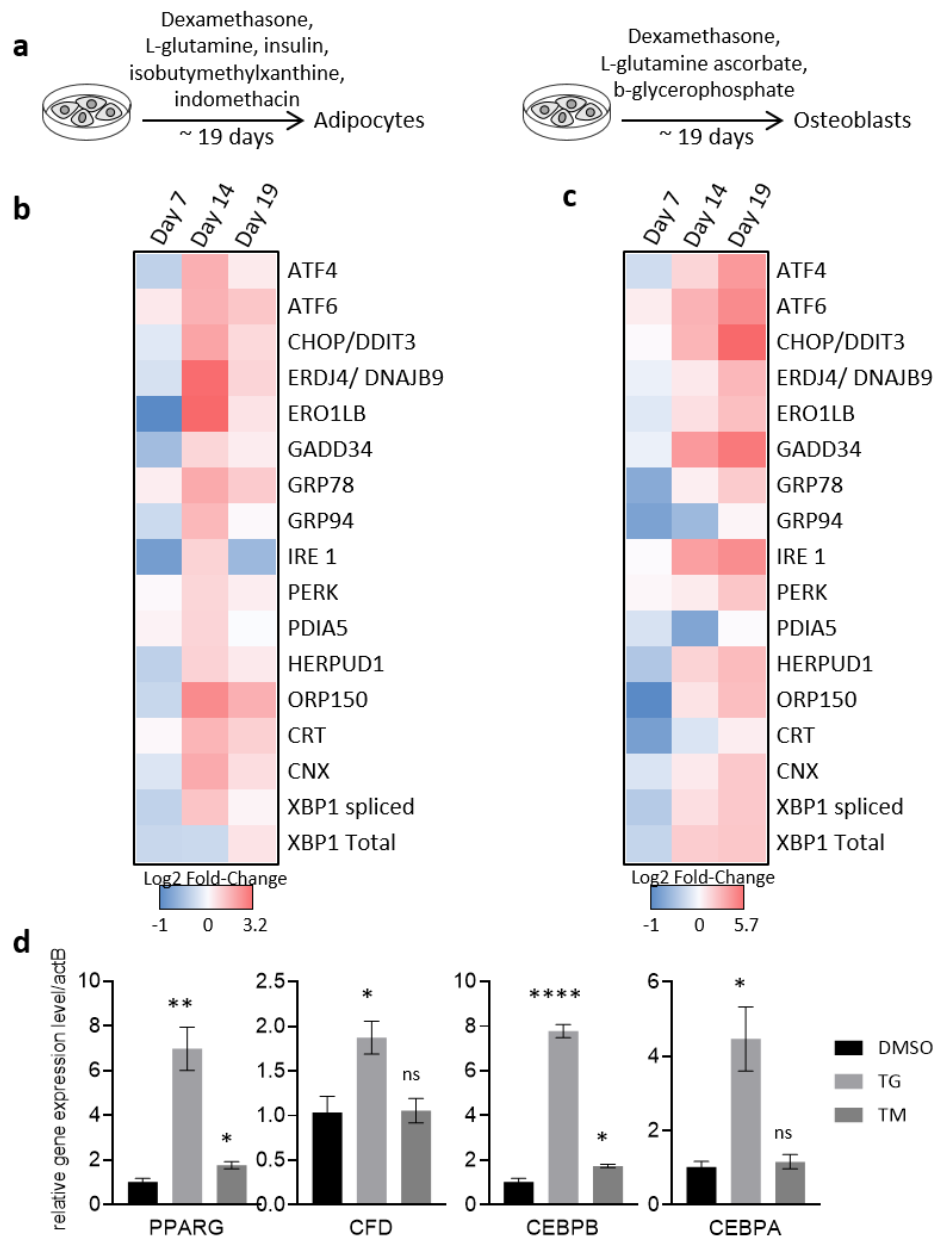
Figure 4.5: Differentiating MSCs activate ER stress and ER stress inducers activate adipogenic marker genes in MSCs. (a) Schematic representation of adipogenic and osteogenic differentiation of MSCs with the respective cocktails used. **(b-c)** Heat map with differentially regulated UPR-related genes during MSC adipogenic or osteogenic differentiation from three different biological replicates (HD1, HD2, HD3). Data are plotted as fold-change as compared to undifferentiated MSCs. **(b)** UPR activation was observed after 14 days of adipogenesis induction and declined at day 19. **(c)** UPR activation was observed after two and three weeks of osteogenesis induction. **(d)** Expression of adipogenesis markers genes (PPARγ, CFD, CEBPβ, CEBPα) in healthy donors MSCs treated with ER stress inducers, TG and TM, for 24 hours. MSCs treated with DMSO are used as controls. Results represent average of 3 technical replicates. Y-axis is displayed in linear scale. Asterisks, where indicated, are *p<0.05; **p<0.01; ***p<0.001; unpaired two-tailed t-test. All error bars indicate S.E.M.

4.1.3. Modelling UPR

I next sought to model UPR activation induced by AML in MSCs in order to investigate its effects on MSC homeostasis independently from any other stresses. To this purpose, each UPR arm was modelled by using a gain-of-function approach. Lentivirus-based bicistronic vectors were designed with a doxycycline (dox)-inducible system, enabling artificial and selective activation of one of the UPR branches (Figures 4.6 and 4.7). More specifically, the intraluminal ER sensor domains of PERK
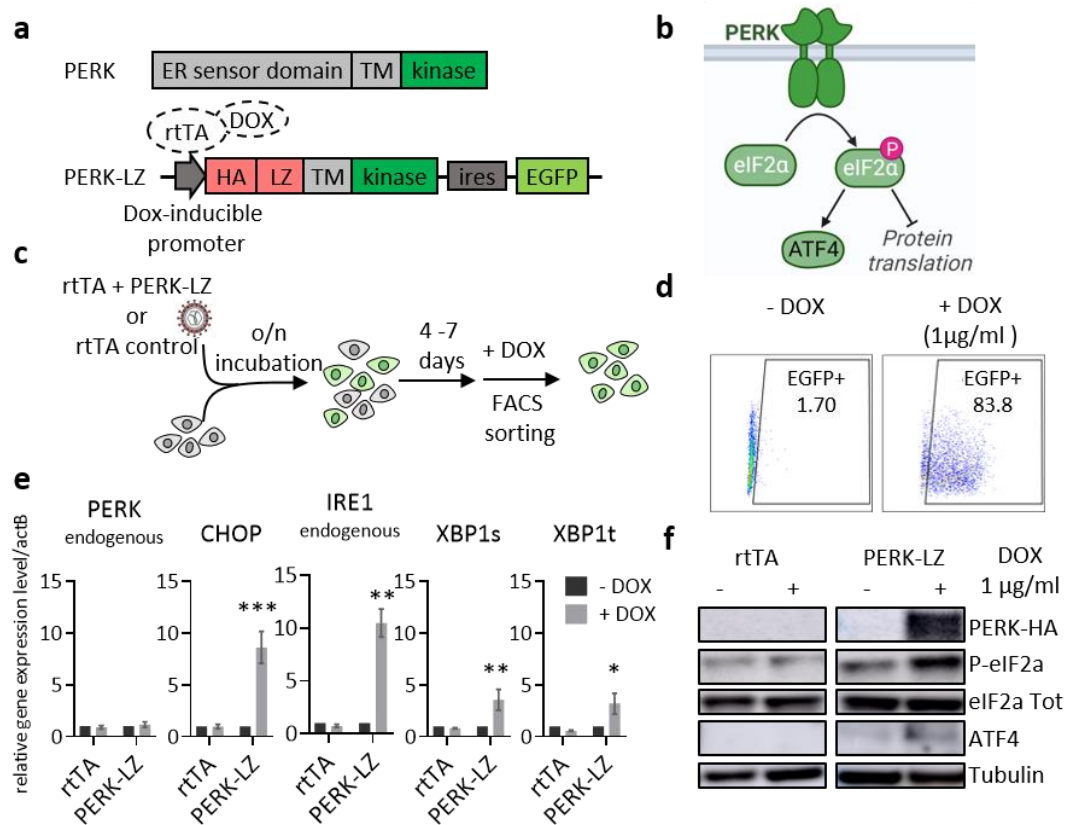
Figure 4.6: Generation and validation of PERK gain-of-function plasmid. (a) *Schematic representation of PERK sequence domains and of PERK gain-of-function plasmid (PERK-LZ).* ***(b)*** *Schematic representation of PERK arm signalling pathway.* ***(c)*** *Schematic representation of the workflow to transduce MSc with the gain-of-function plasmid: MSC are stably co-transduced with the trans-activator vector (rtTA) and PERK-LZ vector. After 3 to 4 days of expansion, cells are treated with dox to induce the recombinant protein and EGFP expression. Effectively transduced cells are then sorted on EGFP.* ***(d)*** *Dot plot showing EGFP+ cells upon 1μg/ml doxycycline treatment of successfully transduced MSCs with rtTA and PERK-LZ vectors (+DOX). Untreated transduced MSCs are used as controls (-DOX). Untransduced EGFP negative cells are used to set GFP thresholds (not shown).* ***(e)*** *qPCR analysis of mRNA levels of UPR genes and* ***(f)*** *western blot analysis of PERK-LZ (HA tag) and PERK targets ATF4 and P-eIF2a protein levels upon 1μg/ml dox treatment in MSCs transduced with both rtTA vector and PERK-LZ. Controls are represented by untreated MSCs transduced with both rtTA vector and PERK-LZ, and MSCs transduced with the rtTA vector alone, in presence or absence of doxycycline. All error bars indicate s.e.m. [TM: transmembrane domain; LZ: leucine-zipper domain; HA: Human influenza hemagglutinin (HA) tag; rtTA: reverse tetracycline-controlled transactivator; dox: doxycycline].*

and IRE1 were replaced by a c-Jun leucine zipper (LZ) fused to an HA-tag (PERK-LZ, IRE1-LZ). Thus, the addition of dox induces specific expression with subsequent dimerization and activation of the recombinant proteins, PERK-LZ or IRE1-LZ. EGFP, used as a reporter gene, was cloned after an internal ribosome entry site (IRES)-sequence, and its expression is induced upon dox treatment as well (Figure 4.6a and 4.7a). Validation of the constructs and doxycycline titration was performed on MSCs stably transduced with rtTA vector, expressing the dox-induced trans-activator, and one of the gain-of-function vectors, PERK-LZ (PERK-MSC, Figure 4.6) or IRE1-LZ (IRE1-MSC, Figure 4.7). MSCs stably transduced with the rtTA vector alone were used as controls (Figure 4.6c) (see also Supplementary Chapter 6.2).
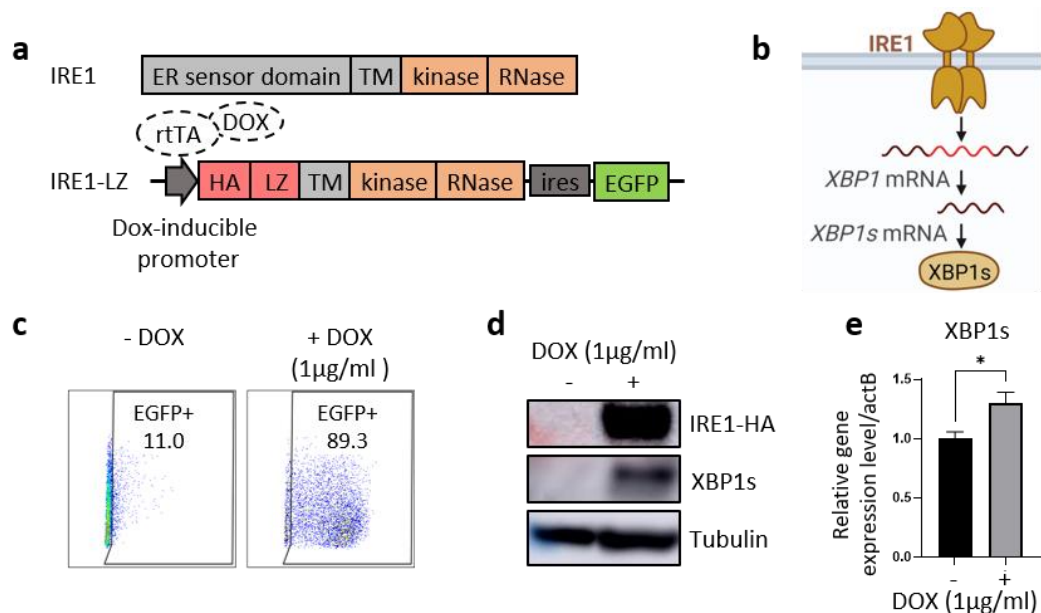
Figure 4.7: Generation and validation of IRE1 gain-of-function plasmid. (a) *Schematic representation of IRE1 sequence domains and of IRE1 gain-of-function plasmid (IRE1-LZ).* ***(b)*** *Schematic representation of IRE1 arm signalling pathway.* ***(c)*** *Dot plot showing GFP+ cells upon dox treatment of successfully transduced MSCs with rtTA and IRE1-LZ vectors (+DOX). Untreated transduced MSC are used as controls (-DOX). Untransduced GFP- cells are used to set GFP thresholds (not shown).* ***(d)*** *qPCR analysis of XBP1s and* ***(e)*** *Western blot analysis of IRE1-LZ (HA tag) and XBP1s protein levels upon dox treatment in MSCs transduced with both rtTA vector and IRE1-LZ as compared to untreated controls. All error bars indicate S.E.M. [TM: transmembrane domain; LZ: leucine-zipper domain; HA: Human influenza hemagglutinin (HA) tag; rtTA: reverse tetracycline-controlled transactivator; dox: doxycycline].*

Treatment with 1µg/ml dox, induced the expression of EGFP with both PERK-LZ and IRE1-LZ vectors (Figure 4.6d and 4.7c). Dox treatment of PERK-MSCs induced the expression of PERK-LZ (Figure 4.6f), detected with anti-HA antibody, and the expression of its target genes, as shown by western blot and qPCR analysis (Figure

4.6e and 4.6f). These were not expressed in dox absence. Given that the luminal domain in both PERK-LZ and IRE1-LZ was deleted and substituted with the LZ domain and the HA-tag, I designed primers specific for the luminal domain sequences of PERK and IRE1 to detect selectively the levels of the endogenous proteins. Dox treatment and PERK-LZ expression did not lead to increased expression of endogenous PERK, suggesting that CHOP and ATF4 induction and phosphorylation of eiF2α were mediated specifically by PERK-LZ. Of note, PERK-LZ activation led to increased expression of the endogenous IRE1 and XBP1s genes, suggesting a possible cross-talk between the two UPR branches, PERK and IRE1, a mechanism previously reported (Tsuru et al., 2016). Dox treatment of IRE1-MSCs induced the expression of IRE1-LZ (Figure 4.7d), detected with anti-HA antibody, and increased the expression of the IRE1 target XBP1s mRNA and protein (Figure 4.7d and 4.7e), which were not expressed in dox absence. These data show that UPR branch activation can be modelled with this approach.

4.1.4. PERK-MSCs have reduced proliferation capacities

I then used the gain-of-function vectors to study the effects of UPR activation on MSCs biology. PERK-MSCs showed reduced proliferative capacities with respect to IRE1-MSCs and rtTA-MSCs control, as shown by the cell proliferation assay (Figure 4.8a). Since UPR activation regulates apoptosis, I thought to test if the reduced cell number was due to increased apoptosis in PERK-MSC. To this purpose, I monitored cell toxicity and apoptosis by flow cytometry using Annexin V binding assay at days 1, 3 and 6-post dox treatment (Figure 4.8b). Surprisingly, less apoptosis was observed at day 1 upon PERK activation in MSCs compared to rtTA-MSCs controls. This effect was not seen at 3 and 6 where apoptotic levels of PERK-MSC, rtTA-MSCs and IRE1-MSCs are similar and show no differences, suggesting that apoptosis is not responsible for the decrease in cell numbers. Therefore, I asked whether a decrease in cell cycle could be responsible for the phenotype observed and tested the effects of PERK and IRE1 activation on MSCs cell cycle. We observed that PERK-LZ induced a cytostatic effect on MSCs, which significantly accumulated in the G0/1 phase of the cell cycle on day 1 and day 3 (Figure 4.8c). PERK-MSCs showed also a significant

reduction of cells in the S and G2/M phases at day 3, which could explain their reduced proliferative potential. Conversely, IRE1-MSCs showed a slight increase of cells in the S phase at day 1, as compared to both rtTA-MSCs and PERK-MSC. However, the number of cells in the S phase decreased at day 3, accompanied by an increase of cells in the G1/0 phase, although to a lesser extent compared to PERK-MSCs. Finally, phenotypic analysis of transduced MSCs showed an altered CD73 and CD105 expression on PERK-MSC at different time points (Figure 4.8d). Overall, PERK activation but not IRE1 alters MSC biology and identity. Despite ectopic PERK expression inducing endogenous IRE1 and XBP1s expression (Figure 4.6e), this activation does not seem to be relevant to rescue the phenotype.
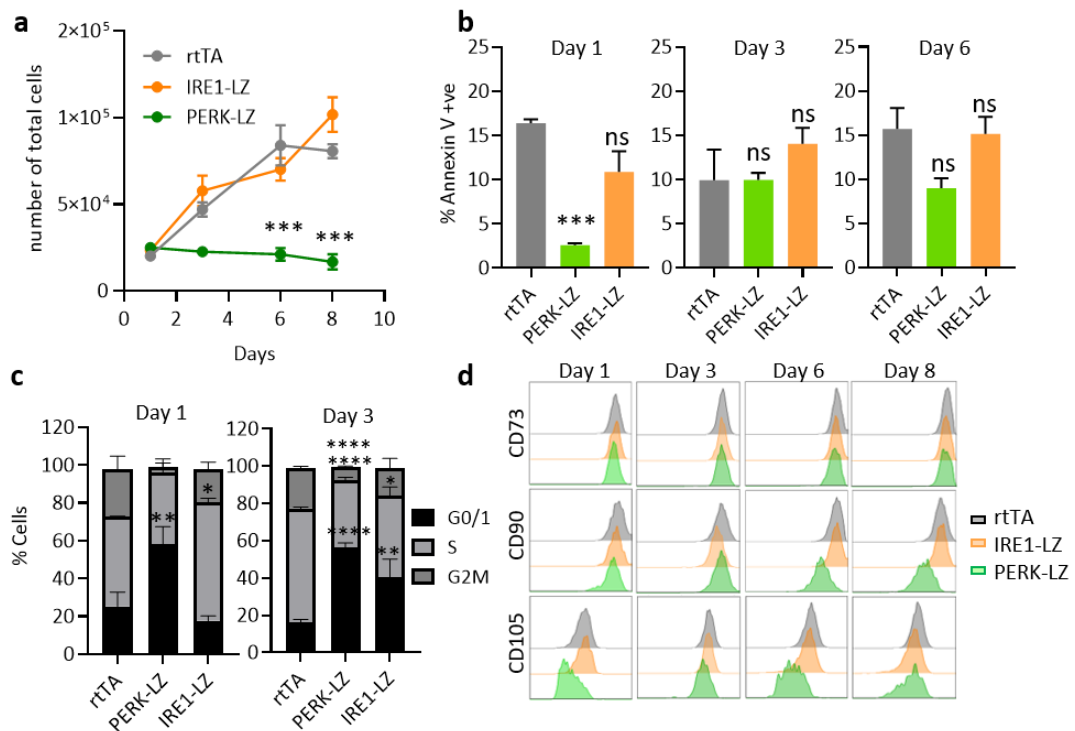
Figure 4.8: PERK-LZ reduces MSC proliferation and induces a cytostatic effect on MSCs. *rtTA-MSCs (rtTA), IRE1-MSCs (IRE1-LZ) and PERK-MSC (PERK-LZ) were treated with 1µg/ml doxycycline and analysed for different phenotypes at several time points. **(a)** Cell proliferation assay by counting cells using trypan blue staining and haemocymeter. **(b)** Apoptosis analysis performed by quantifying percentage of Annexin V+ cells with flow-cytometry. **(c)** Cell cycle analysis of DAPI stained cells after fixation and permeabilisation. **(d)** Representative histograms plots showing known MSC markers CD73, CD90 and CD105 (Dominici at al., 2006). Unstained cells were used as control to set the threshold for the analysis with flow cytometry. Results represent average of 3 technical replicates. Asterisks, where indicated, are *p<0.05; **p<0.01; ***p<0.001; ****p<0.0001 with respect to rtTA controls; unpaired two-tailed t-test. All error bars indicate S.E.M. LZ: leucine-zipper domain; HA: Human influenza hemagglutinin (HA) tag; rtTA: reverse tetracycline-controlled transactivator.*

4.1.5. Ectopic expression of PERK but not IRE1 inhibits adipogenesis

Since MSCs can be differentiated into adipocytes and osteoblasts *in vitro* (Figures 3.2), and UPR activation was observed during the differentiation of healthy MSCs (Figures 4.5), I analysed the effect of PERK-LZ and IRE1-LZ overexpression on MSCs differentiation (Figures 4.9 and 4.10). To this end, transduced cells with either PERK-LZ or IRE1-LZ were grown in adipogenic media in the presence or absence of doxycycline (dox). Cells transduced with rtTA alone were used as transduction control while transduced cells grown in a normal MSC medium, in the presence or absence of doxycycline, were used as differentiation control. After 14 days of adipogenic induction, PERK-MSCs still expressed EGFP (Figure 4.9a) and PERK-downstream effectors (Figure 4.9b), indicating that PERK expression was stable over time. Increased expression of adipogenic marker genes, *PPARγ* and *CFD*, as compared to cells not induced for adipogenic differentiation indicated that adipogenesis induction was successful (Figure 4.9c). However, upon dox treatment PERK-MSC presented with a decrease in the formation of mature adipocytes (Figure 4.9d) and a decrease in Oil Red O staining, reflecting a reduction of their intracellular fat deposit (Figure 4.9d-e). Furthermore, PERK-MSCs had reduced expression of several adipogenic marker genes (Figure 4.9f) as compared to rtTA and dox-untreated PERK-MSC controls, overall suggesting that normal adipogenesis was disrupted. The inhibition of adipocytes differentiation recapitulates what can be observed through histological analysis of BM trephines samples from AML patients, where BM adipocytes frequency and size are dramatically reduced, compared to BM trephines obtained from healthy donors (HD) (Boyd et al., 2017) (Figure 4.9g).

Despite increased expression of IRE1 and its target XBP1s upon PERK-LZ induction (Figure 4.9b), ectopic overexpression of IRE1 with IRE1-LZ did not affect MSC adipogenesis potential to differentiate into mature adipocytes, and RT-qPCR of the adipogenic marker genes rtTA and IRE1-LZ showed similar profiles (Figure 4.10). This indicates that IRE1 overexpression does not alter adipogenesis in MSCs and that the loss of adipogenic potential upon PERK-LZ is independent of IRE1 signalling.
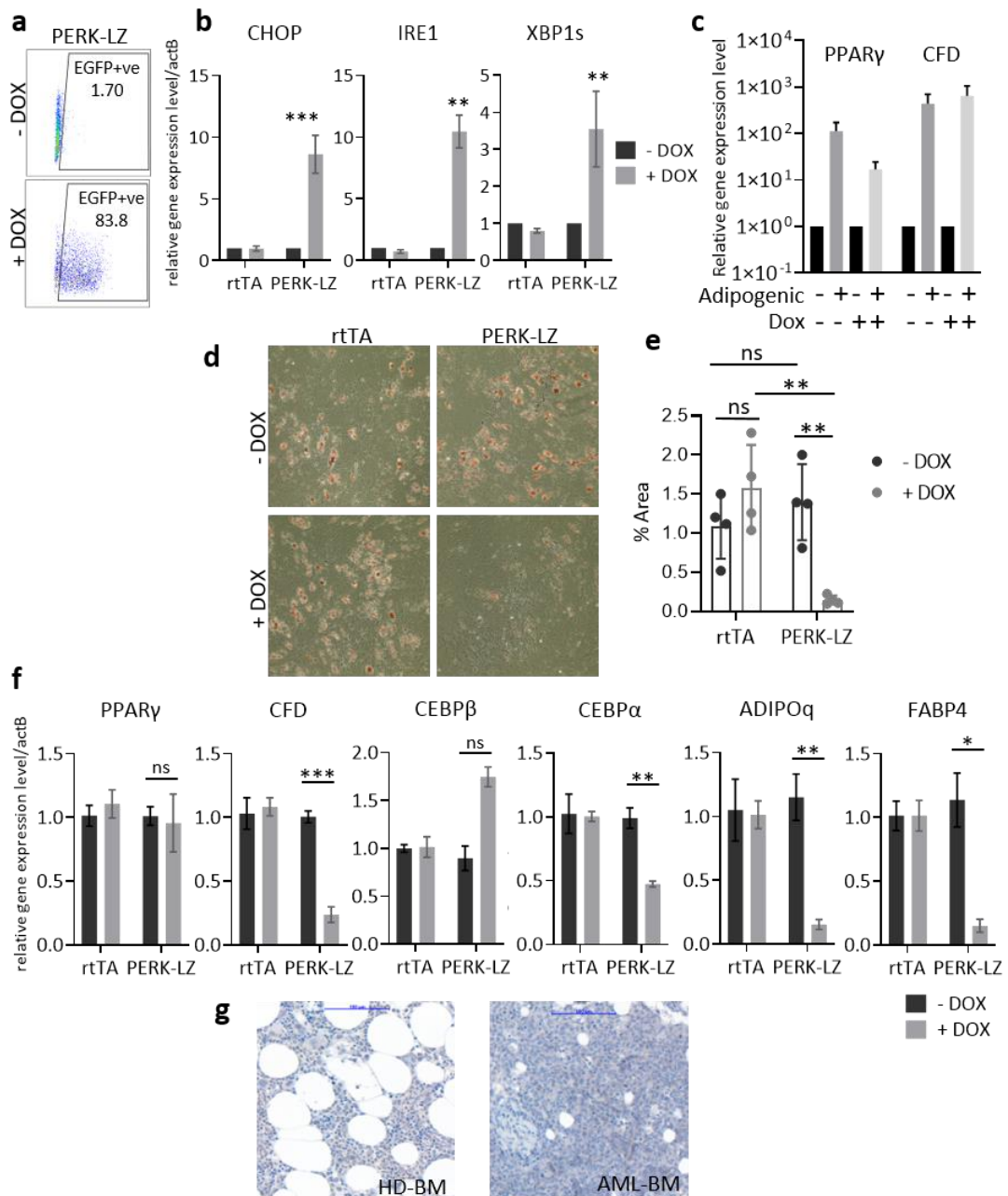
Figure 4.9: PERK-LZ inhibits adipogenic differentiation in MSCs. *PERK-MSCs or rtTA-MSCs were cultured in adipogenic standard conditions in presence or absence of 0.5 µg/ml doxycycline (DOX) for 19 days and differentiation status was assessed with expression of adipogenic marker genes at day 14 and Oil red O staining at day 19. **(a)** Representative dot-plots showing EGFP expression of PERK-MSC at day 14 of adipogenesis induction. **(b)** Histograms of PERK-target genes at day 14, showing activation of the pathway when PERK-LZ is induced with dox. Activation is not observed in dox-untreated PERK-MSCs nor in rtTA-MSCs controls. **(c)** Histograms of adipogenic marker genes PPARγ and CFD at day 14 in PERK-MSCs kept in adipogenic medium or normal medium. Increased expression of PPARγ and CFD in adipogenic-induced PERK-MSCs, presented as fold-change with respect to MSC not induced with adipogenic medium, indicates successful differentiation. **(d)** Picture of adipocytes taken with a bright-field microscope, after staining with Oil Red O. **(e)** Absolute quantification of Oil Red O staining using ImageJ. **(f)** Histograms of adipogenic marker genes at day 14 of PERK-MSCs and rtTA-MSCs, in dox presence (+DOX) or absence (-DOX). Data of dox-treated cells are presented as fold-change with respect to dox-untreated cells. **(g)** Haematoxylin staining of BM trephine slides from one healthy-donor BM sample and one AML-BM showing reduced adipocyte (white holes) frequency in AML BM trephine. Asterisks, where indicated, are *p<0.05; **p<0.01; ***p<0.001; ****p<0.0001; unpaired two-tailed t-test; results are shown as the mean ± SEM; ns: nonsignificant.*
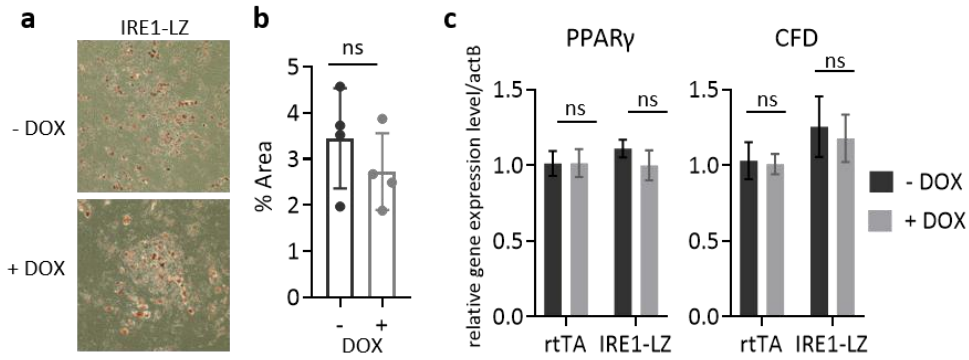
Figure 4.10: IRE1-LZ does not affect adipogenic differentiation in MSCs. *IRE1-MSCs or rtTA-MSCs were cultured in adipogenic standard conditions in presence or absence of 0.5 µg/ml doxycycline (dox) for 19 days. Differentiation status was assessed with marker genes (PPARγ and CFD) expression at day 14 and Oil red O staining at day 19.* ***(a)*** *Picture of adipocytes, stained with Oil Red O, taken with a bright-field microscope.* ***(b)*** *Absolute quantification of Oil Red O staining using ImageJ. Results represent average of two biological replicates.* ***(c)*** *Histograms of adipogenic marker genes PPARγ and CFD at day 14 of IRE1-MSCs kept in adipogenic medium in dox presence (Dox+) or absence (Dox-). Data represents 2 biological repeats and results are shown as the mean ± SEM; ns: nonsignificant.*

We next investigated the transcriptomic consequences of PERK ectopic expression in MSCs grown in adipogenic differentiation conditions. RNA sequencing of the adipogenic-induced PERK-MSCs confirmed increased expression of PERK as compared to rtTA-MSCs controls (Figure 4.11b), with the upregulation of ER stress and UPR (Figure 4.11c and d). Moreover, GSEA showed downregulation of adipogenic pathways in the PERK-MSCs cells, including PPARγ signalling, adipogenesis and fatty acid metabolism gene sets (Figure 4.11c and d) which is in agreement with the phenotype observed.

Conversely, when MSCs were cultured in osteogenic stimulating conditions, PERK or IRE1 induction did not seem to induce significant changes in their capacities to differentiate into osteoblasts (Figure 4.12). No morphological and phenotypic differences were observed in PERK-MSCs or IRE1-MSCs with respect to control cells, as showed by Alizarin staining quantification (Figure 4.12a-b) and analysis of *BMP2* and *RUNX2* marker genes expression (Figure 4.12c), with osteogenesis being successfully induced in all three conditions (Figure 4.12d).
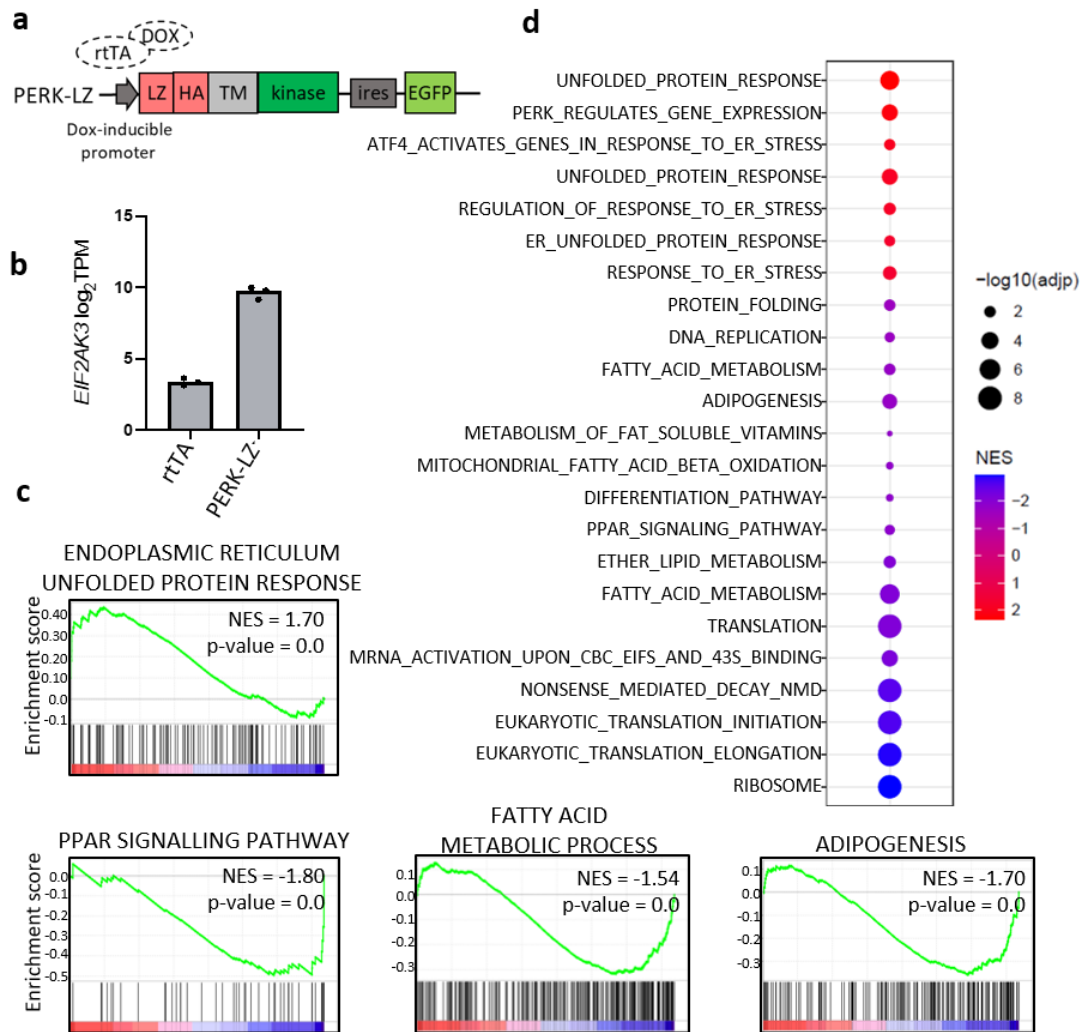
Figure 4.11: PERK-LZ ectopic expression suppress adipogenic pathways in MSCs. *PERK-MSCs and rtTA-MSCs were cultured in adipogenic standard conditions in presence of 1 µg/ml doxycycline (dox) for 19 days. RNA-seq analysis was performed at day 14. **(a)** Schematic representation of PERK-LZ gain-of-function vector. **(b)** Reads Per Kilobase Million (RPKM) of PERK transcript EIF2AK3 in PERK-MSC vs rtTA-MSC. **(c)** Gene set enrichment analysis (GSEA) plots showing upregulation of endoplasmic reticulum unfolded protein response and downregulation of adipogenesis, PPAR signalling, and fatty acid metabolism gene sets in PERK-MSCs compared to rtTA-MSCs when cultured in adipogenic media for 14 days. **(d)** Dot plots of GSEA showing normalized enrichment scores (NES) in PERK-MSCs compared to rtTA-MSCs when cultured in adipogenic media for 14 days.*
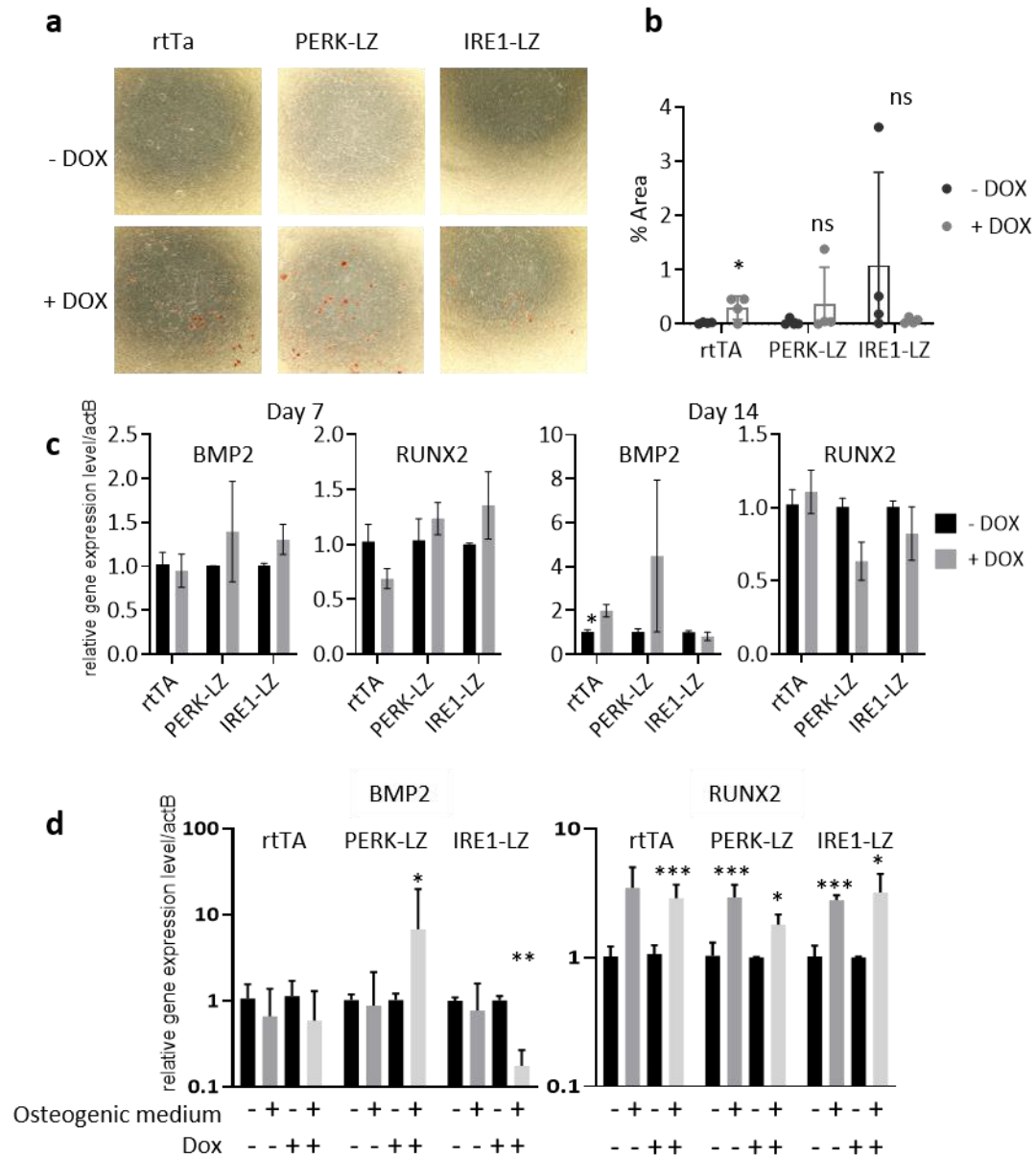
Figure 4.12: Ectopic expression of PERK or IRE1 does not affect osteogenesis differentiation in MSCs. *PERK-MSCs, IRE1-MSCs or rtTA-MSCs were cultured in osteogenic standard conditions in presence or absence of 0.5 µg/ml doxycycline (dox) for 19 days. Differentiation status was assessed with marker genes (BMP2 and RUNX2) expression at day 14 and Alizarin staining at day 19. **(a)** Picture of osteoblasts, stained with Alizarin, taken with a bright-field microscope. **(b)** Absolute quantification of Alizarin staining using ImageJ. Results represent average of two biological replicates. **(c)** Histograms of osteogenic marker genes BMP2 and RUNX2 at day 7 and day 14 of rtTA-MSCs, PERK-MSCs and IRE1-MSCs kept in osteogenic medium in dox presence (+ Dox) or absence (- Dox). Data represents 2 biological repeats. Y-axis in shown in linear scale. **(d)** Histograms of osteogenic marker genes BMP2 and RUNX2 at day 14 of cells kept in standard MSC culturing conditions or osteogenic medium, in presence or absence of dox. Y-axis in shown in logarithmic scale. Asterisks, where indicated, are *p<0.05; **p<0.01; ***p<0.001; ****p<0.0001; unpaired two-tailed t-test; results are shown as the mean ± SEM; ns: nonsignificant.*

4.1.6. GATA3 expression during ER stress and adipogenesis

I next sought mechanisms that could explain ER stress-induced reduction of adipogenesis. Adipogenesis is regulated by a complex and highly orchestrated gene expression program, which includes the upregulation of transcription factors of the C/EBP family and PPARγ (Chapter 1.1.2.3.) These, cooperatively interact to drive the expression of downstream genes necessary for the generation and maintenance of the adipogenic phenotype, such as genes involved in lipid metabolism and accumulation, and insulin sensitivity (Ambele et al., 2020; Christopher E. Lowe et al., 2011). GATA3, KLF1 and CHOP are, on the other hand, negative regulators of terminal adipogenesis and can be referred to as pre-adipocyte marker genes. These act as molecular gatekeepers that control the transition from pre-adipocytes to adipocytes. Evidence in murine cells suggests that GATA3 is upregulated in pre-adipocytes and negatively regulates PPARγ, thereby preventing cells from fully differentiating into adipocytes (Tong et al., 2000; Tong et al., 2005). Furthermore, GATA3 was found to be upregulated upon ER stress in human and murine pre-adipocytes (Tong et al., 2016), representing thus a good candidate for the adipogenesis decrease observed in our model. Indeed, 24-hour treatment with the ER stress inducers Thapsigargin (TG) and Tunicamycin (TM) induced *GATA3* expression in healthy donor MSCs (Figure 4.13a), recapitulating previous findings. However, the increase could only be observed at the transcriptomic level, while GATA3 protein levels could not be evaluated due to the weak signal on the blot. Although we could not detect a significant change in *GATA3* expression during the adipogenic differentiation of healthy donor MSCs at days 7, 14 and 19 of differentiation (Figure 4.13b), we observed a dramatic increase in GATA3 expression upon ectopic expression of PERK-LZ during adipogenic differentiation (Figure 4.13c). A similar increase did not occur upon expression of IRE1-LZ or in control rtTA-MSCs (Figure 4.13c). Due to the poor specificity of the antibody, an increase in GATA3 expression could not be evaluated at the protein level. The increase in GATA3 expression in adipogenic-induced PERK-MSCs could be also appreciated in our RNA-sequencing data, confirming the qPCR analysis (Figure 4.13d). Despite being still preliminary, these data seem to point for a GATA3 increase upon ER stress and advocate for further investigation of this

mechanism. Indeed, we could speculate that PERK expression blocks MSC in a pre-adipocytes state. Thereby MSCs express adipogenic marker genes (Figure 4.9c), but cannot complete the terminal differentiation into mature adipocytes (Figure 4.9) as *GATA3* expression is maintained high in an ER stress-dependent manner. However,
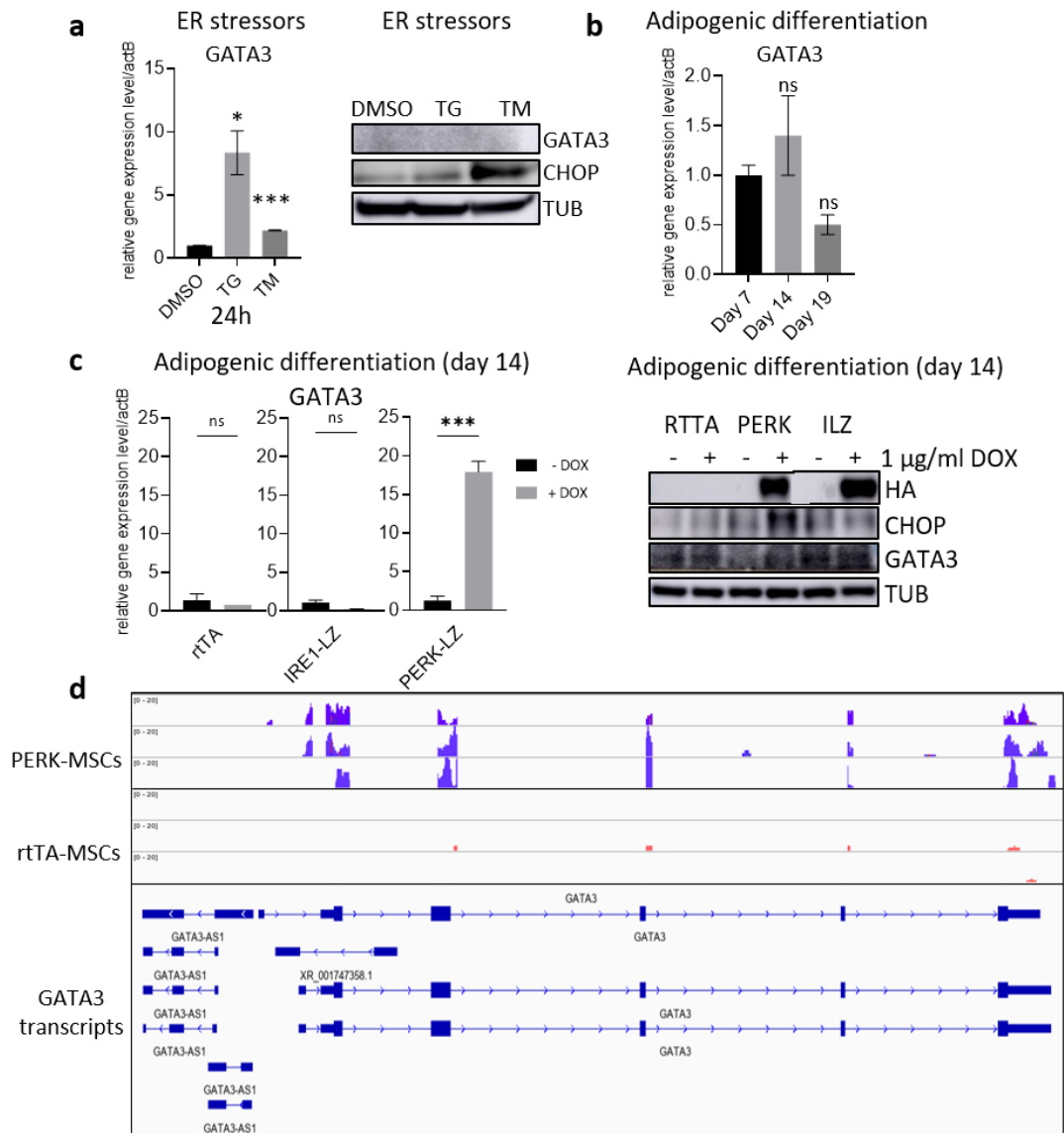
***Figure 4.13: GATA3 expression during ER stress activation. (a)** GATA3 mRNA levels measured by qPCR and western blot of GATA3 and PERK target CHOP protein levels in MSC treated for 24 hours with 250 nM Thapsigargin (TG) or 1µg/ml Tunicamycin (TM). Controls are represented by DMSO 0.1%-treated MSCs. **(b)** GATA3 mRNA levels measured by qPCR at different time points in HD-MSCs grown in adipogenic conditions. **(c)** GATA3 mRNA levels measured by qPCR and western blot analysis of GATA3, CHOP and HA-tag (PERK-LZ and IRE1-LZ) protein levels in PERK-MSCs, IRE1-MSCs and rtTA controls grown in adipogenic conditions for 14 days in presence or absence of 0.5 µg/ml dox. **(d)** Integrative Genomics Viewer (IGV) visualisation of sequencing coverage of GATA3 transcripts in PERK-MSCs or rtTA-MSCs treated with dox for 48 hours. Results are shown as mean S.E.M. Y-axis is displayed in linear scale. Asterisks are *p<0.05; **p<0.01; ***p<0.001; ****p<0.0001; ns: nonsignificant. [HA: Human influenza hemagglutinin tag; rtTA: reverse tetracycline-controlled transactivator; dox: doxycycline].*

it remains to be determined if GATA3 increased expression translates into a functional protein.

4.2. Effects of PERK activation in MSCs on haematopoiesis

Chapters 3 and 4.1 provided experimental evidence that AML growth alters MSC niche homeostasis, affecting their identity and compromising adipocytes maturation through UPR induction and activation of PERK. As mentioned in the Introduction (Chapter 1.1.2.1), MSCs integrity within the BM is essential for maintaining healthy and efficient haematopoiesis, as these cells provide essential signals, such as extracellular matrix (ECM) proteins, cytokines and growth factors that regulate HSC maintenance. Combined clinical and experimental model research demonstrated that AML impairs healthy haematopoiesis, by impeding haematopoietic stem cells differentiation, consequently inducing cytopenia and BM failure (Boyd et al., 2017; Miraki-Moud et al., 2013), one of the major causes of morbidity and mortality of leukaemia. However, it is still unclear whether AML cells directly inhibit normal haematopoiesis or whether this is mediated via alterations of the bone marrow microenvironment. This hypothesis of niche-induced haematopoiesis alterations is further corroborated by animal model results showing that specific modifications within the BM niche led to the development of haematological malignancies (Kode et al., 2014; Raaijmakers et al., 2010). For these reasons, understanding how changes within the MSC niche could affect haematopoiesis is essential to elucidate leukaemogenesis.

4.2.1. PERK expression in MSCs results in hematopoietic lineage skewing with increased myeloid cells *in vivo*

To determine whether PERK overexpression in MSCs could affect their capacity to support hematopoietic stem and progenitor cells (HSPCs) and regulate their function,

we used a humanized BM niche *in vivo* (Figure 4.14a; Passaro, Abarrategi, et al., 2017). Collagen-based scaffolds (also called organoids) were injected with human PERK-MSCs and human healthy cord blood (CB) CD34$^+$ HSPCs and subcutaneously implanted into immunodeficient mice. After six weeks to allow the development of the humanized BM niche (organoids) *in vivo*, the mice were fed with a doxycycline solution to induce the expression and activation of PERK. The mice were kept on the same doxycycline regimen for six weeks to mimic the effects of AML progression within the niche and to study the impact of these changes/alterations on hematopoietic stem and progenitor cells. Mice with rtTA-MSCs scaffolds were used as controls, along with mice fed with a solution that did not contain doxycycline. After six weeks of treatment, the mice were sacrificed to retrieve the organoids, the BM and the spleen. Samples were then analysed by flow cytometry to study the organoids' niche composition and the differentiation capabilities of HSPCs. Figure 4.14b shows that both human CD90$^+$ CD73$^+$ MSCs and mouse CD51$^+$ MSCs (that colonised the scaffold) contributed to the formation of the organoids, equally in both PERK-LZ and control mice. Furthermore, the organoids were, as expected, well vascularised by the murine CD31 endothelial cells, allowing the transport of oxygen and nutrients to the organoids. While PERK expression in MSCs had no significant effect on the total number of human haematopoietic CD45$^+$ cells within the organoids, it led to a shift towards myeloid lineage development, with PERK-MSCs being more supportive of CD33$^+$ myeloid cells (Figure 4.14b). This shift was accompanied by a compensatory although a non-significant decrease in the CD19$^+$ lymphocytes, while CD3$^+$ lymphocyte numbers remained unvaried between PERK-MSCs and control mice. Interestingly, although PERK expression in MSCs had no significant effect on the total number of CD45$^+$ cells within the organoids, more human CD45$^+$ cells colonised and engrafted the murine BM in PERK-MSCs mice. This finding suggests that ectopic expression of PERK within the niche might generate a hostile environment for healthy haematopoietic cells that egress to the bone marrow. Overall, this data supports the hypothesis that PERK-MSCs affect HSPCs growth favouring myeloid lineage skewing.
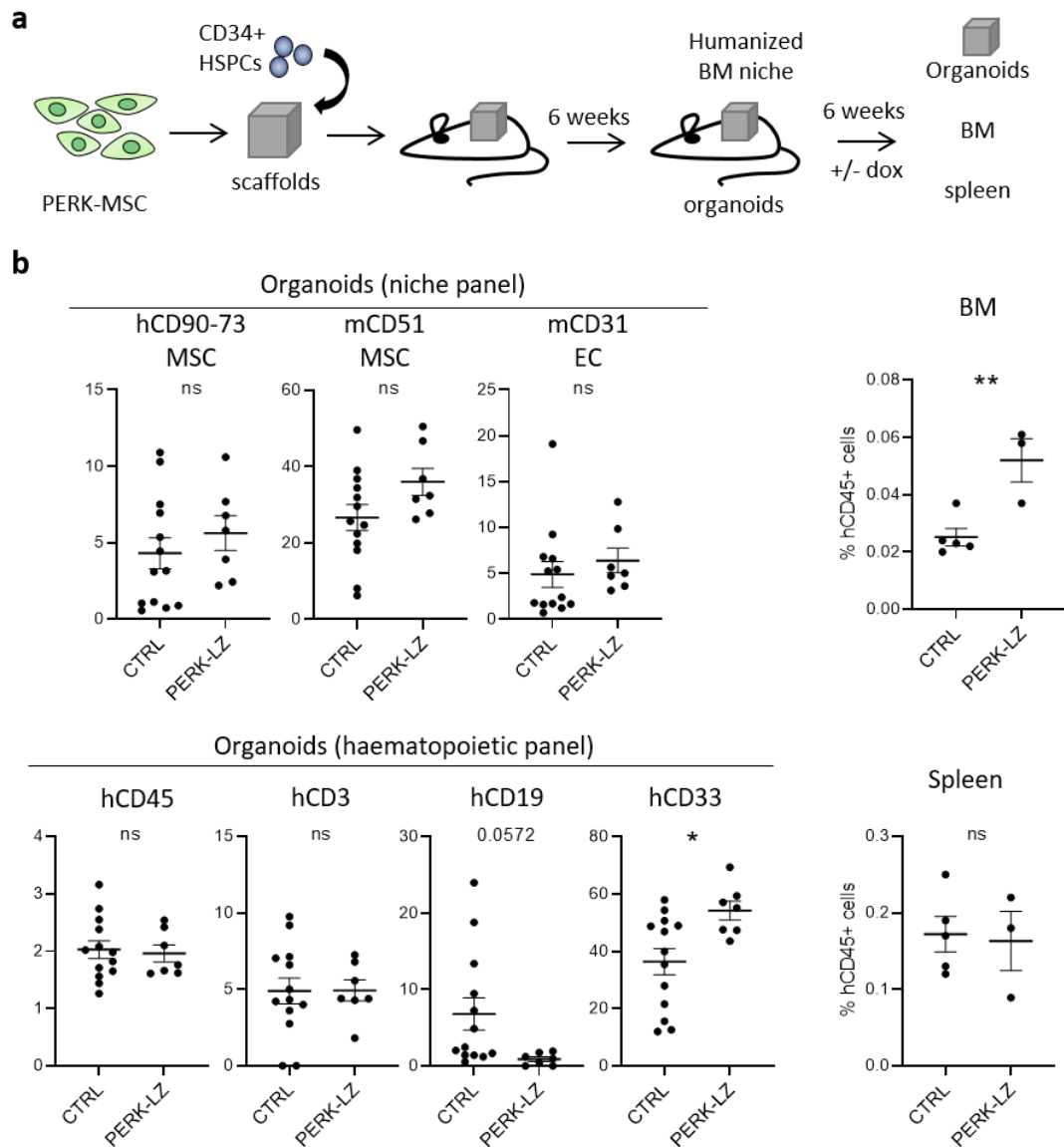
Figure 4.14: PERK-LZ ectopic expression in MSCs induces hematopoietic lineage skewing in vivo. (a) *Schematic representation of procedure to obtain humanised bone marrow niches (organoids) in mice: Scaffolds are injected with PERK-MSCs or rtTA-MSCs and CD34+ hematopoietic stem and progenitor cells (HSPCs) and subcutaneously implanted into mice. After 6 weeks, to allow organoids to form, mice were watered with a doxycycline (dox) solution once a week for the remaining time to induce expression of the transgene and mimic AML development and progression. Dox-untreated mice are used as controls. After 6 weeks, mice are sacrificed and organoids, bone marrow (BM) and spleen are harvested for further analysis.* **(b)** *Dot plot representing flow cytometry analysis of organoids, BM and spleen samples collected from mice. Organoids were analysed with a 'niche panel' comprising of anti-human CD90 and CD73 for detecting human MSCs, anti-mouse CD51 for murine MSCs and anti-mouse CD31 for murine endothelial cells (EC), and a 'haematopoietic panel' comprising of all anti-human antibodies: CD45 as pan-haematopoietic marker, CD3 and CD19 for lymphocytes and CD33 for myeloid cells. Each dot represent one organoid. Spleen and BM were analysed to determine percentages of human CD45. Each dot represents one mouse. Asterisks, where indicated, are *p<0.05; **p<0.01; ***p<0.001; ****p<0.0001; ns: nonsignificant; unpaired two-tailed t-test; results are shown as the mean ± SEM.*

4.2.2. PERK expression in MSCs results in matrisome and secretome alterations

To get insights into possible mechanisms by which PERK activation in MSCs may affect haematopoiesis, I performed RNA sequencing and proteomic analysis on PERK-MSCs upon doxycycline treatment. These experiments were performed at 48 hours to allow the transcription and translation of the putative PERK-induced genes and activation of the downstream pathways. Doxycycline-treated rtTA-MSCs were used as controls. RNA-sequencing analysis results confirmed the upregulation of ER stress and UPR pathways in PERK-MSCs, which was accompanied by a downregulation of protein translation and RNA processing pathways (Figure 4.15a), which are known consequences of PERK activation. Moreover, GSEA showed downregulation of adipogenic pathways and fatty acid metabolism in PERK-MSCs cells (Figure 4.15a), supporting previous data (Chapters 1.3.4.3., 4.1.2, and 4.1.5) which demonstrated that UPR signalling governs adipogenesis and that excessive activation abrogates it.

Interestingly, the RNA sequencing analysis identified genes involved in the extracellular matrix (ECM) organisation, regulation and ECM receptor interaction (*THBS1*, *IGFBP2*, *SERPINE2*) as preferentially downregulated in PERK-MSCs, along with downregulation of genes involved in cell adhesion molecules, collagen formation and deposition (*COL1A2*, *COL3A1*, *COL5A1*, *COL1A1*, *DCN*) (Figure 4.15a). Further functional annotation analysis indicated that many signalling pathways known to be implicated in haematopoiesis regulation were downregulated in PERK-MSCs (Figure 4.15a), with a negative enrichment of HSPC niche gene set (Figure 4.15b) (Lim et al., 2016), suggestive of a weakened supportive role of these cells. Furthermore, PERK-MSCs presented with an altered expression of growth factors and cytokines known to be involved in HSC maintenance and regulation such as *CXCL2*, *IL6*, *SCF*, *CXCL12*, *IGF1* and *IGF2* (Figure 4.15c) (Pinho & Frenette, 2019; Waclawiczek et al., 2020). Gene ontology analysis of our proteomic data showed downregulation of ECM- and collagen-related pathways in PERK-MSCs, recapitulating RNA sequencing data (Figure 4.15d). Given these changes in ECM of PERK-MSCs in both data sets, we next performed a matrisome analysis on our transcriptomic data and proteomic data to enrich for signalling molecules and environmental local cues that

could affect haematopoiesis (Figure 4.15e). Despite a low overlap between the transcriptomic and proteomic data, the matrisome signature confirmed the altered extracellular-matrix composition and organisation with a marked decrease in ECM regulators, ECM proteins and collagens in both data sets (Figure 4.15e). Furthermore, the matrisome enrichment revealed an upregulation of secreted factors, particularly in the transcriptomic data, with FGF2 being overexpressed in both data sets. FGF2, or fibroblast growth factor 2, is a growth factor secreted by stromal cells and has been implicated in the regulation of proliferation and differentiation of both MSCs and HSPCs (Itkin et al., 2012; L. Xiao et al., 2010; Yoon et al., 2017), particularly during stress conditions (Itkin et al., 2012; Philippe et al., 2016). Furthermore, FGF2 expression is mediated via non-canonical translation pathways upon PERK induction (Philippe et al., 2016), making FGF2 a causative candidate of the observed phenotype. Collectively these results, despite preliminary, demonstrated that in conditions of increased PERK activity, the molecular signature of MSCs is altered and their HSPC-supporting functions are probably impaired.
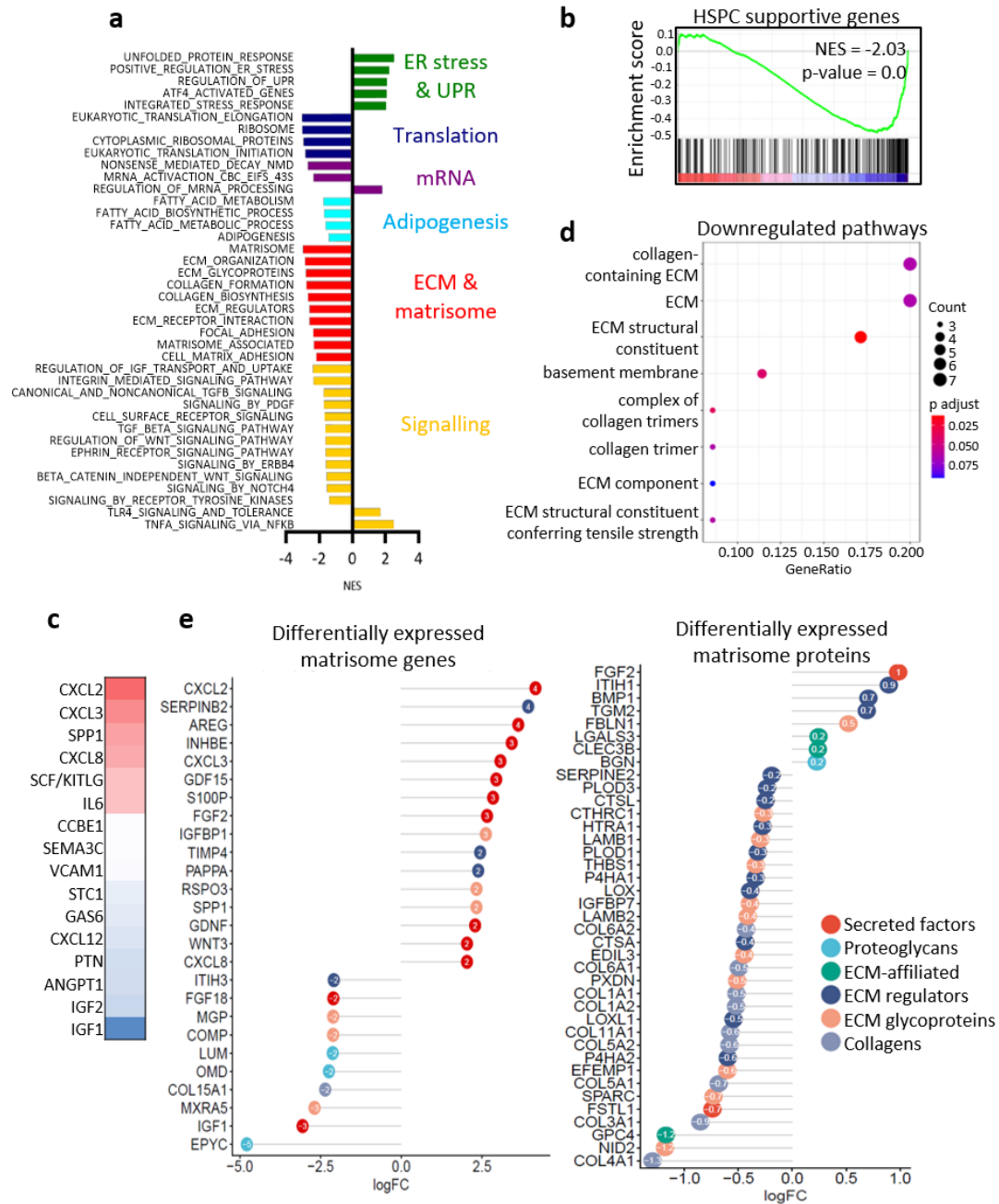
Figure 4.15: PERK-LZ ectopic expression alters MSC secretome and matrisome. (a) *Bar plot of GSEA showing positive or negative normalized enrichment scores (NES) in PERK-MSCs compared to rtTA-MSCs treated for 48 hours with 1 µg/ml doxycycline. Pathways with adjusted enrichment p-value of less than 0.05 are included in the figure. Categories within the same biological process (colour) are ordered by enrichment fold change (shown on the x-axis). **(b)** GSEA plot showing downregulation of genes expressed in HSC supportive stromal cell [gene set: M2581]. **(c)** Heatmap of selected genes (Pinho & Frenette, 2019; Waclawiczek et al., 2020; Wilkinson, Igarashi & Nakauchi 2020) encoding for growth factors or cytokines secreted by stromal cells and involved in HSC maintenance and regulation that were differentially expressed in PERK-MSCs compared to rtTA-MSCs. **(d)** Gene ontology analysis based on differentially expressed proteins in PERK-MSCs compared to rtTA-MSCs, showing downregulated pathways. The X-axis is the ratio of the number of DE proteins in the corresponding pathway to the number of total proteins identified in the pathway. The colour of the points represent the p-value of the hypergeometric test. The size of the dot represents the number of DE proteins in the corresponding pathway. **(e)** Matrisome analysis of differentially expressed matrisome genes and proteins respectively in PERK-MSCs compared to rtTA-MSCs. Numbers within the dots represent the logFC and dots are colour-coded based on the different matrisome categories.*

126

Chapter 5

Discussion

My study highlights two main findings. First, acute myeloid leukaemia (AML) profoundly remodels the bone marrow (BM) stromal niche, altering mesenchymal stromal cell (MSC) transcriptome, proteome and secretome. Second, with combined *in vivo* and *in vitro* approaches, I identified ER stress activation and unfolded protein response (UPR) as the driver of AML-induced changes in MSC capacities to differentiate into adipocytes and sustain healthy hematopoietic cell homeostasis. These findings are in agreement with and complement recent evidence showing that leukaemic cells induce considerable modifications in the BM microenvironment, affecting its architecture and the different cell populations present (Schroeder et al., 2016). Similar to previous reports (Geyh et al., 2016), our analysis of MSCs isolated from the BM of AML patients (AML-MSCs) compared to healthy donor-derived MSCs (HD-MSCs) indicated a growth deficiency of AML-MSCs (Figure 3.3), which was accompanied by a downregulation of cell cycle and DNA replication pathways, both at transcriptomic and proteomic levels (Figure 3.3 & 3.4). In addition to changes in gene expression and proliferation potential (Geyh et al., 2016), other studies have also reported that AML-MSCs exhibit other molecular and functional alterations, including translocations, reduced clonogenic potential, higher senescence, and impaired differentiation (Azadniv et al., 2020; Battula et al., 2017; Blau et al., 2011; Bonilla et al., 2019; Chandran et al., 2015). However, despite the consensus in recognising that AML alters the BM microenvironment to better suit its propagation, there has been contrasting evidence regarding the specific changes. Where some groups observed an increase in the adipogenic potential in MSCs isolated from AML patients (Azadniv et al., 2020), others reported a decrease in adipocytes in BM biopsies (Boyd et al., 2017). Similarly, some groups showed a reduced osteogenic differentiation capacity of AML-derived MSCs (Bonilla et al., 2019; Geyh et al., 2016), while another study reported an increase in osteogenic differentiation in AML-derived MSC and MSC co-cultured with AML cell line (Battula et al., 2017). These

discrepancies could be caused by differences in the lineage-associated genes used to assess the differentiation status, thereby not accurately discriminating precursors from mature cell type, or by differences in the *ex vivo* and *in vitro* models and approaches used by the authors, that ranged from expanded healthy donors-derived and AML-derived MSC to trephine biopsies or co-cultures conditions. The use of different models could thus result in the modelling of different stages of the disease, alongside with variable, and sometimes limited, numbers of patients in the cohorts and the fact that different alterations observed may be dependent on the specific AML molecular subgroup. These *in vitro* and *ex vivo* data are complemented by experiments in mouse models, which show a progressive loss of mature osteoblasts (Duarte et al., 2018) and adipocytes (Boyd et al., 2017) with increased severity of the disease, and an expansion of MSCs primed for osteoblastic differentiation at later stages (Hanoun et al., 2014). Despite discrepancies, all findings advocate for an altered MSC niche where the balance between adipogenic and osteogenic differentiation is profoundly disturbed.

The molecular mechanisms responsible for these alterations and their consequences are not yet fully elucidated. Our analysis of the transcriptome of MSCs isolated from the BM of AML patients and AML patient-derived xenograft (PDX) mice (Passaro et al., 2021) revealed an upregulation of UPR pathways (Figure 4.1 & Figure 4.4), which was replicated in the *ex vivo* co-cultures (Figure 4.3 & Supplemtary Figure 6.2) and may be responsible for the MSC adaptation to the stress induced by the leukaemic growth. Activation of UPR has been reported in AML blasts, haematopoietic stem and progenitor cells (HSPC) and recently also in MSCs and osteoblasts of a mouse AML model (Doron et al., 2018; Rouault-Pierre et al., 2013; van Galen et al., 2018), suggesting that ER stress may be involved in the pathogenesis of AML. UPR has been historically linked to protein overload and protein regulation, but it has become more and more recognised that UPR might play important roles in many cellular mechanisms, including cell fate decisions such as osteogenesis and adipogenesis (Chapter 1.3.4). Indeed, I showed that MSCs differentiating into adipocytes and osteoblasts broadly activate UPR-target genes (Figure 4.5) and ER stressor treatment induces expression of adipogenic genes in immature MSCs (Figure 4.5d), suggesting

that the physiological level of the UPR may be required for adipogenesis to occur. Consistently, suppression of UPR impedes differentiation (Yang et al., 2004). While UPR activation appears to be instrumental and necessary to guide MSCs differentiation, excessive ER stress activity is instead detrimental and represses adipogenesis (Agostinis & Afshin, 2012). This biological paradox is known as hormetic ER stress, a process by which cells are exposed to mild stressors that ultimately lead to beneficial adaptations, including enhanced lifespan and increased protein folding capacity, required for secretory cells such as adipocytes and osteoblasts. Interestingly, studies on hormetic ER stress revealed a dose-dependent response, in which a milder dose triggers a stimulatory beneficial effect while a high dose causes an inhibitory adverse effect (Luchsinger, 2021). By using a unique inducible system (Figure 4.6 & 4.7, Supp. Figure 6.3 & 6.4), I showed that constitutive PERK activation completely abrogates adipogenesis in MSCs, impeding lipid accumulation and reducing expression of adipogenic marker genes, and, in particular, markers of mature adipocytes such as adipsin, also known as CFD, adiponectin, and FABP4 (Figure 4.9). These results are consistent with previous reports (Han et al., 2013) and with the dramatic reduction of adipocytes observed in the BM of AML patients and AML mouse models (Boyd et al., 2017). Conversely, constitutive activation of IRE1 does not seem to induce changes in MSC differentiation capabilities (Figures 4.10) (Han et al., 2013). As adipogenic marker genes were still expressed in conditions of PERK overexpression (Figure 4.9c) and levels of PPARγ and early adipogenic marker genes such as C/EBPβ were unaltered (Figure 4.9f), we hypothesised that the cells initiated differentiation but were trapped in a pre-adipocytes state. A proposed mechanism for UPR-induced block of adipogenesis involves the induction of CHOP, which stoichiometrically dimerises with C/EBP transcription factors and represses their activity by preventing them from binding adipogenic target genes (Figure 1.11) (Batchvarova et al., 1995; Kaspar et al., 2021). CHOP is a direct target of PERK and was dramatically increased in PERK-MSCs (Figure 4.9b and 4.13c), which could potentially explain the adipogenesis blockage observed even in presence of unaltered expression of C/EBPβ; however, further experiments are necessary to confirm the interaction of CHOP and C/EBPs in our conditions. Nevertheless, consistent with the hypothesis that UPR causes the cells to be trapped in a pre-

adipocyte status, GATA3, a pre-adipocyte marker and repressor of mature adipogenesis (Tong et al., 2000), was upregulated in PERK-MSCs (Figure 4.13). GATA3 is a direct target of UPR activation (Figure 4.13) (Qiang et al., 2016), is specifically expressed in pre-adipocytes, and blocks the maturation into fully differentiated adipocytes, in part by interacting with C/EBPs (Tong et al., 2005), which again, could explain the high levels of C/EBPs despite the adipogenesis arrest. It cannot be ruled out that the phenotype could be, at least in part, due to alteration in the cell cycle and reduced proliferation potential observed in MSCs upon ectopic expression of PERK (Figure 4.8). PERK has been shown to play a role in cell cycle inhibition (Hamanaka et al., 2005; Zhimeng Wu et al., 2017), and cell cycle regulators are finely tuned during cell differentiation (Batsali et al., 2017), thereby seeking further investigation. Of note, despite the alterations in the cell cycle, PERK-MSC retained the capability to differentiate into osteoblasts (Figure 4.12) suggesting that the phenotype may not be dependent on cell cycle variations.

While BM adipocytes have largely been deemed negative regulators of haematopoiesis, other evidence suggests that they provide important support in the regeneration of blood lineages (Zhou et al., 2017), and leukaemic suppression of adipocytes within the BM have been associated with imbalanced regulation of endogenous haematopoietic stem and progenitor cells with compromised myelo-erythroid maturation (Boyd et al., 2017).

Defective haematopoiesis is a hallmark of AML and predisposes patients to life-threatening complications such as haemorrhage and infections, thereby it is important to assess how AML-induced niche damages feedback on haematopoiesis. MSCs constitute an essential component of the BM niche not only because they contribute to the cellular diversity of the BM by differentiating into osteoblasts and adipocytes and through the development and maintenance of the sinusoidal network (Muguruma et al., 2006; Sacchetti et al., 2007), but also by directly sustaining haematopoiesis, through secretion of HSC-supporting factors. Given this, while it is essential to study the effects of the absence of adipocytes within the BM niche (Boyd et al., 2017), we also wanted to understand MSC's broader role. Using a state-of-art humanised *in vivo* niche (Passaro, Abarrategi, et al., 2017) to mimic the UPR

activation caused by AML propagation, we showed that the stressed niche affects proper production of blood cell lineages and becomes an unfavourable environment for healthy hematopoietic cells while favouring myeloid-biased cells growth (Figure 4.14). Furthermore, using a transcriptomic approach, we identified common niche-supportive factors and pathways as being altered when PERK was ectopically expressed in MSCs (Figure 4.15). Proteomic and matrisome analysis further revealed alterations in signalling receptors and extracellular matrix composition (Figure 4.15), indicating that also cell-to-cell or cell-to-matrix contacts may be disrupted, possibly contributing to the compromised haematopoiesis. Efforts from several research groups provided evidence that chemical and/or genetic rescue of AML-induced changes in the microenvironment in mouse models were able to offset the niche-damaging effects of AML and rescue BM failure (Boyd et al., 2017; Duarte et al., 2018; Krevvata et al., 2014; Passaro, Di Tullio, et al., 2017). Therefore, our work provides a rationale to target UPR to restore MSC homeostasis and capabilities to differentiate into adipocytes and sustain healthy blood production.

Finally, I also show that e*x vivo* human cultures and co-cultures represent a valid surrogate model to study AML and BM microenvironment in a human context and to overcome some limitations of the murine models. While murine models have been essential to study HSC, AML and the BM niche, the requirements for pre-conditioning (irradiation or myeloablation) of immunodeficient mice are likely to alter the BM microenvironment. In addition, the fact that the mouse niche does not fully recapitulate the human BM and lacks some cross-reactivity signals renders the study of the niche in xenotransplantation hazardous (Theocharides et al., 2016). The scaffolds developed by Dominique Bonnet's lab and other groups (Passaro, Abarrategi, et al., 2017) and implanted into immunodeficient mice can provide a humanized niche in murine models. However, they also come with technical challenges such as the colonisation of the scaffold by murine haematopoietic and stroma cells, irradiation of the recipient in some models and a limited amount of material recovered. Overall, although the 2D *ex vivo* culture cannot convey the complexity of the BM niche, it offers the opportunity to better understand cell-to-cell interactions and deregulated pathways that alters the MSC niche during AML

expansion in a controlled parameter environment. MSCs have a great propensity for *ex vivo* expansion (Dominici et al., 2006). Despite extensively passaged cells and manipulation may induce alterations, the *ex vivo* culture remains the gold standard to study human MSCs due to the lack of definitive markers for prospective isolation and due to their low frequency in the BM (<0.01%) impeding the harvest of cells in sufficient numbers for certain applications (Méndez-Ferrer et al., 2020).

In conclusion, the data discussed in the present work provide new insights into the alterations observed in the MSC niche upon AML expansion and show that UPR activation via PERK orchestrates the AML-induced microenvironment alterations (Figure 5.1). Our findings are corroborated by recent reports indicating that AML affects the BM niche components, creating an aberrant, self-reinforcing microenvironment while impairing its functions in supporting HSC and their progeny.
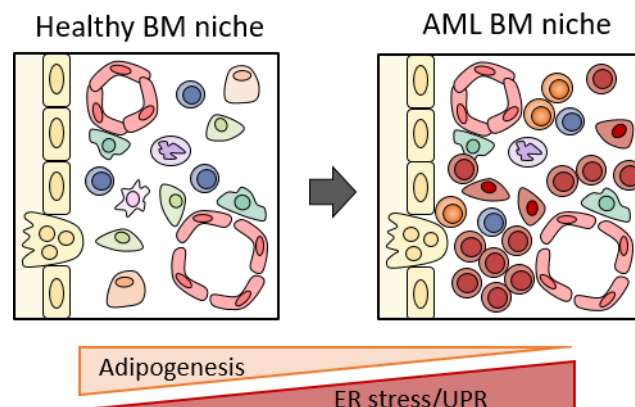
Figure 5.1: AML growth alters the MSC transcriptional program, activating the unfolded protein response (UPR) in MSCs and blocking adipogenic differentiation. AML cells (in red) invade the BM niche causing MSC to respond to the stress by activating UPR signalling pathway. When UPR is induced, MSC lose the capability to differentiate into adipocytes, leading to a drastic reduction of adipocytes in the BM niche. Furthermore, UPR activation in MSCs leads to lineage skewing in HSCs (orange cells).

Chapter 6

Supplementary information

6.1. Establishing 2D co-cultures

To assess the effects of acute myeloid leukaemia (AML) expansion on stroma cells, I established a 2D co-culture system where stroma cells, such as primary mesenchymal stromal cells (MSC) or a murine stromal cell line called MS-5, are cultured with AML cells or healthy controls for several days. The AML cells used were primary samples (Figure 4.3) or the AML cell lines OCI-AML3, THP1 and HL60 (Supplementary Figures 6.1 and 6.2). Before further analysis, however, it is necessary to isolate stroma cells from the haematopoietic fractions. For this purpose, we thought to use immunomagnetic cell sorting as it represented a relatively quick procedure, with a low risk of stressing the cells. However, the techniques yielded very variable purity levels, impeding further molecular and functional analysis of the different fractions (Supplementary Figure 6.1a-b). One of the reasons for such variability was probably due to differences in cell numbers. Culturing MSCs with different numbers of OCI-AML3 cells (Supplementary Figure 6.1c), I could assess that the purity levels of MSCs after immunomagnetic isolation were inversely proportional to the number of OCI-AML3. Furthermore, MSCs purity levels were low even when co-cultured with 2-3 million OCI-AML3, despite the kit ensuring the purity of isolation up to 7 million cells. To ensure the issue was not operational as some clumps were present after harvesting of the cells, I used different concentrations of ethylenediaminetetraacetic acid (EDTA) while harvesting and isolating the cells, as EDTA inhibits clotting by chelating calcium. Nevertheless, the use of EDTA did not improve purity levels (not shown). We reached good purity levels by increasing the number of incubations and washes during the isolation of the cells (Supplementary Figure 6.1d).
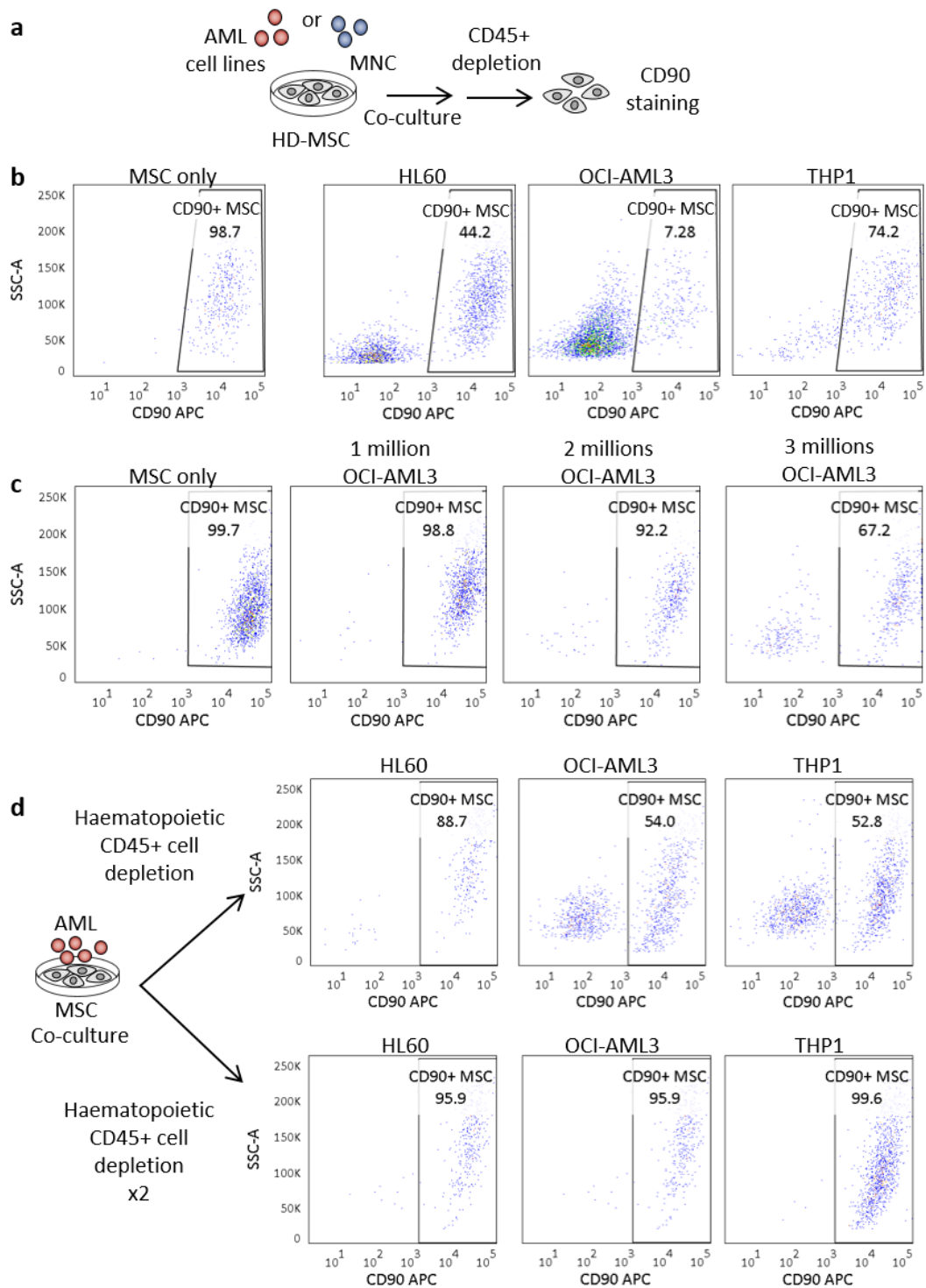
Supplementary Figure 6.1: Optimisation of immunomagnetic cell depletion of CD45 negative MSCs from 2D co-cultures. (a) *Schematic representation of 2D co-cultures, followed by hematopoietic CD45+ cell depletion and CD90 staining of CD45- fractions. **(b-d)** Dot plots show CD90+ MSCs purity levels of the CD45- fractions. **(b)** MSCs are co-cultured with 100,000 AML cells (AML cell lines: HL60, THP1 or OCI-AML3) for up to 14 days. **(c)** MSCs are co-cultured with one, two or three millions OCI-AML3 cells for 24 hours **(d)** MSCs are co-cultured with 100,000 AML cells (AML cell lines: HL60, THP1 or OCI-AML3) for 14 days. Hematopoietic CD45+ cell are depleted via immunomagnetic isolation to purify MSCs. A fraction of the CD45- population is subjected to another round (x2) of CD45+ depletion to increase purity.*

We next tested whether AML growth led to ER stress and UPR signalling in MSCs: MSCs were co-cultured with AML cell lines, THP1, OCI-AML3 and HL60 or with healthy mononuclear cell (MNC) controls for up to 14 days (Supplementary Figure 6.2a).
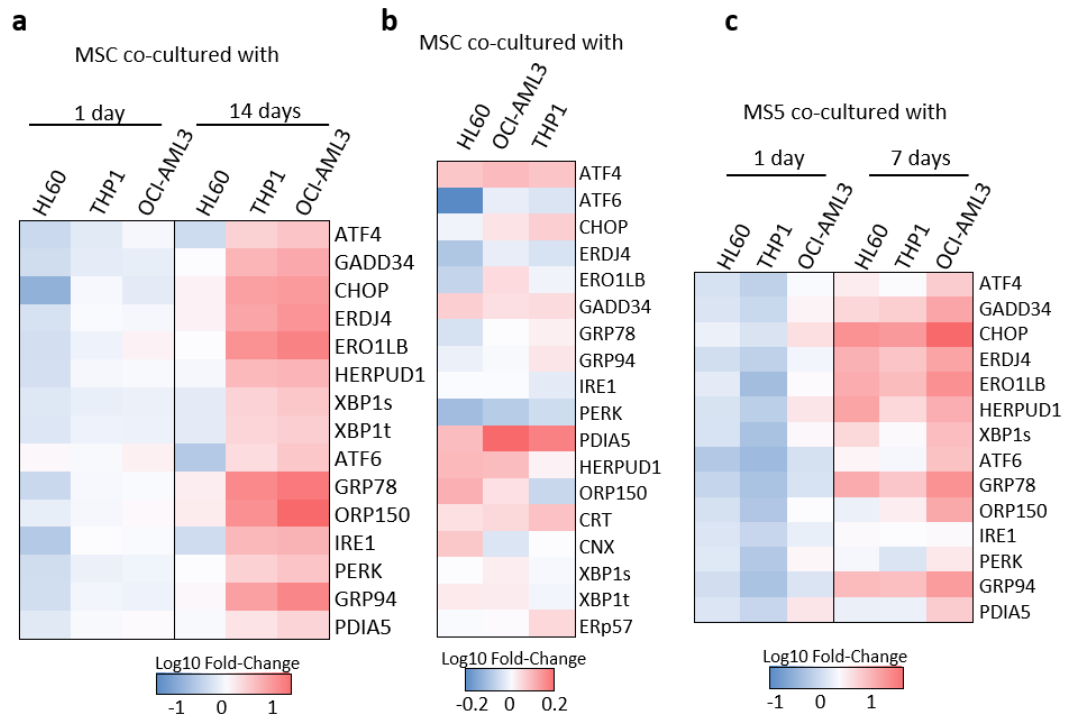
Supplementary Figure 6.2: AML cell lines induce ER stress in MSCs. (a) *Healthy-donor MSCs are co-cultured with 100,000 AML cells (AML cell lines: HL60, THP1 or OCI-AML3) or 100,000 healthy MNC controls for up to 14 days. At each time point, hematopoietic CD45+ cell were depleted with immunomagnetic isolation to purify MSCs. Heat map with differentially regulated UPR-related genes upon 1-day and 14-days of MSC cultured with the three different AML cell lines. Data are plotted as fold-change as compared to MSC cultured with healthy MNC controls.* ***(b)*** *Healthy-donor MSCs are co-cultured with one million AML cells (HL60, THP1 or OCI-AML3) or one million healthy MNC controls for 24 hours. Hematopoietic CD45+ cell are depleted by immunomagnetic isolation. Heat map shows differentially regulated UPR-related genes in MSC cultured with the three different AML cell lines. Data, from three different biological replicates, are plotted as fold-change as compared to MSC cultured with healthy MNC controls).* ***(c)*** *Heat map with differentially regulated UPR-related genes upon 1-day and 7-day of MS5 cultured with AML cell lines HL60, THP1 and OCI-AML3. Data are plotted as fold-change as compared to MS5 cultured with healthy MNC controls from one biological replicate.*

While one-day co-cultures did not seem to induce UPR in MSCs, a widespread overexpression of UPR-related genes was observed in MSCs upon 14-day co-cultures with AML cell lines, as compared to cultures with healthy MNC controls. In particular, UPR activation was induced by THP1 and OCI-AML3 cell lines and not by HL60, indicating that the effects of AML growth on the stroma may be dependent on the particular AML genetic background. To ensure the ER stress activation was not due to the physical crowdedness of the wells, I co-cultured MSCs with 1 million THP1,

135

OCI-AML3 and HL60 cell lines or 1 million MNC cells (Supplementary Figure 6.2b) revealing a significant activation of some UPR-target genes, indicating that AML-induced ER stress on MSC could not be accounted for physical crowdedness alone. UPR activation was also observed on an MS-5 stroma upon seven-day cultures with the three AML cell lines as compared to healthy MNC controls (Supplementary Figure 6.2c). Shorter co-culture times were used for MS-5 as, being a cell line, the cells are not contact-inhibited and, without irradiation, they can overgrow within the well. Irradiation on the other hand would affect the subsequent molecular analysis. This, together with the fact that AML cell line growth is independent of the stroma, leads us to use primary AML samples co-cultured with primary MSCs to better assess the crosstalk between these cells (Chapter 4.1).
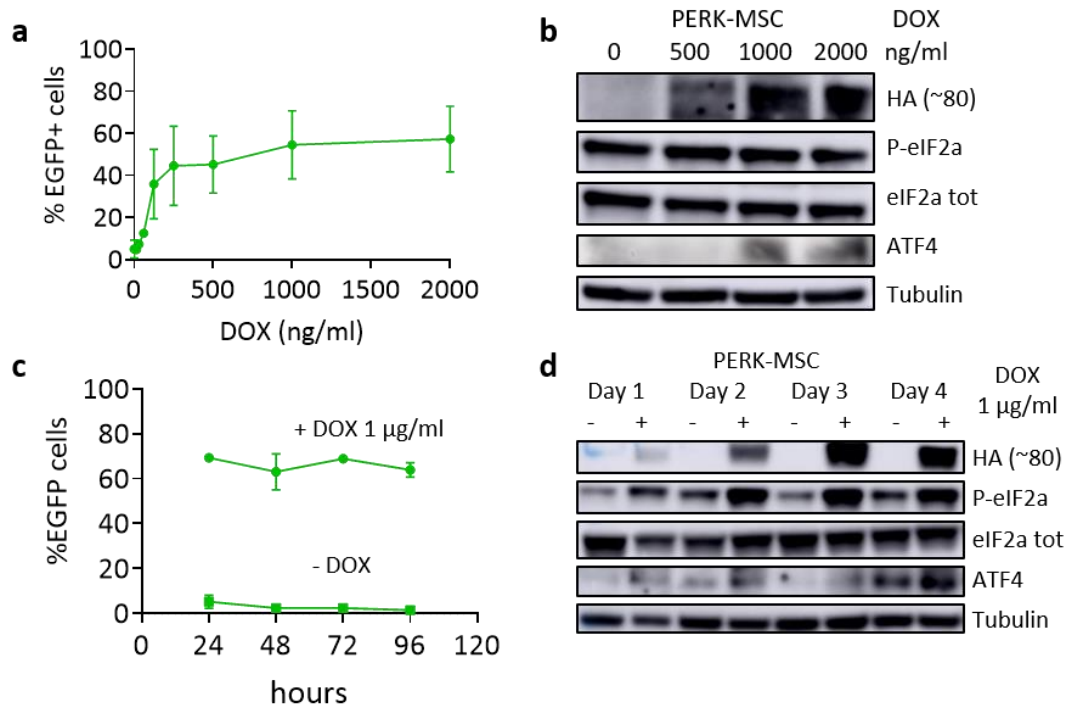
Supplementary Figure 6.3: Doxycycline titration for PERK-LZ gain-of-function plasmid. (a) *Line graph showing EGFP+ cells percentage of successfully transduced MSCs with rtTA and PERK-LZ vectors (PERK-MSCs) upon 24 hours treatment with increasing doxycycline (DOX) concentrations. Untransduced GFP-cells are used to set GFP thresholds (not shown).* ***(b)*** *Western blot analysis of PERK-LZ (HA tag) protein levels and PERK downstream effectors ATF4 and P-eIF2α of PERK-MSCs treated for 24 hours with increasing dose of doxycycline (DOX).* ***(c)*** *Line graph showing EGFP+ cells percentage of PERK-MSCs cells treated with 1μg/ml of doxycycline (DOX) at different time points.* ***(d)*** *Western blot analysis of PERK-LZ (HA tag) protein levels and PERK downstream effectors ATF4 and P-eIF2α of PERK-MSCs treated with 1μg/ml doxycycline (DOX) at different time points. All error bars indicate s.e.m. [LZ: leucine-zipper domain; HA: Human influenza hemagglutinin (HA) tag; rtTA: reverse tetracycline-controlled transactivator; dox: doxycycline].*

6.2. Doxycycline dosage

Doxycycline (DOX) titration and dosing time of the PERK-LZ and IRE1-LZ gain-of-function constructs (Chapter 4.1.3) was performed on mesenchymal stromal cells (MSCs) stably transduced with the trans-activator vector (rtTA) and one of the two constructs, monitoring EGFP expression and protein levels of HA-tagged recombinant proteins, PERK-LZ and IRE1-LZ, and targets genes of each branch. EGFP expression was induced in a doxycycline concentration-dependent manner, reaching a plateau at 1000 ng/ml (Supplementary Figure 6.3a and 6.4a). Similarly, the expression of PERK-LZ and IRE1-LZ, detected with anti-HA antibody, and of the targets, ATF4 and P-eIF2a and XBP1s respectively, was doxycycline-inducible and increased in a dox-concentration-dependent manner (Supplementary Figure 6.3b and 6.4b), reaching a
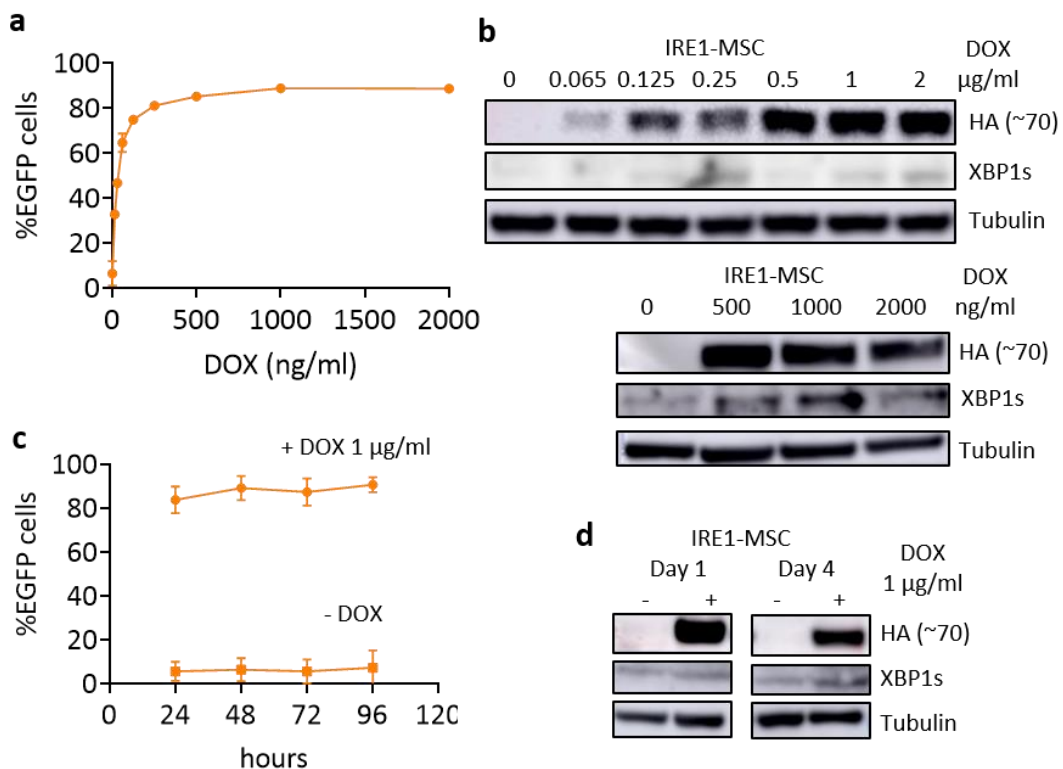
Supplementary Figure 6.4: Doxycycline titration for IRE1-LZ gain-of-function plasmid (a) *Line graph showing EGFP+ cells percentage of successfully transduced MSCs with rtTA and IRE1-LZ vectors (IRE1-MSCs) upon 24 hours treatment with increasing doxycycline (DOX) concentrations. Untransduced GFP- cells are used to set GFP thresholds (not shown).* ***(b)*** *Western blot analysis of IRE1-LZ (HA tag) protein levels and IRE1 downstream effectors XBP1s of IRE1-MSCs treated for 24 hours with increasing dose of doxycycline (DOX).* ***(c)*** *Line graph showing EGFP+ cells percentage of IRE1-MSCs cells treated with 1µg/ml of doxycycline (DOX) at different time points.* ***(d)*** *Western blot analysis of IRE1-LZ (HA tag) protein levels and IRE1 downstream effectors XBP1s of IRE1-MSCs treated with 1µg/ml doxycycline (DOX) at different time points. All error bars indicate s.e.m. [LZ: leucine-zipper domain; HA: Human influenza hemagglutinin (HA) tag; rtTA: reverse tetracycline-controlled transactivator; dox: doxycycline].*

plateau at 1000 ng/ml. To test whether the PERK-LZ, IRE1-LZ activation was stable over time, transduced cells were treated with 1000 ng/ml doxycycline and harvested at different time points. EGFP+ expression (Supplementary Figure 6.3c and 6.4c), and expression of PERK-LZ and IRE1-LZ and their targets were detectable at different time points (Supplementary Figure 6.3d and 6.4d), allowing a stable expression of the constructs.

6.3. Transmissible ER stress

Activation of UPR has been reported in AML blasts, haematopoietic stem and progenitor cells (HSPC) and in MSCs and osteoblasts of a mouse AML model (Doron et al., 2018; Rouault-Pierre et al., 2013; van Galen et al., 2018). The induction of the UPR in cancer cells can trigger the release of soluble factors that can transmit ER stress to other cells, in a phenomenon termed transmissible ER stress (TERS). These UPR-based intercellular signalling mechanisms allow cancer cells to reshape the microenvironment to better suit their growth and gain fitness (Doron et al., 2018; Willert et al., 2017). In recent years, different methods of intercellular communication have been identified including gap-junctions, exosomal vesicles and tunnelling nanotubules, which allow the passage of soluble factors and mRNAs. mRNAs may be translated in the acceptor cells (Mittelbrunn & Sánchez-Madrid, 2012), transducing a biological effect, and affecting the phenotype of the cells. To assess the existence of such crosstalk between AML blast, HSPCs and MSCs we sought to investigate if UPR-related mRNAs were transferred between stromal cells and normal/leukemic cells. We used a co-culture system comprising a stroma murine cell line, MS-5, together with human blood cells and species-specific qPCR primers, to discriminate human mRNAs that may be transferred from AML cells into murine stroma cells and vice versa. Species-specific qPCR primers were designed by using Primer-BLAST (NCBI) (Table 2.2 and Supplementary Table 6.1). The murine primers panel was first validated by using the chemical ER stress inducers thapsigargin (TG) and tunicamycin (TM), similar to validation performed for the human primers (Chapter 4.1.1, Figure 4.2). MS-5 were treated with the two ER stress-inducers for 6

hours which caused the increase in expression of UPR-target genes, as compared to DMSO-treated controls (Supplementary Figure 6.5a). Validation of species specificity of the primers was performed on mRNA isolated from murine MS-5 and human THP1 leukemic cells. The species-specific qPCR primers showed no cross-reactivity as murine primers allowed specific amplification of murine mRNAs, without amplifying human ones (Supplementary Figure 6.5c). Similarly, human primers did not amplify murine genes (Supplementary Figure 6.5d).
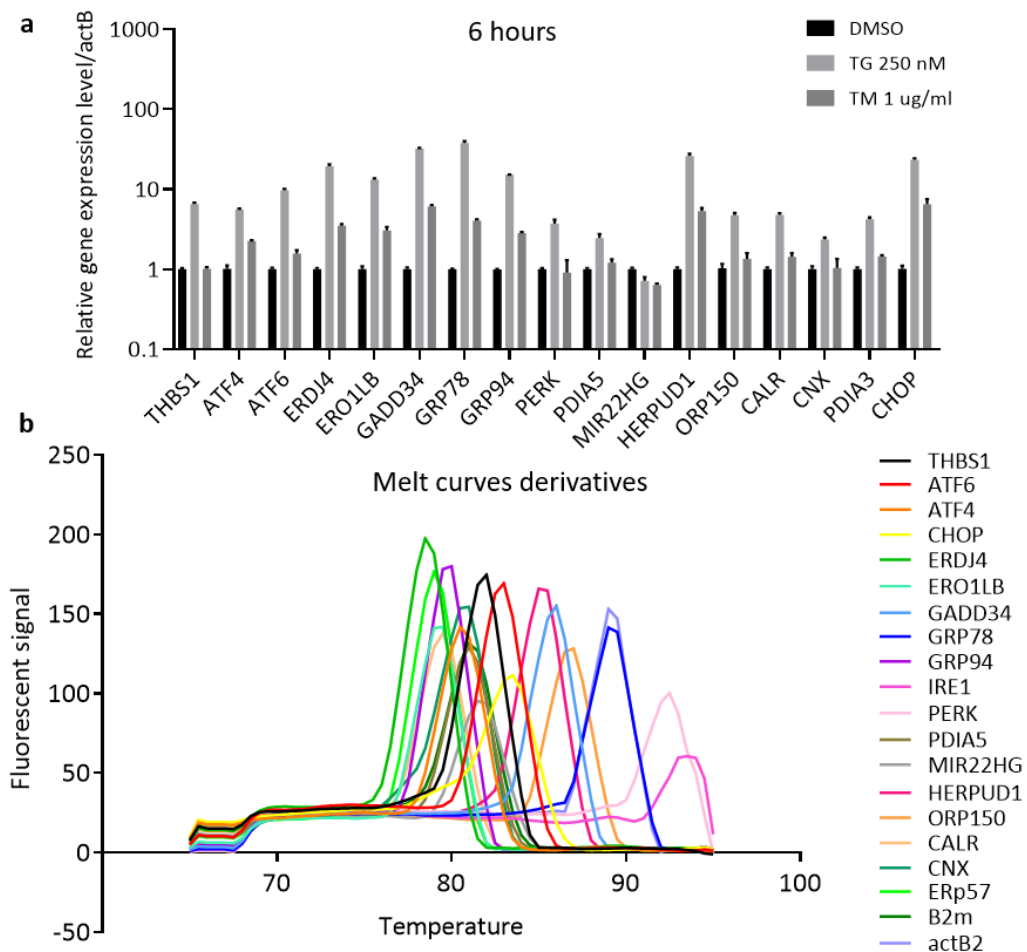
***Supplementary Figure 6.5: UPR-related genes qPCR panel validation for murine and human primers. (a)** mRNA levels for UPR-related genes measured by qPCR in MS5 treated for 6 hours with 250 nM Thapsigargin (TG) or 1μg/ml Tunicamycin (TM). mRNA levels are expressed as fold-change relative to vehicle (DMSO 0.1%)-treated cells. Results are shown as mean s.d. of three technical replicates. Y-axis is displayed in logarithmic scale. All error bars indicate s.d. (b) Dissociation curves were generated to check for the presence of aspecific amplicons or primer dimers, which would be visible as additional peaks. Each line represents the dissociation curve of one qPCR reaction, colours indicate different genes. **(c-d) overleaf** Amplification curves of qPCR reactions for UPR-related genes using murine primers **(c)** or human primers **(d).** THP1 human cell line and MS5 mouse cell line were treated with 1 μg/ml Tunicamycin for 6 hours to induce ER stress. After RNA isolation and retrotranscription, qPCR reactions were performed by using different concentrations of cDNA. Each graph represents the amplification curve for one gene. Murine primers **(c)** amplified specifically and efficiently murine mRNAs (green lines), without amplifying human ones (red lines). Similarly, human primers **(d)** did not amplify murine genes.*

c   Primers for mouse genes
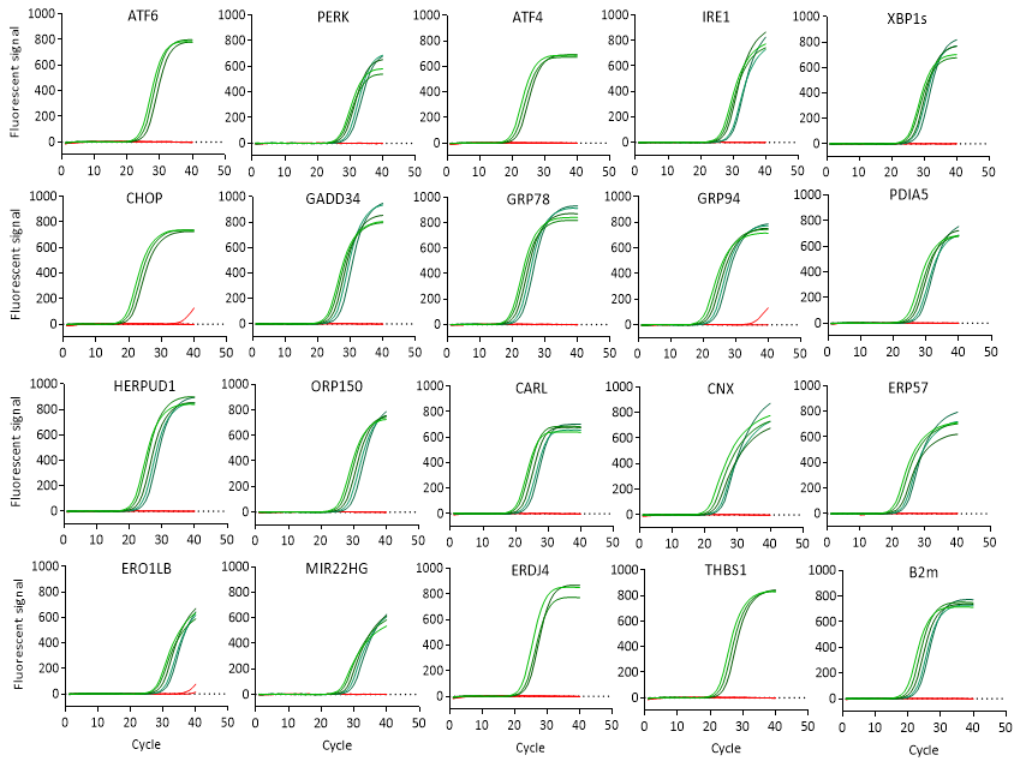
d   Primers for human genes

[cDNA]	[cDNA]
MS5 5 ng/ul	THP1 5 ng/ul
MS5 2.5 ng/ul	THP1 2.5 ng/ul
MS5 1.25 ng/ul	THP1 1.25 ng/ul
MS5 0.625 ng/ul	THP1 0.625 ng/ul
MS5 0.3125 ng/ul	THP1 0.3125 ng/ul

140
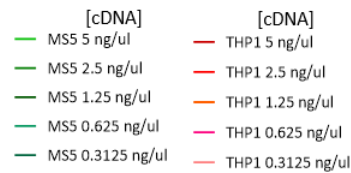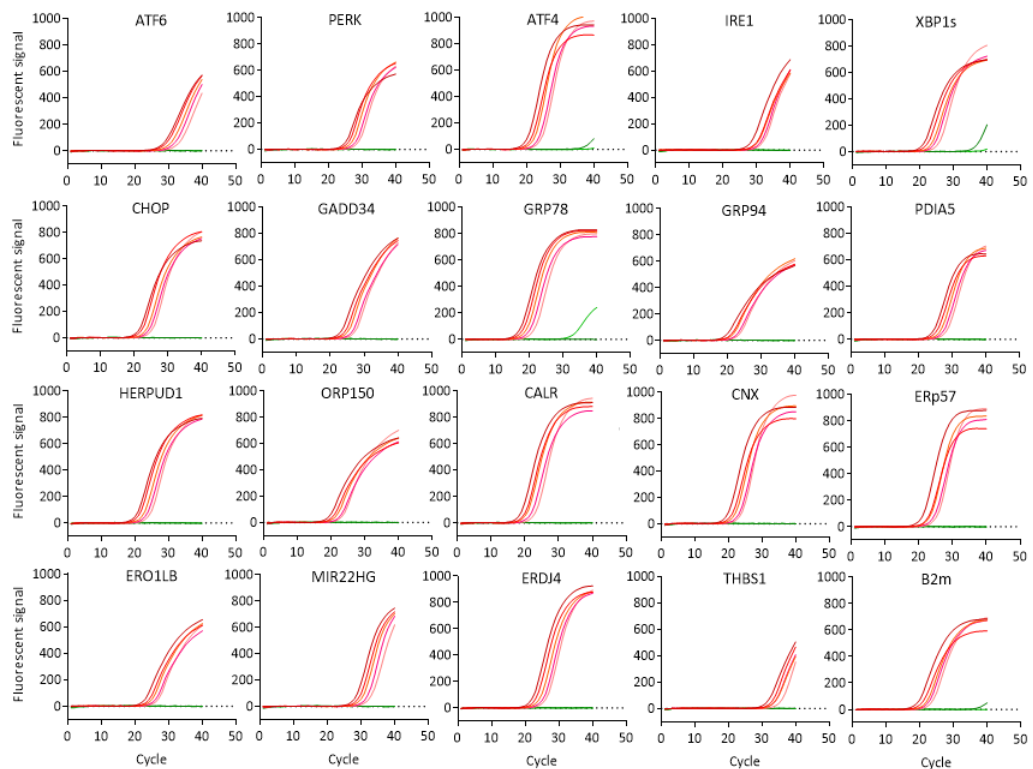
Supplementary Table 6.1: qPCR primer for mouse cDNA

	Forward	Reverse
ATF4	GCGCTCTTCACGAAATCCAG	CATGTTGTGGGGCTTTGCTG
ATF6	CCATGTGGTGAATGTGCTGC	AGCACAGCGATATCCGAACC
CHOP	CCCAGGAAACGAAGAGGAAG	CTTTGGGATGTGCGTGTGAC
CNX	CTAAATCAGATGCCAGCACTCC	TCATCTACTTCCCACTTTCCATCAT
CRT	CTGAATACAAGGGCGAGTGGA	GCATCGGGGGAGTATTCAGG
ERDJ4	GTCGGGGCGCACAGGTTAT	GGCAGACTTTGGCACACCTA
ERO1LB	ACTGCTTCAAGCCTCGATCT	GCTGGCATGGAGTCCTGATA
ERp57	GGACTGCTGATGGAATTGTCA	TGCCCATCACTGAATAAATCCC
GADD34	GAGAAGACCAAGGGACGTGG	AGCGAAGTGTACCTTCCGAG
GRP78	GCCTGTTGCTGGACTCCTAAG	GAACACACCGACGCAGGAAT
GRP94	GTCAAAGGTGTTGTGGATTCCG	TGCCGAACTCCTTCCAGAAA
HERPUD1	ATTCCGCAGCGACGTTTTCT	GTCCTGGTTGGCAGCATCTC
IRE 1	CCGTCCAAGGCCTCCTTTTCT	TCCACTCAGACAAGCATGAGGAC
MIR22HG	TGCCTATCATCCGGAAGTGT	TGAGGCTCCATGTTGGATGAG
ORP150	CTGGTGCGCGAGACGC	CATCACAGCCAATGTGTCGCTC
PDIA5	TGGCTGGGATGAACGTCTAC	AACCGCCCCTTCTCGAAATA
PERK	CATGAGCCCAGAGCAGATTCA	GGGTGCTGAATGGGTAGAGG
THBS1	ACCGGTTATATCAGAGTGGTGAT	AGCGCTGGTTATGATTGGCAG
XBP1 spliced	TGACGAGGTTCCAGAGGTG	CTGCACCTGCTGCGGACTCAG
XBP1 Total	CTACTCTTATCTGGCCAGCCC	TTTTTCAGTTCCTCCGCAGC
actB	CTTCTTTGCAGCTCCTTCGTT	TTCTGACCCATTCCCACCATC

Supplementary Table 6.2: Top 200 upregulated genes in AML-MSC vs HD-MSC

Threshold has been applied to display genes with adj. P.value < 0.05.

Ensembl.id	Gene.name	logFC	P.Value	adj.P.Val
ENSG00000279399	AL356095.2	4.884507439	0.000787894	0.02504565
ENSG00000182389	CACNB4	3.447270918	0.001826386	0.039396992
ENSG00000158258	CLSTN2	2.481884021	0.000236666	0.012104285
ENSG00000143036	SLC44A3	2.157640259	0.000459046	0.01832826
ENSG00000076344	RGS11	2.135954061	0.002701078	0.047979817
ENSG00000198947	DMD	2.044020944	0.000361678	0.015811876
ENSG00000226686	LINC01535	2.022156246	0.00284676	0.049347187
ENSG00000067992	PDK3	1.985991287	0.00113354	0.030199707
ENSG00000106025	TSPAN12	1.872325746	0.000214496	0.01140854
ENSG00000128274	A4GALT	1.736664631	0.000310953	0.014406511
ENSG00000108639	SYNGR2	1.72454147	0.000755179	0.024422225
ENSG00000197381	ADARB1	1.608064753	0.001924869	0.040687375
ENSG00000104936	DMPK	1.600270865	0.002244144	0.043349701
ENSG00000262576	PCDHGA4	1.526280911	0.000109766	0.008005833
ENSG00000187498	COL4A1	1.466362258	0.001156036	0.030468487
ENSG00000178695	KCTD12	1.418779587	4.66E-05	0.005480983
ENSG00000153823	PID1	1.404538868	0.001173046	0.030751768
ENSG00000173210	ABLIM3	1.350423126	0.00234859	0.043964226
ENSG00000180921	FAM83H	1.317273556	0.00282052	0.049173965
ENSG00000145284	SCD5	1.307826862	7.17E-05	0.006484554
ENSG00000204682	MIR1915HG	1.254194498	0.00284809	0.049347187
ENSG00000197903	H2BC12	1.230947891	0.001201014	0.030934514
ENSG00000140450	ARRDC4	1.209698504	4.11E-05	0.0054069
ENSG00000274180	NATD1	1.208234017	0.000271139	0.01322746
ENSG00000204959	ARHGEF34P	1.195141178	0.002813373	0.049168942
ENSG00000147027	TMEM47	1.186479905	0.002204541	0.043076255
ENSG00000258727	AL135999.1	1.171477441	0.002311218	0.043767571
ENSG00000118523	CCN2	1.158017166	0.000495627	0.019266663
ENSG00000152137	HSPB8	1.157999084	0.001052653	0.029406588
ENSG00000134871	COL4A2	1.153449794	0.000404085	0.017106853
ENSG00000107738	VSIR	1.098979036	0.001775347	0.038922902
ENSG00000143162	CREG1	1.095187236	0.000609036	0.021569551
ENSG00000183775	KCTD16	1.079435625	0.001843653	0.039557459
ENSG00000163453	IGFBP7	1.074021987	0.000304311	0.014278402
ENSG00000119280	C1orf198	1.070480627	0.001506337	0.034568333
ENSG00000088899	LZTS3	1.06189403	0.000640511	0.022414844
ENSG00000092969	TGFB2	1.060383228	0.00054732	0.020287658
ENSG00000206503	HLA-A	1.050227239	0.00017344	0.010303594
ENSG00000099337	KCNK6	1.038404033	0.001005017	0.028695563
ENSG00000159348	CYB5R1	1.016636234	0.000114931	0.008180062
ENSG00000137266	SLC22A23	1.00193725	0.002385048	0.044479637
ENSG00000119938	PPP1R3C	1.000716149	0.001442014	0.034075696
ENSG00000162433	AK4	0.99242404	0.000546243	0.020287658
ENSG00000122707	RECK	0.970284224	6.41E-05	0.006185243
ENSG00000000971	CFH	0.96357267	8.84E-05	0.007192515
ENSG00000186815	TPCN1	0.958156272	0.001396792	0.033549215
ENSG00000124762	CDKN1A	0.956212195	0.001371356	0.033395343
ENSG00000115963	RND3	0.927237278	0.00286994	0.049448265
ENSG00000169604	ANTXR1	0.920646907	0.000291012	0.013941968
ENSG00000100439	ABHD4	0.89703207	0.001383368	0.033549215
ENSG00000204580	DDR1	0.894857187	0.000110348	0.008008643
ENSG00000204520	MICA	0.891556679	0.001421897	0.033783006
ENSG00000102452	NALCN	0.877187447	0.002303861	0.043767571
ENSG00000174080	CTSF	0.873836376	0.000131959	0.009000684
ENSG00000139508	SLC46A3	0.86768888	0.001467401	0.034305961
ENSG00000100307	CBX7	0.855326183	0.002850367	0.049347187
ENSG00000134030	CTIF	0.851827697	0.001321117	0.032878407
ENSG00000001461	NIPAL3	0.849948663	0.00048844	0.019130383
ENSG00000198542	ITGBL1	0.847317115	0.001085641	0.029840959
ENSG00000178033	CALHM5	0.815050361	0.002827011	0.049173965
ENSG00000182261	NLRP10	0.813009133	0.00246578	0.045467247
ENSG00000114626	ABTB1	0.805189156	0.000505056	0.01950628
ENSG00000110628	SLC22A18	0.790344749	0.001353936	0.033227198
ENSG00000173482	PTPRM	0.764979043	0.001981145	0.041168135
ENSG00000104763	ASAH1	0.762444213	0.000938639	0.027746175
ENSG00000167702	KIFC2	0.756738149	0.002194543	0.042994949
ENSG00000125629	INSIG2	0.755434545	0.002764657	0.048627521

ENSG00000048392	RRM2B	0.752075503	0.001459636	0.034305961
ENSG00000065809	FAM107B	0.746844755	0.001283541	0.032254232
ENSG00000197696	NMB	0.742051482	0.001097306	0.029882823
ENSG00000123989	CHPF	0.740387757	0.001385243	0.033549215
ENSG00000132824	SERINC3	0.730092163	0.000105246	0.007930877
ENSG00000122786	CALD1	0.72893978	0.000941634	0.027746175
ENSG00000034152	MAP2K3	0.728492512	0.002421877	0.044938938
ENSG00000131018	SYNE1	0.728390443	0.000253353	0.012567835
ENSG00000172667	ZMAT3	0.725275838	0.000300112	0.014171651
ENSG00000127415	IDUA	0.724192317	0.002855724	0.049381903
ENSG00000136156	ITM2B	0.719097018	0.000926227	0.027512312
ENSG00000144583	MARCHF4	0.715981837	0.002121986	0.042345742
ENSG00000152409	JMY	0.71505252	0.001077139	0.029718134
ENSG00000116209	TMEM59	0.714856642	2.63E-05	0.004358651
ENSG00000093010	COMT	0.712194187	0.002576651	0.046591924
ENSG00000174132	FAM174A	0.711750663	0.001017117	0.028817662
ENSG00000113273	ARSB	0.707992151	0.00052946	0.020071448
ENSG00000165912	PACSIN3	0.704020908	0.002607192	0.04679504
ENSG00000181458	TMEM45A	0.700491894	0.001349449	0.033191041
ENSG00000130962	PRRG1	0.699396213	0.001490652	0.03442335
ENSG00000111897	SERINC1	0.696908069	5.97E-05	0.005981795
ENSG00000197746	PSAP	0.689710022	0.001163109	0.030545613
ENSG00000187098	MITF	0.688213875	0.001179384	0.030790408
ENSG00000197081	IGF2R	0.683354606	0.000684255	0.022888333
ENSG00000101460	MAP1LC3A	0.680546749	6.55E-05	0.006185243
ENSG00000164463	CREBRF	0.680505687	0.002449119	0.045273369
ENSG00000134574	DDB2	0.672392937	0.000699053	0.023159675
ENSG00000157978	LDLRAP1	0.667228725	0.000608716	0.021569551
ENSG00000164187	LMBRD2	0.660648133	0.002055209	0.041764689
ENSG00000025293	PHF20	0.659230359	0.00223456	0.04331812
ENSG00000137103	TMEM8B	0.65486798	0.00043935	0.017885028
ENSG00000183723	CMTM4	0.654135854	0.000654605	0.0225544
ENSG00000152894	PTPRK	0.651975422	0.000426364	0.017630691
ENSG00000167740	CYB5D2	0.650266264	0.001952118	0.040892808
ENSG00000076351	SLC46A1	0.641259095	0.002585665	0.046648677
ENSG00000132376	INPP5K	0.641081116	0.000918859	0.027403937
ENSG00000100284	TOM1	0.631658297	4.52E-05	0.005462563
ENSG00000003402	CFLAR	0.631476547	0.001400244	0.033549215
ENSG00000013392	RWDD2A	0.630546504	0.001295548	0.032461406
ENSG00000182534	MXRA7	0.630181776	0.000139288	0.00931749
ENSG00000129493	HEATR5A	0.629899354	0.001230307	0.031523666
ENSG00000243749	TMEM35B	0.629862075	0.002071043	0.041798194
ENSG00000140391	TSPAN3	0.629003644	2.95E-05	0.004665939
ENSG00000166046	TCP11L2	0.625080273	0.002768569	0.048627521
ENSG00000141542	RAB40B	0.623760471	0.00172725	0.038358835
ENSG00000158467	AHCYL2	0.622264329	7.68E-05	0.006775297
ENSG00000133872	SARAF	0.619434504	0.000204073	0.011094492
ENSG00000099785	MARCHF2	0.619097322	0.001397685	0.033549215
ENSG00000170385	SLC30A1	0.618307909	0.000548055	0.020287658
ENSG00000107679	PLEKHA1	0.615310864	3.86E-05	0.005269205
ENSG00000166946	CCNDBP1	0.614030618	0.000707316	0.023359424
ENSG00000103227	LMF1	0.613058621	0.001393741	0.033549215
ENSG00000106211	HSPB1	0.606544053	0.002588756	0.046648677
ENSG00000182372	CLN8	0.60592829	0.001130843	0.030182452
ENSG00000137414	FAM8A1	0.604534599	5.93E-05	0.005981795
ENSG00000042445	RETSAT	0.601070426	0.001140179	0.030267121
ENSG00000126458	RRAS	0.600050297	0.000859273	0.026210493
ENSG00000090581	GNPTG	0.598999615	0.000248389	0.012405127
ENSG00000153214	TMEM87B	0.598903406	0.000677989	0.022805504
ENSG00000105404	RABAC1	0.598643416	0.000638768	0.022407062
ENSG00000165943	MOAP1	0.597770142	0.000588561	0.021201132
ENSG00000220205	VAMP2	0.594608708	0.001897913	0.040233446
ENSG00000113732	ATP6V0E1	0.589984823	0.000413723	0.017415382
ENSG00000148848	ADAM12	0.588962763	0.002487935	0.045761232
ENSG00000106052	TAX1BP1	0.587618431	0.000114382	0.008180062
ENSG00000198832	SELENOM	0.586146453	0.000441012	0.017885028
ENSG00000269556	TMEM185A	0.585163591	0.001068496	0.029647233
ENSG00000183722	LHFPL6	0.579007622	0.001785411	0.039002564
ENSG00000171928	TVP23B	0.571192617	4.39E-05	0.005462563
ENSG00000166311	SMPD1	0.569181708	0.001197088	0.030887391
ENSG00000213625	LEPROT	0.566892448	0.001105303	0.029889838

ENSG00000106771	TMEM245	0.566578286	0.00156832	0.035493646
ENSG00000197324	LRP10	0.566409647	0.000327964	0.014867358
ENSG00000050130	JKAMP	0.566299505	0.002050397	0.041764689
ENSG00000126391	FRMD8	0.565107255	0.002046673	0.041764027
ENSG00000119801	YPEL5	0.562374189	0.002267036	0.043489892
ENSG00000168936	TMEM129	0.561862989	0.000188711	0.010757257
ENSG00000144357	UBR3	0.559185037	0.000562479	0.020563298
ENSG00000107331	ABCA2	0.558884324	0.001384126	0.033549215
ENSG00000030582	GRN	0.557054649	0.001109736	0.029889838
ENSG00000163697	APBB2	0.556258052	0.001432455	0.033929827
ENSG00000176046	NUPR1	0.552143706	0.000357226	0.015733045
ENSG00000140941	MAP1LC3B	0.55122112	0.000233626	0.012015672
ENSG00000107372	ZFAND5	0.548101114	0.001522215	0.034824215
ENSG00000129625	REEP5	0.548090083	0.001466787	0.034305961
ENSG00000116604	MEF2D	0.546345472	0.000252753	0.012567835
ENSG00000153904	DDAH1	0.545515838	0.001191762	0.030858047
ENSG00000109016	DHRS7B	0.545054336	0.001568341	0.035493646
ENSG00000101290	CDS2	0.543177802	0.000631103	0.022244113
ENSG00000110057	UNC93B1	0.540549251	0.00210722	0.042296558
ENSG00000168216	LMBRD1	0.538147979	0.0026503	0.047329544
ENSG00000143753	DEGS1	0.536183935	0.001345519	0.033149717
ENSG00000177666	PNPLA2	0.533565618	0.002082469	0.041971303
ENSG00000239305	RNF103	0.533265926	0.000517438	0.019801083
ENSG00000139190	VAMP1	0.531866836	0.002758212	0.048627521
ENSG00000128590	DNAJB9	0.530195276	0.000405233	0.017106853
ENSG00000063660	GPC1	0.52515629	0.001993481	0.041285513
ENSG00000162604	TM2D1	0.523153751	0.000246291	0.012342187
ENSG00000186111	PIP5K1C	0.520094143	0.00109094	0.029850237
ENSG00000126524	SBDS	0.517158024	0.001462632	0.034305961
ENSG00000013288	MAN2B2	0.516162616	0.001151486	0.03045754
ENSG00000171105	INSR	0.512891566	0.002122743	0.042345742
ENSG00000263465	SRSF8	0.512297665	0.001921342	0.04067116
ENSG00000063854	HAGH	0.511988974	0.001496687	0.034508113
ENSG00000152492	CCDC50	0.506418981	0.001331838	0.032978101
ENSG00000105856	HBP1	0.504100735	0.000267894	0.013112586
ENSG00000149557	FEZ1	0.503415756	0.002534161	0.046264928
ENSG00000164331	ANKRA2	0.502512763	0.002514696	0.046076849
ENSG00000090674	MCOLN1	0.499447895	0.000922314	0.027451414
ENSG00000169826	CSGALNACT2	0.492080156	0.000647896	0.022483638
ENSG00000005486	RHBDD2	0.491061116	0.000389114	0.016616863
ENSG00000090238	YPEL3	0.48900998	0.000546499	0.020287658
ENSG00000168300	PCMTD1	0.484979899	0.002149621	0.042346076
ENSG00000120725	SIL1	0.484467465	0.002126837	0.042345742
ENSG00000119537	KDSR	0.483510276	0.000200388	0.011001722
ENSG00000083097	DOP1A	0.481451074	0.000947708	0.027758622
ENSG00000017260	ATP2C1	0.481213163	0.000814807	0.025326062
ENSG00000136854	STXBP1	0.48087355	0.000742449	0.024093607
ENSG00000145391	SETD7	0.479256741	0.000966813	0.028090401
ENSG00000198380	GFPT1	0.478538737	0.002548302	0.046456544
ENSG00000189339	SLC35E2B	0.461590273	0.00094729	0.027758622
ENSG00000100647	SUSD6	0.460826848	0.000812911	0.025320531
ENSG00000144455	SUMF1	0.457546284	0.002577372	0.046591924
ENSG00000174307	PHLDA3	0.457306107	0.001462547	0.034305961
ENSG00000135452	TSPAN31	0.454135724	0.001127729	0.030153951
ENSG00000068971	PPP2R5B	0.452668503	0.002114027	0.042345742
ENSG00000103042	SLC38A7	0.452217681	0.00212786	0.042345742
ENSG00000164117	FBXO8	0.449280087	0.00212944	0.042345742
ENSG00000197530	MIB2	0.449225253	0.002208546	0.04307794
ENSG00000114019	AMOTL2	0.447604084	0.002504663	0.045954172
ENSG00000186591	UBE2H	0.446312374	0.000419007	0.017537573
ENSG00000100949	RABGGTA	0.445290825	0.002690565	0.047979817
ENSG00000182220	ATP6AP2	0.443025974	0.000297592	0.01414331

Supplementary Table 6.3: Top 200 downregulated genes in AML-MSC vs HD-MSC.

Threshold has been applied to display genes with adj.P.value < 0.05.

Ensembl.id	Gene.name	logFC	P.Value	adj.P.Val
ENSG00000130052	STARD8	-1.482240701	0.001515576	0.034726255
ENSG00000147536	GINS4	-1.483084661	7.54E-05	0.006690825
ENSG00000131747	TOP2A	-1.486232228	0.000206595	0.01118425
ENSG00000123975	CKS2	-1.491925167	0.000200849	0.011001722
ENSG00000073111	MCM2	-1.502231696	5.70E-06	0.002799675
ENSG00000130592	LSP1	-1.507348659	0.001161983	0.030545613
ENSG00000196220	SRGAP3	-1.512229049	0.001762128	0.038727953
ENSG00000186871	ERCC6L	-1.513333635	1.67E-05	0.003583247
ENSG00000137310	TCF19	-1.514667655	2.10E-06	0.00206795
ENSG00000165490	DDIAS	-1.518223631	2.33E-05	0.004036172
ENSG00000100479	POLE2	-1.523151426	0.000695903	0.023159675
ENSG00000100297	MCM5	-1.530493491	2.41E-06	0.002092082
ENSG00000154920	EME1	-1.532820647	0.001365087	0.03329772
ENSG00000146670	CDCA5	-1.533645083	1.86E-06	0.00206795
ENSG00000138160	KIF11	-1.538616667	8.24E-05	0.007081064
ENSG00000138182	KIF20B	-1.539346403	1.19E-05	0.003281923
ENSG00000189057	FAM111B	-1.539791059	0.002065859	0.041798194
ENSG00000075702	WDR62	-1.542396202	4.97E-06	0.002799675
ENSG00000011426	ANLN	-1.551122825	0.000116173	0.008228732
ENSG00000158402	CDC25C	-1.555581953	0.001176504	0.030787637
ENSG00000164109	MAD2L1	-1.55997804	1.23E-05	0.003281923
ENSG00000118193	KIF14	-1.561770411	0.000238466	0.012104285
ENSG00000174371	EXO1	-1.561922636	0.000193156	0.010861691
ENSG00000164649	CDCA7L	-1.564920934	0.000189838	0.010757257
ENSG00000105011	ASF1B	-1.56521261	2.39E-06	0.002092082
ENSG00000092853	CLSPN	-1.566276843	8.28E-07	0.002032286
ENSG00000119969	HELLS	-1.572790972	2.04E-05	0.003844446
ENSG00000127423	AUNIP	-1.574498795	0.000168283	0.010287628
ENSG00000106462	EZH2	-1.576616788	2.72E-05	0.004456856
ENSG00000102057	KCND1	-1.578218981	0.002046567	0.041764027
ENSG00000071539	TRIP13	-1.581372633	7.85E-06	0.002965282
ENSG00000080986	NDC80	-1.584093962	1.95E-05	0.00372342
ENSG00000175063	UBE2C	-1.584690983	4.60E-05	0.005469156
ENSG00000142731	PLK4	-1.587469285	7.43E-06	0.002965282
ENSG00000013810	TACC3	-1.595108814	6.33E-06	0.002965282
ENSG00000176890	TYMS	-1.596945361	9.52E-06	0.003051814
ENSG00000024526	DEPDC1	-1.608845116	5.55E-05	0.005773009
ENSG00000135476	ESPL1	-1.612885729	1.84E-05	0.00370074
ENSG00000171848	RRM2	-1.61494535	1.53E-05	0.00347877
ENSG00000112742	TTK	-1.623436894	2.54E-05	0.004255794
ENSG00000137812	KNL1	-1.634689623	7.67E-06	0.002965282
ENSG00000167513	CDT1	-1.641948639	9.31E-06	0.003051814
ENSG00000143387	CTSK	-1.64240952	0.002520732	0.046076849
ENSG00000075218	GTSE1	-1.646781079	4.49E-06	0.002799675
ENSG00000183856	IQGAP3	-1.648405861	7.68E-06	0.002965282
ENSG00000166831	RBPMS2	-1.648857856	0.000429411	0.017630691
ENSG00000203760	CENPW	-1.651995196	5.44E-05	0.005773009
ENSG00000156970	BUB1B	-1.663369826	2.18E-05	0.003919346
ENSG00000152253	SPC25	-1.66425934	8.19E-05	0.007081064
ENSG00000137804	NUSAP1	-1.666318339	1.23E-06	0.00206795
ENSG00000187741	FANCA	-1.667441372	1.88E-06	0.00206795
ENSG00000145386	CCNA2	-1.669495066	0.000474451	0.018841207
ENSG00000197299	BLM	-1.669848466	1.86E-05	0.00370074
ENSG00000035499	DEPDC1B	-1.672811885	0.00021996	0.011451158
ENSG00000171320	ESCO2	-1.67314006	5.53E-05	0.005773009
ENSG00000122966	CIT	-1.676328352	8.51E-05	0.007081064
ENSG00000169607	CKAP2L	-1.677426561	1.04E-05	0.003051814
ENSG00000134690	CDCA8	-1.68075789	3.16E-05	0.004847071
ENSG00000186185	KIF18B	-1.685035389	1.29E-05	0.003322318
ENSG00000093009	CDC45	-1.696140208	4.81E-05	0.005536632
ENSG00000135451	TROAP	-1.697277134	0.000169651	0.010301197
ENSG00000101447	FAM83D	-1.697292675	0.000432614	0.017704716
ENSG00000076382	SPAG5	-1.699946914	5.45E-05	0.005773009
ENSG00000230615	AL139220.2	-1.705622527	0.000735274	0.024012378
ENSG00000166851	PLK1	-1.709485279	0.000217961	0.011427839
ENSG00000111665	CDCA3	-1.716501688	5.53E-05	0.005773009
ENSG00000171241	SHCBP1	-1.716577859	4.77E-06	0.002799675

ENSG00000117724	CENPF	-1.718955496	4.36E-05	0.005462563
ENSG00000131153	GINS2	-1.727281097	6.70E-07	0.002032286
ENSG00000168078	PBK	-1.72831119	1.41E-05	0.003397978
ENSG00000163808	KIF15	-1.733291401	2.52E-05	0.004255794
ENSG00000237649	KIFC1	-1.734413312	7.69E-06	0.002965282
ENSG00000139354	GAS2L3	-1.744178092	4.73E-05	0.005482126
ENSG00000101057	MYBL2	-1.75021539	4.97E-05	0.005674845
ENSG00000066279	ASPM	-1.752763261	5.04E-05	0.005713594
ENSG00000087586	AURKA	-1.759537496	8.53E-05	0.007081064
ENSG00000117632	STMN1	-1.763008696	6.51E-05	0.006185243
ENSG00000106976	DNM1	-1.764023017	0.00289586	0.049783789
ENSG00000149948	HMGA2	-1.767148425	0.002836303	0.04927742
ENSG00000198901	PRC1	-1.775466577	0.00023348	0.012015672
ENSG00000148773	MKI67	-1.778019171	1.74E-06	0.00206795
ENSG00000154839	SKA1	-1.780233207	1.37E-05	0.003397978
ENSG00000231007	CDC20P1	-1.788554166	0.0014871	0.03442335
ENSG00000178999	AURKB	-1.792294962	6.72E-05	0.006227129
ENSG00000138180	CEP55	-1.793762569	6.49E-05	0.006185243
ENSG00000167900	TK1	-1.795503515	3.77E-05	0.00526287
ENSG00000143228	NUF2	-1.798827035	0.000103807	0.007930877
ENSG00000121152	NCAPH	-1.800702746	1.02E-05	0.003051814
ENSG00000166803	PCLAF	-1.810961399	4.91E-06	0.002799675
ENSG00000104147	OIP5	-1.812528727	2.09E-05	0.003844446
ENSG00000072571	HMMR	-1.812792012	0.000238981	0.012104285
ENSG00000134057	CCNB1	-1.814360996	0.000344638	0.015293827
ENSG00000085999	RAD54L	-1.815328371	0.000138032	0.009285936
ENSG00000117399	CDC20	-1.8256704	0.000136284	0.009252884
ENSG00000187951	AC091057.1	-1.827799418	0.000771316	0.024650336
ENSG00000179750	APOBEC3B	-1.828656962	8.79E-06	0.003051814
ENSG00000100162	CENPM	-1.850229958	4.20E-05	0.005432792
ENSG00000157456	CCNB2	-1.856943159	8.60E-05	0.007081064
ENSG00000115163	CENPA	-1.85871891	0.000175233	0.010368293
ENSG00000090889	KIF4A	-1.881472214	1.78E-05	0.00370074
ENSG00000085840	ORC1	-1.88606667	0.000197713	0.010992085
ENSG00000169679	BUB1	-1.887241143	3.55E-05	0.0050544
ENSG00000117650	NEK2	-1.90112913	0.000179466	0.010492325
ENSG00000164611	PTTG1	-1.902288435	4.32E-05	0.005462563
ENSG00000186193	SAPCD2	-1.903570386	9.41E-05	0.007537419
ENSG00000068489	PRR11	-1.907415973	2.11E-06	0.00206795
ENSG00000129195	PIMREG	-1.926434533	1.77E-05	0.00370074
ENSG00000064692	SNCAIP	-1.931869182	0.001762142	0.038727953
ENSG00000276043	UHRF1	-1.932824159	3.93E-05	0.005269205
ENSG00000111206	FOXM1	-1.946456873	8.64E-06	0.003051814
ENSG00000259316	AC087632.2	-1.95122914	7.78E-06	0.002965282
ENSG00000126787	DLGAP5	-1.960406197	6.24E-05	0.006126276
ENSG00000129810	SGO1	-1.963198811	6.17E-05	0.006124148
ENSG00000065328	MCM10	-1.96366687	1.50E-05	0.003447107
ENSG00000110492	MDK	-1.976413498	7.48E-07	0.002032286
ENSG00000175305	CCNE2	-1.980604482	0.000170605	0.010301348
ENSG00000165480	SKA3	-1.999089413	1.41E-06	0.00206795
ENSG00000089685	BIRC5	-2.014906679	0.000107885	0.007987311
ENSG00000100526	CDKN3	-2.069581504	0.000709991	0.023359424
ENSG00000113368	LMNB1	-2.072962056	7.70E-06	0.002965282
ENSG00000075213	SEMA3A	-2.077677964	0.002216237	0.04307794
ENSG00000157551	KCNJ15	-2.120013689	0.001108321	0.029889838
ENSG00000112984	KIF20A	-2.158338873	0.000159955	0.01002815
ENSG00000028137	TNFRSF1B	-2.263482888	0.001415713	0.033695804
ENSG00000196460	RFX8	-2.321414742	0.000221163	0.011473234
ENSG00000261373	VPS9D1-AS1	-2.39804426	0.002023203	0.041469211
ENSG00000263513	FAM72C	-2.436775253	0.000916141	0.027378305
ENSG00000106785	TRIM14	-2.487534337	0.000159079	0.01001584
ENSG00000173376	NDNF	-2.55428404	0.002053513	0.041764689
ENSG00000102879	CORO1A	-2.655962158	0.00080311	0.025228622
ENSG00000238266	LINC00707	-3.234670712	0.002340983	0.043935934

Supplementary Table 6.4: Top 200 upregulated genes in PERK-MSC vs rtTA-MSC.

Threshold has been applied to display genes with adj.P.value < 0.05.

Ensembl.id	Gene.name	logFC	P.Value	adj.P.Val
ENSG00000225420	AC104134.1	9.466788059	2.72E-09	3.66E-08
ENSG00000170689	HOXB9	7.73754905	7.39E-09	8.26E-08
ENSG00000160179	ABCG1	7.460544864	4.35E-08	3.55E-07
ENSG00000172071	EIF2AK3	7.166229665	4.44E-22	6.54E-18
ENSG00000078081	LAMP3	6.584222846	3.79E-09	4.79E-08
ENSG00000133134	BEX2	6.488232224	2.16E-08	1.97E-07
ENSG00000110680	CALCA	6.231485715	1.20E-06	5.96E-06
ENSG00000189410	SH2D5	6.039973629	3.23E-08	2.78E-07
ENSG00000006128	TAC1	5.816711185	1.21E-06	6.01E-06
ENSG00000115602	IL1RL1	5.676712408	3.72E-06	1.58E-05
ENSG00000102683	SGCG	5.444761864	7.65E-07	4.03E-06
ENSG00000134548	SPX	5.313575611	2.39E-08	2.15E-07
ENSG00000155961	RAB39B	5.144694496	4.03E-11	1.21E-09
ENSG00000205609	EIF3CL	5.085765321	0.02471922	0.040627875
ENSG00000272196	H2AC19	4.97146717	0.011738054	0.020888604
ENSG00000163884	KLF15	4.943996546	8.11E-11	2.08E-09
ENSG00000163347	CLDN1	4.74246665	3.40E-15	1.44E-12
ENSG00000258667	HIF1A-AS3	4.677625391	2.08E-07	1.33E-06
ENSG00000254835	RNF185-AS1	4.57048878	7.05E-05	0.000214005
ENSG00000279484	KLHL30-AS1	4.475214344	1.03E-07	7.32E-07
ENSG00000164683	HEY1	4.462324964	4.81E-06	1.97E-05
ENSG00000181585	TMIE	4.413102972	3.71E-07	2.16E-06
ENSG00000130487	KLHDC7B	4.398220787	8.03E-11	2.07E-09
ENSG00000204334	ERICH2	4.356666187	3.67E-05	0.000119737
ENSG00000163216	SPRR2D	4.242852843	2.54E-05	8.62E-05
ENSG00000205923	CEMP1	4.208323072	0.01434951	0.024974759
ENSG00000162772	ATF3	4.162288007	1.74E-15	9.88E-13
ENSG00000081041	CXCL2	4.156037854	5.16E-08	4.10E-07
ENSG00000123892	RAB38	4.13301734	8.06E-08	5.95E-07
ENSG00000239467	AC007405.3	4.052707944	1.03E-06	5.22E-06
ENSG00000102032	RENBP	4.012619509	3.40E-05	0.000111556
ENSG00000197632	SERPINB2	3.930664394	7.78E-05	0.000233807
ENSG00000171658	NMRAL2P	3.889454109	8.47E-10	1.39E-08
ENSG00000196866	H2AC7	3.86979183	0.000480463	0.001190691
ENSG00000250509	AC034213.1	3.867518315	2.77E-05	9.29E-05
ENSG00000278202	AC243919.2	3.724562349	0.001592935	0.003462483
ENSG00000145777	TSLP	3.683850614	7.59E-11	1.99E-09
ENSG00000224712	NPIPA3	3.660370852	0.003584012	0.007152973
ENSG00000170909	OSCAR	3.642946951	3.61E-10	7.05E-09
ENSG00000109321	AREG	3.623759062	4.20E-07	2.41E-06
ENSG00000255663	AP002373.1	3.604900872	0.005539951	0.010606899
ENSG00000156453	PCDH1	3.591523888	5.70E-13	4.72E-11
ENSG00000261499	AC233699.1	3.555334755	0.002769021	0.005666896
ENSG00000115604	IL18R1	3.512376501	8.51E-08	6.25E-07
ENSG00000258186	SLC7A5P2	3.509725404	0.000578727	0.001401445
ENSG00000256040	PAPPA-AS1	3.500810422	0.001338753	0.002976736
ENSG00000243742	RPLP0P2	3.474861937	4.65E-12	2.18E-10
ENSG00000258964	AL137129.1	3.427651569	0.003025714	0.006137662
ENSG00000188487	INSC	3.42670615	0.00258699	0.005329902
ENSG00000139269	INHBE	3.420618168	8.40E-12	3.51E-10
ENSG00000285901	AC008012.1	3.328072052	0.000184163	0.000504044
ENSG00000271992	AL354872.1	3.296870339	0.006671516	0.012545174
ENSG00000275493	AL627230.1	3.287350351	0.000571351	0.001386545
ENSG00000156510	HKDC1	3.249971548	7.53E-08	5.62E-07
ENSG00000023445	BIRC3	3.194638552	7.43E-11	1.96E-09
ENSG00000276148	AC084824.5	3.155626006	0.004728695	0.009199507
ENSG00000197409	H3C4	3.152211437	0.002224176	0.00465133
ENSG00000183598	H3C13	3.138565997	0.003144024	0.006354904
ENSG00000154319	FAM167A	3.077900175	1.70E-12	1.03E-10
ENSG00000163734	CXCL3	3.071575444	2.51E-06	1.13E-05
ENSG00000196302	AC146944.1	3.008003483	0.022854117	0.03786233
ENSG00000136404	TM6SF1	2.974351763	1.19E-09	1.84E-08
ENSG00000124635	H2BC11	2.967743108	2.58E-05	8.73E-05
ENSG00000168918	INPP5D	2.961222367	2.38E-07	1.50E-06
ENSG00000150594	ADRA2A	2.953575267	2.68E-06	1.20E-05
ENSG00000130513	GDF15	2.941632354	9.11E-19	4.47E-15
ENSG00000147509	RGS20	2.938377248	1.86E-07	1.21E-06

ENSG00000259522	AL136295.4	2.900247456	0.014658376	0.025470203
ENSG00000087074	PPP1R15A	2.891717631	1.37E-19	1.01E-15
ENSG00000165121	AL353743.1	2.887507466	1.39E-08	1.37E-07
ENSG00000183775	KCTD16	2.874364058	4.14E-14	7.34E-12
ENSG00000173535	TNFRSF10C	2.848290512	2.09E-06	9.65E-06
ENSG00000116761	CTH	2.847793383	4.43E-15	1.68E-12
ENSG00000163993	S100P	2.842729654	0.002691098	0.005521997
ENSG00000165891	E2F7	2.842522698	2.95E-14	6.04E-12
ENSG00000186642	PDE2A	2.838333978	1.62E-06	7.75E-06
ENSG00000178773	CPNE7	2.827146532	1.48E-05	5.33E-05
ENSG00000179242	CDH4	2.820976748	1.09E-12	7.65E-11
ENSG00000272168	CASC15	2.811859125	3.24E-11	1.02E-09
ENSG00000185950	IRS2	2.760373825	8.52E-14	1.24E-11
ENSG00000137825	ITPKA	2.754815038	0.000157733	0.000439547
ENSG00000154928	EPHB1	2.752573662	1.49E-07	9.98E-07
ENSG00000123329	ARHGAP9	2.746505616	6.90E-06	2.71E-05
ENSG00000145002	FAM86B2	2.743320321	0.000949301	0.00219011
ENSG00000163393	SLC22A15	2.738646538	1.73E-14	4.24E-12
ENSG00000184254	ALDH1A3	2.723178312	4.56E-14	7.82E-12
ENSG00000075643	MOCOS	2.71903926	6.70E-14	1.02E-11
ENSG00000012223	LTF	2.713432406	0.001540954	0.00336289
ENSG00000197989	SNHG12	2.711291225	6.28E-15	2.01E-12
ENSG00000152463	OLAH	2.705895393	0.001975878	0.004184362
ENSG00000274213	AC015912.3	2.702132027	9.08E-05	0.000269266
ENSG00000135842	NIBAN1	2.692452128	1.37E-16	1.55E-13
ENSG00000140961	OSGIN1	2.67804428	1.93E-13	2.22E-11
ENSG00000261717	AC009163.5	2.668338037	0.030977501	0.049661755
ENSG00000188818	ZDHHC11	2.66209498	0.000385615	0.00097717
ENSG00000116717	GADD45A	2.659234856	6.90E-18	2.45E-14
ENSG00000131737	KRT34	2.657853005	1.80E-16	1.77E-13
ENSG00000138685	FGF2	2.656951307	5.93E-17	9.86E-14
ENSG00000100292	HMOX1	2.651616284	1.92E-16	1.77E-13
ENSG00000141682	PMAIP1	2.650923763	6.26E-13	5.04E-11
ENSG00000146678	IGFBP1	2.618481838	0.001230331	0.002762032
ENSG00000230825	AC005532.1	2.611454367	9.71E-06	3.66E-05
ENSG00000145819	ARHGAP26	2.603853302	5.67E-13	4.72E-11
ENSG00000099812	MISP	2.5979348	1.43E-08	1.41E-07
ENSG00000224864	AC011447.1	2.591577044	0.005267084	0.010139808
ENSG00000055163	CYFIP2	2.583526006	1.24E-11	4.80E-10
ENSG00000108448	TRIM16L	2.57970366	3.16E-14	6.22E-12
ENSG00000171791	BCL2	2.557790828	8.34E-09	9.03E-08
ENSG00000228409	CCT6P1	2.545818808	1.09E-08	1.12E-07
ENSG00000273542	H4C12	2.544474781	0.009072473	0.016534481
ENSG00000175567	UCP2	2.534675289	0.000811327	0.001899457
ENSG00000158079	PTPDC1	2.522511226	1.75E-13	2.07E-11
ENSG00000118971	CCND2	2.512998252	2.71E-06	1.21E-05
ENSG00000165113	GKAP1	2.512553311	5.26E-08	4.17E-07
ENSG00000250846	EPHA5-AS1	2.511299607	0.021657903	0.036087523
ENSG00000178718	RPP25	2.501011063	2.67E-08	2.38E-07
ENSG00000241322	CDRT1	2.492469924	2.61E-09	3.54E-08
ENSG00000249859	PVT1	2.487639384	4.75E-13	4.25E-11
ENSG00000101255	TRIB3	2.471612539	1.01E-17	2.47E-14
ENSG00000197837	H4-16	2.462281042	0.00018678	0.000510733
ENSG00000245025	AC107959.1	2.448277326	1.56E-08	1.51E-07
ENSG00000165030	NFIL3	2.445619307	8.62E-15	2.56E-12
ENSG00000157150	TIMP4	2.442249728	2.03E-06	9.41E-06
ENSG00000245848	CEBPA	2.437122031	1.28E-05	4.70E-05
ENSG00000054356	PTPRN	2.420535463	2.28E-07	1.44E-06
ENSG00000253616	AC107959.3	2.409624829	0.011263068	0.02010648
ENSG00000182752	PAPPA	2.382828813	6.02E-13	4.96E-11
ENSG00000157557	ETS2	2.382646773	5.22E-13	4.50E-11
ENSG00000254352	AC100854.1	2.377652995	0.012743476	0.022444666
ENSG00000111012	CYP27B1	2.358274488	0.000144101	0.000405084
ENSG00000272138	LINC01607	2.358149259	0.00119969	0.002698477
ENSG00000243686	RPLP1P11	2.355662229	0.01653829	0.028352178
ENSG00000206341	HLA-H	2.355350521	0.012422229	0.021957612
ENSG00000160917	CPSF4	2.355326498	3.71E-16	2.87E-13
ENSG00000178860	MSC	2.349416704	1.04E-15	6.63E-13
ENSG00000073756	PTGS2	2.334663555	2.48E-10	5.18E-09
ENSG00000146374	RSPO3	2.329679904	2.35E-05	8.04E-05
ENSG00000118785	SPP1	2.329153029	4.11E-06	1.73E-05

ENSG00000259867	AC105411.1	2.327234378	2.67E-05	8.97E-05
ENSG00000196152	ZNF79	2.323709795	2.75E-11	9.10E-10
ENSG00000256433	AC005840.2	2.315692094	0.003968072	0.007850356
ENSG00000213147	RPL23AP60	2.30412963	0.027608625	0.044900968
ENSG00000251393	AC005280.1	2.293842198	0.002358908	0.004905955
ENSG00000168621	GDNF	2.287539674	2.72E-14	5.64E-12
ENSG00000178607	ERN1	2.273024327	9.81E-13	7.09E-11
ENSG00000198342	ZNF442	2.269846518	5.62E-08	4.40E-07
ENSG00000119703	ZC2HC1C	2.25142101	7.82E-05	0.000234789
ENSG00000277998	AC107075.1	2.250920382	0.015617009	0.026942083
ENSG00000113448	PDE4D	2.248181083	4.27E-13	3.95E-11
ENSG00000223547	ZNF844	2.247769671	1.88E-12	1.11E-10
ENSG00000180730	SHISA2	2.243803532	7.27E-09	8.17E-08
ENSG00000258150	AC133555.3	2.239322892	0.023235057	0.038402748
ENSG00000172059	KLF11	2.236872901	5.48E-13	4.67E-11
ENSG00000123689	G0S2	2.227424127	7.59E-12	3.22E-10
ENSG00000113742	CPEB4	2.22575404	3.27E-14	6.34E-12
ENSG00000270882	H4C14	2.221908928	1.69E-10	3.76E-09
ENSG00000220920	AL023807.1	2.21635173	0.017672344	0.03010367
ENSG00000104689	TNFRSF10A	2.209963675	2.79E-07	1.71E-06
ENSG00000238258	AL121748.1	2.201104574	0.006946634	0.013020962
ENSG00000106948	AKNA	2.195232598	1.05E-13	1.44E-11
ENSG00000120889	TNFRSF10B	2.179952127	8.31E-18	2.45E-14
ENSG00000188573	FBLL1	2.178436338	1.16E-06	5.77E-06
ENSG00000011347	SYT7	2.175524303	7.13E-10	1.22E-08
ENSG00000164463	CREBRF	2.175081192	7.41E-11	1.96E-09
ENSG00000177453	NIM1K	2.165382621	3.49E-08	2.96E-07
ENSG00000059728	MXD1	2.155097127	6.06E-15	2.01E-12
ENSG00000179598	PLD6	2.151240363	2.40E-09	3.30E-08
ENSG00000256633	PDE2A-AS2	2.147856201	0.001865472	0.003975122
ENSG00000169594	BNC1	2.143425956	5.33E-15	1.91E-12
ENSG00000157510	AFAP1L1	2.142013829	5.23E-08	4.15E-07
ENSG00000143178	TBX19	2.137900134	1.09E-08	1.12E-07
ENSG00000185710	SMG1P4	2.13241149	0.000169806	0.000468141
ENSG00000105499	PLA2G4C	2.131152934	1.32E-09	2.01E-08
ENSG00000232956	SNHG15	2.121350277	5.64E-13	4.72E-11
ENSG00000131480	AOC2	2.116178511	4.20E-05	0.000134941
ENSG00000177363	LRRN4CL	2.111802027	1.50E-10	3.45E-09
ENSG00000131941	RHPN2	2.099488643	3.30E-10	6.51E-09
ENSG00000143469	SYT14	2.094555843	8.70E-06	3.33E-05
ENSG00000227354	RBM26-AS1	2.091213381	1.17E-05	4.31E-05
ENSG00000170989	S1PR1	2.088021451	1.24E-10	2.94E-09
ENSG00000213244	H3P4	2.087425112	0.000630183	0.001511148
ENSG00000175197	DDIT3	2.077544209	9.07E-16	6.36E-13
ENSG00000288632	AC133555.6	2.060037701	4.97E-09	5.95E-08
ENSG00000198208	RPS6KL1	2.05847707	8.63E-06	3.30E-05
ENSG00000124191	TOX2	2.04751859	1.64E-08	1.56E-07
ENSG00000004799	PDK4	2.042009347	3.37E-05	0.000110804
ENSG00000166455	C16orf46	2.036971844	0.005102822	0.009853195
ENSG00000188613	NANOS1	2.036469317	4.65E-08	3.75E-07
ENSG00000108379	WNT3	2.0348232	8.47E-10	1.39E-08
ENSG00000120149	MSX2	2.034123599	0.000510544	0.001257623
ENSG00000169429	CXCL8	2.033721816	1.97E-05	6.86E-05
ENSG00000151012	SLC7A11	2.030643437	2.41E-14	5.28E-12
ENSG00000159388	BTG2	2.029779093	4.75E-14	7.96E-12
ENSG00000256664	AC025423.2	2.027982373	6.57E-10	1.15E-08
ENSG00000169087	HSPBAP1	2.021237164	9.87E-11	2.46E-09
ENSG00000223345	H2BP1	2.012651274	0.003043136	0.006166212
ENSG00000263647	BPTFP1	2.002650685	0.019510553	0.032840052
ENSG00000234585	CCT6P3	1.996124716	1.11E-08	1.14E-07
ENSG00000169122	FAM110B	1.995081017	8.07E-12	3.40E-10
ENSG00000237296	SMG1P1	1.993920668	1.20E-08	1.22E-07
ENSG00000178764	ZHX2	1.991634094	4.54E-12	2.14E-10

Supplementary Table 6.5: Top 200 downregulated genes in PERK-MSC vs rtTA-MSC.

Threshold has been applied to display genes with adj.P.value < 0.05.

Ensembl.id	Gene.name	logFC	P.Value	adj.P.Val
ENSG00000263424	AC110597.3	-6.788732178	0.000284306	0.000744124
ENSG00000083782	EPYC	-4.78420146	8.24E-06	3.18E-05
ENSG00000274985	PTCHD3P1	-4.187800734	0.018772522	0.031742864
ENSG00000285815	GET1-SH3BGR	-4.003909762	0.001727108	0.003712501
ENSG00000262633	AC005670.2	-3.954283974	0.000641366	0.001535464
ENSG00000264578	AC009630.3	-3.594962496	0.005885117	0.011202253
ENSG00000249839	AC011330.1	-3.380644262	0.001665054	0.003595902
ENSG00000277991	FP236241.1	-3.294709537	0.00813391	0.015002115
ENSG00000174792	ODAPH	-3.289562826	0.000602211	0.001451158
ENSG00000255498	AC068385.1	-3.154592807	0.008247057	0.015182294
ENSG00000017427	IGF1	-3.057887048	1.57E-06	7.57E-06
ENSG00000094963	FMO2	-3.039135091	0.002254902	0.004705591
ENSG00000222032	AC112721.2	-2.96602299	0.000970241	0.002231433
ENSG00000132465	JCHAIN	-2.878408855	0.000300741	0.000782967
ENSG00000173432	SAA1	-2.736257489	0.002605852	0.005365011
ENSG00000137869	CYP19A1	-2.712787452	0.006741239	0.012664967
ENSG00000101825	MXRA5	-2.687158536	6.64E-12	2.91E-10
ENSG00000118137	APOA1	-2.680202596	0.004986711	0.009649227
ENSG00000269707	AC018730.1	-2.649452767	0.012447338	0.021996717
ENSG00000276997	AL513314.2	-2.596325815	0.008098446	0.01494606
ENSG00000254910	AC136475.2	-2.527011918	0.022925705	0.037955323
ENSG00000231231	LINC01423	-2.495969637	0.000131611	0.000373825
ENSG00000237476	LINC01637	-2.486344227	0.000724745	0.001713362
ENSG00000197361	FBXL22	-2.482489414	6.65E-10	1.16E-08
ENSG00000229720	AL109924.1	-2.475967251	0.000933334	0.002159237
ENSG00000275400	AC006001.4	-2.465236441	0.020724049	0.034672656
ENSG00000267827	AC011468.2	-2.46041089	0.026904696	0.043848107
ENSG00000151418	ATP6V1G3	-2.456329642	0.000491666	0.001216001
ENSG00000236094	LINC00545	-2.448299996	0.017018452	0.029124505
ENSG00000077943	ITGA8	-2.4143521	9.43E-08	6.81E-07
ENSG00000163017	ACTG2	-2.391639357	1.20E-11	4.68E-10
ENSG00000204291	COL15A1	-2.355525623	6.75E-09	7.70E-08
ENSG00000225937	PCA3	-2.350131576	0.018151542	0.030788242
ENSG00000270953	AC007938.3	-2.331971279	0.001936608	0.004110496
ENSG00000165409	TSHR	-2.329118328	6.22E-06	2.47E-05
ENSG00000183801	OLFML1	-2.254063395	1.15E-08	1.18E-07
ENSG00000273062	AL449106.1	-2.246449137	5.90E-06	2.36E-05
ENSG00000127083	OMD	-2.24082239	5.50E-06	2.22E-05
ENSG00000267395	DM1-AS	-2.237563092	0.023334331	0.038532246
ENSG00000214110	LDHAP4	-2.228128423	0.001109557	0.002518815
ENSG00000266441	AP005205.2	-2.220532418	0.003882846	0.007690124
ENSG00000281501	SEPSECS-AS1	-2.192034992	0.030529703	0.049039917
ENSG00000244952	AC123768.1	-2.191161796	0.023175376	0.038312703
ENSG00000106538	RARRES2	-2.19003513	1.18E-09	1.83E-08
ENSG00000259343	TMC3-AS1	-2.165039431	1.57E-05	5.62E-05
ENSG00000267414	SETBP1-DT	-2.154704529	3.35E-07	1.99E-06
ENSG00000134198	TSPAN2	-2.141245135	1.28E-10	2.98E-09
ENSG00000139329	LUM	-2.124323606	1.29E-12	8.51E-11
ENSG00000105664	COMP	-2.112014964	2.69E-15	1.28E-12
ENSG00000111341	MGP	-2.110035492	1.84E-12	1.09E-10
ENSG00000156427	FGF18	-2.10419246	2.58E-05	8.72E-05
ENSG00000228495	LINC01013	-2.100205313	0.000413841	0.001040996
ENSG00000169282	KCNAB1	-2.092378285	2.71E-12	1.45E-10
ENSG00000162267	ITIH3	-2.090011602	0.00114879	0.002598268
ENSG00000261783	AC009054.2	-2.084841461	0.016308806	0.027994599
ENSG00000109625	CPZ	-2.055793395	1.59E-05	5.69E-05
ENSG00000106236	NPTX2	-2.018163837	0.01599768	0.027518251
ENSG00000272478	AL020996.3	-1.981461077	0.028163227	0.045727224
ENSG00000104953	TLE6	-1.972998054	0.028716307	0.046507348
ENSG00000131386	GALNT15	-1.972492848	1.80E-07	1.17E-06
ENSG00000250722	SELENOP	-1.967570089	1.64E-07	1.08E-06
ENSG00000112559	MDFI	-1.96404578	6.14E-06	2.44E-05
ENSG00000234160	AL513165.1	-1.947283708	0.02717719	0.044262829
ENSG00000124212	PTGIS	-1.93075766	1.23E-14	3.17E-12
ENSG00000086991	NOX4	-1.92936091	3.69E-06	1.57E-05
ENSG00000270136	MICOS10-NBL1	-1.925808813	0.025974695	0.042487531

ENSG00000230838	LINC01614	-1.924458488	9.94E-11	2.47E-09
ENSG00000155011	DKK2	-1.91390351	1.57E-07	1.05E-06
ENSG00000127954	STEAP4	-1.896593125	0.000483353	0.001197249
ENSG00000273723	SUGT1-DT	-1.892737508	0.000985267	0.002261755
ENSG00000188338	SLC38A3	-1.87287511	3.72E-06	1.58E-05
ENSG00000106819	ASPN	-1.86159194	9.14E-05	0.000270967
ENSG00000101265	RASSF2	-1.845722335	3.11E-09	4.06E-08
ENSG00000064205	CCN5	-1.843497758	4.60E-12	2.16E-10
ENSG00000258818	RNASE4	-1.836736303	1.61E-10	3.64E-09
ENSG00000213057	C1orf220	-1.836200335	4.66E-06	1.92E-05
ENSG00000142583	SLC2A5	-1.829083478	1.81E-08	1.71E-07
ENSG00000283537	AC073264.3	-1.824423794	0.009635242	0.017435031
ENSG00000160161	CILP2	-1.821466912	6.51E-09	7.46E-08
ENSG00000029559	IBSP	-1.803921516	0.009753865	0.017636683
ENSG00000006606	CCL26	-1.802720427	1.00E-05	3.77E-05
ENSG00000112562	SMOC2	-1.799207869	0.015456892	0.026687729
ENSG00000185432	METTL7A	-1.787459658	3.70E-08	3.11E-07
ENSG00000115252	PDE1A	-1.784876074	0.000687579	0.001633361
ENSG00000123500	COL10A1	-1.783624042	2.38E-07	1.50E-06
ENSG00000099998	GGT5	-1.783069967	1.70E-07	1.12E-06
ENSG00000268941	LINC01711	-1.78193008	0.001142906	0.002586152
ENSG00000105427	CNFN	-1.764263527	0.010277925	0.018473182
ENSG00000270728	AL035413.1	-1.759551414	0.026941393	0.043893348
ENSG00000103485	QPRT	-1.753392156	2.14E-06	9.86E-06
ENSG00000143416	SELENBP1	-1.751636084	6.05E-12	2.69E-10
ENSG00000166816	LDHD	-1.746866465	2.81E-06	1.25E-05
ENSG00000141750	STAC2	-1.746670442	0.000323068	0.000833583
ENSG00000127241	MASP1	-1.746298873	2.37E-08	2.14E-07
ENSG00000106483	SFRP4	-1.745474936	3.11E-09	4.07E-08
ENSG00000011465	DCN	-1.741375713	5.29E-17	9.86E-14
ENSG00000178776	C5orf46	-1.738974543	5.34E-05	0.000167107
ENSG00000143196	DPT	-1.727089698	3.47E-05	0.000113529
ENSG00000182389	CACNB4	-1.72687889	1.79E-08	1.69E-07
ENSG00000267397	AC090229.1	-1.714798465	0.007789449	0.014435466
ENSG00000175899	A2M	-1.700234895	1.77E-10	3.88E-09
ENSG00000109107	ALDOC	-1.687831594	3.89E-10	7.44E-09
ENSG00000185924	RTN4RL1	-1.68631838	4.62E-06	1.91E-05
ENSG00000260342	AC138811.2	-1.682715806	0.007375328	0.013744081
ENSG00000007237	GAS7	-1.680492763	6.79E-10	1.18E-08
ENSG00000106823	ECM2	-1.680301419	1.72E-11	6.29E-10
ENSG00000132329	RAMP1	-1.679542155	1.06E-07	7.54E-07
ENSG00000273017	AP000240.1	-1.676871959	0.028543584	0.046283581
ENSG00000137745	MMP13	-1.675878603	8.73E-05	0.000259924
ENSG00000149131	SERPING1	-1.672402392	2.11E-13	2.30E-11
ENSG00000254154	CRYZL2P-SEC16B	-1.667361757	1.12E-05	4.16E-05
ENSG00000158008	EXTL1	-1.66335319	2.21E-13	2.37E-11
ENSG00000259948	AC124068.1	-1.662079407	9.86E-05	0.000289188
ENSG00000128606	LRRC17	-1.658236954	4.66E-10	8.57E-09
ENSG00000135549	PKIB	-1.646576941	4.07E-06	1.71E-05
ENSG00000272674	PCDHB16	-1.645679716	7.44E-05	0.000224576
ENSG00000268603	AC053503.4	-1.63973261	0.013445022	0.023578801
ENSG00000120324	PCDHB10	-1.63967359	4.35E-06	1.82E-05
ENSG00000124208	TMEM189-UBE2V1	-1.629635172	8.22E-07	4.29E-06
ENSG00000135744	AGT	-1.620196985	0.021130486	0.035292534
ENSG00000115457	IGFBP2	-1.615195819	1.90E-16	1.77E-13
ENSG00000108950	FAM20A	-1.612254286	1.34E-11	5.14E-10
ENSG00000188783	PRELP	-1.610188979	1.44E-08	1.42E-07
ENSG00000258704	SRP54-AS1	-1.603286631	0.015239741	0.026362228
ENSG00000100626	GALNT16	-1.592929449	1.31E-12	8.55E-11
ENSG00000157570	TSPAN18	-1.592751699	1.46E-12	9.30E-11
ENSG00000263873	THY1-AS1	-1.582900553	2.80E-10	5.67E-09
ENSG00000169314	C22orf15	-1.579886876	0.007311365	0.013636959
ENSG00000183160	TMEM119	-1.575732638	2.49E-15	1.22E-12
ENSG00000102265	TIMP1	-1.575603838	1.51E-13	1.88E-11
ENSG00000162645	GBP2	-1.574864747	2.07E-13	2.29E-11
ENSG00000260081	AF274858.1	-1.572174891	0.009866585	0.017803355
ENSG00000270562	AC097634.1	-1.548870553	0.004869503	0.009443515
ENSG00000115461	IGFBP5	-1.547892798	2.57E-12	1.42E-10
ENSG00000170962	PDGFD	-1.546243601	0.000103807	0.000302369
ENSG00000250056	LINC01018	-1.545879674	9.94E-07	5.07E-06
ENSG00000211448	DIO2	-1.544847079	4.77E-07	2.67E-06

ENSG00000227533	SLC2A1-AS1	-1.544619958	0.000283597	0.000742533
ENSG00000164188	RANBP3L	-1.54447325	7.04E-06	2.76E-05
ENSG00000214274	ANG	-1.543296681	1.60E-08	1.54E-07
ENSG00000196154	S100A4	-1.541271718	1.91E-07	1.24E-06
ENSG00000130592	LSP1	-1.538877555	2.09E-13	2.29E-11
ENSG00000113212	PCDHB7	-1.533481025	5.66E-06	2.27E-05
ENSG00000185885	IFITM1	-1.532683944	2.66E-08	2.37E-07
ENSG00000141469	SLC14A1	-1.531791411	6.73E-14	1.02E-11
ENSG00000239332	LINC01119	-1.525863767	1.13E-06	5.64E-06
ENSG00000153246	PLA2R1	-1.520823233	3.09E-10	6.17E-09
ENSG00000280721	LINC01943	-1.515249585	0.012383193	0.021901751
ENSG00000172061	LRRC15	-1.513351275	4.06E-10	7.63E-09
ENSG00000164122	ASB5	-1.509113767	6.08E-05	0.000187771
ENSG00000143387	CTSK	-1.505791668	1.57E-11	5.85E-10
ENSG00000082196	C1QTNF3	-1.505173833	3.76E-07	2.19E-06
ENSG00000108176	DNAJC12	-1.502076706	0.00143637	0.003165127
ENSG00000128422	KRT17	-1.499123322	2.64E-10	5.42E-09
ENSG00000108947	EFNB3	-1.498504614	1.03E-07	7.36E-07
ENSG00000265690	AC074143.1	-1.497443755	0.002171669	0.004560969
ENSG00000072952	IRAG1	-1.495903332	1.12E-11	4.46E-10
ENSG00000276600	RAB7B	-1.495111622	2.09E-10	4.47E-09
ENSG00000205403	CFI	-1.494788444	2.75E-07	1.69E-06
ENSG00000100100	PIK3IP1	-1.493600638	3.57E-10	6.99E-09
ENSG00000173227	SYT12	-1.492027137	1.25E-10	2.94E-09
ENSG00000154864	PIEZO2	-1.491588794	3.80E-13	3.65E-11
ENSG00000213316	LTC4S	-1.491473323	2.38E-07	1.50E-06
ENSG00000260751	AC008870.2	-1.489495227	0.001889501	0.004021672
ENSG00000154096	THY1	-1.486248961	1.45E-15	8.56E-13
ENSG00000233098	CCDC144NL-AS1	-1.486211434	1.45E-05	5.22E-05
ENSG00000185585	OLFML2A	-1.484568	4.03E-09	5.02E-08
ENSG00000116774	OLFML3	-1.484232074	4.39E-15	1.68E-12
ENSG00000170271	FAXDC2	-1.482527578	4.60E-08	3.72E-07
ENSG00000160307	S100B	-1.480026525	0.000384508	0.000974866
ENSG00000150687	PRSS23	-1.478287907	2.75E-16	2.25E-13
ENSG00000087303	NID2	-1.470876545	6.09E-15	2.01E-12
ENSG00000079150	FKBP7	-1.465838598	1.20E-11	4.68E-10
ENSG00000130600	H19	-1.464130298	1.97E-05	6.85E-05
ENSG00000173114	LRRN3	-1.461270164	4.44E-06	1.85E-05
ENSG00000273192	AL671710.1	-1.460364963	0.00795589	0.014716149
ENSG00000167244	IGF2	-1.455368243	2.96E-12	1.55E-10
ENSG00000179403	VWA1	-1.45303014	8.21E-13	6.29E-11
ENSG00000101955	SRPX	-1.452490273	1.34E-12	8.67E-11
ENSG00000149380	P4HA3	-1.450223241	4.14E-10	7.75E-09
ENSG00000143355	LHX9	-1.447513321	2.53E-09	3.46E-08
ENSG00000287978	AC245407.2	-1.44521884	0.017779511	0.030250064
ENSG00000146250	PRSS35	-1.445203469	0.003225917	0.006505261
ENSG00000107796	ACTA2	-1.444521051	9.69E-16	6.49E-13
ENSG00000137142	IGFBPL1	-1.441018089	3.18E-07	1.91E-06
ENSG00000143320	CRABP2	-1.440889366	8.49E-12	3.52E-10
ENSG00000100196	KDELR3	-1.439170457	8.70E-15	2.56E-12
ENSG00000118292	C1orf54	-1.437581714	1.03E-07	7.34E-07
ENSG00000130203	APOE	-1.436388133	0.003554285	0.007100377
ENSG00000226237	GAS1RR	-1.436089519	6.76E-05	0.000206473
ENSG00000162878	PKDCC	-1.435668735	1.38E-09	2.08E-08
ENSG00000276523	AC025287.3	-1.433192005	0.03030551	0.048738248
ENSG00000089472	HEPH	-1.432489675	4.21E-12	2.04E-10
ENSG00000135643	KCNMB4	-1.431601372	0.005023327	0.009709877
ENSG00000171631	P2RY6	-1.42564242	1.18E-06	5.89E-06
ENSG00000101463	SYNDIG1	-1.425394151	0.001629208	0.003529353
ENSG00000129009	ISLR	-1.421319731	1.56E-13	1.91E-11
ENSG00000019991	HGF	-1.419720888	3.71E-09	4.71E-08
ENSG00000141854	MISP3	-1.418750146	0.000224715	0.000603265
ENSG00000151320	AKAP6	-1.416931494	1.41E-06	6.87E-06

Supplementary Table 6.6: Differentially expressed proteins in AML-MSC vs HD-MSC.

Threshold has been applied to display genes with p-value < 0.05.

	p-value	fold change
HTRA1	0.022545768	1.665126033
ARSB	0.031646108	1.5627713
GRN	0.020618655	1.244205006
HAGH	0.005208822	1.124610108
APOE	0.036442005	0.94911715
GMFB	0.039906541	0.94600379
SMPD1	0.008439313	0.936352582
CTIF	0.016557352	0.890681354
FTH1	0.009318071	0.85042022
TXNRD1	0.024624661	0.830481685
PPP1R7	0.03049154	0.821771085
PRKAB2	0.018213642	0.809553281
MYO1D	0.011474962	0.793268084
BLMH	0.036485397	0.704575958
L3HYPDH	0.023199323	0.702426078
PGM1	0.02765441	0.702399467
MIF	0.043561421	0.699961026
C10orf67	0.031788689	0.686226718
GYG1	0.007611317	0.671484707
ADK	0.048122852	0.659247349
PDLIM1	0.0159567	0.645653978
STXBP1	0.005862714	0.606907912
CYB5A	0.042703694	0.604921902
TAGLN2	0.041616431	0.592075657
ASAP1	0.04992611	0.588198022
VDAC3	0.049826939	0.585688604
CTSD	0.005316123	0.584600458
PDCD6	0.041827786	0.573538069
GYS1	0.026790703	0.555793398
NEXN	0.030255437	0.537732498
TOM1	6.59E-05	0.518704503
PRKAR2A	0.019429745	0.504613605
AKT3	0.04050811	0.499703412
AP2A2	0.015046274	0.493267515
PRDX5	0.010549302	0.486358147
PGK1	0.020734565	0.485803508
PRDX4	0.021038229	0.479886117
na.16	0.039014284	0.478713408
CNN3	0.025379544	0.475151381
PKLR	0.022294871	0.453734141
FNTA	0.016983883	0.442811839
CSRP1	0.0317136	0.400372022
MTOR	0.005722364	0.39915523
EML4	0.024699806	0.399082073
YARS1	0.035259243	0.398089752
ADRM1	0.04676765	0.386626147
NHLRC2	0.006383983	0.386464936
PAFAH1B2	0.018281837	0.373780846
NARS1	0.033959653	0.344313494
ROCK1	0.035331614	0.339498832
RNPEP	0.019457818	0.330411963
TES	0.026019522	0.322953496
IQGAP2	0.012481298	0.319918845
LRPPRC	0.028312425	0.31245201
PDLIM7	0.012309664	0.307438816
MYH9	0.028656865	0.303210457
NIT2	0.014816669	0.301900196
FTSJ3	0.033773935	0.291818679
MYL6	0.015767467	0.268891918
DCTD	0.036308492	0.264895736
AP2B1	0.024346058	0.263075274
GRHPR	0.046032795	0.253951479
GNB2	0.028593733	0.25311279
SRI	0.025910144	0.233090632
GDI1	0.000505582	0.230195103

SNX17	0.015790073	0.227031249
GUK1	0.049838494	0.221683159
MYL9	0.049102745	0.216846217
PRKAB1	0.049312201	0.21358623
TRIM25	0.013948966	0.19730175
ARHGAP17	0.027172156	0.17292333
PAFAH1B1	0.007508296	0.126553249
DYNC1I2	0.007110236	-0.084046313
GOLGA3	0.035585298	-0.100719024
PSMD8	0.028289104	-0.134644298
UFD1	0.0286126	-0.151768385
PPIH	0.041916419	-0.168876912
HNRNPA0	0.025612283	-0.1726743
PPP6R2	0.021910424	-0.18616668
FXR1	0.039531991	-0.194587333
TUBA8	0.044115737	-0.200405582
ACTR3	0.023218246	-0.200644712
GNL1	0.04650732	-0.204561439
NAP1L4	0.000654626	-0.204623311
CAND1	0.035399392	-0.20471621
RAB1B	0.041871814	-0.207327481
COPS4	0.020251217	-0.210015041
UBQLN1	0.019757797	-0.212249019
STK39	0.016565575	-0.2186923
PSMD6	0.049620979	-0.21967642
GART	0.040684246	-0.220630603
PCBP2	0.002683736	-0.223472308
DYNC1H1	0.003753719	-0.224583927
HSPA2	0.014773057	-0.228437174
na.13	0.004282841	-0.229109886
SRP19	0.040779784	-0.232867865
SRSF9	0.017992258	-0.242196748
WDR1	0.03403358	-0.244135352
HNRNPD	0.030056793	-0.245507851
XRCC5	0.02390803	-0.24602934
TRIP10	0.025642488	-0.248860889
PSMD7	0.021563685	-0.251365496
COPA	0.026508753	-0.25151318
EIF1	0.00104115	-0.252289614
HNRNPA3	0.04850295	-0.255220758
NAPG	0.003213094	-0.255377917
EWSR1	0.004959923	-0.255749556
PEPD	0.010014412	-0.259965123
SRSF1	0.020700979	-0.262470067
RBMX	0.033739105	-0.26479279
RPL4	0.044343664	-0.269910155
ADSS2	0.034641221	-0.273108303
PSMD13	0.034434715	-0.277811727
RIC8A	0.037590475	-0.282137459
EIF4H	0.010804144	-0.282942005
UBQLN4	0.039822427	-0.286732062
CBX3	0.014114173	-0.28731745
SFPQ	0.041416552	-0.29026981
VCP	0.008186238	-0.291503441
HNRNPK	0.044959473	-0.302695892
GSPT1	0.002616402	-0.302696108
HNRNPU	0.011625093	-0.304615396
ESYT1	0.043944092	-0.305372153
U2AF2	0.045218137	-0.305756095
PPP6R3	0.024121874	-0.308942706
CSTF3	0.04305693	-0.310985908
ARHGEF12	0.008498577	-0.312806236
PSMD3	0.016842061	-0.313554935
SF3A1	0.039632965	-0.316539648
SAE1	0.019267207	-0.318848923
PRKACB	0.049953632	-0.320402201
PSPC1	0.003369741	-0.322233752
RPS8	0.021680533	-0.322430875
SMU1	0.029787811	-0.327364092
UBA6	0.032340636	-0.330768582
SNAP29	0.01458147	-0.335268234

HSP90AB1	0.01749355	-0.336500152
ATXN10	0.040970566	-0.337089919
RPL34	0.035149741	-0.339731457
RPL27A	0.032265564	-0.341389062
SRSF11	0.007142137	-0.344533101
OPLAH	0.012713855	-0.346130255
ARL2BP	0.032362655	-0.348797929
HNRNPH1	0.019088412	-0.351130921
DYNLT1	0.007287316	-0.353851525
SH3GL1	0.03096228	-0.358773258
RPS28	0.016216269	-0.359548932
SF3A2	0.019340718	-0.360798666
ACP1	0.036273758	-0.361656609
UBXN1	0.020943918	-0.364225947
PACS1	0.022103538	-0.367045174
LSM7	0.017976384	-0.369938303
XRCC6	0.00359585	-0.370213758
HDAC2	0.04444248	-0.371472996
ANP32E	0.023953626	-0.372984223
WDR18	0.025730864	-0.377185489
CPSF6	0.044558013	-0.378460173
CDV3	0.033444801	-0.378972291
SNRPD2	0.030751565	-0.381596648
DTYMK	0.012159679	-0.381783404
RPS20	0.027876585	-0.382873051
HSP90AB2P	0.020848155	-0.38289815
ABCF2	0.016022136	-0.383009601
GALE	0.010554716	-0.384711012
ZNF207	0.048296936	-0.384853392
RPS5	0.029314951	-0.386641112
ZC3H15	0.048214986	-0.386852734
SF3B3	0.01507517	-0.389181704
EVPL	0.022994638	-0.393996362
BZW1	0.020923062	-0.394233508
NUDT21	0.03891154	-0.399167532
UMPS	0.0268541	-0.399335927
SNRPC	0.020875984	-0.401042789
RPL7A	0.048830367	-0.40345349
HSP90AA1	0.043989444	-0.404484892
MATR3	0.045248578	-0.406141656
RBM25	0.019062025	-0.409626628
ACAT1	0.044261289	-0.410684082
API5	0.013584817	-0.411184284
SF3B6	0.032150252	-0.412296759
ELAVL1	0.017351413	-0.413132549
HNRNPF	0.013611008	-0.413388249
SUPT16H	0.006392913	-0.414382034
NUP205	0.041107086	-0.416069845
RBM8A	0.014751868	-0.421557581
CTNNBL1	0.003483221	-0.423384842
SRGAP2	0.017361888	-0.424600442
PABPN1	0.028261917	-0.425798353
RANGAP1	0.040761334	-0.428170432
TRIP12	0.006079017	-0.429345486
CCDC93	0.043135308	-0.430753721
HNRNPA1	0.039954607	-0.432480899
RBM42	0.007757065	-0.434640285
HNRNPDL	0.021229701	-0.434971461
DDX17	0.026786439	-0.435830634
RBM12	0.036630584	-0.440019856
TRAP1	0.012695944	-0.44134771
RNMT	0.004724854	-0.445001931
MTMR6	0.002047247	-0.449201047
SET	0.032816563	-0.451301508
CSDE1	0.011652686	-0.45165352
KHSRP	0.045231183	-0.452917932
DR1	0.031537707	-0.456447934
CEP170	0.040337102	-0.456948963
NUDT16	0.035893008	-0.45752961
RPL10A	0.027873201	-0.458492948
SSRP1	0.004657348	-0.458841346

HSPH1	0.042637625	-0.460528343
DDX5	0.031232839	-0.461841298
RANBP1	0.022272907	-0.462342567
HNRNPC	0.009515498	-0.476140952
IPO9	0.041295486	-0.476362595
RPL13A	0.040511354	-0.479409083
SF3B5	0.009283893	-0.483001802
na.4	0.013132317	-0.486221159
TRIM28	0.017334067	-0.496935235
RBBP7	0.028747957	-0.500178126
CHERP	0.046374478	-0.501544162
SNRNP200	0.001107389	-0.503372439
GLRX3	0.013874747	-0.507605113
HMGB1	0.042213603	-0.511698786
TBC1D23	0.02575967	-0.514803928
FAM50A	0.012985671	-0.515633447
CDK11A	0.003770697	-0.518884994
NUP37	0.032214601	-0.520145116
WBP11	0.015366252	-0.521886687
ANKMY2	0.040674763	-0.527360236
NAA15	0.004180283	-0.531529364
WNK2	0.006208372	-0.536373102
RBM17	0.024695185	-0.546327884
SF1	0.042384404	-0.554381326
SART1	0.003982986	-0.554849265
CAPRIN1	0.041824257	-0.561462261
PHAX	0.029889473	-0.564480048
SRP14	0.031595718	-0.566752249
RRM1	0.027444784	-0.571005077
EHD4	0.009715839	-0.580031154
ST13	0.00019237	-0.5847274
HPRT1	0.004889852	-0.588860032
HNRNPLL	0.042642208	-0.594707124
PRKACA	0.008787184	-0.5956977
FHL3	0.022637967	-0.612033359
na.23	0.02502672	-0.61290339
GIT1	0.015235548	-0.614166566
ELP2	0.015222453	-0.617358128
RPL36A	0.01621351	-0.621780208
CPSF7	0.033767491	-0.622803864
MRFAP1	0.031556446	-0.633840047
NCBP1	0.041022111	-0.634293567
HAT1	0.048963057	-0.638635889
SRRM1	0.042793211	-0.648156327
DRAP1	0.037661277	-0.668375096
ACTC1	0.006139896	-0.669838906
PCNA	0.010828774	-0.673700014
DCPS	0.029454212	-0.680678213
SUGT1	0.0481177	-0.685536009
ITCH	0.018306189	-0.695933937
NCOA5	0.004807209	-0.711551927
NAT10	0.020198285	-0.732750352
HDAC1	0.025932634	-0.743942088
PSME4	0.02302128	-0.75397131
NUBP1	0.005394658	-0.760209916
GCC2	0.04473061	-0.766333545
DIS3	0.036034107	-0.770737659
ILKAP	0.007932285	-0.774908109
AKT1	0.027797659	-0.782991905
NELFA	0.017536874	-0.784264386
DIAPH1	0.021307618	-0.78782382
CD2BP2	0.037721553	-0.808077538
DNAJC9	0.01972179	-0.822022339
SLC9A3R1	0.04698426	-0.829905338
ARHGEF17	0.002156571	-0.831716769
CDC42EP3	0.026846543	-0.835587421
DUT	0.027592264	-0.847996907
NASP	0.006899078	-0.86335316
TMEM43	0.005968835	-0.878769631
SCYL2	0.04701174	-0.883961045
CAB39	0.0238363	-0.89455215

FAF1	0.02057595	-0.894901615
NXN	0.026359454	-0.936114959
MCM2	0.019912033	-0.941499763
TM9SF2	0.005987737	-0.95483946
CYFIP1	0.045929905	-0.960325837
PIN4	0.02640286	-0.966632977
CRNKL1	0.034485503	-1.007315531
GRWD1	0.024994769	-1.060608399
POSTN	0.033929211	-1.069694746
BCCIP	0.006923841	-1.071215282
SYNE1	0.03097442	-1.115111511
IRF2BP2	0.012637733	-1.176015183
CIITA	0.035841474	-1.196530901
STMN1	0.022273862	-1.218529046
NQO1	0.045881095	-1.235448434
HCFC1	0.015209058	-1.243867198
UBE2O	0.011834891	-1.286430032
PCOLCE	0.049664359	-1.472830733
ACOT9	0.047301842	-1.484321658
TNC	0.013828871	-1.493958387
MCM3	0.024374164	-1.508040511
NFATC4	0.02166397	-1.517982181
MCM7	0.01886051	-1.535652543
NEMF	0.046666903	-1.612136768
CRYM.AS1	0.032035375	-1.638686144
BPNT2	0.006763791	-1.650885098
SMC4	0.042373658	-1.867079389
NOTCH2	0.039288207	-1.898108175

Supplementary Table 6.7: Differentially expressed proteins in PERK-MSC vs rtTA-MSC.

Threshold has been applied to display genes with p-value < 0.05.

	p-value	fold change
PTPN14	0.000529572	3.134648031
NIBAN1	0.000480618	2.374047471
ATG3	0.016905621	1.762432818
ALDH1A3	0.005874449	1.342939783
COBLL1	0.00890098	1.181809951
SQSTM1	0.000454345	1.090380803
TBC1D13	0.02739241	1.048735988
FGF2	0.001944035	0.983171954
ITIH1	0.002167988	0.896438216
NUP214	0.024528825	0.825548716
OAS3	0.0024285	0.759360359
H1.10	0.01021069	0.716835871
CBSL	0.009382952	0.716310381
TNS3	0.044208754	0.710337682
ASNS	0.01286739	0.708442325
BMP1	0.000585703	0.706902302
SSU72	0.001329635	0.69925024
TGM2	7.20E-05	0.691456112
SHFL	0.017887351	0.689773313
RBPMS	0.024451999	0.686026127
KRT31	0.034468792	0.672548533
HSPB6	0.011821411	0.670255486
CDK20	0.000147174	0.617024856
PSPH	0.00525915	0.593298185
UNC45A	0.003066945	0.588286573
KRT76	0.007258915	0.56961008
PUS1	0.002982371	0.548291817
GOT1	6.72E-05	0.547655085
WARS1	0.002005438	0.542442768
DCTN3	0.016656962	0.528390839
FBLN1	0.002318397	0.521680378
COPG2	0.028471894	0.514334081
CDK5	0.004423047	0.474266381
KRT19	0.031103695	0.459306399
PSAT1	2.53E-05	0.458023868
CARS1	0.014649193	0.457443558
IGF2BP2	0.021653933	0.452198178
CNRIP1	0.048768196	0.448904619
FAM114A2	0.046530634	0.446819343
KRT1	0.009653533	0.442902169
SART3	0.031715174	0.442886623
TSR1	0.044227872	0.429561047
DYNC1LI1	0.038682074	0.411025596
NQO1	0.01726053	0.408964655
CD2AP	0.047399005	0.406719606
SORBS2	0.016936555	0.400773963
G6PD	0.028302896	0.399729762
LARS1	0.016240884	0.398204943
na.22	0.048527942	0.391259024
BICD2	0.022432205	0.390306836
GARS1	0.001659722	0.386696456
UAP1L1	0.048578476	0.378683517
PYGM	0.003344077	0.377542514
PHGDH	0.022369603	0.371913057
CTTNBP2NL	0.004306429	0.367674228
KRT34	0.001790319	0.363088076
PYGB	0.022795175	0.354124259
EIF1AX	0.012960258	0.342149146
GDI2	0.007071164	0.341246557
TSG101	0.012692936	0.334494728
TXNRD1	0.000165138	0.334347218
SNX18	0.021775336	0.32755852
PFN2	0.046751509	0.32666986
KRT14	0.001254973	0.325851201
GAR1	0.011022221	0.324546965
LANCL1	0.02279575	0.322184261

UCHL1	0.043347405	0.321836897
CSE1L	0.011540488	0.318974643
EEF1E1	0.026630927	0.317602226
MTAP	0.04501935	0.311664708
AK2	0.026619119	0.306634306
GTPBP4	0.026173152	0.306569641
GSDME	0.035841369	0.306406617
H2AC1	0.026454195	0.304074165
ARPC3	0.024472166	0.301469649
NPM1	0.001486385	0.301107654
KCTD12	0.012415707	0.299020169
EPS8L2	0.042802154	0.289217464
PMM2	0.028116122	0.288507019
FARSB	0.020018204	0.285366521
LYPLA1	0.025702922	0.283209379
PDLIM2	2.08E-05	0.276223079
DDX1	0.000195209	0.276220798
TPP1	0.013602065	0.274187819
AARS1	0.004708228	0.272968334
DDAH1	0.0027234	0.272623166
GSR	0.000447211	0.271179746
TUBB	0.002440506	0.269820135
SARS1	0.022541879	0.265378717
UBA5	0.029937597	0.262626873
TUBA1A	0.010062956	0.262521849
CASP4	0.017333385	0.262110638
MTX2	0.038746266	0.259383069
TOLLIP	0.026484642	0.258654219
TIGAR	0.033053113	0.256526695
HEXA	0.025217829	0.255622064
H2BC4	0.036160002	0.254958736
DPYSL3	0.015860343	0.250861057
ANKFY1	0.038554989	0.245670702
LGALS3	0.005192128	0.243862297
NUP62	0.045900707	0.24210409
CLEC3B	0.022655131	0.237710801
PGLS	0.003684224	0.235511861
VASP	0.010380181	0.231375931
GMFB	0.016366289	0.229904697
BGN	0.009635358	0.227672463
EIF1	0.005065701	0.225312944
PPP6R2	0.00431054	0.222520826
NT5C2	0.003257365	0.222182006
DDX39A	0.003323023	0.221996091
GMPS	0.020781587	0.2218027
TUBA1C	0.031397758	0.220543914
ABRACL	0.042143582	0.219627048
KPNA4	0.042357047	0.217381175
STAT1	0.041136489	0.212417328
RANBP6	0.030498386	0.209120973
GMPPB	0.015527426	0.206852677
CDV3	0.024573312	0.204525801
DNM3	0.007646556	0.202911766
COMMD1	0.028873998	0.202635278
ROCK1	0.047568082	0.201255408
PDLIM7	0.00252272	0.201186352
CCT3	0.014095997	0.200737736
TP53I3	0.027479107	0.199112144
C11orf54	0.003983513	0.198839203
SRSF3	0.047853061	0.197516849
TUBA8	0.015889561	0.194926408
KARS1	0.031218689	0.193930059
HNRNPL	0.012457455	0.191239039
EIF5A	0.044742634	0.190288782
DPYSL2	0.008700491	0.189158833
CIRBP	0.039567825	0.1887439
CAPN2	0.010218786	0.188643192
PGM2	0.014101001	0.188320076
HYPK	0.035561522	0.188226336
EIF4G3	0.018604931	0.186626831
NARS1	0.03514785	0.184782855

MYL6	0.041401224	0.183315485
DAZAP1	0.016469421	0.18050571
DYNLT1	0.048844154	0.179546809
ESD	0.014440667	0.178102487
EEF1B2	0.007701807	0.176667034
PDXK	0.043139504	0.176301532
TLN1	0.002323213	0.17447807
HNRNPK	0.01779793	0.173615198
GART	0.024564001	0.170953956
YARS1	0.01795016	0.16890468
FSCN1	0.026519832	0.167037909
CAMK2G	0.047700958	0.165846778
DNM2	0.041932654	0.165610193
MBNL1	0.041410067	0.164518927
BAG2	0.002952919	0.16408887
PSMC1	0.0055006	0.162910567
TALDO1	0.046581164	0.162396051
PXK	0.034384884	0.161582442
CFL2	0.003904426	0.160122745
PABPC4	0.025246566	0.156222989
PSMA5	0.013447609	0.156078509
GAK	0.037910746	0.154740809
RNH1	0.015128725	0.154725284
CBR1	0.041368019	0.154261598
CAPNS1	0.032496961	0.153458873
HNRNPD	0.012998749	0.153035866
YWHAZ	0.039131001	0.142095769
PGM3	0.027670858	0.141083527
SFPQ	0.001587191	0.140989242
PSMA6	0.028084955	0.139900109
CLIC1	0.015392115	0.136890523
GSTP1	0.040252327	0.135675046
SRP72	0.042827241	0.13452171
ANP32B	0.021968699	0.13309216
TTLL12	0.010156147	0.131356146
GPI	0.047809251	0.12595741
PTK2	0.028642219	0.12314393
RPL6	0.005147897	0.119337697
CAST	0.03713811	0.11823457
ACTN1	0.013257331	0.118143233
NNMT	0.044867314	0.11560958
UBE2D1	0.010344414	0.114860642
TUBB8	0.029431756	0.113541514
PSMC3	0.030739301	0.107490747
RUVBL1	0.037082461	0.100356909
LAP3	0.008950404	0.098990034
CCT6A	0.044165251	0.094068097
PDLIM1	0.017726383	0.091615728
NAGK	0.024010012	0.090262403
NME2	0.010586594	0.074067992
DCTN2	0.006240192	0.06007034
RCN3	0.024229337	-0.087918441
DDX5	0.037483639	-0.097950107
FKBP10	0.013521055	-0.132994426
STK38L	0.03247778	-0.134476165
DNAJA2	0.028217556	-0.137575905
EIF3CL	0.015296759	-0.139088916
TRAP1	0.016206004	-0.1495199
RBBP7	0.001871058	-0.153709048
SNX3	0.02204892	-0.162840777
PDIA3	0.030011299	-0.162943927
PDIA4	0.048314399	-0.165420536
CALR	0.037912676	-0.177877562
PPP2R5E	0.046887204	-0.181610529
NUDT21	0.048489605	-0.182486548
CNN1	0.008436146	-0.189073713
SERPINE2	0.035796448	-0.190846254
CALU	0.01111352	-0.20058293
GLRX3	0.012245855	-0.202222558
GRB2	0.002084698	-0.203654695
UGP2	0.012584316	-0.212297279

PRKAR1A	0.002594121	-0.21377359
SKP1	0.006223226	-0.215311485
UROD	0.026375502	-0.220931637
KIF2A	0.037594908	-0.222035289
PLOD3	0.022066204	-0.234518631
CDC42EP3	0.034395328	-0.235559685
HSP90AB1	0.039420339	-0.236131447
GSTM3	0.015140196	-0.24013627
HDLBP	0.039522528	-0.241488935
RPS25	0.004047536	-0.247070132
CTSL	0.012597225	-0.248612831
GRHPR	0.003341866	-0.252340844
MYO1D	0.039786906	-0.255023032
PDIA5	0.035387033	-0.261056818
CTHRC1	0.043913428	-0.26697893
SUGT1	0.006699882	-0.270062186
HSP90AA1	0.026326409	-0.272479569
CNPY2	0.028218908	-0.274530969
HTRA1	0.049175702	-0.275555316
HSP90B1	0.012800068	-0.275940841
CRTAP	0.015518842	-0.280004595
AKAP12	0.018673833	-0.292782221
DNAJB11	0.010198557	-0.296672078
LAMB1	0.0428759	-0.297261276
CSDE1	0.027025478	-0.300707567
SLAIN2	0.042628033	-0.303202233
GIT1	0.017378317	-0.308451163
NCOA5	0.022277789	-0.30853024
CKB	0.004695091	-0.314349391
P3H3	0.00345297	-0.316557004
SPATS2L	0.012975711	-0.31757169
SDF2	0.015505181	-0.318513747
PLOD1	0.01176245	-0.318880919
ARHGEF17	0.043292845	-0.323973533
RPL31	0.04764057	-0.326887865
PRKCSH	0.040046629	-0.328155895
THBS1	0.007274306	-0.338485028
MGLL	0.039357367	-0.339711289
P4HA1	0.006850549	-0.340567161
PTS	0.01238389	-0.34453489
NEK7	0.027227692	-0.352892082
HSPB7	0.002549318	-0.353110104
ELAVL1	0.032180914	-0.355186589
P3H1	0.00272965	-0.359891014
HSBP1	0.002775147	-0.376018396
SRGAP2	0.027286635	-0.381330398
PCNA	0.004244951	-0.384659525
NOMO1	0.007467138	-0.384961336
LOX	0.015559553	-0.390781522
IGFBP7	0.017224704	-0.393222662
LAMB2	0.042372933	-0.413518938
KRT72	0.028221243	-0.416309175
ARL2BP	0.005435466	-0.426800728
COL6A2	0.006481757	-0.428624534
CTSA	0.039996799	-0.437782279
ACLY	0.020086662	-0.442057406
EDIL3	0.00834937	-0.445874774
CPSF1	0.010287746	-0.448334894
DYNLT3	0.019661247	-0.452560232
ASMTL	0.026317894	-0.461742239
na.19	0.021819349	-0.4639471
FKBP14	0.019126157	-0.465273868
GTF2I	0.015145905	-0.468912933
ACOX1	0.027690275	-0.469774367
GABARAPL2	0.014337251	-0.478261773
COG1	0.008766567	-0.48234009
POLR2L	0.034673511	-0.485820343
COL6A1	0.041612782	-0.495697373
SDF4	0.0333528	-0.498758985
ZC3H15	0.000283761	-0.498938757
FTO	0.045257199	-0.502735074

DAB2	0.011623246	-0.506887811
STAT2	0.004311367	-0.507170944
PXDN	0.026973987	-0.511506401
COL1A1	0.036391509	-0.518090292
SELENOM	0.000599078	-0.521195816
COL1A2	0.015746499	-0.521346872
FLOT1	0.037265247	-0.532008271
DEPTOR	0.023305629	-0.545103026
LOXL1	0.045748156	-0.545485001
SIL1	0.037397303	-0.555889239
CETN2	0.013064618	-0.56325259
NDRG3	0.023997538	-0.573407932
COL11A1	0.002954601	-0.5743961
SMPD1	0.0247581	-0.576947146
COL5A2	0.025109947	-0.582265321
GNAS	0.036673221	-0.587713932
CEMIP	0.012732403	-0.588497513
RPS15A	0.027360908	-0.590375942
P4HA2	0.00580181	-0.598316138
EFEMP1	0.033784011	-0.602660402
SYT5	0.027977787	-0.608858617
ZC3HAV1	0.021182191	-0.641163598
SCARB2	0.021639671	-0.64217701
CHMP3	0.043440904	-0.651772048
WASHC5	0.010459051	-0.660370312
COL5A1	0.000281171	-0.682643965
OPLAH	0.030344481	-0.709857357
BAIAP2	0.025448655	-0.726747833
MCM6	0.017929891	-0.729971496
SPARC	0.033662691	-0.730617255
ADI1	0.0164541	-0.730674111
FSTL1	0.005206133	-0.741023062
ATP6V1D	0.026991907	-0.775035921
RIPOR1	0.034414267	-0.78275622
DDX17	1.53E-05	-0.798235967
SELENBP1	0.005585448	-0.839507127
COL3A1	0.004443222	-0.852763598
na.1	0.021746723	-0.869700961
PPP1R14A	0.033686777	-0.873438768
TXNDC9	0.000565332	-0.880775094
NEU1	0.004340233	-0.909671062
EFHD1	0.044786313	-0.936492371
LIMS3	0.000605791	-0.971644359
LXN	0.001718743	-1.042258859
UBQLN2	0.027698257	-1.0731934
GPC4	0.01011968	-1.172806223
NID2	0.001459483	-1.181137638
BCCIP	0.00222083	-1.200476219
KIAA1671	0.038682317	-1.259056288
COL4A1	0.005524678	-1.296858919
TBC1D10B	0.041160849	-1.321009791
GALNT5	0.015731707	-1.607315288
IWS1	0.038245731	-1.614613968
MINPP1	0.00147216	-1.686560641
SRSF7	0.009253309	-2.102904162
CEP97	0.012556231	-2.28519392

Supplementary Table 6.8: Top 100 upregulated phosphorylated sites in AML-MSC vs HD-MSC.

Threshold has been applied to display genes with p-value < 0.05.

	p-value	fold change
MAP1S(S741);	0.002766105	10.86099805
ARHGEF17(S509);	0.018519924	10.32993473
EML4(S918);EML4(S938);EML4(T921);EML4(S946);	0.025970172	10.1497191
TITIN_HUMAN; 21091-21097_no_mod;	0.0373574	9.950245643
GOLGA4(S266);GOLGA4(M240);	0.045432329	9.530405096
PRKCA(T497);PRKCB(T500);PRKCG(T514);	0.022752785	9.168987435
BCL9L(S116);	0.022355888	8.399219683
MAST3(S709);	0.007908204	7.967313698
MAST3(Y708);	0.007908204	7.967313698
HSPB7(S92);	0.043106864	3.701696612
LUC7L2(T17);	0.007434336	3.477165653
TNKS1BP1(S1383);	0.02041828	3.311020033
LMOD1(M29);LMOD1(S12);	0.045527543	3.235904799
VIM(S438);	0.009293305	2.987058892
UBR4(T2715);	0.022825235	2.970198572
FAM129B(K620);(S641);(S646);	0.002865852	2.918778604
ABLIM3(R384);ABLIM3(M387);ABLIM3(S388);	0.033043819	2.784419768
FILIP1L(S1053);	0.026306337	2.661895632
PTRF(T376);PTRF(S379);	0.004066721	2.557164048
ATG14(S29);	0.007051795	2.366293541
SH3RF1(S735);SH3RF1(T741);	0.031726274	2.349797344
KIAA1671(K1016);KIAA1671(S1019);	0.049958058	2.23579554
ADARB1(S26);	0.007919198	2.183057532
PANK4(S393);	0.037466606	2.141283749
PANK4(Y377);	0.037466606	2.141283749
STK38L(S282);	0.030145493	1.945644504
STK38L(Y281);	0.030145493	1.945644504
NEXN(T156);NEXN(T158);	0.044692984	1.886603443
NOC2L(S22);NOC2L(S26);NOC2L(S28);	0.038088641	1.863809336
PTRF(S175);	0.014566501	1.801840966
PTRF(S202);	0.0117561	1.777647206
VAMP4(S30);	0.048070312	1.721493
PTRF(S365);PTRF(S387);PTRF(S389);PTRF(S366);	0.009709144	1.719368826
EEF1D(S133);	0.002599557	1.709080557
EEF1D(M135);EEF1D(S133);	0.002599557	1.709080557
XPC(S883);XPC(S891);	0.012870776	1.692092375
LBH(T69);	0.037522202	1.672200587
PTRF(S365);PTRF(S387);PTRF(S389);	0.008529388	1.639498061
MPRIP(S991);	0.02334411	1.587971891
NAV3(S275);	0.044607709	1.568058264
PDCD4(S76);	0.036940414	1.562593349
EPN1(T412);	0.013744319	1.55036872
PRKCA(Y504);PRKCB(Y507);PRKCG(Y521);	0.021872159	1.520798239
EIF2AK4(T667);	0.043968008	1.511526515
EDC3(T300);	0.045893041	1.496209692
LMO7(Y752);	0.020629965	1.401448435
WDR44(S50);	0.002896797	1.366322214
MAP3K3(S337);	0.025424852	1.361149405
PKN1(T772);	0.034859654	1.358522098
MYH9(S1114);	0.046438668	1.327466278
CALD1(S131);	0.02921352	1.318938529
LMO7(S895);	0.003885257	1.304314507
PPP1R3D(S46);	0.049478256	1.300994312
FERMT2(T172);	0.032942152	1.273953451
PRKCA(T501);PRKCB(T504);PRKCG(T518);	0.028311261	1.234654888
ARHGEF2(S932);	0.04057818	1.224876194
GOLGA4(S266);	0.008728978	1.156738011
MAP1B(S1421);	0.018370084	1.156651832
EPB41L2(S38);	0.039407879	1.155267337
VIM(S83);	0.024854574	1.145157096
AHNAK(S5739);	0.032222458	1.114350915
LMO7(S751);	0.032594203	1.103439505
WASL(Y256);	0.036813949	1.102680857
ARHGEF2(S932);ARHGEF2(R927);	0.049405219	1.083225848
PLEC(S720);	0.039064839	1.078674694
FAM54B(S103);	0.045083809	1.070221028

SIPA1L1(S208);	0.000177063	1.043226103
SIPA1L1(Y206);	0.000177063	1.043226103
THRAP3(S320);	0.015737042	1.029639037
PURB(S298);PURB(S304);	0.002017042	0.994708474
PURB(S304);	0.002017042	0.994708474
KIAA0284(T1137);	0.004323786	0.983419061
MAP1S(T782);	0.015416153	0.975530142
AKAP2(S630);	0.017586737	0.967553378
TPD52L2(T23);	0.046267638	0.962806364
HNRNPUL2(S168);	0.001914476	0.962205002
VCL(S288);	0.030073932	0.953776983
LMO7(S1597);	0.045270641	0.903790025
PRKACA(S339);	0.02311485	0.879496829
MAP1B(S828);	0.018336456	0.877748969
SMARCA2(S1512);(S1516);(S1528);	0.00157537	0.86799755
MAP1B(S828);MAP1B(T837);	0.030634185	0.848475621
CANX(T562);	0.003117662	0.844219724
CAMK2D(S333);	0.025554431	0.837245256
LMO7(S997);	0.023733041	0.812277213
EPS8(R656);EPS8(S664);	0.025044521	0.805122684
SYNJ2(S1122);	0.009404135	0.780175414
MAP2K2(S30);	0.048596873	0.762184021
CDC42EP4(S64);	0.025039597	0.757882798
AHNAK(S5731);	0.043061567	0.725694048
CANX(S564);	0.010446042	0.721347299
YWHAE(S213);	0.036525139	0.707172557
LMNB1(S23);	0.039849445	0.701371993
FAM129B(S641);	0.003990268	0.689275396
TUBA4A(S340);TUBA1B(S340);	0.042290317	0.685797314
FCHO2(S403);	0.001452307	0.674201071
CALD1(T791);	0.046369474	0.663259378
NEXN(T156);	0.036542725	0.663135833
AHNAK(T4999);	0.03539749	0.66135832
NEXN(T172);	0.02852431	0.659145402
MAP1B(S1406);	0.04427429	0.525266235
ZC3H18(S46);	0.047502441	0.507546903

Supplementary Table 6.9: Top 100 downregulated phosphorylated sites in AML-MSC vs HD-MSC.

Threshold has been applied to display genes with p-value < 0.05.

	p-value	fold change
RBM5(S624);	0.02370662	-12.64430163
RBM5(Y620);	0.02370662	-12.64430163
CSDA(T65);	0.040350804	-12.28592923
MYO9B(S1405);	0.038560196	-11.06964131
UBE2O(S1167);(S1196);(S1201);	0.004993318	-10.31119599
MAN2A1(S80);MAN2A1(S82);	0.036809792	-9.895624059
KDM1A(S126);(S137);(M123);	0.001239259	-9.624764339
EEF2K(S18);	0.017685039	-7.365904344
PRRX1(T71);PRRX1(S72);PRRX1(S74);	0.000512898	-5.26071872
STXBP5(R689);STXBP5(S692);	0.005355	-4.785690574
NFATC4(T119);NFATC4(S142);	0.006891191	-4.560202295
SLC38A10(S802);	0.003851575	-4.286281361
TJP1(S968);	7.89E-05	-4.116118558
NOLC1(T607);NOLC1(T610);	0.01998977	-3.981087195
DEK(S51);	0.009516766	-3.907581936
PNKP(T118);	0.017592679	-3.621641631
GOLM1(T255);	0.012254307	-3.557691901
GOLM1(R248);GOLM1(T255);	0.012254307	-3.557691901
SLC38A10(S685);	0.031104047	-3.531417474
BAP1(Y394);	0.000685807	-3.456439563
ZFP106(S639);	0.015410567	-3.389442988
SPAST(S243);	0.00757308	-3.262848615
RANBP2(T1399);	0.039953266	-3.230244976
IVNS1ABP(S325);IVNS1ABP(S326);	0.029111191	-3.12287909
RALGPS2(S329);	0.003497857	-3.016121525
CASC4(S374);	0.002838377	-3.014669172
SRRM2(S1542);	0.014947635	-2.988917341
LMO7(S955);LMO7(S968);	0.025890102	-2.957111825
MLL2(S654);	0.004097772	-2.948813161
ARHGAP29(S589);	0.00933194	-2.8454591
HIST1H1C(S36);D(S37);E(S36);	0.004903857	-2.812502926
BCAR3(R80);BCAR3(T86);	0.004471813	-2.803555506
KDM1A(S126);KDM1A(S137);	0.029563779	-2.799827085
CDYL(T230);	0.00962951	-2.783363231
GPATCH8(S1175);	0.006563855	-2.690232775
SPTY2D1(Y587);	0.007492006	-2.67069769
CCDC165(T1417);CCDC165(S1421);	0.023803332	-2.639175486
FAM198B(S199);	0.028925221	-2.608219549
SRRM2(S2272);	0.000802523	-2.598546585
SRRM2(M2268);SRRM2(S2272);	0.000802523	-2.598546585
DOCK10(T322);	0.049437176	-2.592418665
B4GALT1(S73);	0.0012475	-2.548439539
BCL7C(S114);	0.005112466	-2.543953719
FAM134C(T310);(S320);(T307);(S313);	0.001470217	-2.52516818
09/09/18 00:00:00(T49);	0.012176885	-2.484544631
TMPO(S184);	0.035664504	-2.390999685
TMPO(R173);(S180);(S184);	0.035664504	-2.390999685
NDRG3(S335);	0.008896832	-2.356451159
CASC4(S328);	0.007499194	-2.34560265
TSR2(S142);	0.033621444	-2.337223838
SCARF2(S651);SCARF2(S653);	0.048820776	-2.317081023
SMARCA4(S613);	0.025099076	-2.314915329
PPFIBP1(T428);	0.017116857	-2.290133295
PRR12(T733);PRR12(S747);	0.002183402	-2.231763075
RBM12B(S839);	0.049605568	-2.223340018
TP53BP1(S1426);	0.007359877	-2.189044293
SMC4(T48);	0.017917752	-2.169609742
TBC1D4(T749);TBC1D4(S750);	0.009064705	-2.150715168
EML4(S917);	0.040115178	-2.082283245
KIFAP3(S60);	0.01273114	-2.053406063
MLLT10(S705);	0.030308316	-2.05212768
SLC4A1AP(S82);	0.010894735	-2.051574297
MED24(T875);	0.049401434	-2.049454422
FN1(S2384);	0.002908448	-2.045208755
FN1(M2373);FN1(S2384);	0.002908448	-2.045208755
AKAP11(T1100);	0.032291262	-2.027332

GGNBP2(S360);	0.015818268	-2.019444902
ZC3HC1(S321);	0.027530723	-2.002099993
RFC1(S71);	0.013724175	-1.997101533
RFC1(S71);RFC1(S73);	0.013724175	-1.997101533
RFC1(S71);RFC1(Y67);	0.013724175	-1.997101533
MIER1(S383);	0.000843689	-1.992394792
COPB2(T861);	0.00945371	-1.986807563
CHAMP1(S427);	0.049397841	-1.978847463
STMN1(S38);	0.006872457	-1.961654509
TOP2A(S1387);	0.019840281	-1.942601346
ZC3H13(S993);	0.00719457	-1.934185214
PRUNE2(T2091);PRUNE2(S2104);	0.038067829	-1.931598663
ADAMTSL1(S976);	0.019418779	-1.929916929
CCDC86(S113);(S102);(R94);	0.00049994	-1.920495193
NOP2(S786);	0.002340507	-1.907795029
ZC3H13(S207);ZC3H13(S211);	0.035097643	-1.899904165
DOCK10(S12);	0.032892516	-1.897494448
RSF1(S604);	0.00172405	-1.894550042
PLEC(S149);	0.001292622	-1.892727147
ERCC6L(S1069);	0.013043901	-1.877237984
METTL3(T45);	0.003500743	-1.872692871
OTUD4(S1005);	0.008070024	-1.865403136
NEXN(M566);NEXN(S564);	0.013257204	-1.853716182
WRAP53(S99);	0.020282582	-1.847244615
TMPO(R173);TMPO(Y183);	0.015471508	-1.846945539
WNK1(S167);	0.007660298	-1.838436134
MCM2(S40);	0.026775794	-1.838009676
SLC9A3R1(S280);	0.040761732	-1.827740024
TMPO(S66);TMPO(S67);	0.004344659	-1.822315055
URI1(S372);	0.002473778	-1.820963809
CD44(S704);	0.01891548	-1.8183773
ATF7IP(S113);	0.010552024	-1.817059185
COPR5(S87);COPR5(T93);	0.045171888	-1.813467085
COPR5(T93);	0.045171888	-1.813467085
RNF4(S94);RNF4(S95);	0.014202683	-1.811525975

Supplementary Table 6.10: Top 100 upregulated phosphorylated sites in PERK-MSC vs rtTA-MSC.

Threshold has been applied to display genes with p-value < 0.05.

	p-value	fold change
HECW2(T50);	0.024972827	8.473329654
C9orf78(S15);C9orf78(S17);	0.008870779	3.203485173
AMOTL1(S793);AMOTL1(S805);	0.024726268	3.122075486
KIAA1671(K1016);KIAA1671(S1019);	0.03571599	2.817130874
SQSTM1(S272);SQSTM1(S266);	0.041014563	2.616862585
GIT2(M431);GIT2(S421);GIT2(S415);	0.028431321	2.557237997
ANKRD17(S2059);	0.045637571	2.352431205
SPP1(S308);SPP1(S310);	0.006159753	2.078002512
HIRIP3(S196);HIRIP3(S199);	0.011749233	2.003029812
PDCD4(S76);	0.047321687	1.934938261
MAGED2(S190);MAGED2(S191);MAGED2(T200);	0.04993015	1.76825276
TWF1(T148);	0.005721464	1.650331149
TWF1(Y137);	0.005721464	1.650331149
CRBG3_HUMAN_Phospho (ST);	0.03772598	1.633773785
NUCKS1(S61);	0.00773403	1.562965782
ANKS1A(S649);	0.028700066	1.529333632
WRAP53(S85);	0.044098283	1.523336775
AKAP12(S128);	0.037873898	1.479426225
DTD1(S194);DTD1(S196);	0.007197261	1.473863295
NDRG3(T329);	0.000376418	1.455568979
TLN2(S1643);TLN1(S1641);	0.046405941	1.453538099
PRKCA(T497);PRKCB(T500);PRKCG(T514);	0.001716135	1.408046232
NUCKS1(S58);	0.044704937	1.393865096
CAMK2D(S330);CAMK2D(S334);	0.008783566	1.331637306
HNRNPC(S306);	0.029809721	1.287001907
MARK1(Y222);MARK4(Y221);MARK2(Y215);MARK3(Y218);	0.024430464	1.276155328
RANBP3(S96);RANBP3(S100);	0.0383009	1.27372544
NDRG1(S330);NDRG1(S336);	0.024686639	1.265197884
MARK1(S219);MARK4(S218);MARK2(S212);MARK3(S215);	0.023932122	1.262954147
PRKCD(T511);	0.021961473	1.241424522
PRKCD(M655);PRKCD(S664);	0.029981614	1.236870825
RAI14(S293);RAI14(S296);	0.007992605	1.228319689
RAI14(S293);	0.014038353	1.181187371
MYH9(S1943);	0.014889689	1.178864634
SRRM2(T1063);(S1069);(S1072);(S1073);	0.009876777	1.173237735
HNRNPUL2(S168);	0.018714911	1.158601414
ATN1(S73);ATN1(S77);	0.017498991	1.152777015
PCDHGC3(S60);CEP170(S1160);PLIN5(S203);	0.005980881	1.098684275
TGFBR2(S352);	0.005980881	1.098684275
ROBO4(T122);	0.005980881	1.098684275
MAP3K7(S367);	0.005980881	1.098684275
VIM(S83);	0.030294327	1.094048353
VIM(S29);	0.007484128	1.071697843
VIM(Y30);	0.007484128	1.071697843
SF3B1(S242);	0.008931043	1.058261445
APBB2(S160);	0.02280867	1.042644337
HTT(S417);HTT(S429);	0.033479629	1.03562391
PRKCA(Y504);PRKCB(Y507);PRKCG(Y521);	0.011435364	1.011617004
RANBP3(S96);	0.045850558	1.009323549
OSBP(S351);	0.034308731	1.005648201
OSBP(M350);OSBP(M368);OSBP(S351);	0.034308731	1.005648201
SRRM2(S1320);SRRM2(S1326);SRRM2(S1329);	0.04385755	1
SRRM2(S778);SRRM2(S780);	0.013215678	0.987360257
SRRM2(S780);	0.013215678	0.987360257
DKC1(T496);	0.000438005	0.966452179
ARHGEF2(T153);	0.035024202	0.959777709
NOC2L(S673);	0.001199657	0.959065646
VCL(S288);	0.034035789	0.951994627
SF3B1(S242);SF3B1(T248);	0.000956344	0.935989909
DDX51(S83);	0.007867053	0.903784685
PPP2R5D(R86);PPP2R5D(S89);PPP2R5D(S90);	0.002505269	0.893315179
FIP1L1(S304);	0.048764277	0.892499821
SRRM1(S752);SRRM1(S754);SRRM1(S756);	0.045493105	0.891363203
IWS1(S398);IWS1(S400);	0.011288117	0.890404909
SLK(S781);	0.0336849	0.889397359
ATXN2L(T681);ATXN2L(S684);	0.014076049	0.878176259

PRKCA(T501);PRKCB(T504);PRKCG(T518);	0.02627243	0.8754497
MICAL3(S1152);MICAL3(S1156);	0.037499514	0.866633239
CAMK2D(S333);	0.000264526	0.857042046
EXOC1(S470);	0.028512189	0.850135817
MAP1B(S828);MAP1B(T837);	0.03367544	0.829716957
PRPF4B(S292);PRPF4B(S294);	0.005928589	0.826392961
NDRG1(S333);	0.046699834	0.823210601
PURB(S298);PURB(S304);	0.009212531	0.776722267
PURB(S304);	0.009212531	0.776722267
ACLY(S455);	0.029616945	0.774808945
TCEAL3(S125);TCEAL6(S125);TCEAL5(S131);	0.029107414	0.750607162
ARHGEF2(S932);	0.036550295	0.745580796
DOCK7(S894);DOCK7(S905);	0.0272977	0.743834097
SRSF2(T25);	0.040567544	0.732739461
PPFIBP1(S466);	0.014817512	0.731310731
UBD(S111);	0.014817512	0.731310731
VIM(S214);	0.034674092	0.726156599
OTOP3(S18);OTOP3(S23);	0.025660184	0.71429776
ARHGAP19(T402);ARHGAP19(T404);	0.025660184	0.71429776
PALLD(S893);	0.012927413	0.703188582
ANKS3(T319);	0.019136966	0.693969532
HMGN1(T83);	0.019914077	0.687080283
VASP(T315);	0.037891595	0.679632419
RBM34(S14);	0.001370155	0.67211445
LRRFIP2(T316);LRRFIP2(S323);	0.029477651	0.66970077
DDX42(T98);	0.035859256	0.668503715
SPTBN1(S2184);	0.030484967	0.66732447
TCEA1(T96);	0.003881421	0.667150267
RABGEF1(R307);RABGEF1(S310);	0.028183459	0.662717658
RBM12B(T640);	0.025844883	0.658857772
TNS3(T692);	0.047916337	0.65798193
FOXK1(S213);	0.018863584	0.649813645
PSIP1(S102);	0.042037038	0.633315607
PSIP1(K100);PSIP1(S102);	0.042037038	0.633315607
TCEAL3(S65);	0.034351564	0.624441513

Supplementary Table 6.11: Top 100 downregulated phosphorylated sites in PERK-MSC vs rtTA-MSC.

Threshold has been applied to display genes with p-value < 0.05.

	p-value	fold change
TJAP1(S300);	0.005760353	-15.60495531
DBN1(T377);	0.02508509	-11.43556653
MED24(T875);	0.019691556	-10.67713126
FOXK1(M237);FOXK1(T245);FOXK1(S249);FOXK1(S253);	0.038720862	-10.2824908
BCL7C(S114);	0.014382601	-10.0911481
SPECC1L(S385);	0.009022308	-9.517170641
WDR47(S312);	0.010934896	-9.503426221
CC2D1A(S455);	0.033077987	-9.309596934
SLC4A1AP(S82);	0.038855082	-7.206144576
STMN1(S63);	0.00243401	-7.118908789
CAMK2G(R284);CAMK2G(T287);	0.020935702	-5.97938121
SORBS3(S547);	0.018865279	-4.278388978
WRAP53(S99);	0.023721483	-3.869707298
ASAP1(S1027);	0.005912218	-3.768508854
LATS1(K608);LATS1(T611);	0.013687188	-3.651226478
FTSJ3(S10);	0.033737926	-3.599972488
ZBTB3(S369);	0.048460896	-3.453627048
KIF1B(S1054);	0.00219291	-3.408589661
MAP3K7(S439);	0.002910949	-3.286103127
AKAP12(S1390);	0.006130528	-3.13100602
AMOTL2(T45);	0.02301473	-3.060143317
CDC40(S43);	0.024351194	-2.892574022
STXBP5(R689);STXBP5(S692);	0.02116534	-2.821827035
TBC1D2(S436);	0.011009157	-2.798005295
FAM91A1(T362);	0.004747056	-2.773840555
RABGAP1L(S496);	0.02986732	-2.727462439
KIAA1429(T184);	0.00575875	-2.713195597
FRMD6(S525);	0.033680366	-2.704440492
RIN2(S484);	0.021696047	-2.67956928
MAP1B(R2140);MAP1B(T2158);MAP1B(S2180);	0.015634611	-2.661040069
MTMR3(T619);	0.04160887	-2.586783616
MTMR3(Y614);	0.04160887	-2.586783616
SPATS2L(S115);	0.022362452	-2.49607392
BUD13(S325);	0.002657808	-2.469917092
SNX17(S421);	0.025644236	-2.418825072
GAPVD1(S1116);	0.049093705	-2.347906941
DIDO1(S805);DIDO1(S809);	0.023549207	-2.347300816
PHRF1(S973);	0.020471072	-2.321399872
TNKS1BP1(S1103);	0.028315283	-2.311076995
SKA3(S155);	0.039132068	-2.283633853
TCF3(S381);	0.019633237	-2.210090488
REPS1(S115);	0.038204992	-2.184816644
FAM198B(S199);	0.030394606	-2.181799195
PDLIM4(S132);	0.04547644	-2.176600266
MLL2(S654);	0.049153659	-2.15490496
KSR1(S567);	0.011529849	-2.144804497
MEF2D(S98);	0.005272304	-2.107520084
NSRP1(S40);	0.025471661	-2.102863691
PRRC2C(M776);PRRC2C(S779);	0.033864242	-2.076359381
LARP1(T858);	0.010232263	-2.069274458
SRRM2(S1398);	0.023913148	-2.06355056
FILIP1L(S791);	0.042742323	-1.956260378
PPP1R10(T315);	0.034524267	-1.953892015
ZRANB2(Y167);	0.044601691	-1.902603237
NAV1(S806);	0.016857627	-1.861826338
MAPKAP1(S512);	0.000287	-1.857941792
SP100(S18);	0.012189149	-1.829473869
SP100(M24);SP100(S18);	0.012189149	-1.829473869
ANLN(S189);	0.004345095	-1.799646827
ABL1(S915);	0.022310296	-1.791058297
MARK2(S456);	0.029559579	-1.780774098
TRIP12(S310);	0.004811418	-1.771625136
FOXC2(S240);	0.021060063	-1.740067498
DGCR8(S377);	0.038300426	-1.721158791
ANXA1(S37);	0.025012043	-1.684086035
ANXA1(Y39);	0.025012043	-1.684086035

NCOR2(S956);	0.008866193	-1.671208413
TRAFD1(S415);	0.002419878	-1.662065653
EPS15(T572);	0.038937254	-1.640765933
EIF4G1(T202);EIF4G1(S204);	0.009926319	-1.638068314
CDK14(S24);	0.033842059	-1.63794615
ANKRD17(T12);	0.010061679	-1.630082331
AFAP1(S277);AFAP1(S278);AFAP1(S282);	0.009140193	-1.619282574
WWTR1(R63);WWTR1(S70);	0.038107616	-1.603427097
WWTR1(R63);WWTR1(S69);WWTR1(S70);	0.038107616	-1.603427097
SRRM2(S1397);	0.000571481	-1.589272931
SRRM2(M1396);SRRM2(S1397);	0.000571481	-1.589272931
PIKFYVE(T309);	0.00703607	-1.587465008
FNDC1(M554);FNDC1(S537);FNDC1(T538);	0.020415715	-1.586339502
FNDC1(M554);FNDC1(T538);	0.020415715	-1.586339502
FNDC1(M554);FNDC1(S537);FNDC1(T538);1	0.020415715	-1.586339502
MYCBP2(S3467);	0.013549124	-1.572154724
VPS13D(S1045);	0.017169409	-1.551854189
ATN1(S103);	0.022439123	-1.54549106
MAP1B(R2077);MAP1B(S2087);	0.043114287	-1.544610713
FNDC1(M554);FNDC1(T538);FNDC1(S555);	0.017150682	-1.540066483
FNDC1(M554);FNDC1(T538);FNDC1(S555);1	0.017150682	-1.540066483
DOCK7(T909);DOCK7(S910);	0.004257516	-1.535934674
DOCK7(S910);	0.004257516	-1.535934674
NAV1(S652);	0.011303691	-1.514062695
SMC4(T48);	0.045020727	-1.497341043
PRKD1(T217);	0.026783621	-1.495957495
RB1(S37);	0.01706312	-1.4915122
TNK2(Y827);	0.006785054	-1.490093464
NFIX(S306);	0.002655146	-1.487351347
MAST2(S148);	0.018856685	-1.481298942
ATAT1(S315);	0.010025815	-1.478286967
SRRM1(S773);	0.01410407	-1.47614867
SLAIN2(S391);	0.032573048	-1.463413316

Supplementary Table 6.12: AML patients characteristics

Mutations in leukaemic cells	VAF
AML01	
NRAS,CSDE1	0.474
GATA2,GATA2-AS1	0.066
GATA2,GATA2-AS1	0.409
KIT	0.459
TET2	0.476
TET2	0.523
TET2	0.48
CUX1	0.086
EZH2	0.484
RP13-46H24.1,HRAS,LRRC56	0.999
RUNX1	0.068
STAG2	0.06
BCORL1	0.999
BCORL1	0.052
AML02	
NRAS,CSDE1	0.485
GATA2,GATA2-AS1	0.083
GATA2,GATA2-AS1	0.389
CUX1	0.451
CUX1	0.463
CUX1	0.485
ETV6	0.208
TP53	0.959
TP53	0.981
ASXL1	0.997
RUNX1	0.07
KDM6A	0.993
STAG2	0.076
BCORL1	0.996
BCORL1	0.066
AML03	
GATA2,GATA2-AS1	0.357
TET2	0.492
TET2	0.996
CUX1	0.997
CUX1	0.993
TP53	0.992
ASXL1	0.461
RUNX1	0.064
RUNX1	0.419
RUNX1	0.486
RUNX1	0.551
U2AF1	0.484
STAG2	0.115
BCORL1	0.998
BCORL1	0.063
BCORL1	0.053
AML04	
Mutations in leukaemic cells	
Not available	

References

Agostinis, P., & Afshin, S. (Eds.). (2012). *Endoplasmic Reticulum Stress in Health and Disease*. Springer Netherlands. https://doi.org/10.1007/978-94-007-4351-9

Alberts, B., Johnson, A., & Lewis, J. (2002). The Endoplasmic Reticulum. In *Molecular Biology of the Cell* (4th ed.). Garland Science. https://www.ncbi.nlm.nih.gov/books/NBK26841/

Almanza, A., Carlesso, A., Chintha, C., Creedican, S., Doultsinos, D., Leuzzi, B., Luís, A., McCarthy, N., Montibeller, L., More, S., Papaioannou, A., Püschel, F., Sassano, M. L., Skoko, J., Agostinis, P., de Belleroche, J., Eriksson, L. A., Fulda, S., Gorman, A. M., … Samali, A. (2019). Endoplasmic reticulum stress signalling – from basic mechanisms to clinical applications. *FEBS Journal*, *286*(2), 241–278. https://doi.org/10.1111/febs.14608

Ambele, M. A., Dhanraj, P., Giles, R., & Pepper, M. S. (2020). Adipogenesis: A complex interplay of multiple molecular determinants and pathways. *International Journal of Molecular Sciences*, *21*(12), 1–27. https://doi.org/10.3390/ijms21124283

Andrzejewska, A., Lukomska, B., & Janowski, M. (2019). Concise Review: Mesenchymal Stem Cells: From Roots to Boost. *Stem Cells*, *37*(7), 855–864. https://doi.org/10.1002/stem.3016

Armes, H., Bewicke-Copley, F., Rio-Machin, A., Di Bella, D., Philippe, C., Wozniak, A., Tummala, H., Wang, J., Ezponda, T., Prosper, F., Dokal, I., Vulliamy, T., Kilpivaara, O., Wartiovaara-Kautto, U., Fitzgibbon, J., & Rouault-Pierre, K. (2022). Germline ERCC excision repair 6 like 2 (ERCC6L2) mutations lead to impaired erythropoiesis and reshaping of the bone marrow microenvironment. *British Journal of Haematology*, *June*, 1–11. https://doi.org/10.1111/bjh.18466

Azadniv, M., Myers, J. R., McMurray, H. R., Guo, N., Rock, P., Coppage, M. L., Ashton, J., Becker, M. W., Calvi, L. M., & Liesveld, J. L. (2020). Bone marrow mesenchymal stromal cells from acute myelogenous leukemia patients demonstrate

adipogenic differentiation propensity with implications for leukemia cell support. *Leukemia*, *34*(2), 391–403. https://doi.org/10.1038/s41375-019-0568-8

Bandyopadhyay, A., Tsuji, K., Cox, K., Harfe, B. D., Rosen, V., & Tabin, C. J. (2006). Genetic analysis of the roles of BMP2, BMP4, and BMP7 in limb patterning and skeletogenesis. *PLoS Genetics*, *2*(12), 2116–2130. https://doi.org/10.1371/journal.pgen.0020216

Barroso, I., Gurnell, M., Crowley, V. E. F., Agostini, M., Schwabe, J. W., Soos, M. A., Maslen, G. L., Williams, T. D. M., Lewis, H., Schafer, A. J., Chatterjee, V. K. K., & O'Rahilly, S. (1999). Dominant negative mutations in human PPARγ associated with severe insulin resistance, diabetes mellitus and hypertension. *Nature*, *402*(6764), 880–883. https://doi.org/10.1038/47254

Baryawno, N., Przybylski, D., Kowalczyk, M. S., Kfoury, Y., Severe, N., Gustafsson, K., Kokkaliaris, K. D., Mercier, F., Tabaka, M., Hofree, M., Dionne, D., Papazian, A., Lee, D., Ashenberg, O., Subramanian, A., Vaishnav, E. D., Rozenblatt-Rosen, O., Regev, A., & Scadden, D. T. (2019). A Cellular Taxonomy of the Bone Marrow Stroma in Homeostasis and Leukemia. *Cell*, 1–18. https://doi.org/10.1016/j.cell.2019.04.040

Basseri, S., Lhoták, Š., Sharma, A. M., & Austin, R. C. (2009). The chemical chaperon 4-phenylbutyrate inhibits adipogenesis by modulating the unfolded protein response. *Journal of Lipid Research*, *50*(12), 2486–2501. https://doi.org/10.1194/jlr.M900216-JLR200

Batchvarova, N., Wang, X. Z., & Ron, D. (1995). Inhibition of adipogenesis by the stress-induced protein CHOP (Gadd153). *EMBO Journal*, *14*(19), 4654–4661. https://doi.org/10.1002/j.1460-2075.1995.tb00147.x

Batsali, A. K., Pontikoglou, C., Koutroulakis, D., Pavlaki, K. I., Damianaki, A., Mavroudi, I., Alpantaki, K., Kouvidi, E., Kontakis, G., & Papadaki, H. A. (2017). Differential expression of cell cycle and WNT pathway-related genes accounts for differences in the growth and differentiation potential of Wharton's jelly and

bone marrow-derived mesenchymal stem cells. *Stem Cell Research and Therapy*, *8*(1), 1–17. https://doi.org/10.1186/s13287-017-0555-9

Battula, V. L., Le, P. M., Sun, J. C., Nguyen, K., Yuan, B., Zhou, X., Sonnylal, S., McQueen, T., Ruvolo, V., Michel, K. A., Ling, X., Jacamo, R., Shpall, E., Wang, Z., Rao, A., Al-Atrash, G., Konopleva, M., Davis, R. E., Harrington, M. A., … Andreeff, M. (2017). AML-induced osteogenic differentiation in mesenchymal stromal cells supports leukemia growth. *JCI Insight*, *2*(13), 1–18. https://doi.org/10.1172/jci.insight.90036

Baum, C. M., Weissman, I. L., Tsukamoto, A. S., Buckle, A. M., & Peault, B. (1992). Isolation of a candidate human hematopoietic stem-cell population. *Proceedings of the National Academy of Sciences of the United States of America*, *89*(7), 2804–2808. https://doi.org/10.1073/pnas.89.7.2804

Beck, D., Niessner, H., Smalley, K. S. M., Flaherty, K., Paraiso, K. H. T., Busch, C., Sinnberg, T., Vasseur, S., Iovanna, J. L., Drießen, S., Stork, B., Wesselborg, S., Schaller, M., Biedermann, T., Bauer, J., Lasithiotakis, K., Weide, B., Eberle, J., Schittek, B., … Meier, F. (2013). Vemurafenib potently induces endoplasmic reticulum stress-mediated apoptosis in BRAFV600E melanoma cells. *Science Signaling*, *6*(260). https://doi.org/10.1126/scisignal.2003057

Becker, A. J., Mcculloch, E. A., & Till, J. E. (1963). Cytological Demonstration of the Clonal Nature of Spleen Colonies Derived from Transplanted Mouse Marrow Cells. *Nature*, *197*(4866), 452–454. https://doi.org/10.1038/197452a0

Bensidhoum, M., Chapel, A., Francois, S., Demarquay, C., Mazurier, C., Fouillard, L., Bouchet, S., Bertho, J. M., Gourmelon, P., Aigueperse, J., Charbord, P., Gorin, N. C., Thierry, D., & Lopez, M. (2004). Homing of in vitro expanded Stro-1. *Blood*, *103*(9), 3313–3319. https://doi.org/10.1182/blood-2003-04-1121.Supported

Bhatia, M., Wang, J. C. Y., Kapp, U., Bonnet, D., & Dick, J. E. (1997). Purification of primitive human hematopoietic cells capable of repopulating immune-deficient mice. *Proceedings of the National Academy of Sciences of the United States of America*, *94*(10), 5320–5325. https://doi.org/10.1073/pnas.94.10.5320

Blau, O., Baldus, C. D., Hofmann, W. K., Thiel, G., Nolte, F., Burmeister, T., Türkmen, S., Benlasfer, O., Schümann, E., Sindram, A., Molkentin, M., Mundlos, S., Keilholz, U., Thiel, E., & Blau, I. W. (2011). Mesenchymal stromal cells of myelodysplastic syndrome and acute myeloid leukemia patients have distinct genetic abnormalities compared with leukemic blasts. *Blood*, *118*(20), 5583–5592. https://doi.org/10.1182/blood-2011-03-343467

Bobrovnikova-Marjon, E., Hatzivassiliou, G., Grigoriadou, C., Romero, M., Cavener, D. R., Thompson, C. B., & Diehl, J. A. (2008). PERK-dependent regulation of lipogenesis during mouse mammary gland development and adipocyte differentiation. *Proceedings of the National Academy of Sciences of the United States of America*, *105*(42), 16314–16319. https://doi.org/10.1073/pnas.0808517105

Bonilla, X., Vanegas, N. D. P., & Vernot, J. P. (2019). Acute leukemia induces senescence and impaired osteogenic differentiation in mesenchymal stem cells endowing leukemic cells with functional advantages. *Stem Cells International*, *2019*. https://doi.org/10.1155/2019/3864948

Bonnet, D., & Dick, J. E. (1997). Human acute myeloid leukemia is organized as a hierarchy that originates from a primitive hematopoietic cell. *Nature Medicine*, *3*(7), 730–737. https://doi.org/10.1038/nm0797-730

Bousette, N., Abbasi, C., Chis, R., & Gramolini, A. O. (2014). Calnexin silencing in mouse neonatal cardiomyocytes induces Ca2+ cycling defects, ER stress, and apoptosis. *Journal of Cellular Physiology*, *229*(3), 374–383. https://doi.org/10.1002/jcp.24459

Boyd, A. L., Reid, J. C., Salci, K. R., Aslostovar, L., Benoit, Y. D., Shapovalova, Z., Nakanishi, M., Porras, D. P., Almakadi, M., Campbell, C. J. V., Jackson, M. F., Ross, C. A., Foley, R., Leber, B., Allan, D. S., Sabloff, M., Xenocostas, A., Collins, T. J., & Bhatia, M. (2017). Acute myeloid leukaemia disrupts endogenous myelo-erythropoiesis by compromising the adipocyte bone marrow niche. *Nature Cell Biology*, *19*(11), 1336–1347. https://doi.org/10.1038/ncb3625

Bullinger, L., Döhner, K., & Dohner, H. (2017). Genomics of acute myeloid leukemia diagnosis and pathways. *Journal of Clinical Oncology*, *35*(9), 934–946. https://doi.org/10.1200/JCO.2016.71.2208

Cai, H., Zou, J., Wang, W., & Yang, A. (2021). BMP2 induces hMSC osteogenesis and matrix remodeling. *Molecular Medicine Reports*, *23*(2), 1–12. https://doi.org/10.3892/mmr.2020.11764

Calvi, L. M., Adams, G. B., Weibrecht, K. W., Weber, J. M., Olson, D. P., Knight, M. C., Martin, R. P., Schipani, E., Divieti, P., Bringhurst, F. R., Milner, L. A., Kronenberg, H. M., & Scadden, D. T. (2003). Osteoblastic cells regulate the haematopoietic stem cell niche. *Nature*, *425*(6960), 841–846. https://doi.org/10.1038/nature02040

Cao, Z., Umek, R. M., & McKnight, S. L. (1991). Regulated expression of three C/EBP isoforms during adipose conversion of 3T3-L1 cells. *Genes and Development*, *5*(9), 1538–1552. https://doi.org/10.1101/gad.5.9.1538

Cattoretti, G., Schiro, R., Orazi, A., Soligo, D., & Colombo, M. P. (1993). Bone marrow stroma in humans: Anti-nerve growth factor receptor antibodies selectively stain reticular cells in vivo and in vitro. *Blood*, *81*(7), 1726–1738. https://doi.org/10.1182/blood.v81.7.1726.bloodjournal8171726

Chandran, P., Le, Y., Li, Y., Sabloff, M., Mehic, J., Rosu-Myles, M., & Allan, D. S. (2015). Mesenchymal stromal cells from patients with acute myeloid leukemia have altered capacity to expand differentiated hematopoietic progenitors. *Leukemia Research*, *39*(4), 486–493. https://doi.org/10.1016/j.leukres.2015.01.013

Chen, D., Harris, M. A., Rossini, G., Dunstan, C. R., Dallas, S. L., Feng, J. Q., Mundy, G. R., & Harris, S. E. (1997). Bone morphogenetic protein 2 (BMP-2) enhances BMP-3, BMP-4, and bone cell differentiation marker gene expression during the induction of mineralized bone matrix formation in cultures of fetal rat calvarial osteoblasts. *Calcified Tissue International*, *60*(3), 283–290. https://doi.org/10.1007/s002239900230

Chen, H., Yuan, R., Zhang, Y., Zhang, X., Chen, L., Zhou, X., Yuan, Z., Nie, Y., Li, M., Mo,

D., & Chen, Y. (2016). ATF4 regulates SREBP1c expression to control fatty acids synthesis in 3T3-L1 adipocytes differentiation. *Biochimica et Biophysica Acta - Gene Regulatory Mechanisms*, *1859*(11), 1459–1469. https://doi.org/10.1016/j.bbagrm.2016.07.010

Chipurupalli, S., Kannan, E., Tergaonkar, V., D'Andrea, R., & Robinson, N. (2019). Hypoxia Induced ER Stress Response as an Adaptive Mechanism in Cancer. *International Journal of Molecular Sciences*, *20*(3), 749. https://doi.org/10.3390/ijms20030749

Civin, C. I., Strauss, L. C., Brovall, C., Fackler, M. J. O., Schwartz, J. F., & Shaper, J. H. (1984). Antigenic analysis of hematopoiesis . III . A hematopoietic progenitor cell surface antigen defined by a monoclonal antibody raised against KG-1a cells . Information about subscribing to The Journal of Immunology is online at : . A Hematopoietic Progenito. *The Journal of Immunology*, *133*(1), 157–165.

Cohen, D. M., Won, K.-J., Nguyen, N., Lazar, M. A., Chen, C. S., & Steger, D. J. (2015). ATF4 licenses C/EBPβ activity in human mesenchymal stem cells primed for adipogenesis. *ELife*, *4*, 1–20. https://doi.org/10.7554/elife.06821

Corces-Zimmerman, M. R., Hong, W.-J., Weissman, I. L., Medeiros, B. C., & Majeti, R. (2014). Preleukemic mutations in human acute myeloid leukemia affect epigenetic regulators and persist in remission. *Proceedings of the National Academy of Sciences*, *111*(7), 2548–2553. https://doi.org/10.1073/pnas.1324297111

Corces, M. R., Buenrostro, J. D., Wu, B., Greenside, P. G., Chan, S. M., Koenig, J. L., Snyder, M. P., Pritchard, J. K., Kundaje, A., Greenleaf, W. J., Majeti, R., & Chang, H. Y. (2016). Lineage-specific and single-cell chromatin accessibility charts human hematopoiesis and leukemia evolution. *Nature Genetics*, *48*(10), 1193–1203. https://doi.org/10.1038/ng.3646

Corre, J., Planat-Benard, V., Corberand, J. X., Pénicaud, L., Casteilla, L., & Laharrague, P. (2004). Human bone marrow adipocytes support complete myeloid and lymphoid differentiation from human CD34+ cells. *British Journal of*

Haematology, *127*(3), 344–347. https://doi.org/10.1111/j.1365-2141.2004.05198.x

Corselli, M., Chin, C. J., Parekh, C., Sahaghian, A., Wang, W., Ge, S., Evseenko, D., Wang, X., Montelatici, E., Lazzari, L., Crooks, G. M., & Péault, B. (2013). Perivascular support of human hematopoietic stem/progenitor cells. *Blood*, *121*(15), 2891–2901. https://doi.org/10.1182/blood-2012-08-451864

Cox, G., Boxall, S. A., Giannoudis, P. V., Buckley, C. T., Roshdy, T., Churchman, S. M., McGonagle, D., & Jones, E. (2012). High abundance of CD271 + multipotential stromal cells (MSCs) in intramedullary cavities of long bones. *Bone*, *50*(2), 510–517. https://doi.org/10.1016/j.bone.2011.07.016

Cunha, D. A., Hekerman, P., Ladrière, L., Bazarra-Castro, A., Ortis, F., Wakeham, M. C., Moore, F., Rasschaert, J., Cardozo, A. K., Bellomo, E., Overbergh, L., Mathieu, C., Lupi, R., Hai, T., Herchuelz, A., Marchetti, P., Rutter, G. A., Eizirik, D. L., & Cnop, M. (2008). Initiation and execution of lipotoxic ER stress in pancreatic β-cells. *Journal of Cell Science*, *121*(14), 2308–2318. https://doi.org/10.1242/jcs.026062

Day, T. F., Guo, X., Garrett-Beal, L., & Yang, Y. (2005). Wnt/β-catenin signaling in mesenchymal progenitors controls osteoblast and chondrocyte differentiation during vertebrate skeletogenesis. *Developmental Cell*, *8*(5), 739–750. https://doi.org/10.1016/j.devcel.2005.03.016

De Kouchkovsky, I., & Abdul-Hay, M. (2016). 'Acute myeloid leukemia: A comprehensive review and 2016 update.' *Blood Cancer Journal*, *6*(7). https://doi.org/10.1038/bcj.2016.50

Delépine, M., Nicolino, M., Barrett, T., Golamaully, M., Mark Lathrop, G., & Julier, C. (2000). EIF2AK3, encoding translation initiation factor 2-α kinase 3, is mutated in patients with Wolcott-Rallison syndrome. *Nature Genetics*, *25*(4), 406–409. https://doi.org/10.1038/78085

Diaz de la Guardia, R., Lopez-Millan, B., Lavoie, J. R., Bueno, C., Castaño, J., Gómez-Casares, M., Vives, S., Palomo, L., Juan, M., Delgado, J., Blanco, M. L.,

Nomdedeu, J., Chaparro, A., Fuster, J. L., Anguita, E., Rosu-Myles, M., & Menéndez, P. (2017). Detailed Characterization of Mesenchymal Stem/Stromal Cells from a Large Cohort of AML Patients Demonstrates a Definitive Link to Treatment Outcomes. *Stem Cell Reports*, *8*(6), 1573–1586. https://doi.org/10.1016/j.stemcr.2017.04.019

DiMascio, L., Voermans, C., Uqoezwa, M., Duncan, A., Lu, D., Wu, J., Sankar, U., & Reya, T. (2007). Identification of Adiponectin as a Novel Hemopoietic Stem Cell Growth Factor. *The Journal of Immunology*, *178*(6), 3511–3520. https://doi.org/10.4049/jimmunol.178.6.3511

Ding, L., & Morrison, S. J. (2013). Haematopoietic stem cells and early lymphoid progenitors occupy distinct bone marrow niches. *Nature*, *495*(7440), 231–235. https://doi.org/10.1038/nature11885

Ding, L., Saunders, T. L., Enikolopov, G., & Morrison, S. J. (2012). Endothelial and perivascular cells maintain haematopoietic stem cells. *Nature*, *481*(7382), 457–462. https://doi.org/10.1038/nature10783

Döhner, H., Estey, E., Grimwade, D., Amadori, S., Appelbaum, F. R., Büchner, T., Dombret, H., Ebert, B. L., Fenaux, P., Larson, R. A., Levine, R. L., Lo-Coco, F., Naoe, T., Niederwieser, D., Ossenkoppele, G. J., Sanz, M., Sierra, J., Tallman, M. S., Tien, H.-F., … Bloomfield, C. D. (2017). Diagnosis and management of AML in adults: 2017 ELN recommendations from an international expert panel. *Blood*, *129*(4), 424–447. https://doi.org/10.1182/blood-2016-08-733196

Döhner, H., Wei, A. H., Appelbaum, F. R., Craddock, C., DiNardo, C. D., Dombret, H., Ebert, B. L., Fenaux, P., Godley, L. A., Hasserjian, R. P., Larson, R. A., Levine, R. L., Miyazaki, Y., Niederwieser, D., Ossenkoppele, G., Röllig, C., Sierra, J., Stein, E. M., Tallman, M. S., … Löwenberg, B. (2022). Diagnosis and management of AML in adults: 2022 recommendations from an international expert panel on behalf of the ELN. *Blood*, *140*(12), 1345–1377. https://doi.org/10.1182/blood.2022016867

Domen, J., Cheshier, S. H., & Weissman, I. L. (2000). The role of apoptosis in the

regulation of hematopoietic stem cells: Overexpression of BCL-2 increases both their number and repopulation potential. *Journal of Experimental Medicine*, *191*(2), 253–263. https://doi.org/10.1084/jem.191.2.253

Dominici, M., Le Blanc, K., Mueller, I., Slaper-Cortenbach, I., Marini, F. C., Krause, D. S., Deans, R. J., Keating, A., Prockop, D. J., & Horwitz, E. M. (2006). Minimal criteria for defining multipotent mesenchymal stromal cells. The International Society for Cellular Therapy position statement. *Cytotherapy*, *8*(4), 315–317. https://doi.org/10.1080/14653240600855905

Doron, B., Abdelhamed, S., Butler, J. T., Hashmi, S. K., Horton, T. M., & Kurre, P. (2018). Transmissible ER stress reconfigures the AML bone marrow compartment. *Leukemia*. https://doi.org/10.1038/s41375-018-0254-2

Doulatov, S., Notta, F., Laurenti, E., & Dick, J. E. (2012). Hematopoiesis: A human perspective. *Cell Stem Cell*, *10*(2), 120–136. https://doi.org/10.1016/j.stem.2012.01.006

Drevinge, C., Karlsson, L. O., Ståhlman, M., Larsson, T., Perman Sundelin, J., Grip, L., Andersson, L., Borén, J., & Levin, M. C. (2013). Cholesteryl Esters Accumulate in the Heart in a Porcine Model of Ischemia and Reperfusion. *PLoS ONE*, *8*(4), 2–9. https://doi.org/10.1371/journal.pone.0061942

Duarte, D., Hawkins, E. D., Akinduro, O., Ang, H., De Filippo, K., Kong, I. Y., Haltalli, M., Ruivo, N., Straszkowski, L., Vervoort, S. J., McLean, C., Weber, T. S., Khorshed, R., Pirillo, C., Wei, A., Ramasamy, S. K., Kusumbe, A. P., Duffy, K., Adams, R. H., … Lo Celso, C. (2018). Inhibition of Endosteal Vascular Niche Remodeling Rescues Hematopoietic Stem Cell Loss in AML. *Cell Stem Cell*, *22*(1), 64-77.e6. https://doi.org/10.1016/j.stem.2017.11.006

Ducy, P., Amling, M., Takeda, S., Priemel, M., Schilling, A. F., Beil, F. T., Shen, J., Vinson, C., Rueger, J. M., & Karsenty, G. (2000). Leptin inhibits bone formation through a hypothalamic relay: A central control of bone mass. *Cell*, *100*(2), 197–207. https://doi.org/10.1016/S0092-8674(00)81558-5

Ducy, P., Starbuck, M., Priemel, M., Shen, J., Pinero, G., Geoffroy, V., Amling, M., &

Karsteny, G. (1999). Erratum: A Cbfa1-dependent genetic pathway controls bone formation beyond embryonic development (Genes and Development (1999) 13 (1025-1036)). *Genes and Development*, *13*(14), 1898.

Ducy, P., Zhang, R., Geoffroy, V., Ridall, A. L., & Karsenty, G. (1997). Osf2/Cbfa1: A transcriptional activator of osteoblast differentiation. *Cell*, *89*(5), 747–754. https://doi.org/10.1016/S0092-8674(00)80257-3

Duncavage, E. J., Schroeder, M. C., O'Laughlin, M., Wilson, R., MacMillan, S., Bohannon, A., Kruchowski, S., Garza, J., Du, F., Hughes, A. E. O., Robinson, J., Hughes, E., Heath, S. E., Baty, J. D., Neidich, J., Christopher, M. J., Jacoby, M. A., Uy, G. L., Fulton, R. S., … Spencer, D. H. (2021). Genome Sequencing as an Alternative to Cytogenetic Analysis in Myeloid Cancers. *New England Journal of Medicine*, *384*(10), 924–935. https://doi.org/10.1056/nejmoa2024534

Eletto, D., Eletto, D., Dersh, D., Gidalevitz, T., & Argon, Y. (2014). Protein Disulfide Isomerase A6 Controls the Decay of IRE1α Signaling via Disulfide-Dependent Association. *Molecular Cell*, *53*(4), 562–576. https://doi.org/10.1016/j.molcel.2014.01.004

Féral, K., Jaud, M., Philippe, C., Bella, D. Di, Pyronnet, S., Rouault-Pierre, K., Mazzolini, L., & Touriol, C. (2021). ER stress and unfolded protein response in leukemia: Friend, foe, or both? *Biomolecules*, *11*(2), 1–31. https://doi.org/10.3390/biom11020199

Freytag, S. O., Paielli, D. L., & Gilbert, J. D. (1994). Ectopic expression of the CCAAT/enhancer-binding protein α promotes the adipogenic program in a variety of mouse fibroblastic cells. *Genes and Development*, *8*(14), 1654–1663. https://doi.org/10.1101/gad.8.14.1654

Friedenstein, A., Chailakhjan, R., & Lalykina, K. (1970). THE DEVELOPMENT OF FIBROBLAST COLONIES IN MONOLAYER CULTURES OF GUINEA-PIG BONE MARROW AND SPLEEN CELLS. *Cell Proliferation*, *3*(4), 393–403. https://doi.org/10.1111/j.1365-2184.1970.tb00347.x

Friedenstein, A., Chailakhyan, R., Latsinik, N., Panasyuk, A., & Keiliss-Borok, I. (1974).

Stromal Cells Responsible for Transferring the Microenvironment of the Hemopoietic Tissues. In *Transplantation* (Vol. 17, Issue 4, pp. 331–340). https://doi.org/10.1097/00007890-197404000-00001

Fu, S., Yang, L., Li, P., Hofmann, O., Dicker, L., Hide, W., Lin, X., Watkins, S. M., Ivanov, A. R., & Hotamisligil, G. S. (2011). Aberrant lipid metabolism disrupts calcium homeostasis causing liver endoplasmic reticulum stress in obesity. *Nature*, *473*(7348), 528–531. https://doi.org/10.1038/nature09968

Gass, J. N., Gifford, N. M., & Brewer, J. W. (2002). Activation of an unfolded protein response during differentiation of antibody-secreting B cells. *Journal of Biological Chemistry*, *277*(50), 49047–49054. https://doi.org/10.1074/jbc.M205011200

Gass, J. N., Gunn, K. E., Sriburi, R., & Brewer, J. W. (2004). Stressed-out B cells? Plasma-cell differentiation and the unfolded protein response. *Trends in Immunology*, *25*(1), 17–24. https://doi.org/10.1016/j.it.2003.11.004

Geyh, S., Rodríguez-Paredes, M., Jäger, P., Khandanpour, C., Cadeddu, R. P., Gutekunst, J., Wilk, C. M., Fenk, R., Zilkens, C., Hermsen, D., Germing, U., Kobbe, G., Lyko, F., Haas, R., & Schroeder, T. (2016). Functional inhibition of mesenchymal stromal cells in acute myeloid leukemia. *Leukemia*, *30*(3), 683–691. https://doi.org/10.1038/leu.2015.325

Göttgens, B. (2015). Regulatory network control of blood stem cells. *Blood*, *125*(17), 2614–2620. https://doi.org/10.1182/blood-2014-08-570226

Gray, S., Feinberg, M. W., Hull, S., Kuo, C. T., Watanabe, M., Sen, S., Depina, A., Haspel, R., & Jain, M. K. (2002). The Krüppel-like factor KLF15 regulates the insulin-sensitive glucose transporter GLUT4. *Journal of Biological Chemistry*, *277*(37), 34322–34328. https://doi.org/10.1074/jbc.M201304200

Greenbaum, A., Hsu, Y. M. S., Day, R. B., Schuettpelz, L. G., Christopher, M. J., Borgerding, J. N., Nagasawa, T., & Link, D. C. (2013). CXCL12 in early mesenchymal progenitors is required for haematopoietic stem-cell maintenance. *Nature*, *495*(7440), 227–230.

https://doi.org/10.1038/nature11926

Grimwade, D., Ivey, A., & Huntly, B. J. P. (2016). *Molecular Landscape Aml*. *127*(1), 29–41. https://doi.org/10.1182/blood-2015-07-604496.have

Gronthos, S., Zannettino, A. C. W., Hay, S. J., Shi, S., Graves, S. E., Kortesidis, A., & Simmons, P. J. (2003). Molecular and cellular characterisation of highly purified stromal stem cells derived from human bone marrow. *Journal of Cell Science*, *116*(9), 1827–1835. https://doi.org/10.1242/jcs.00369

Gunn, K. E., Gifford, N. M., Mori, K., & Brewer, J. W. (2004). A role for the unfolded protein response in optimizing antibody secretion. *Molecular Immunology*, *41*(9), 919–927. https://doi.org/10.1016/j.molimm.2004.04.023

Hamamura, K., & Yokota, H. (2007). Stress to endoplasmic reticulum of mouse osteoblasts induces apoptosis and transcriptional activation for bone remodeling. *FEBS Letters*, *581*(9), 1769–1774. https://doi.org/10.1016/j.febslet.2007.03.063

Hamanaka, R. B., Bennett, B. S., Cullinan, S. B., & Diehl, J. A. (2005). PERK and GCN2 Contribute to eIF2α Phosphorylation and Cell Cycle Arrest after Activation of the Unfolded Protein Response Pathway. *Molecular Biology of the Cell*, *16*(12), 5493–5501. https://doi.org/10.1091/mbc.e05-03-0268

Han, J., & Kaufman, R. J. (2016). The role of ER stress in lipid metabolism and lipotoxicity. *Journal of Lipid Research*, *57*(8), 1329–1338. https://doi.org/10.1194/jlr.R067595

Han, J., Murthy, R., Wood, B., Song, B., Wang, S., Sun, B., Malhi, H., & Kaufman, R. J. (2013). ER stress signalling through eIF2α and CHOP, but not IRE1α, attenuates adipogenesis in mice. *Diabetologia*, *56*(4), 911–924. https://doi.org/10.1007/s00125-012-2809-5

Hanoun, M., Zhang, D., Mizoguchi, T., Pinho, S., Pierce, H., Kunisaki, Y., Lacombe, J., Armstrong, S. A., Dührsen, U., & Frenette, P. S. (2014). Acute myelogenous leukemia-induced sympathetic neuropathy promotes malignancy in an altered hematopoietic stem cell Niche. *Cell Stem Cell*, *15*(3), 365–375.

https://doi.org/10.1016/j.stem.2014.06.020

Hetz, C. (2012). The unfolded protein response: Controlling cell fate decisions under ER stress and beyond. *Nature Reviews Molecular Cell Biology*, *13*(2), 89–102. https://doi.org/10.1038/nrm3270

Hetz, C., & Papa, F. R. (2018). The Unfolded Protein Response and Cell Fate Control. *Molecular Cell*, *69*(2), 169–181. https://doi.org/10.1016/j.molcel.2017.06.017

Higa, A., Taouji, S., Lhomond, S., Jensen, D., Fernandez-Zapico, M. E., Simpson, J. C., Pasquet, J.-M., Schekman, R., & Chevet, E. (2014). Endoplasmic Reticulum Stress-Activated Transcription Factor ATF6α Requires the Disulfide Isomerase PDIA5 To Modulate Chemoresistance. *Molecular and Cellular Biology*, *34*(10), 1839–1849. https://doi.org/10.1128/mcb.01484-13

Hilton, M. J., Tu, X., Wu, X., Bai, S., Zhao, H., Kobayashi, T., Kronenberg, H. M., Teitelbaum, S. L., Ross, F. P., Kopan, R., & Long, F. (2008). Notch signaling maintains bone marrow mesenchymal progenitors by suppressing osteoblast differentiation. *Nature Medicine*, *14*(3), 306–314. https://doi.org/10.1038/nm1716

Hino, S. I., Kondo, S., Yoshinaga, K., Saito, A., Murakami, T., Kanemoto, S., Sekiya, H., Chihara, K., Aikawa, Y., Hara, H., Kudo, T., Sekimoto, T., Funamoto, T., Chosa, E., & Imaizumi, K. (2010). Regulation of ER molecular chaperone prevents bone loss in a murine model for osteoporosis. *Journal of Bone and Mineral Metabolism*, *28*(2), 131–138. https://doi.org/10.1007/s00774-009-0117-z

Hishida, T., Nishizuka, M., Osada, S., & Imagawa, M. (2009). The role of C/EBPδ in the early stages of adipogenesis. *Biochimie*, *91*(5), 654–657. https://doi.org/10.1016/j.biochi.2009.02.002

Hoogenkamp, M., Lichtinger, M., Krysinska, H., Lancrin, C., Clarke, D., Williamson, A., Mazzarella, L., Ingram, R., Jorgensen, H., Fisher, A., Tenen, D. G., Kouskoff, V., Lacaud, G., & Bonifer, C. (2009). Early chromatin unfolding by RUNX1: A molecular explanation for differential requirements during specification versus maintenance of the hematopoietic gene expression program. *Blood*, *114*(2),

299–309. https://doi.org/10.1182/blood-2008-11-191890

Hu, C. C. A., Dougan, S. K., McGehee, A. M., Love, J. C., & Ploegh, H. L. (2009). XBP-1 regulates signal transduction, transcription factors and bone marrow colonization in B cells. *EMBO Journal*, *28*(11), 1624–1636. https://doi.org/10.1038/emboj.2009.117

Hu, E., Tontonoz, P., & Spiegelman, B. M. (1995). Transdifferentiation of myoblasts by the adipogenic transcription factors PPARγ and C/EBPα. *Proceedings of the National Academy of Sciences of the United States of America*, *92*(21), 9856–9860. https://doi.org/10.1073/pnas.92.21.9856

Huang, J. C., Basu, S. K., Zhao, X., Chien, S., Fang, M., Oehler, V. G., Appelbaum, F. R., & Becker, P. S. (2015). Mesenchymal stromal cells derived from acute myeloid leukemia bone marrow exhibit aberrant cytogenetics and cytokine elaboration. *Blood Cancer Journal*, *5*(4). https://doi.org/10.1038/bcj.2015.17

Imai, T., Takakuwa, R., Marchand, S., Dentz, E., Bornert, J. M., Messaddeq, N., Wendling, O., Mark, M., Desvergne, B., Wahli, W., Chambon, P., & Metzger, D. (2004). Peroxisome proliferator-activated receptor γ is required in mature white and brown adipocytes for their survival in the mouse. *Proceedings of the National Academy of Sciences of the United States of America*, *101*(13), 4543–4547. https://doi.org/10.1073/pnas.0400356101

Itkin, T., Ludin, A., Gradus, B., Gur-Cohen, S., Kalinkovich, A., Schajnovitz, A., Ovadya, Y., Kollet, O., Canaani, J., Shezen, E., Coffin, D. J., Enikolopov, G. N., Berg, T., Piacibello, W., Hornstein, E., & Lapidot, T. (2012). FGF-2 expands murine hematopoietic stem and progenitor cells via proliferation of stromal cells, c-Kit activation, and CXCL12 down-regulation. *Blood*, *120*(9), 1843–1855. https://doi.org/10.1182/blood-2011-11-394692

Iwakoshi, N. N., Lee, A. H., Vallabhajosyula, P., Otipoby, K. L., Rajewsky, K., & Glimcher, L. H. (2003). Plasma cell differentiation and the unfolded protein response intersect at the transcription factor XBP-I. *Nature Immunology*, *4*(4), 321–329. https://doi.org/10.1038/ni907

Jacobson, L. O., Simmons, E. L., Marks, E. K., & Eldredge, J. H. (1951). Recovery from Radiation Injury. *Science*, *113*(2940), 510–511. https://doi.org/10.1126/science.113.2940.510

Jacquemyn, J., Cascalho, A., & Goodchild, R. E. (2017). The ins and outs of endoplasmic reticulum-controlled lipid biosynthesis. *EMBO Reports*, *18*(11), 1905–1921. https://doi.org/10.15252/embr.201643426

Jang, W. G., Kim, E. J., Kim, D. K., Ryoo, H. M., Lee, K. B., Kim, S. H., Choi, H. S., & Koh, J. T. (2012). BMP2 protein regulates osteocalcin expression via Runx2-mediated Atf6 gene transcription. *Journal of Biological Chemistry*, *287*(2), 905–915. https://doi.org/10.1074/jbc.M111.253187

Jaud, J., Philippe, P., Bella, D., Tang, T., Pyronnet, P., Laurell, L., Mazzolini, M., Rouault-Pierre, R.-P., & Touriol, T. (2020). Translational Regulations in Response to Endoplasmic Reticulum Stress in Cancers. *Cells*, 1–30. https://doi.org/10.3390/cells9030540

Jaud, M., Philippe, C., Di Bella, D., Tang, W., Pyronnet, S., Laurell, H., Mazzolini, L., Rouault-Pierre, K., & Touriol, C. (2020). Translational Regulations in Response to Endoplasmic Reticulum Stress in Cancers. *Cells*, *9*(3), 540. https://doi.org/10.3390/cells9030540

Johansson, B., & Harrison, C. J. (2010). Acute Myeloid Leukemia. *Cancer Cytogenetics*, 45–139. https://doi.org/10.1002/9781118010136.ch5

Kaspar, S., Oertlin, C., Szczepanowska, K., Kukat, A., Senft, K., Lucas, C., Brodesser, S., Hatzoglou, M., Larsson, O., Topisirovic, I., & Trifunovic, A. (2021). Adaptation to mitochondrial stress requires CHOP-directed tuning of ISR. *Science Advances*, *7*(22), eabf0971. https://doi.org/10.1126/sciadv.abf0971

Khwaja, A., Bjorkholm2, M., Gale1, R. E., Levine3, R. L., Jordan4, C. T., , Gerhard Ehninger5, C. D. B., Estey7, E., , Alan Burnett8, J. J. C., & David A. Scheinberg10, D. B. and D. C. L. (2016). *Acute myeloid leukaemia*.

Kiyoi, H., Kawashima, N., & Ishikawa, Y. (2020). FLT3 mutations in acute myeloid leukemia: Therapeutic paradigm beyond inhibitor development. *Cancer Science*,

111(2), 312–322. https://doi.org/10.1111/cas.14274

Kode, A., Manavalan, J. S., Mosialou, I., Bhagat, G., Rathinam, C. V., Luo, N., Khiabanian, H., Lee, A., Murty, V. V., Friedman, R., Brum, A., Park, D., Galili, N., Mukherjee, S., Teruya-Feldstein, J., Raza, A., Rabadan, R., Berman, E., & Kousteni, S. (2014). Leukaemogenesis induced by an activating β-catenin mutation in osteoblasts. *Nature*, *506*(7487), 240–244. https://doi.org/10.1038/nature12883

Komori, T., Yagi, H., Nomura, S., Yamaguchi, A., Sasaki, K., Deguchi, K., Shimizu, Y., Bronson, R. ., Gao, Y.-H., Inada, M., Sato, M., Okamoto, R., Kitamura, Y., Yoshiki, S., & Kishimoto, T. (1997). Targeted Disruption of Results in a Complete Lack of Bone Formation owing to Maturational Arrest of Osteoblasts. *Cell*, *89*(5), 755–764. https://doi.org/10.1016/S0092-8674(00)80258-5

Konopleva, M., Konoplev, S., Hu, W., Zaritskey, A. Y., Afanasiev, B. V., & Andreeff, M. (2002). Stromal cells prevent apoptosis of AML cells by up-regulation of anti-apoptotic proteins. *Leukemia*, *16*(9), 1713–1724. https://doi.org/10.1038/sj.leu.2402608

Kornblau, S. M., Ruvolo, P. P., Wang, R. Y., Battula, V. L., Shpall, E. J., Ruvolo, V. R., McQueen, T., Qui, Y. H., Zeng, Z., Pierce, S., Jacamo, R., Yoo, S. Y., Le, P. M., Sun, J., Hail, N., Konopleva, M., & Andreeff, M. (2018). Distinct protein signatures of acute myeloid leukemia bone marrow-derived stromal cells are prognostic for patient survival. *Haematologica*, *103*(5), 810–821. https://doi.org/10.3324/haematol.2017.172429

Kozutsumi, Y., Segal, M., Normington, K., Gething, M. J., & Sambrook, J. (1988). The presence of malfolded proteins in the endoplasmic reticulum signals the induction of glucose-regulated proteins. *Nature*, *332*(6163), 462–464. https://doi.org/10.1038/332462a0

Krause, D., Fackler, M., Civin, C., & May, W. (1996). CD34: structure, biology, and clinical utility. *Blood*, *87*(1), 1–13. https://doi.org/10.1182/blood.V87.1.1.1

Krevvata, M., Silva, B. C., Manavalan, J. S., Galan-Diez, M., Kode, A., Matthews, B. G.,

Park, D., Zhang, C. A., Galili, N., Nickolas, T. L., Dempster, D. W., Dougall, W., Teruya-Feldstein, J., Economides, A. N., Kalajzic, I., Raza, A., Berman, E., Mukherjee, S., Bhagat, G., & Kousteni, S. (2014). Inhibition of leukemia cell engraftment and disease progression in mice by osteoblasts. *Blood*, *124*(18), 2834–2846. https://doi.org/10.1182/blood-2013-07-517219

Kumar, B., Garcia, M., Weng, L., Jung, X., Murakami, J. L., Hu, X., McDonald, T., Lin, A., Kumar, A. R., Digiusto, D. L., Stein, A. S., Pullarkat, V. A., Hui, S. K., Carlesso, N., Kuo, Y. H., Bhatia, R., Marcucci, G., & Chen, C. C. (2018). Acute myeloid leukemia transforms the bone marrow niche into a leukemia-permissive microenvironment through exosome secretion. *Leukemia*, *32*(3), 575–587. https://doi.org/10.1038/leu.2017.259

Kunisaki, Y., Bruns, I., Scheiermann, C., Ahmed, J., Pinho, S., Zhang, D., Mizoguchi, T., Wei, Q., Lucas, D., Ito, K., Mar, J. C., Bergman, A., & Frenette, P. S. (2013). Arteriolar niches maintain haematopoietic stem cell quiescence. *Nature*, *502*(7473), 637–643. https://doi.org/10.1038/nature12612

Laurenti, E., & Dick, J. E. (2012). Molecular and functional characterization of early human hematopoiesis. *Annals of the New York Academy of Sciences*, *1266*(1), 68–71. https://doi.org/10.1111/j.1749-6632.2012.06577.x

Laurenti, E., Frelin, C., Xie, S., Ferrari, R., Dunant, C. F., Zandi, S., Neumann, A., Plumb, I., Doulatov, S., Chen, J., April, C., Fan, J. B., Iscove, N., & Dick, J. E. (2015). CDK6 levels regulate quiescence exit in human hematopoietic stem cells. *Cell Stem Cell*, *16*(3), 302–313. https://doi.org/10.1016/j.stem.2015.01.017

Laurenti, E., & Göttgens, B. (2018). From haematopoietic stem cells to complex differentiation landscapes. *Nature*, *553*(7689), 418–426. https://doi.org/10.1038/nature25022

Le Blanc, K., & Ringdén, O. (2007). Immunomodulation by mesenchymal stem cells and clinical experience. *Journal of Internal Medicine*, *262*(5), 509–525. https://doi.org/10.1111/j.1365-2796.2007.01844.x

Lee, A.-H., Iwakoshi, N. N., & Glimcher, L. H. (2003). XBP-1 Regulates a Subset of

Endoplasmic Reticulum Resident Chaperone Genes in the Unfolded Protein Response. *Molecular and Cellular Biology*, *23*(21), 7448–7459. https://doi.org/10.1128/MCB.23.21.7448-7459.2003

Lee, B., Thirunavukkarasu, K., Zhou, L., Pastore, L., Baldini, A., Hecht, J., Geoffrey, V., Ducy, P., & Karsenty, G. (1997). Missense mutations abolishing DNA binding of the osteoblast-specific transcription factor OSF2/CBFA1 in cleidocranial dysplasia. *Nature Genetics*, *16*(3), 307–310. https://doi.org/10.1038/ng0797-307

Lefterova, M. I., Zhang, Y., Steger, D. J., Schupp, M., Schug, J., Cristancho, A., Feng, D., Zhuo, D., Stoeckert, C. J., Liu, X. S., & Lazar, M. A. (2008). PPARγ and C/EBP factors orchestrate adipocyte biology via adjacent binding on a genome-wide scale. *Genes and Development*, *22*(21), 2941–2952. https://doi.org/10.1101/gad.1709008

Ley, T. J., Ding, L., Walter, M. J., McLellan, M. D., Lamprecht, T., Larson, D. E., Kandoth, C., Payton, J. E., Baty, J., Welch, J., Harris, C. C., Lichti, C. F., Townsend, R. R., Fulton, R. S., Dooling, D. J., Koboldt, D. C., Schmidt, H., Zhang, Q., Osborne, J. R., … Wilson, R. K. (2010). DNMT3A Mutations in Acute Myeloid Leukemia. *New England Journal of Medicine*, *363*(25), 2424–2433. https://doi.org/10.1056/NEJMoa1005143

Ley, T. J., Miller, C., Ding, L., Raphael, B. J., Mungall, A. J., Robertson, G., Hoadley, K., Triche, T. J., Laird, P. W., Baty, J. D., Fulton, L. L., Fulton, R., Heath, S. E., Kalicki-Veizer, J., Kandoth, C., Klco, J. M., Koboldt, D. C., Kanchi, K. L., Kulkarni, S., … Wilson, R. K. (2013). Genomic and epigenomic landscapes of adult de novo acute myeloid leukemia. *New England Journal of Medicine*, *368*(22), 2059–2074. https://doi.org/10.1056/NEJMoa1301689

Li, D., Yea, S., Li, S., Chen, Z., Narla, G., Banck, M., Laborda, J., Tan, S., Friedman, J. M., Friedman, S. L., & Walsh, M. J. (2005). Krüppel-like factor-6 promotes preadipocyte differentiation through histone deacetylase 3-dependent repression of DLK1. *Journal of Biological Chemistry*, *280*(29), 26941–26952. https://doi.org/10.1074/jbc.M500463200

Li, H., Ghazanfari, R., Zacharaki, D., Ditzel, N., Isern, J., Ekblom, M., Méndez-Ferrer, S., Kassem, M., & Scheding, S. (2014). Low/negative expression of PDGFR-α identifies the candidate primary mesenchymal stromal cells in adult human bone marrow. *Stem Cell Reports*, *3*(6), 965–974. https://doi.org/10.1016/j.stemcr.2014.09.018

Li, Y., Ge, C., Long, J. P., Begun, D. L., Rodriguez, J. A., Goldstein, S. A., & Franceschi, R. T. (2012). Biomechanical stimulation of osteoblast gene expression requires phosphorylation of the RUNX2 transcription factor. *Journal of Bone and Mineral Research*, *27*(6), 1263–1274. https://doi.org/10.1002/jbmr.1574

Lim, M., Pang, Y., Ma, S., Hao, S., Shi, H., Zheng, Y., Hua, C., Gu, X., Yang, F., Yuan, W., & Cheng, T. (2016). Altered mesenchymal niche cells impede generation of normal hematopoietic progenitor cells in leukemic bone marrow. *Leukemia*, *30*(1), 154–162. https://doi.org/10.1038/leu.2015.210

Long, F. (2012). Building strong bones: Molecular regulation of the osteoblast lineage. *Nature Reviews Molecular Cell Biology*, *13*(1), 27–38. https://doi.org/10.1038/nrm3254

Lorenz, E., Uphoff, D., Reid, T. R., & Shelton, E. (1951). Modification of irradiation injury in mice and guinea pigs by bone marrow injections. *Journal of the National Cancer Institute*, *12*(1), 197–201. https://doi.org/10.1093/jnci/12.1.197

Lowe, C. E., Dennis, R. J., Obi, U., O'Rahilly, S., & Rochford, J. J. (2012). Investigating the involvement of the ATF6α pathway of the unfolded protein response in adipogenesis. *International Journal of Obesity*, *36*(9), 1248–1251. https://doi.org/10.1038/ijo.2011.233

Lowe, Christopher E., O'Rahilly, S., & Rochford, J. J. (2011). Adipogenesis at a glance. *Journal of Cell Science*, *124*(16), 2681–2686. https://doi.org/10.1242/jcs.079699

Lowenberg, B., Downing, J. R., & Burnett, A. (1999). Acute Myeloid Leukemia. *New England Journal of Medicine*, *341*(14), 1051–1062. https://doi.org/10.1056/NEJM199909303411407

Luchsinger, L. L. (2021). Hormetic endoplasmic reticulum stress in hematopoietic

stem cells. *Current Opinion in Hematology*, *28*(6), 417–423. https://doi.org/10.1097/MOH.0000000000000668

Lundgren, M., De Franco, E., Arnell, H., & Fischler, B. (2019). Practical management in Wolcott-Rallison syndrome with associated hypothyroidism, neutropenia, and recurrent liver failure: A case report. *Clinical Case Reports*, *7*(6), 1133–1138. https://doi.org/10.1002/ccr3.2168

Lymperi, S., Horwood, N., Marley, S., Gordon, M. Y., Cope, A. P., & Dazzi, F. (2008). Strontium can increase some osteoblasts without increasing hematopoietic stem cells. *Blood*, *111*(3), 1173–1181. https://doi.org/10.1182/blood-2007-03-082800

Ma, Y., Shimizu, Y., Mann, M. J., Jin, Y., & Hendershot, L. M. (2010). Plasma cell differentiation initiates a limited ER stress response by specifically suppressing the PERK-dependent branch of the unfolded protein response. *Cell Stress and Chaperones*, *15*(3), 281–293. https://doi.org/10.1007/s12192-009-0142-9

Madsen, M. S., Siersbæk, R., Boergesen, M., Nielsen, R., & Mandrup, S. (2014). Peroxisome Proliferator-Activated Receptor γ and C/EBPα Synergistically Activate Key Metabolic Adipocyte Genes by Assisted Loading. *Molecular and Cellular Biology*, *34*(6), 939–954. https://doi.org/10.1128/mcb.01344-13

Majeti, R., Park, C. Y., & Weissman, I. L. (2007). Identification of a Hierarchy of Multipotent Hematopoietic Progenitors in Human Cord Blood. *Cell Stem Cell*, *1*(6), 635–645. https://doi.org/10.1016/j.stem.2007.10.001

Medyouf, H. (2017). The microenvironment in human myeloid malignancies: Emerging concepts and therapeutic implications. *Blood*, *129*(12), 1617–1626. https://doi.org/10.1182/blood-2016-11-696070

Méndez-Ferrer, S., Bonnet, D., Steensma, D. P., Hasserjian, R. P., Ghobrial, I. M., Gribben, J. G., Andreeff, M., & Krause, D. S. (2020). Bone marrow niches in haematological malignancies. *Nature Reviews. Cancer*. https://doi.org/10.1038/s41568-020-0245-2

Méndez-Ferrer, S., Michurina, T. V., Ferraro, F., Mazloom, A. R., MacArthur, B. D.,

Lira, S. A., Scadden, D. T., Ma'ayan, A., Enikolopov, G. N., & Frenette, P. S. (2010). Mesenchymal and haematopoietic stem cells form a unique bone marrow niche. *Nature*, *466*(7308), 829–834. https://doi.org/10.1038/nature09262

Miller, R. S., Diaczok, D., & Cooke, D. W. (2007). Repression of GLUT4 expression by the endoplasmic reticulum stress response in 3T3-L1 adipocytes. *Biochemical and Biophysical Research Communications*, *362*(1), 188–192. https://doi.org/10.1016/j.bbrc.2007.07.176

Miraki-Moud, F., Anjos-Afonso, F., Hodby, K. A., Griessinger, E., Rosignoli, G., Lillington, D., Jia, L., Davies, J. K., Cavenagh, J., Smith, M., Oakervee, H., Agrawal, S., Gribben, J. G., Bonnet, D., & Taussig, D. C. (2013). Acute myeloid leukemia does not deplete normal hematopoietic stem cells but induces cytopenias by impeding their differentiation. *Proceedings of the National Academy of Sciences*, *110*(33), 13576–13581. https://doi.org/10.1073/pnas.1301891110

Mittelbrunn, M., & Sánchez-Madrid, F. (2012). Intercellular communication: Diverse structures for exchange of genetic information. *Nature Reviews Molecular Cell Biology*, *13*(5), 328–335. https://doi.org/10.1038/nrm3335

Montero, A., Okada, Y., Tomita, M., Ito, M., Tsurukami, H., Nakamura, T., Doetschman, T., Coffin, J. D., & Hurley, M. M. (2000). Disruption of the fibroblast growth factor-2 gene results in decreased bone mass and bone formation. *Journal of Clinical Investigation*, *105*(8), 1085–1093. https://doi.org/10.1172/JCI8641

Mori, T., Sakaue, H., Iguchi, H., Gomi, H., Okada, Y., Takashima, Y., Nakamura, K., Nakamura, T., Yamauchi, T., Kubota, N., Kadowaki, T., Matsuki, Y., Ogawa, W., Hiramatsu, R., & Kasuga, M. (2005). Role of krüppel-like factor 15 (KLF15) in transcriptional regulation of adipogenesis. *Journal of Biological Chemistry*, *280*(13), 12867–12875. https://doi.org/10.1074/jbc.M410515200

Morikawa, S., Mabuchi, Y., Kubota, Y., Nagai, Y., Niibe, K., Hiratsu, E., Suzuki, S., Miyauchi-Hara, C., Nagoshi, N., Sunabori, T., Shimmura, S., Miyawaki, A., Nakagawa, T., Suda, T., Okano, H., & Matsuzaki, Y. (2009). Prospective

identification, isolation, and systemic transplantation of multipotent mesenchymal stem cells in murine bone marrow. *Journal of Experimental Medicine*, *206*(11), 2483–2496. https://doi.org/10.1084/jem.20091046

Morrison, S. J., & Scadden, D. T. (2014). The bone marrow niche for haematopoietic stem cells. *Nature*, *505*(7483), 327–334. https://doi.org/10.1038/nature12984

Muguruma, Y., Yahata, T., Miyatake, H., Sato, T., Uno, T., Itoh, J., Kato, S., Ito, M., Hotta, T., & Ando, K. (2006). Reconstitution of the functional human hematopoietic microenvironment derived from human mesenchymal stem cells in the murine bone marrow compartment. *Blood*, *107*(5), 1878–1887. https://doi.org/10.1182/blood-2005-06-2211

Mundlos, S., Otto, F., Mundlos, C., Mulliken, J. B., Aylsworth, A. S., Albright, S., Lindhout, D., Cole, W. G., Henn, W., Knoll, J. H. M., Owen, M. J., Mertelsmann, R., Zabel, B. U., & Olsen, B. R. (1997). Mutations involving the transcription factor CBFA1 cause cleidocranial dysplasia. *Cell*, *89*(5), 773–779. https://doi.org/10.1016/S0092-8674(00)80260-3

Mupo, A., Celani, L., Dovey, O., Cooper, J. L., Grove, C., Rad, R., Sportoletti, P., Falini, B., Bradley, A., & Vassiliou, G. S. (2013). A powerful molecular synergy between mutant Nucleophosmin and Flt3-ITD drives acute myeloid leukemia in mice. *Leukemia*, *27*(9), 1917–1920. https://doi.org/10.1038/leu.2013.77

Murray, L., Chen, B., Galy, A., Chen, S., Tushinski, R., Uchida, N., Negrin, R., Tricot, G., Jagannath, S., Vesole, D., Barlogie, B., Hoffman, R., & Tsukamoto, A. (1995). Enrichment of human hematopoietic stem cell activity in the CD34+Thy- 1+Lin subpopulation from mobilized peripheral blood. *Blood*, *85*(2), 368–378. https://doi.org/10.1182/blood.v85.2.368.bloodjournal852368

Nakashima, K., Zhou, X., Kunkel, G., Zhang, Z., Deng, J. M., Behringer, R. R., & de Crombrugghe, B. (2002). The Novel Zinc Finger-Containing Transcription Factor Osterix Is Required for Osteoblast Differentiation and Bone Formation. *Cell*, *108*(1), 17–29. https://doi.org/10.1016/S0092-8674(01)00622-5

Naveiras, O., Nardi, V., Wenzel, P. L., Hauschka, P. V., Fahey, F., & Daley, G. Q. (2009).

Bone-marrow adipocytes as negative regulators of the haematopoietic microenvironment. *Nature*, *460*(7252), 259–263. https://doi.org/10.1038/nature08099

Nielsen, R., Pedersen, T. Å., Hagenbeek, D., Moulos, P., Siersbæk, R., Megens, E., Denissov, S., Børgesen, M., Francoijs, K. J., Mandrup, S., & Stunnenberg, H. G. (2008). Genome-wide profiling of PPARγ:RXR and RNA polymerase II occupancy reveals temporal activation of distinct metabolic pathways and changes in RXR dimer composition during adipogenesis. *Genes and Development*, *22*(21), 2953–2967. https://doi.org/10.1101/gad.501108

Nishio, Y., Dong, Y., Paris, M., O'Keefe, R. J., Schwarz, E. M., & Drissi, H. (2006). Runx2-mediated regulation of the zinc finger Osterix/Sp7 gene. *Gene*, *372*(1–2), 62–70. https://doi.org/10.1016/j.gene.2005.12.022

Notta, F., Doulatov, S., Laurenti, E., Poeppl, A., Jurisica, I., & Dick, J. E. (2011). Isolation of single human hematopoietic stem cells capable of long-term multilineage engraftment. *Science*, *333*(6039), 218–221. https://doi.org/10.1126/science.1201219

Notta, F., Zandi, S., Takayama, N., Dobson, S., Gan, O. I., Wilson, G., Kaufmann, K. B., McLeod, J., Laurenti, E., Dunant, C. F., McPherson, J. D., Stein, L. D., Dror, Y., & Dick, J. E. (2016). Distinct routes of lineage development reshape the human blood hierarchy across ontogeny. *Science*, *351*(6269), aab2116–aab2116. https://doi.org/10.1126/science.aab2116

Obacz, J., Avril, T., Rubio-Patiño, C., Bossowski, J. P., Igbaria, A., Ricci, J. E., & Chevet, E. (2019). Regulation of tumor–stroma interactions by the unfolded protein response. *FEBS Journal*, *286*(2), 279–296. https://doi.org/10.1111/febs.14359

Oishi, Y., Manabe, I., Tobe, K., Tsushima, K., Shindo, T., Fujiu, K., Nishimura, G., Maemura, K., Yamauchi, T., Kubota, N., Suzuki, R., Kitamura, T., Akira, S., Kadowaki, T., & Nagai, R. (2005). Krüppel-like transcription factor KLF5 is a key regulator of adipocyte differentiation. *Cell Metabolism*, *1*(1), 27–39. https://doi.org/10.1016/j.cmet.2004.11.005

Omatsu, Y., Sugiyama, T., Kohara, H., Kondoh, G., Fujii, N., Kohno, K., & Nagasawa, T. (2010). The Essential Functions of Adipo-osteogenic Progenitors as the Hematopoietic Stem and Progenitor Cell Niche. *Immunity*, *33*(3), 387–399. https://doi.org/10.1016/j.immuni.2010.08.017

Orkin, S. H., & Zon, L. I. (2008). Hematopoiesis: An Evolving Paradigm for Stem Cell Biology. *Cell*, *132*(4), 631–644. https://doi.org/10.1016/j.cell.2008.01.025

Otto, F., Thornell, A. P., Crompton, T., Denzel, A., Gilmour, K. C., Rosewell, I. R., Stamp, G. W. H., Beddington, R. S. P., Mundlos, S., Olsen, B. R., Selby, P. B., & Owen, M. J. (1997). Cbfa1, a candidate gene for cleidocranial dysplasia syndrome, is essential for osteoblast differentiation and bone development. *Cell*, *89*(5), 765–771. https://doi.org/10.1016/S0092-8674(00)80259-7

Papaemmanuil, E., Gerstung, M., Bullinger, L., Gaidzik, V. I., Paschka, P., Roberts, N. D., Potter, N. E., Heuser, M., Thol, F., Bolli, N., Gundem, G., Van Loo, P., Martincorena, I., Ganly, P., Mudie, L., McLaren, S., O'Meara, S., Raine, K., Jones, D. R., … Campbell, P. J. (2016). Genomic Classification and Prognosis in Acute Myeloid Leukemia. *The New England Journal of Medicine*, *374*(23), 2209–2221. https://doi.org/10.1056/NEJMoa1516192

Park, S. J., Li, C., & Chen, Y. M. (2021). Endoplasmic Reticulum Calcium Homeostasis in Kidney Disease: Pathogenesis and Therapeutic Targets. *American Journal of Pathology*, *191*(2), 256–265. https://doi.org/10.1016/j.ajpath.2020.11.006

Passaro, D., Abarrategi, A., Foster, K., Ariza-McNaughton, L., & Bonnet, D. (2017). Bioengineering of humanized bone marrow microenvironments in mouse and their visualization by live imaging. *Journal of Visualized Experiments*, *2017*(126), 1–13. https://doi.org/10.3791/55914

Passaro, D., Di Tullio, A., Abarrategi, A., Rouault-Pierre, K., Foster, K., Ariza-McNaughton, L., Montaner, B., Chakravarty, P., Bhaw, L., Diana, G., Lassailly, F., Gribben, J., & Bonnet, D. (2017). Increased Vascular Permeability in the Bone Marrow Microenvironment Contributes to Disease Progression and Drug Response in Acute Myeloid Leukemia. *Cancer Cell*, *32*(3), 324-341.e6.

https://doi.org/10.1016/j.ccell.2017.08.001

Passaro, D., Garcia-Albornoz, M., Diana, G., Chakravarty, P., Ariza-McNaughton, L., Batsivari, A., Borràs-Eroles, C., Abarrategi, A., Waclawiczek, A., Ombrato, L., Malanchi, I., Gribben, J., & Bonnet, D. (2021). Integrated OMICs unveil the bone-marrow microenvironment in human leukemia. *Cell Reports*, *35*(6), 109119. https://doi.org/10.1016/j.celrep.2021.109119

Perman, J. C., Boström, P., Lindbom, M., Lidberg, U., StÅhlman, M., Hägg, D., Lindskog, H., Täng, M. S., Omerovic, E., Hultén, L. M., Jeppsson, A., Petursson, P., Herlitz, J., Olivecrona, G., Strickland, D. K., Ekroos, K., Olofsson, S. O., & Borén, J. (2011). The VLDL receptor promotes lipotoxicity and increases mortality in mice following an acute myocardial infarction. *Journal of Clinical Investigation*, *121*(7), 2625–2640. https://doi.org/10.1172/JCI43068

Philippe, C., Dubrac, A., Quelen, C., Desquesnes, A., Van Den Berghe, L., Ségura, C., Filleron, T., Pyronnet, S., Prats, H., Brousset, P., & Touriol, C. (2016). PERK mediates the IRES-dependent translational activation of mRNAs encoding angiogenic growth factors after ischemic stress. *Science Signaling*, *9*(426), 1–9. https://doi.org/10.1126/scisignal.aaf2753

Pietras, E. M., Warr, M. R., & Passegué, E. (2011). Cell cycle regulation in hematopoietic stem cells. *Journal of Cell Biology*, *195*(5), 709–720. https://doi.org/10.1083/jcb.201102131

Pievani, A., Donsante, S., Tomasoni, C., Corsi, A., Dazzi, F., Biondi, A., Riminucci, M., & Serafini, M. (2021). Acute myeloid leukemia shapes the bone marrow stromal niche in vivo. *Haematologica*, *106*(3), 865–870. https://doi.org/10.3324/haematol.2020.247205

Pinho, S., & Frenette, P. S. (2019). Haematopoietic stem cell activity and interactions with the niche. *Nature Reviews Molecular Cell Biology*, *20*(May). https://doi.org/10.1038/s41580-019-0103-9

Pinho, S., Lacombe, J., Hanoun, M., Mizoguchi, T., Bruns, I., Kunisaki, Y., & Frenette, P. S. (2013). PDGFRα and CD51 mark human Nestin+ sphere-forming

mesenchymal stem cells capable of hematopoietic progenitor cell expansion. *Journal of Experimental Medicine*, *210*(7), 1351–1367. https://doi.org/10.1084/jem.20122252

Porter, K. R., Claude, A., & Fullam, E. F. (1945). A study of tissue culture cells by electron microscopy: Methods and preliminary observations. *Journal of Experimental Medicine*, *81*(3), 233–246. https://doi.org/10.1084/jem.81.3.233

Qiang, G., Kong, H. W., Fang, D., McCann, M., Yang, X., Du, G., Blüher, M., Zhu, J., & Liew, C. W. (2016). The obesity-induced transcriptional regulator TRIP-Br2 mediates visceral fat endoplasmic reticulum stress-induced inflammation. *Nature Communications*, *7*, 1–14. https://doi.org/10.1038/ncomms11378

Raaijmakers, M. H. G. P., Mukherjee, S., Guo, S., Zhang, S., Kobayashi, T., Schoonmaker, J. A., Ebert, B. L., Al-Shahrour, F., Hasserjian, R. P., Scadden, E. O., Aung, Z., Matza, M., Merkenschlager, M., Lin, C., Rommens, J. M., & Scadden, D. T. (2010). Bone progenitor dysfunction induces myelodysplasia and secondary leukaemia. *Nature*, *464*(7290), 852–857. https://doi.org/10.1038/nature08851

Reimold, A. M., Iwakoshi, N. N., Manis, J., Vallabhajosyula, P., Szomolanyi-Tsuda, E., Gravallese, E. M., Friend, D., Grusby, M. J., Alt, F., & Glimcher, L. H. (2001). Plasma cell differentiation requires the transcription factor XBP-1. *Nature*, *412*(6844), 300–307. https://doi.org/10.1038/35085509

Rix, B., Maduro, A. H., Bridge, K. S., & Grey, W. (2022). Markers for human haematopoietic stem cells: The disconnect between an identification marker and its function. *Frontiers in Physiology*, *13*. https://doi.org/10.3389/fphys.2022.1009160

Ron, D., & Habener, J. F. (1992). CHOP, a novel developmentally regulated nuclear protein that dimerizes with transcription factors C/EBP and LAP and functions as a dominant-negative inhibitor of gene transcription. *Genes and Development*, *6*(3), 439–453. https://doi.org/10.1101/gad.6.3.439

Ron, D., & Walter, P. (2007). Signal integration in the endoplasmic reticulum unfolded protein response. *Nature Reviews Molecular Cell Biology*, *8*(7), 519–529.

https://doi.org/10.1038/nrm2199

Rosen, E. D., Hsu, C. H., Wang, X., Sakai, S., Freeman, M. W., Gonzalez, F. J., & Spiegelman, B. M. (2002). C/EBPα induces adipogenesis through PPARγ: A unified pathway. *Genes and Development*, *16*(1), 22–26. https://doi.org/10.1101/gad.948702

Rosen, E. D., Sarraf, P., Troy, A. E., Bradwin, G., Moore, K., Milstone, D. S., Spiegelman, B. M., & Mortensen, R. M. (1999). PPARγ is required for the differentiation of adipose tissue in vivo and in vitro. *Molecular Cell*, *4*(4), 611–617. https://doi.org/10.1016/S1097-2765(00)80211-7

Rouault-Pierre, K., Lopez-Onieva, L., Foster, K., Anjos-Afonso, F., Lamrissi-Garcia, I., Serrano-Sanchez, M., Mitter, R., Ivanovic, Z., de Verneuil, H., Gribben, J., Taussig, D., Rezvani, H. R., Mazurier, F., & Bonnet, D. (2013). HIF-2α Protects Human Hematopoietic Stem/Progenitors and Acute Myeloid Leukemic Cells from Apoptosis Induced by Endoplasmic Reticulum Stress. *Cell Stem Cell*, *13*(5), 549–563. https://doi.org/10.1016/j.stem.2013.08.011

Rutkovskiy, A., Stensløkken, K.-O., & Vaage, I. J. (2016). Osteoblast Differentiation at a Glance. *Medical Science Monitor Basic Research*, *22*, 95–106. https://doi.org/10.12659/msmbr.901142

Ryu, K. Y., Jeon, E. J., Leem, J., Park, J. H., & Cho, H. (2020). Regulation of adipsin expression by endoplasmic reticulum stress in adipocytes. *Biomolecules*, *10*(2). https://doi.org/10.3390/biom10020314

Sacchetti, B., Funari, A., Michienzi, S., Di Cesare, S., Piersanti, S., Saggio, I., Tagliafico, E., Ferrari, S., Robey, P. G., Riminucci, M., & Bianco, P. (2007). Self-Renewing Osteoprogenitors in Bone Marrow Sinusoids Can Organize a Hematopoietic Microenvironment. *Cell*, *131*(2), 324–336. https://doi.org/10.1016/j.cell.2007.08.025

Saito, A., Ochiai, K., Kondo, S., Tsumagari, K., Murakami, T., Cavener, D. R., & Imaizumi, K. (2011). Endoplasmic reticulum stress response mediated by the PERK-eIF2α-ATF4 pathway is involved in osteoblast differentiation induced by

BMP2. *Journal of Biological Chemistry*, *286*(6), 4809–4818. https://doi.org/10.1074/jbc.M110.152900

Schepers, K., Pietras, E. M., Reynaud, D., Flach, J., Binnewies, M., Garg, T., Wagers, A. J., Hsiao, E. C., & Passegué, E. (2013). Myeloproliferative neoplasia remodels the endosteal bone marrow niche into a self-reinforcing leukemic niche. *Cell Stem Cell*, *13*(3), 285–299. https://doi.org/10.1016/j.stem.2013.06.009

Schröder, M. (2008). Endoplasmic reticulum stress responses. In *Cellular and Molecular Life Sciences* (Vol. 65, Issue 6). https://doi.org/10.1007/s00018-007-7383-5

Schroeder, T., Geyh, S., Germing, U., & Haas, R. (2016). Mesenchymal stromal cells in myeloid malignancies. *Blood Research*, *51*(4), 225–232. https://doi.org/10.5045/br.2016.51.4.225

Schwarz, D. S., & Blower, M. D. (2016). The endoplasmic reticulum: Structure, function and response to cellular signaling. *Cellular and Molecular Life Sciences*, *73*(1), 79–94. https://doi.org/10.1007/s00018-015-2052-6

Sen Banerjee, S., Feinberg, M. W., Watanabe, M., Gray, S., Haspel, R. L., Denkinger, D. J., Kawahara, R., Hauner, H., & Jain, M. K. (2003). The Krüppel-like factor KLF2 inhibits peroxisome proliferator-activated receptor-γ expression and adipogenesis. *Journal of Biological Chemistry*, *278*(4), 2581–2584. https://doi.org/10.1074/jbc.M210859200

Sepulveda, D., Rojas-Rivera, D., Rodríguez, D. A., Groenendyk, J., Köhler, A., Lebeaupin, C., Ito, S., Urra, H., Carreras-Sureda, A., Hazari, Y., Vasseur-Cognet, M., Ali, M. M. U., Chevet, E., Campos, G., Godoy, P., Vaisar, T., Bailly-Maitre, B., Nagata, K., Michalak, M., … Hetz, C. (2018). Interactome Screening Identifies the ER Luminal Chaperone Hsp47 as a Regulator of the Unfolded Protein Response Transducer IRE1α. *Molecular Cell*, *69*(2), 238-252.e7. https://doi.org/10.1016/j.molcel.2017.12.028

Seraihi, A. F. Al, Tawana, K., Charrot, S., Bödör, C., & Butler, T. (2019). *Genomics & Diagnostics in Acute Myeloid Leukaemia*. 1–23.

https://doi.org/10.1039/9781782628217-00001

Sha, H., He, Y., Chen, H., Wang, C., Zenno, A., Shi, H., Yang, X., Zhang, X., & Qi, L. (2009). The IRE1α-XBP1 Pathway of the Unfolded Protein Response Is Required for Adipogenesis. *Cell Metabolism*, *9*(6), 556–564. https://doi.org/10.1016/j.cmet.2009.04.009

Shafat, M. S., Gnaneswaran, B., Bowles, K. M., & Rushworth, S. A. (2017). The bone marrow microenvironment – Home of the leukemic blasts. *Blood Reviews*, *31*(5), 277–286. https://doi.org/10.1016/j.blre.2017.03.004

Shlush, L. I., Zandi, S., Mitchell, A., Chen, W. C., Brandwein, J. M., Gupta, V., Kennedy, J. A., Schimmer, A. D., Schuh, A. C., Yee, K. W., McLeod, J. L., Doedens, M., Medeiros, J. J. F., Marke, R., Kim, H. J., Lee, K., McPherson, J. D., Hudson, T. J., Brown, A. M. K., … Dick, J. E. (2014). Identification of pre-leukaemic haematopoietic stem cells in acute leukaemia. *Nature*, *506*(7488), 328–333. https://doi.org/10.1038/nature13038

Špehar Uroić, A., Mulliqi Kotori, V., Rojnić Putarek, N., Kušec, V., & Dumić, M. (2014). Primary hypothyroidism and nipple hypoplasia in a girl with Wolcott-Rallison syndrome. *European Journal of Pediatrics*, *173*(4), 529–531. https://doi.org/10.1007/s00431-013-2189-y

Sugiyama, T., Kohara, H., Noda, M., & Nagasawa, T. (2006). Maintenance of the Hematopoietic Stem Cell Pool by CXCL12-CXCR4 Chemokine Signaling in Bone Marrow Stromal Cell Niches. *Immunity*, *25*(6), 977–988. https://doi.org/10.1016/j.immuni.2006.10.016

Takeda, S., Elefteriou, F., Levasseur, R., Liu, X., Zhao, L., Parker, K. L., Armstrong, D., Ducy, P., & Karsenty, G. (2002). Leptin regulates bone formation via the sympathetic nervous system. *Cell*, *111*(3), 305–317. https://doi.org/10.1016/S0092-8674(02)01049-8

Tamori, Y., Masugi, J., Nishino, N., & Kasuga, M. (2002). Role of peroxisome proliferator-activated receptor-γ in maintenance of the characteristics of mature 3T3-L1 adipocytes. *Diabetes*, *51*(7), 2045–2055.

https://doi.org/10.2337/diabetes.51.7.2045

Tanaka, T., Yoshida, N., Kishimoto, T., & Akira, S. (1997). Defective adipocyte differentiation in mice lacking the C/EBPβ and/or C/EBPδ gene. *EMBO Journal*, *16*(24), 7432–7443. https://doi.org/10.1093/emboj/16.24.7432

Tang, C. H. A., Ranatunga, S., Kriss, C. L., Cubitt, C. L., Tao, J., Pinilla-Ibarz, J. A., Del Valle, J. R., & Hu, C. C. A. (2014). Inhibition of ER stress-associated IRE-1/XBP-1 pathway reduces leukemic cell survival. *Journal of Clinical Investigation*, *124*(6), 2585–2598. https://doi.org/10.1172/JCI73448

Tang, Q. Q., Otto, T. C., & Lane, M. D. (2003). CCAAT/enhancer-binding protein β is required for mitotic clonal expansion during adipogenesis. *Proceedings of the National Academy of Sciences of the United States of America*, *100*(3), 850–855. https://doi.org/10.1073/pnas.0337434100

Theocharides, A. P. A., Rongvaux, A., Fritsch, K., Flavell, R. A., & Manz, M. G. (2016). Humanized hemato-lymphoid system mice. *Haematologica*, *101*(1), 5–19. https://doi.org/10.3324/haematol.2014.115212

Tikhonova, A. N., Dolgalev, I., Hu, H., Sivaraj, K. K., Hoxha, E., Cuesta-Domínguez, Á., Pinho, S., Akhmetzyanova, I., Gao, J., Witkowski, M., Guillamot, M., Gutkin, M. C., Zhang, Y., Marier, C., Diefenbach, C., Kousteni, S., Heguy, A., Zhong, H., Fooksman, D. R., … Aifantis, I. (2019). The bone marrow microenvironment at single-cell resolution. *Nature*, *569*(7755), 222–228. https://doi.org/10.1038/s41586-019-1104-8

Till, J. E., & McCulloch, E. A. (1961). A Direct Measurement of the Radiation Sensitivity of Normal Mouse Bone Marrow Cells. *Radiation Research*, *14*(2), 213. https://doi.org/10.2307/3570892

Tohmonda, T., Miyauchi, Y., Ghosh, R., Yoda, M., Uchikawa, S., Takito, J., Morioka, H., Nakamura, M., Iwawaki, T., Chiba, K., Toyama, Y., Urano, F., & Horiuchi, K. (2011). The IRE1α-XBP1 pathway is essential for osteoblast differentiation through promoting transcription of Osterix. *EMBO Reports*, *12*(5), 451–457. https://doi.org/10.1038/embor.2011.34

Tong, Q., Dalgin, G., Xu, H., Ting, C. N., Leiden, J. M., & Hotamisligil, G. S. (2000). Function of GATA transcription factors in preadipocyte-adipocyte transition. *Science*, *290*(5489), 134–138. https://doi.org/10.1126/science.290.5489.134

Tong, Q., Tsai, J., Tan, G., Dalgin, G., & Hotamisligil, G. S. (2005). Interaction between GATA and the C/EBP Family of Transcription Factors Is Critical in GATA-Mediated Suppression of Adipocyte Differentiation. *Molecular and Cellular Biology*, *25*(2), 706–715. https://doi.org/10.1128/mcb.25.2.706-715.2005

Tontonoz, P., Hu, E., & Spiegelman, B. M. (1994). Stimulation of adipogenesis in fibroblasts by PPARγ2, a lipid-activated transcription factor. *Cell*, *79*(7), 1147–1156. https://doi.org/10.1016/0092-8674(94)90006-X

Touw, I., & Lowenberg, B. (1983). No stimulative effect of adipocytes on hematopoiesis in long-term human bone marrow cultures. *Blood*, *61*(4), 770–774. https://doi.org/10.1182/blood.v61.4.770.bloodjournal614770

Tsuru, A., Imai, Y., Saito, M., & Kohno, K. (2016). Novel mechanism of enhancing IRE1α-XBP1 signalling via the PERK-ATF4 pathway. *Scientific Reports*, *6*, 1–8. https://doi.org/10.1038/srep24217

Tu, B. P., & Weissman, J. S. (2004). Oxidative protein folding in eukaryotes: Mechanisms and consequences. *Journal of Cell Biology*, *164*(3), 341–346. https://doi.org/10.1083/jcb.200311055

Urra, H., Dufey, E., Avril, T., Chevet, E., & Hetz, C. (2016). Endoplasmic Reticulum Stress and the Hallmarks of Cancer. *Trends in Cancer*, *2*(5), 252–262. https://doi.org/10.1016/j.trecan.2016.03.007

Valdez, B. C., Brammer, J. E., Li, Y., Murray, D., Liu, Y., Hosing, C., Nieto, Y., Champlin, R. E., & Andersson, B. S. (2015). Romidepsin targets multiple survival signaling pathways in malignant T cells. *Blood Cancer Journal*, *5*(10). https://doi.org/10.1038/bcj.2015.83

Van Galen, P., Kreso, A., Mbong, N., Kent, D. G., Fitzmaurice, T., Chambers, J. E., Xie, S., Laurenti, E., Hermans, K., Eppert, K., Marciniak, S. J., Goodall, J. C., Green, A. R., Wouters, B. G., Wienholds, E., & Dick, J. E. (2014). The unfolded protein

response governs integrity of the haematopoietic stem-cell pool during stress. *Nature*, *510*(7504), 268–272. https://doi.org/10.1038/nature13228

van Galen, P., Mbong, N., Kreso, A., Schoof, E. M., Wagenblast, E., Ng, S. W. K., Krivdova, G., Jin, L., Nakauchi, H., & Dick, J. E. (2018). Integrated Stress Response Activity Marks Stem Cells in Normal Hematopoiesis and Leukemia. *Cell Reports*, *25*(5), 1109-1117.e5. https://doi.org/10.1016/j.celrep.2018.10.021

Vassiliou, G. S., Cooper, J. L., Rad, R., Li, J., Rice, S., Uren, A., Rad, L., Ellis, P., Andrews, R., Banerjee, R., Grove, C., Wang, W., Liu, P., Wright, P., Arends, M., & Bradley, A. (2011). Mutant nucleophosmin and cooperating pathways drive leukemia initiation and progression in mice. *Nature Genetics*, *43*(5), 470–476. https://doi.org/10.1038/ng.796

Velten, L., Haas, S. F., Raffel, S., Blaszkiewicz, S., Islam, S., Hennig, B. P., Hirche, C., Lutz, C., Buss, E. C., Nowak, D., Boch, T., Hofmann, W., Ho, A. D., Huber, W., Trumpp, A., Essers, M. A. G., & Steinmetz, L. M. (2017). Human haematopoietic stem cell lineage commitment is a continuous process. *Nature Cell Biology*, *19*(4), 271–281. https://doi.org/10.1038/ncb3493

Visnjic, D., Kalajzic, Z., Rowe, D. W., Katavic, V., Lorenzo, J., & Aguila, H. L. (2004). Hematopoiesis is severely altered in mice with an induced osteoblast deficiency. *Blood*, *103*(9), 3258–3264. https://doi.org/10.1182/blood-2003-11-4011

Waclawiczek, A., Hamilton, A., Rouault-Pierre, K., Abarrategi, A., Albornoz, M. G., Miraki-Moud, F., Bah, N., Gribben, J., Fitzgibbon, J., Taussig, D., & Bonnet, D. (2020). Mesenchymal niche remodeling impairs hematopoiesis via stanniocalcin 1 in acute myeloid leukemia. *Journal of Clinical Investigation*, *130*(6), 3038–3050. https://doi.org/10.1172/JCI133187

Walter, P., & Ron, D. (2011). The Unfolded Protein Response: From Stress Pathway to Homeostatic Regulation. *Science*, *334*(6059), 1081–1086. https://doi.org/10.1126/science.1209038

Wang, F., Mullican, S. E., DiSpirito, J. R., Peed, L. C., & Lazar, M. A. (2013). Lipoatrophy and severe metabolic disturbance in mice with fat-specific deletion of PPARγ.

Proceedings of the National Academy of Sciences of the United States of America, *110*(46), 18656–18661. https://doi.org/10.1073/pnas.1314863110

Wasnik, S., Tiwari, A., Kirkland, M. A., & Pande, G. (2012). Osteohematopoietic Stem Cell Niches in Bone Marrow. In *International Review of Cell and Molecular Biology* (1st ed., Vol. 298). Elsevier Inc. https://doi.org/10.1016/B978-0-12-394309-5.00003-1

Wei, J., Sheng, X., Feng, D., McGrath, B., & Cavener, D. R. (2008). PERK is essential for neonatal skeletal development to regulate osteoblast proliferation and differentiation. *Journal of Cellular Physiology*, *217*(3), 693–707. https://doi.org/10.1002/jcp.21543

Willert, K., Chiu, K. T., Nussbacher, J. K., Galimberti, V., Rodvold, J. J., Zanetti, M., Mahadevan, N. R., Hiramatsu, N., & Lin, J. H. (2017). Intercellular transmission of the unfolded protein response promotes survival and drug resistance in cancer cells. *Science Signaling*, *10*(482), eaah7177. https://doi.org/10.1126/scisignal.aah7177

Wiseman, D. H. (2011). Donor Cell Leukemia: A Review. *Biology of Blood and Marrow Transplantation*, *17*(6), 771–789. https://doi.org/10.1016/j.bbmt.2010.10.010

Wolock, S. L., Krishnan, I., Tenen, D. E., Matkins, V., Camacho, V., Patel, S., Agarwal, P., Bhatia, R., Tenen, D. G., Klein, A. M., & Welner, R. S. (2019). Mapping Distinct Bone Marrow Niche Populations and Their Differentiation Paths. *Cell Reports*, *28*(2), 302-311.e5. https://doi.org/10.1016/j.celrep.2019.06.031

Wu, J., & Kaufman, R. J. (2006). From acute ER stress to physiological roles of the unfolded protein response. *Cell Death and Differentiation*, *13*(3), 374–384. https://doi.org/10.1038/sj.cdd.4401840

Wu, Z, Bucher, N. L., & Farmer, S. R. (1996). Induction of peroxisome proliferator-activated receptor gamma during the conversion of 3T3 fibroblasts into adipocytes is mediated by C/EBPbeta, C/EBPdelta, and glucocorticoids. *Molecular and Cellular Biology*, *16*(8), 4128–4136. https://doi.org/10.1128/mcb.16.8.4128

Wu, Z, Rosen, E. D., Brun, R., Hauser, S., Adelmant, G., Troy, A. E., McKeon, C., Darlington, G. J., & Spiegelman, B. M. (1999). Cross-regulation of C/EBPα and PPARγ controls the transcriptional pathway of adipogenesis and insulin sensitivity. *Molecular Cell*, *3*(2), 151–158. https://doi.org/10.1016/S1097-2765(00)80306-8

Wu, Zhimeng, Li, M., Zheng, W., Hu, Q., Cheng, Z., & Guo, F. (2017). Silencing of both ATF4 and PERK inhibits cell cycle progression and promotes the apoptosis of differentiating chondrocytes. *International Journal of Molecular Medicine*, *40*(1), 101–111. https://doi.org/10.3892/ijmm.2017.2985

Xiao, G., Jiang, D., Ge, C., Zhao, Z., Lai, Y., Boules, H., Phimphilai, M., Yang, X., Karsenty, G., & Franceschi, R. T. (2005). Cooperative interactions between activating transcription factor 4 and Runx2/Cbfa1 stimulate osteoblast-specific osteocalcin gene expression. *Journal of Biological Chemistry*, *280*(35), 30689–30696. https://doi.org/10.1074/jbc.M500750200

Xiao, L., Sobue, T., Esliger, A., Kronenberg, M. S., Coffin, J. D., Doetschman, T., & Hurley, M. M. (2010). Disruption of the Fgf2 gene activates the adipogenic and suppresses the osteogenic program in mesenchymal marrow stromal stem cells. *Bone*, *47*(2), 360–370. https://doi.org/10.1016/j.bone.2010.05.021

Xiong, S., Chng, W. J., & Zhou, J. (2021). Crosstalk between endoplasmic reticulum stress and oxidative stress: a dynamic duo in multiple myeloma. *Cellular and Molecular Life Sciences*, *78*(8), 3883–3906. https://doi.org/10.1007/s00018-021-03756-3

Yamamoto, K., Sato, T., Matsui, T., Sato, M., Okada, T., Yoshida, H., Harada, A., & Mori, K. (2007). Transcriptional Induction of Mammalian ER Quality Control Proteins Is Mediated by Single or Combined Action of ATF6α and XBP1. *Developmental Cell*, *13*(3), 365–376. https://doi.org/10.1016/j.devcel.2007.07.018

Yang, X., & Karsenty, G. (2004). ATF4, the osteoblast accumulation of which is determined post-translationally, can induce osteoblast-specific gene expression

in non-osteoblastic cells. *Journal of Biological Chemistry*, *279*(45), 47109–47114. https://doi.org/10.1074/jbc.M410010200

Yang, X., Matsuda, K., Bialek, P., Jacquot, S., Masuoka, H. C., Schinke, T., Li, L., Brancorsini, S., Sassone-Corsi, P., Townes, T. M., Hanauer, A., & Karsenty, G. (2004). ATF4 is a substrate of RSK2 and an essential regulator of osteoblast biology: Implication for Coffin-Lowry syndrome. *Cell*, *117*(3), 387–398. https://doi.org/10.1016/S0092-8674(04)00344-7

Yeh, W. C., Cao, Z., Classon, M., & McKnight, S. L. (1995). Cascade regulation of terminal adipocyte differentiation by three members of the C/EBP family of leucine zipper proteins. *Genes and Development*, *9*(2), 168–181. https://doi.org/10.1101/gad.9.2.168

Yokota, T., Oritani, K., Takahashi, I., Ishikawa, J., Matsuyama, A., Ouchi, N., Kihara, S., Funahashi, T., Tenner, A. J., Tomiyama, Y., & Matsuzawa, Y. (2000). Adiponectin, a new member of the family of soluble defense collagens, negatively regulates the growth of myelomonocytic progenitors and the functions of macrophages. *Blood*, *96*(5), 1723–1732. https://doi.org/10.1182/blood.v96.5.1723.h8001723_1723_1732

Yoon, K. A., Son, Y., Choi, Y. J., Kim, J. H., & Cho, J. Y. (2017). Fibroblast growth factor 2 supports osteoblastic niche cells during hematopoietic homeostasis recovery after bone marrow suppression. *Cell Communication and Signaling*, *15*(1), 1–11. https://doi.org/10.1186/s12964-017-0181-2

Yu, K., Mo, D., Wu, M., Chen, H., Chen, L., Li, M., & Chen, Y. (2014). Activating transcription factor 4 regulates adipocyte differentiation via altering the coordinate expression of CCATT/enhancer binding protein β and peroxisome proliferator-activated receptor γ. *FEBS Journal*, *281*(10), 2399–2409. https://doi.org/10.1111/febs.12792

Yu, W. H., Li, F. G., Chen, X. Y., Li, J. T., Wu, Y. H., Huang, L. H., Wang, Z., Li, P., Wang, T., Lahn, B. T., & Xiang, A. P. (2012). PPARγ suppression inhibits adipogenesis but does not promote osteogenesis of human mesenchymal stem cells.

International Journal of Biochemistry and Cell Biology, *44*(2), 377–384. https://doi.org/10.1016/j.biocel.2011.11.013

Zhang, J., Niu, C., Ye, L., Huang, H., He, X., Tong, W.-G., Ross, J., Haug, J., Johnson, T., Feng, J. Q., Harris, S., Wiedemann, L. M., Mishina, Y., & Li, L. (2003). Identification of the haematopoietic stem cell niche and control of the niche size. *Nature*, *425*(6960), 836–841. https://doi.org/10.1038/nature02041

Zhang, K., Wong, H. N., Song, B., Miller, C. N., Scheuner, D., & Kaufman, R. J. (2005). The unfolded protein response sensor IRE1α is required at 2 distinct steps in B cell lymphopoiesis. *Journal of Clinical Investigation*, *115*(2), 268–281. https://doi.org/10.1172/jci21848

Zhang, P., McGrath, B., Li, S., Frank, A., Zambito, F., Reinert, J., Gannon, M., Ma, K., McNaughton, K., & Cavener, D. R. (2002). The PERK Eukaryotic Initiation Factor 2α Kinase Is Required for the Development of the Skeletal System, Postnatal Growth, and the Function and Viability of the Pancreas. *Molecular and Cellular Biology*, *22*(11), 3864–3874. https://doi.org/10.1128/mcb.22.11.3864-3874.2002

Zhou, B. O., Yu, H., Yue, R., Zhao, Z., Rios, J. J., Naveiras, O., & Morrison, S. J. (2017). Bone marrow adipocytes promote the regeneration of stem cells and haematopoiesis by secreting SCF. *Nature Cell Biology*, *19*(8), 891–903. https://doi.org/10.1038/ncb3570

Zhou, B. O., Yue, R., Murphy, M. M., Peyer, J. G., & Morrison, S. J. (2014). Leptin-receptor-expressing mesenchymal stromal cells represent the main source of bone formed by adult bone marrow. *Cell Stem Cell*, *15*(2), 154–168. https://doi.org/10.1016/j.stem.2014.06.008

Zhu, J., Garrett, R., Jung, Y., Zhang, Y., Kim, N., Wang, J., Joe, G. J., Hexner, E., Choi, Y., Taichman, R. S., & Emerson, S. G. (2007). Osteoblasts support B-lymphocyte commitment and differentiation from hematopoietic stem cells. *Blood*, *109*(9), 3706–3712. https://doi.org/10.1182/blood-2006-08-041384

Zhu, R. J., Wu, M. Q., Li, Z. J., Zhang, Y., & Liu, K. Y. (2013). Hematopoietic recovery

following chemotherapy is improved by BADGE-induced inhibition of adipogenesis. *International Journal of Hematology*, *97*(1), 58–72. https://doi.org/10.1007/s12185-012-1233-4

Zuo, Y., Qiang, L., & Farmer, S. R. (2006). Activation of CCAAT/enhancer-binding protein (C/EBP) α expression by C/EBPβ during adipogenesis requires a peroxisome proliferator-activated receptor-γ-associated repression of HDAC1 at the C/ebpα gene promoter. *Journal of Biological Chemistry*, *281*(12), 7960–7967. https://doi.org/10.1074/jbc.M510682200